Edgars Edelmers

ORCID 0000-0001-5329-4426

Automated Morphological Structure Detection, Segmentation, and 3D Model Reconstruction from Medical Images Using Artificial Intelligence Deep Neural Network Technologies

Doctoral Thesis – set of publications – for obtaining the scientific degree "Doctor of Science (*PhD*)"

Sector Group – Medical and Health Sciences

Sector – Basic Medicine

Sub-Sector – Anatomy

Supervisors of the Doctoral Thesis:

Dr. med., Associate Professor **Dzintra Kažoka**,
Rīga Stradiņš University, Latvia

Dr. sc. ing., Associate Professor **Katrīna Šmite**,
Riga Technical University, Latvia

Scientific Advisors:

Dr. med., Associate Professor **Maija Radziņa**,
University of Latvia

Dr. sc. comp., Leading Researcher **Kaspars Sudars**,
Institute of Electronics and Computer Science, Latvia

Riga, 2025

Abstract

This research investigates contemporary approaches of automated medical image analysis and the creation of accurate anatomical models. The study aimed to develop and validate artificial intelligence-based methodologies for the automated detection, segmentation, and quantification of diverse morphological structures across various imaging modalities (computed tomography, magnetic resonance tomography, and histological slides). Another significant aim was the creation of extensive protocols for the reconstruction of three-dimensional (3D) anatomical models derived from radiological imaging data. The research results, including 3D printed models and software tools, were intended to improve medical education and clinical diagnostics.

This research has established several protocols for reconstructing 3D anatomical models from data acquired via diverse imaging modalities, including computed tomography, micro-computed tomography, structured-light 3D scanning, and photogrammetry. These digital models were validated through 3D printing and their effective application in anatomy education. Deep neural network architectures, such as U-Net, and YOLO, were systematically trained and evaluated. These models were applied to tasks that included the segmentation of vertebrae and spinal metastatic lesions from computed tomography scans, and the precise quantification of interstitial cells in histological slides. The developed methodologies were further integrated into software tools to demonstrate practical utility and facilitate broader application.

Key findings demonstrate the efficacy of AI models. In vertebral segmentation, the U-Net architecture achieved an F-beta score of 0.96 – meaning that it correctly identified 96 % of vertebral structures while keeping false positives to a minimum – whereas for lytic metastasis detection it reached 0.68, indicating more modest sensitivity and precision in spotting lesions. In histopathology, YOLO-based detectors attained a mean average precision at a 50 % overlap threshold (mAP_{50}) of 92 %, signifying that 92 % of cellular structures were both correctly detected and localised with at least half-area agreement. Finally, the 3D reconstruction workflows consistently produced printed models whose anatomy matched the original specimens to educationally useful degree. This research results confirms that advanced image processing techniques that incorporate deep neural networks can provide reliable, accurate, and reproducible results in the detection and segmentation of morphological structures. The methodologies and software developed offer significant potential to improve medical image analysis, anatomical education, and advance clinical diagnostics.

Keywords: morphology; medical image segmentation; 3D reconstruction; artificial intelligence; deep neural networks; 3D printing; education; medicine.

Anotācija

Automātiska morfoloģisko struktūru noteikšana, segmentēšana un 3D modeļu rekonstrukcija no medicīniskiem attēliem, izmantojot mākslīgā intelekta dziļo neironu tīklu tehnoloģijas

Pētījums ir vērsts uz pieaugošu aktualitāti pēc precīzas, automatizētas medicīnisko attēlu analīzes un atbilstošu anatomisko modeļu izveides. Tā mērķis bija izstrādāt un pārbaudīt uz mākslīgo intelektu (MI) balstītas metodoloģijas, galvenokārt izmantojot dziļos neironu tīklus, lai automatizēti noteiktu, segmentētu un kvantitatīvi noteiktu dažādas morfoloģiskās struktūras dažādās attēlveidošanas modalitātēs (piemēram, datortomogrāfijā (DT), magnētiskās rezonanses tomogrāfijā (MRT) un histoloģiskajos preparātos). Paralēli tika izvirzīts mērķis izstrādāt un validēt visaptverošus protokolus trīsdimensiju (3D) anatomisko modeļu rekonstrukcijai gan no dotiem mākslīgā intelekta segmentētajiem datiem, gan no citiem avotiem, proti, mikro DT un fotogrammetrijas. Pētījumu rezultāti, tostarp izdrukāti modeļi un programmatūras rīki, bija paredzēti medicīnas izglītības un klīniskās diagnostikas uzlabošanai.

Pētījumā tika izstrādāti protokoli 3D anatomisko modeļu rekonstrukcijai no datiem, kas iegūti, izmantojot dažādas attēlveidošanas metodes, tostarp DT, mikro-DT, strukturētu gaismas 3D skenēšanu un fotogrammetriju. Dotie digitālie modeļi tika validēti, izmantojot 3D drukāšanu un to efektīvu izmantošanu anatomijas izglītībā. Tika sistemātiski apmācītas un novērtētas tādas dziļo neironu tīklu arhitektūras kā U-Net un YOLO. Dotie modeļi tika pielietoti skriemeļu un mugurkaula metastātisku bojājumu segmentācijai no datortomogrāfijas skenējumiem, smadzeņu audzēju identificēšanai magnētiskās rezonanses attēlos, pielāgojot mašīnmācīšanās klasifikācijas tīklus ar izskaidrojamu mākslīgo intelektu segmentācijai līdzīgiem rezultātiem, un precīzu starpšūnu kvantitatīvai noteikšanai histoloģiskajos preparātos. Izstrādātās metodoloģijas tālāk tika integrētas programmatūras rīkos, lai demonstrētu praktisko lietderību un veicinātu plašāku to lietojumu.

Galvenie secinājumi liecina par mākslīgā intelekta modeļu efektivitāti. Segmentējot mugurkaulus, U-Net arhitektūra sasniedza F-beta rādītāju 0,96, kas nozīmē, ka tā pareizi identificēja 96 % mugurkaula struktūru, vienlaikus līdz minimumam samazinot viltus pozitīvos rezultātus, savukārt līdzīsko metastāžu noteikšanā tā sasniedza 68 %, kas liecina par mazāku jutību un precizitāti bojājumu noteikšanā. Histopatoloģijā uz YOLO balstītie detektori sasniedza vidējo precizitāti pie 50 % pārklāšanās sliekšņa (mAP_{50}) 92 %, kas nozīmē, ka 92 % šūnu struktūru tika gan pareizi atklātas, gan lokalizētas ar vismaz pusi no platības atbilstību. Visbeidzot, 3D rekonstrukcijas darbplūsmas, kas tika īstenotas, izmantojot viegli pieejamu

programmatūru, konsekventi radīja drukātos modeļus, kuru anatomija atbilda oriģinālajiem paraugiem klīniski noderīgā līmenī.

Modernās attēlu apstrādes metodes, kas ietver dziļos neironu tīklus, var nodrošināt uzticamus, precīzus un reproducējamus rezultātus morfoloģisko struktūru noteikšanā un segmentēšanā. Izstrādātās metodikas un programmatūra piedāvā ievērojamu potenciālu medicīnisko attēlu analīzes uzlabošanai, apmācības pilnveidošanai anatomijā un klīniskās diagnostikas uzlabošanai, tādējādi panākot integrētu mākslīgā intelekta risinājumu nepieciešamību starpdisciplinārās jomās.

Atslēgvārdi: morfoloģija; medicīnisko attēlu segmentācija; 3D rekonstrukcija; mākslīgais intelekts; dziļie neironu tīkli; 3D druka; izglītība; medicīna.

Table of Contents

Abbreviations

AI	Artificial Intelligence
AJP	Aerosol Jet Printing
ANO1	Anoctamin-1 (calcium-activated chloride channel)
BJP	Binder Jet Printing
CPU	Central Processing Unit
CT	Computed Tomography
DICOM	Digital Imaging and Communications in Medicine
DMLS	Direct Metal Laser Sintering
DSC	Dice Similarity Coefficient
EBM	Electron Beam Melting
FDM	Fused Deposition Modelling
FFF	Fused Filament Fabrication (synonym for FDM)
FFPE	Formalin-Fixed, Paraffin-Embedded (tissue)
FOV	Field of View
HGG	High-Grade Glioma
ICC	Interstitial Cells of Cajal
IoU	Intersection-over-Union
mAP	mean Average Precision
mAP50	mAP at IoU = 0.50
mAP50-95	mAP averaged over IoU = 0.50 – 0.95
MRT	Magnetic Resonance Tomography
NIfTI	Neuroimaging Informatics Technology Initiative file format
nnU-Net	“no-new-U-Net” U-Net framework
NRRD	Nearly Raw Raster Data file format
OBJ	Wavefront Object file format
PD-L1	Programmed Death-Ligand 1
PJP	Polyjet Printing
PLA	Polylactic Acid (bioplastic filament)
PVA	Polyvinyl Alcohol (water-soluble support material)
ROI	Region of Interest
RSU	Rīga Stradiņš University
SLM	Selective Laser Melting
SLS	Selective Laser Sintering
STL	Stereolithography file format
U-Net	“U” shaped convolutional network for image segmentation

WSI	Whole-Slide Image
YOLO-v11	You Only Look Once, version 11 (object-detection network)
µCT	Micro Computed Tomography

Introduction

Modern medicine and biology rely heavily on imaging to understand the human body, from large anatomical structures down to the cellular level. Radiological scans like computed tomography (CT) and magnetic resonance tomography (MRT) provide detailed three-dimensional views of organs and tissues. In parallel, digital histology reveals the microscopic world of cells. A common challenge across all these modalities is the sheer volume and complexity of the data, which makes manual analysis time-consuming and subject to variation between experts. To address this, two key technologies offer powerful solutions: artificial intelligence (AI) can automate image analysis with remarkable speed and precision, while 3D printing can transform digital scans into tangible anatomical models. However, these advanced fields often operate independently. This Thesis investigates how to build a unified and reliable workflow that connects them, using AI to automatically analyse medical images at both the anatomical and cellular scales to create accurate 3D models and quantitative reports for education and clinical practice.

Aim of the Thesis

This study aims to develop and validate an artificial intelligence (AI) based methodology that uses deep neural networks for automated detection and segmentation of morphological structures in medical images, as well as to design a protocol to reconstruct three-dimensional (3D) anatomical models from segmented medical imaging data.

Objectives of the Thesis

The following objectives are set to achieve the aim of the Doctoral Thesis:

1 Develop a reproducible protocol to reconstruct anatomically accurate 3D bone models from various medical imaging sources (including CT, µCT, photogrammetry, 3D scanning).

2 Validate the reconstructed bone anatomical models by fabricating them with fused deposition modelling (3D printing).

3 Assemble annotated datasets of segmented morphological structures at two scales, comprising vertebrae with lytic and sclerotic lesions from computed tomography as well as intestinal Cajal cells from immunohistochemically stained histological whole slide images.

4 Train a deep neural network models for the automatic detection and segmentation of these morphological structures.

5 Create and validate the methodologies by implementing them in software for automatic detection and segmentation of morphological structures.

Hypothesis of the Thesis

Advanced image processing techniques, including those utilising deep neural network architectures, can provide reliable and reproducible results in the detection and segmentation of morphological structures with sufficient level of accuracy for both medical diagnostic applications and the reconstruction of anatomical 3D models.

Novelty of the Thesis

Prior to the research conducted in this Doctoral Thesis, the field of medical image analysis had advanced significantly beyond simple manual delineation, yet substantial barriers remained that prevented the seamless integration of these technologies into clinical and educational workflows. The primary challenges in the field had shifted from questions of technical feasibility to issues of scalability, data efficiency, and precision, particularly when dealing with complex pathologies and histological structures.

One of the most significant hurdles was the “Annotation Bottleneck” inherent in modern Deep Learning. While convolutional neural networks, such as the U-Net and V-Net architectures, established a new baseline for medical image segmentation, they introduced a critical dependency on massive, high-quality labelled datasets (Milletari et al., 2016; Ronneberger et al., 2015). Creating these “ground truth” datasets remained a manual, labour-intensive process, often stalling artificial intelligence implementation due to the sheer cost of expert time required to annotate thousands of training examples. Although interactive algorithms like “Graph Cuts” and “Random Walker” were adopted to alleviate this burden, they typically relied on intensity gradients and struggled with the "weak boundaries" common in soft tissues and spinal structures, often requiring substantial user correction that negated their efficiency gains (Boykov & Jolly, 2001; Grady, 2006).

A parallel challenge existed in the domain of digital pathology, specifically regarding the quantification of morphological structures in whole slide images. The quantification of specific cell types, such as interstitial cells of Cajal, was predominantly manual or semi-automated using morphological filters, frequently implemented in legacy commercial image-analysis environments, where user-defined macros and threshold-based routines were tailored for each staining protocol and then laboriously tuned and validated. Standard object detection models utilising horizontal bounding boxes also proved inadequate for these tasks. As noted by Ma et al., when such models are applied to elongated, spindle-shaped cells like interstitial cells of Cajal, they capture excessive background and often suppress adjacent diagonal cells due to high intersection over union overlap, leading to systematic undercounting in dense tissue clusters (Ma et al., 2018). More recent digital pathology ecosystems, including Visiopharm, Definiens Tissue Studio, Image-Pro (Media Cybernetics), Indica Labs’ HALO,

and the Aperio HALO AP platform, provide integrated workflows for whole-slide tissue segmentation and immunohistochemistry scoring, and are now widely used in translational research, clinical trials, and biomarker studies (Escobar Díaz Guerrero et al., 2022; Salo et al., 2024). However, these systems remain proprietary "black boxes": algorithmic details and model parameters are generally inaccessible to end-users, and workflow customisation is constrained by vendor-specific interfaces. In addition, substantial licensing and maintenance costs limit their deployment in many academic and educational settings, despite the availability of open-source alternatives such as Orbit and QuPath, which have demonstrated robust performance for whole-slide image analysis and biomarker quantification but often require considerable technical expertise in scripting, workflow configuration, and computational infrastructure, thereby posing additional barriers for laboratories without dedicated informatics support (Bankhead et al., 2017; Stritt et al., 2020).

In the domain of spinal pathology detection, particularly concerning metastatic lesions, the standard of care relied heavily on manual radiological review. This process is inherently subjective and susceptible to fatigue-related errors, particularly given the high volume of slices in modern high-resolution Computed Tomography scans. Unlike pulmonary nodules, which are contrasted against air, spinal lesions often share similar radiodensity profiles with healthy trabecular bone, making them difficult to isolate using standard density-based thresholding algorithms. While commercial computer-aided detection platforms exist – such as "syngo.via" (Siemens Healthineers) or "Bone VCAR" (GE Healthcare) – these proprietary solutions are often prohibitively expensive and restricted to closed hardware ecosystems (Ha et al., 2017). Furthermore, they typically rely on semi-automated methods that require manual initialisation or seed placement, limiting their utility for fully automated, high-throughput screening compared to end-to-end deep learning approaches (Hammon et al., 2013).

Finally, a distinct technological gap existed in the workflow for 3D anatomical reconstruction. While sophisticated open-source platforms for volumetric segmentation, such as 3D Slicer and ITK-SNAP, were widely accessible, their utility was primarily engineered for diagnostic visualisation rather than manufacturing (Kikinis et al., 2014; Yushkevich et al., 2006). Consequently, the raw surface meshes extracted by these tools frequently exhibited artifacts inherent to slice-based imaging – such as "stair-casing" or terracing effects – along with internal noise and non-manifold geometries (e. g. holes, self-intersections) that render files unprintable. There was a notable absence of validated, unified protocols to bridge this gap using accessible software. Researchers lacked a standardised methodology to systematically convert these raw digital assets into high-fidelity, printable models that balanced the need for

anatomical precision with the topological requirements of additive manufacturing, often forcing reliance on fragmented workflows or expensive industrial computer-aided design solutions.

This Thesis presents practical innovations in artificial intelligence-based medical-image analysis and three-dimensional anatomical reconstruction. Together, the open reconstruction protocol, the segmentation and detection networks, and the custom software application form a coherent, freely available framework that spans data acquisition, artificial intelligence analysis, 3D mesh optimisation, physical fabrication, and educational deployment.

The first major advance comprises the development of deep learning tools for detection and segmentation to separate morphological structures across several imaging domains, addressing the "Annotation Bottleneck" described above. In the context of radiological analysis, the Thesis utilises U-Net models to separate individual vertebrae and classify metastatic lesions in full-resolution computed tomography scans. A key novelty is the introduction of a human-in-the-loop methodology, which iteratively combines artificial intelligence predictions with expert refinement. This approach drastically reduces the time-cost of creating "gold standard" datasets compared to manual annotation. Regarding histological analysis, the Thesis introduces an oriented-box adaptation of the YOLOv11 architecture for the quantification of interstitial cells of Cajal. This specific "nano" model (YOLOv11n-obb) is capable of recognising cells on gigapixel histological slides in real time on standard graphics hardware. This pipeline is supplied as "MorpHista", an open-source program developed in this work that performs tissue masking, inference, post-processing, and quantitative reporting.

The second major advance focuses on 3D anatomical reconstruction and educational integration, establishing a fully documented workflow that transforms data from clinical computed tomography, micro-computed tomography, structured-light scanning, and photogrammetry into anatomically verified, print-ready surface meshes using only open-source software. Newly written repair and simplification steps were developed to reduce printing time while maintaining geometric fidelity. All protocols, parameters, and decision criteria have been published, ensuring that both the workflow and its results can be fully reproduced. Following technical validation, this workflow was subjected to educational validation by being integrated into an undergraduate anatomy course. The pedagogical impact was quantitatively verified: students who learned with the specific three-dimensional printed models generated by this pipeline achieved higher practical scores than earlier cohorts who relied on traditional methods.

Ultimately, this research democratises access to advanced medical imaging technologies. By demonstrating that sophisticated analysis and reconstruction techniques can be implemented with modest resources and shared transparently, the work significantly lowers the technical and financial barriers to innovation. The resulting framework offers a robust

solution for the automated detection of spinal pathologies and the streamlined production of patient-specific educational tools, effectively bridging the gap between theoretical deep learning models and practical application in clinical and academic settings.

1 Review of Literature

1.1 Applications of 3D Reconstruction in Anatomical Education and Clinical Practice

Addressing contemporary educational challenges requires the deliberate deployment of various pedagogical methods and models (Mahlow & Hediger, 2019). Higher education institutions, through their teaching, research and outreach missions, are uniquely positioned to advance sustainable development (Bell et al., 2017). In a period marked by political, economic, and social upheavals, the importance of sustainable development orientated education has increased (Portuguez Castro & Gómez Zermeño, 2020). Sustainability must therefore be conceived as a continuous incremental progression that requires movement in the appropriate direction, and this, in turn, requires a change from knowledge-centred to experience-based learning, supported by specific skills and dispositions.

Within medical education, recent technological, socioeconomic and contextual developments have precipitated notable changes in traditional teaching and learning. The systematic integration of 3D digital technologies into the Human Anatomy curriculum at Rīga Stradiņš University (RSU) has demonstrably improved students' knowledge base, practical skills, and overall performance (Kazoka et al., 2021). Anatomy offers the foundational understanding of the human structure on which all clinical disciplines are based. Although the optimal instructional strategy for anatomy remains a topic of debate, recent innovations delineate clear reform trajectories (Garas et al., 2018; Jeyakumar et al., 2020; Johnson et al., 2019; Memon, 2018). Since 2016 the Department of Morphology at RSU has provided students with the 3D virtual dissection table “Anatomage” and, from 2018, with both 3D printed models and a dedicated 3D printing course.

Human anatomy instruction typically combines lectures, laboratory sessions, and real or virtual dissections, each calibrated to specific learning objectives (Fasel et al., 2016). Practical laboratories interweave lecture content, textbook material, electronic resources, and cadaver preparations, thus introducing theory into direct observation. Digital images and virtual anatomy confer several advantages over traditional methods (Lakhani et al., 2022; Lengyel et al., 2025; Martín, 2018; Ye et al., 2020). High-resolution cross sections deliver fine structural detail, while virtual dissection reduces specimen preparation time and allows simultaneous display of multiple views. Digital data sets are easily stored, organised and retrieved. Continued refinement of these resources is expected to make anatomy teaching more engaging, participatory, and creative (Bücking et al., 2017; Ye et al., 2023).

Parallel advances in 3D printing have catalysed innovation in many sectors, including medicine (Jamróz et al., 2018; J.-Y. Lee et al., 2017). In pedagogy, progress has focused on

combining classical methods with digital approaches. Both the staff and students attest to the efficacy of integrating 3D models and digital imagery into lectures and practical classes (Backhouse et al., 2019; Dee et al., 2021). Beyond higher education, the annual application of 3D printing in clinical settings demonstrably saves and improves lives (N. Lee, 2016; Verner & Merksamer, 2015). Targeted initiatives now invest in training educators to master the fundamentals (AbouHashem et al., 2015), but adoption within schools and universities remains limited (Balestrini & Campo-Celaya, 2016; Smith et al., 2018). Given the demands of the evolving curriculum, increased acceptance is expected from medical educators.

Investment in 3D infrastructure and staff development is essential to realise the pedagogical potential of these technologies (Asghar et al., 2022; Garcia et al., 2018). 3D printing allows students to examine anatomical structures step by step and at multiple scales, fostering mastery of normal anatomy, variations, and pathological conditions. Layer-by-layer fabrication helps learners visualise spatial relationships, plan clinical interventions, and rehearse procedures (Ballard et al., 2018; Diment et al., 2017; Ye et al., 2023).

For clinicians, patient-specific 3D models generated from high-resolution CT data sets facilitate preoperative planning, intraoperative guidance, and interdisciplinary consultation (Lakhani et al., 2022). Reproducible models of defined size and detail offer a substantial advantage for both teaching and training.

Virtual dissection has become a cornerstone of digital transformation. Multiple studies document the educational efficacy of the “Anatomage” table (Baratz et al., 2019; Bharati et al., 2018; Binder et al., 2021). Frozen-section cadaveric data underpin interactive reconstructions that users can section in any plane. High-speed touchscreen displays incorporate digital cross sections, radiological images, and thousands of labelled structures, drawing tools, and extensive case libraries enable human and veterinary applications. Experience at RSU suggests that frequent use of the “Anatomage” technology correlates with better teaching and learning outcomes. Students also use their data sets for research projects, while residents and clinical staff use the technology to develop skills and plan surgeries.

The curricular integration of 3D models can proceed through commercial purchase (Sheth et al., 2016), or by onsite production tailored to local needs (Kong et al., 2016; C. Li et al., 2017; Lim et al., 2016). Many contemporary 3D printers are safe and intuitive enough for students to use, and learners consistently describe this technology as modern, creative, and motivating (Ye et al., 2020). Open-source repositories provide downloadable files that staff can print directly or modify to emphasise or omit particular structures. During model preparation, the duplication process, material selection, and structural composition can be adjusted. Polylactic acid (PLA) 3D printing material is preferred for its ease of use and low cost, but

more complex or durable models may require premium materials (Joseph et al., 2023; Powers et al., 2016). Print times vary widely: simple demonstrators can be produced rapidly for lecture illustration, whereas intricate constructs demand longer fabrication. In addition to departmental resources, students increasingly print custom models for individual study.

In summary, high-resolution digital imaging, virtual dissection, and 3D printing are transforming human anatomy education. These technologies complement, rather than replace, traditional cadaver study (Arráez-Aybar, 2025; K. H. C. Li et al., 2017), collectively supporting a shift toward experiential student-centred learning that equips future clinicians with the knowledge, skills, and attitudes required by contemporary medical practice and sustainable development.

1.1.1 Principles of Anatomical 3D Model Creation

Various methods exist for creating 3D anatomical models (Edelmers et al., 2022; Nath et al., 2021). Model structures, shapes, and sizes can be generated manually using computer software, where the level of detail can be adjusted. For example, a bone model might represent only basic structures or include detailed muscle attachment sites. A more sophisticated method involves creating realistic and highly detailed anatomical models from medical radiological images using computer segmentation techniques. This process allows for the identification of anatomical structures, their variations, pathological processes, and the condition of individual morphological structures (Pujol et al., 2016).

Structures are identified and prepared for segmentation using specialised computer software, then converted to 3D file formats such as stereolithography (STL) or Wavefront Object (OBJ) (Mogali et al., 2018). The resulting models can be printed in various sizes with different levels of detail. In medicine, even minor accuracy of dimensions is critical in certain contexts. This process can provide students and future specialists with a deeper understanding of anatomical structures and their conditions. During classroom lectures and lab work, educators can effectively integrate scaled 3D printed models with students' existing knowledge. This approach allows for a deeper exploration of anatomy by linking it to other core subjects in morphology and clinical studies.

On the basis of experience, the skeletal system is the most accessible for 3D printing anatomical models. The relative simplicity of some bones and their structures allows students to prepare these models with ease. Cross sections and segmentation of medical images can be easily applied in the creation process. 3D printing technology offers numerous possibilities, such as printing individual bones or multiple bones in different sizes. As students gain proficiency, they can attempt to prepare more complex models, such as those of the muscular

system. For other organ systems, students can prepare and print 3D models of organs such as the heart, brain, or kidneys, or specific structures, to improve their understanding of location and function. In later semesters, some students revisit the 3D printing process with a stronger motivation to create more intricate and specialised models.

The increasing availability of 3D printers and advances in segmentation algorithms have boosted the use of 3D printing in medicine, leading to interest in numerous potential medical applications (Yakunina, 2020). Models can be quickly adapted to individual patients, reshaped and 3D printed, offering a cost-effective alternative to commercially available anatomical models. Therefore, 3D printing can be used effectively to teach anatomical structures (Yuen, 2020).

1.1.2 Foundational Processes in 3D Anatomical Modelling: Segmentation, Refinement, and Validation

The initial step involves the acquisition of radiological data, followed by the segmentation of the region of interest. It is a process that divides an image into distinct regions corresponding to structures of interest. Subsequently, this is used to generate a precise computer model of the organs of the patient. The segmentation process is based on the principle that each tissue type is characterised by a specific range of voxel intensities, allowing the differentiation of tissues and the definition of organ boundaries (Talanki et al., 2022). Commercial and free software are available for image segmentation. However, this work exclusively used free and widely accessible software, including the internationally recognised platform “3D Slicer” (Kikinis et al., 2014).

Image segmentation is succeeded by editing and optimising the 3D model to mitigate potential artifacts, optimise the final model size, and enhance anatomical accuracy. Various programs exist for working with 3D models, however, “MeshLab” (Cignoni et al., 2008) offers advantages such as precise control over tools, batch editing, and feature rich user interface. Another programme, “Meshmixer” (Schmidt & Singh, 2010), facilitates manipulation of model morphology. The primary benefits of these programmes include intuitive interfaces and comprehensive documentation.

Errors, such as duplicate points, faces with zero area, non-manifold edges or points, and vertices not referenced by a face, should be corrected during the repair phase prior to printing. Anatomical inaccuracies that may arise during the segmentation process also need to be corrected. Depending on the input data (radiological study type, tomography settings) and the segmentation process, “digital noise” can occur, potentially affecting the quality and smoothness of the model surfaces and introducing artifacts. Smoothing techniques are

necessary to address this. In certain instances, the final model can be created by combining different models.

To ensure the anatomical precision of the model, it is cross-referenced with credible sources such as “Complete Anatomy” (Motsinger, 2020), which serves as a prime example of such a tool, providing an accurate and user-friendly interface to interact with anatomical models. Developed by “3D4Medical” under the auspices of “Elsevier”, “Complete Anatomy” is recognised as a sophisticated educational 3D anatomy platform, with the company having a history of developing medical products since 2009 (Fan et al., 2020; Nair & Lindsey, 2020).

1.1.3 Overview of 3D Printing Technologies for Anatomical Applications

Specialised 3D printing technologies have been developed with distinct functionalities. The selection of techniques is often dictated by specific fabrication processes and raw material requirements to meet high quality standards (Kantaros & Karalekas, 2014). According to the standards set by “American Society for Testing and Materials” (ISO/ASTM 52900), 3D printing methods are categorised into seven groups: binder jetting, directed energy deposition, material extrusion, material jetting, powder bed fusion, sheet lamination, and vat photopolymerization (Aimar et al., 2019; Pérez et al., 2020). The choice of method depends on the intended use and visual appearance of the replica, material properties, and printer capabilities, for example, cost, settings, print time, and volume (Taylor et al., 2018).

Four common additive manufacturing techniques for printing anatomical models are extrusion-based printing (Stefaniak et al., 2019), vat polymerisation-based printing, droplet-based printing, and powder-based printing (Shirazi et al., 2015). Extrusion-based printing is commonly referred to as fused deposition modelling (FDM) or fused filament fabrication (FFF). FDM is a mature technology that involves the extrusion of thermoplastic or composite materials through a heated extrusion head with one or multiple nozzles (Penumakala et al., 2020). Vat polymerisation-based printing is widely used to make complex devices with functional parts and is based on light-curing resin material and selective hardening polymerisation (Revilla-León & Özcan, 2019). Material jetting technology involves the ejection and polymerisation of liquid material droplets through numerous jets, with polymerisation occurring selectively via directed UV light for designed structures (Bezek & Williams, 2023). This category includes aerosol jet printing (AJP), binder jet printing (BJP), and polyjet printing (PJP). Powder-based 3D printing is characterised by its ability to customise fabrication with varied external shapes, internal structures, and porosities (Chin et al., 2020). Common powder-based techniques include selective laser sintering (SLS), selective laser melting (SLM), direct metal laser sintering (DMLS) and electron beam melting (EBM)

(Dev Singh et al., 2021). These techniques differ in their printing processes and product characteristics and rely on localised heating to melt metallic powder for customised product fabrication.

These various 3D printing technologies possess distinct advantages and disadvantages. Extrusion technology is the most widespread and its primary advantage lies in its low printing costs (equipment, maintenance, and materials) and its user-friendly nature (Placone & Engler, 2018). Research indicates that careful tuning of process parameters (layer thickness, extruding temperature, printing speed, retraction distance, etc.) is necessary to achieve desired results with lower-end desktop FDM 3D printers, highlighting existing challenges (Antreas & Piromalis, 2021). Photopolymerisation technologies can be employed when high precision and quality are required (Subedi et al., 2024).

Anatomical 3D reconstruction has been approached using diverse acquisition and modelling strategies, including CT- and μCT-based segmentation, structured-light and laser scanning, photogrammetry workflows, and commercial 3D modelling and printing platforms. These approaches are implemented in heterogeneous software stacks, with substantial variation in how parameters and validation procedures are reported. Most published protocols are framed as case-based "how-to" descriptions aimed at producing individual visualisation or planning models, with limited emphasis on standardised, end-to-end pipelines that can be replicated across institutions using only accessible, low-cost tools. In particular, there is a conspicuous gap in fully documented, reproducible CT-based workflows that cover the complete path from image acquisition and segmentation through mesh repair, optimisation and slicer configuration, explicitly tuned for affordable FDM printers and systematically evaluated for anatomical fidelity and educational utility. The 3D reconstruction and printing protocols developed in this Thesis are designed to address this gap by formalising a transparent, open workflow for bone model generation that is suitable for both teaching and AI dataset creation, with a detailed comparison to existing open-source and commercial solutions (for example, open CT→3D pipelines based on 3D Slicer, MeshLab/Meshmixer and Cura, and commercial platforms such as Materialise Mimics inPrint or syngo.via 3D printing modules) presented in the Discussion section.

1.2 AI in Medical Image Analysis, Diagnostics, and 3D Reconstruction

Artificial intelligence (AI) techniques are increasingly integrated into medical image analysis, offering systematic and reproducible extraction of diagnostically relevant information from complex radiological datasets (Najjar, 2023; Saeed et al., 2023). Contemporary deep-learning models identify subtle textural, morphological, and functional features that may remain imperceptible to human observers, thereby enhancing diagnostic sensitivity and

inter-observer consistency. Improved diagnostic accuracy not only leads to better patient outcomes but also helps avoid unnecessary medical tests. These consume valuable time and financial resources, impose psychological burdens on patients, and may involve exposure to ionising radiation and potentially toxic contrast media (Khalifa & Albadawy, 2024).

Although AI has the ability to automate certain tasks within healthcare specialities that rely heavily on digital information, such as radiology and pathology, it is not expected to replace healthcare professionals entirely. Instead, the goal of AI in healthcare is to improve the skills of clinicians, allowing them to dedicate more time to direct patient care and tasks that require unique human attributes, such as empathy, persuasion, and holistic integration of complex information (Alowais et al., 2023; Bajwa et al., 2021; Gazquez-Garcia et al., 2025; Rony et al., 2024). Integration of AI into healthcare systems presents significant ethical, legal, and practical challenges that require careful consideration and mitigation. More research is essential to fully understand the long-term effects and ensure the safe and effective incorporation of AI-based technologies into routine clinical practice (Ahuja, 2019).

Accurate, automated delineation of anatomical structures and small, localised areas of abnormal tissue changes (pathological foci) is a prerequisite for many downstream tasks in computer-aided diagnosis, therapy planning, and outcome monitoring (Bian et al., 2025). Convolutional neural networks with encoder–decoder topologies have become the methodological standard for such segmentation problems, as they can learn hierarchical feature representations and produce pixel-wise probability maps aligned with the original image dimensions (L. Chen et al., 2021). Among these approaches, U-Net and its derivatives have attained particular prominence in biomedical imaging owing to their ability to recover fine spatial detail while retaining robust contextual information. The U-Net segmentation architecture was initially developed with a focus on medical imaging data analysis (Ronneberger et al., 2015). Its architecture is designed to produce segmentation masks that are the same size as the input image, making it well-suited for indicating the location of potential metastases. A study demonstrated that a deep learning algorithm (DLA) could provide valuable assistance to radiologists in detecting potential spinal cancers on CT scans. The system, which employed an architecture similar to U-Net, achieved a sensitivity of 75 % in identifying potentially malignant spinal bone lesions (Gilberg et al., 2023). This significantly enhanced radiologists' ability to detect incidental lesions that might otherwise go unnoticed due to the primary focus of the scan or diagnostic biases. In this context, AI functions as a “second reader”, substantially increasing detection sensitivity without leading to an excessive rate of false positives. Moreover, AI in metastatic imaging contributes to early detection and therapeutic planning, which are crucial to preventing complications and improving patient

quality of life. Recent research has explored the application of AI approaches in various stages of care for spinal metastasis, including image processing, diagnosis, decision support, and therapeutic assistance (Edelmers, Ņikuļins, et al., 2024). These technologies have shown promising results in terms of increasing work productivity and reducing adverse events; however, further study is required to rigorously evaluate their clinical performance and facilitate their adoption into routine clinical practice (Ong et al., 2022).

Another significant aspect of the role of AI is computational pathology, with contemporary surveys attesting to a transition from handcrafted pipelines to end-to-end deep-learning frameworks that now dominate routine tasks such as tumour detection, grading and prognostication (Komura et al., 2025). Technical progress has moved beyond conventional convolutional networks toward vision transformers whose masked self-supervised pre-training markedly improves data efficiency in whole-slide contexts, and large-scale masked-image-modelling studies demonstrate that scaling self-supervised learning to tens of millions of histology tiles yields pan-cancer representations that outperform contrastive counterparts on 17 downstream tasks (Jiang et al., 2024). Building on such representation learning, foundation models like CHIEF, pretrained on > 60 000 whole-slide images (WSI), deliver state-of-the-art accuracy across cancer-type classification, mutation prediction and survival forecasting while remaining robust to domain shift (X. Wang et al., 2024), and are complemented by the UNI visual backbone that generalises across 19 anatomical sites with minimal fine-tuning (R. J. Chen et al., 2024). Parallel efforts have integrated language grounding, yielding multimodal assistants such as PathChat that couple a pathology-specific encoder with a large language model to answer open-ended diagnostic questions, thereby supporting education and human-in-the-loop decision-making (Lu et al., 2024). Privacy-preserving deployment across centres is facilitated by federated learning frameworks that train gigapixel-scale networks without data pooling, as stated in a 2024 clinical review (Vorontsov et al., 2024). Benchmarking initiatives, for example PathCLIP, extend contrastive vision–language pre-training to histopathology and reveal strong zero-shot robustness but also sensitivity to colour and resolution corruptions (Zheng et al., 2024). Methodological innovation is translating to clinically relevant endpoints: an AI system recently standardised PD-L1 combined-positive-score assessment in triple-negative breast cancer, boosting inter-observer concordance from 0.62 to 0.93 (J. Li et al., 2024). Nevertheless, the imperative for transparent decision pathways has spurred dedicated research on explainability and causality, outlining best practices for rendering model reasoning accessible to pathologists (Plass et al., 2023). Together, these advances – including scalable self-supervision, foundation and multimodal models, federated training, rigorous benchmarking and interpretability – highlight the maturation of

AI from a proof of concept to trustworthy and generalisable tools that are ready to enhance histopathological diagnostics in routine and precision oncology workflows.

In summary, contemporary digital pathology relies on a broad range of approaches, from classical thresholding and morphology-based filters through machine-learning classifiers and fully convolutional segmentation networks to modern object detectors and foundation models, implemented both in open-source research tools and commercial platforms. Yet the vast majority of these methods target broad clinical endpoints such as tumour detection, grading, biomarker scoring and outcome prediction, rather than narrowly defined, functionally specific cell populations. There remains a clear methodological gap in transparently documented, reproducible workflows that focus on quantitative counting of a particular cell type, such as interstitial cells of Cajal within the enteric nervous system. Addressing this gap is a central motivation for the ICC-focused counting pipeline and the "MorpHista" software presented in this Thesis, with a more detailed comparison to existing platforms (for example, open-source environments such as QuPath, Orbit, Cytomine, ImageJ, CellProfiler and Ilastik, and commercial systems such as HALO, Visiopharm, Aiforia, Paige, PathAI, Ibex and Image-Pro) provided in the Discussion section.

AI-Driven Semantic Segmentation in Medical Imaging: Principles and Applications

Semantic segmentation is a critical process in medical radiology, which classifies each pixel in an image to extract detailed anatomical and pathological information (Ahmad et al., 2021). This technique is instrumental in diagnosis, treatment planning, and monitoring of disease progression. However, the implementation of semantic segmentation in medical radiology faces significant challenges, such as scarcity of accurate annotated data. Supervised learning models require extensive labelled data sets for training (Edelmers, Kazoka, et al., 2024). Obtaining precise annotations from experienced radiologists is resource-intensive and time-consuming. Class imbalance, where crucial features, such as tumours, occupy a small image portion, can bias algorithms toward dominant classes, leading to inaccuracies (Schutera et al., 2022). Inter-rater variability among expert radiologists in image interpretation and annotation is common, (Liang et al., 2021) complicating the establishment of a consistent ground truth for training models. Real-time semantic segmentation is required in applications such as image-guided surgeries, adding complexity (Urrea et al., 2024). Computer-aided platforms utilise these advancements to assist medical professionals in clinical decisions related to diagnosis, tracking, and prognosis (Gon Park et al., 2024). The creation of personalised medical images based on patient data enables the visualisation and detection of disease manifestations, enhancing personalised care. AI algorithms are crucial for diagnosing diseases,

planning treatments, and monitoring results. They analyse imaging data to create detailed illustrations of bone dislocations, fractures, or tumours, specifying location, size, shape, and characteristics. AI has surpassed human performance in tasks such as image segmentation (Al-Naser, 2023). Processes various types of medical data, including scanner output, sensor data, or patient metadata. Modern computers with DL algorithms excel at semantic labelling and image classification (Archana & Jeevaraj, 2024). In medical data analysis, these algorithms identify anatomical landmarks, geometric descriptors, centrelines, shape, deformation, and fibre orientation, providing remarkable diagnostic accuracy. Algorithms trained on large data sets can predict results on new data without explicit programming (Jin et al., 2022). Current computer vision algorithms excel in identifying patterns in digital data and achieving human-level accuracy in object detection (Abdel-Jaber et al., 2022).

Image segmentation is fundamental in many medical imaging applications, delineating regions of interest. Traditional methods based on areas and edges face limitations due to nonuniform greyscale, individual differences, and artifacts (J. Wang et al., 2021). Deep learning (DL) has introduced advanced architectures and feature extraction, significantly improving deformed anatomy segmentation, improving diagnostic accuracy, and minimising redundant computations. Automated bone segmentation is crucial for quantitative markers, accurate diagnosis, and computer-aided decision support. In CT and MRT, understanding the pathology and observing changes in bone structures, shape, size, and texture are vital for diagnosis and monitoring (S. Kim et al., 2018). Accurate bone segmentation provides a stable reference for organ registration and localisation. Despite the ease of visual bone observation in CT, challenges like low signal-to-noise ratio, insufficient resolution, and indistinct intensity between spongy substance and soft tissues make precise individual segmentation complex (Fu et al., 2017). Accurate spine segmentation into individual vertebrae is crucial for diagnosing spine illnesses, especially detecting and classifying damage, fractures, lesions, and tumours (Qadri et al., 2023).

Semantically segmented medical datasets are fundamental to the advancement of medical research and technology. Their integration into AI and 3D technologies presents a new era of opportunities. In medical AI, these data sets are indispensable. AI algorithms trained on semantically segmented data have transformed diagnostics by precisely identifying and classifying abnormalities. This helps radiologists and clinicians in early and accurate diagnosis, paving the way for personalised medicine (Rezayi et al., 2022).

3D technologies have benefited significantly from these datasets, allowing detailed anatomical reconstructions (Bücking et al., 2017). Surgeons use these 3D models for meticulous procedural planning, improving patient outcomes, and optimising surgical times. Integrating

these data sets into virtual and augmented reality platforms improves medical training and patient education, providing immersive experiences and real-time surgical guidance (Kanumilli et al., 2024).

Beyond AI and 3D applications, semantically segmented data sets are crucial in telemedicine (Raju et al., 2025). They facilitate real-time sharing and analysis, ensuring access to expert care regardless of location. These data sets are at the forefront of contemporary medical innovation, enhancing current practices, and setting the stage for future advancements.

2 Materials and Methods

2.1 Development and Validation of a 3D Anatomical Model Reconstruction and Printing Protocol

The development and validation of a robust protocol for 3D anatomical model reconstruction and printing formed a cornerstone of this research, aiming to create accurate, accessible, and educationally valuable physical models from diverse imaging sources. This protocol encompassed a multi-stage workflow, from the initial acquisition and preparation of data, to the reconstruction, optimisation, and anatomical validation of a digital model, and finally physical realisation via 3D printing and subsequent evaluation.

2.1.1 Data Acquisition and Preparation for 3D Reconstruction

The generation of accurate and functionally relevant 3D anatomical models is fundamentally dependent on the quality and characteristics of the acquired initial data and its subsequent preparation. This section delineates the methodologies employed for data acquisition from various sources and the preparatory steps undertaken to render these data suitable for the 3D model reconstruction pipelines.

The data sources integral to this investigation were diverse, reflecting a multimodal approach to capture anatomical information. These sources included digital images obtained through conventional photographic techniques, cross-sectional volumetric data derived from advanced medical imaging modalities such as CT and MRT, and surface geometry data acquired via dedicated 3D scanning technologies.

A significant component of the study, particularly concerning the educational intervention, involved the utilisation of digital images and interactive 3D visualisations facilitated by the “Anatomage” (Kavvadia et al., 2023). This system served as a rich repository, providing access to an extensive case library. The database included over 100 high-resolution cross-sections meticulously derived from four prepared human cadaveric specimens, equally distributed between male and female subjects. Furthermore, it contained data from over 50 diverse clinical cases, presenting a variety of visualisation options such as X-rays, CT, and MRT scans. This digital resource enabled students to engage with complex anatomical structures in a virtual environment, facilitating identification and study.

For the creation of physical, tangible 3D printed anatomical models, data acquisition was pursued through three primary techniques: photogrammetry, µCT, and optical 3D scanning of natural anatomical specimens. The selection of the specific data acquisition modality was a deliberate decision, contingent upon the inherent characteristics of the anatomical structure targeted for modelling and the requisite level of morphological detail and dimensional accuracy for the intended application.

The initial preparation of the acquired data was a critical phase, with the specific procedures varying based on the data source. Photographic data intended for photogrammetric processing underwent meticulous post-processing to optimise image quality, ensuring clarity and sharpness essential for accurate 3D reconstruction. Medical imaging data, typically formatted according to the Digital Imaging and Communications in Medicine (DICOM) standard (Bidgood et al., 1997), necessitated import into specialised software platforms designed for medical image analysis and manipulation before further processing could commence. Data captured by dedicated 3D scanners also required initial processing, often involving proprietary software bundled with the scanning hardware, to generate preliminary digital representations.

The foundation for the reconstruction of 3D anatomical models was laid by data obtained through distinct acquisition methods: photogrammetry, μCT, and dedicated 3D scanning. Each method yielded data with unique characteristics, necessitating tailored processing pipelines for effective model generation.

Photogrammetry utilised in this research, involved the systematic acquisition of a series of two-dimensional photographic images capturing a natural anatomical specimen from multiple overlapping perspectives. A high-resolution “Sony, ILCE-7RM2” camera coupled with a “Sigma, 70 mm F2.8 DG MACRO Art” lens was the primary equipment for image capture. Specific photographic parameters were meticulously controlled, including an aperture of f/8.0, a shutter speed of 1/640s, and an ISO sensitivity of 100. The camera’s sensor, boasting a resolution of 42.3 megapixels, was instrumental in obtaining images with sufficient detail to support high-quality texture mapping on the resulting 3D models. The pursuit of optimal sharpness and clarity in the images was paramount, frequently requiring the use of a stable tripod and supplementary artificial light sources to minimise motion blur and ensure consistent illumination. Subsequent to image acquisition, raw photographic data underwent a rigorous post-processing workflow utilising “Adobe Photoshop” (version 23.1.1) and “Capture One 22 Pro” (version 15.0.1.4) software. This process involved adjustments to parameters such as saturation, contrast, and overall colour balance to enhance image quality and prepare the data for photogrammetric software.

μCT provided detailed cross-sectional volumetric data, offering insights into both the external morphology and internal structure of specimens. A “Scanco Medica, μCT50” machine was utilised for this purpose, operating under precisely defined scanning parameters. The scanned area was configured as a cylinder with a diameter of 48 millimetres and a height of 110 millimetres. The X-ray energy was set at 90 peak kilovoltage, with an intensity of 88 microampere, and filtration was achieved using a 0.5 millimetres aluminium filter.

High-resolution presets were consistently applied, resulting in a field of view (FOV) of 49.6 millimetres, a voxel size of 24.2 micrometres, and an integration time of 1500 milliseconds. Initial processing of the raw μCT data was performed using the proprietary software supplied with the μCT machine. The processed data was subsequently exported in the standardised DICOM file format, which is widely compatible with medical imaging software and necessary for the subsequent 3D model creation workflow. An additional source of CT data was utilised from the "New Mexico Decedent Image Database" project (Edgar et al., n.d.). This database provided CT scans acquired using a specific protocol characterised by a peak kilovoltage of 120, milliampere-seconds of 200, a scan length ranging from 800 to 1000 millimetres, a scan FOV of 500 millimetres, a pitch of 0.942, collimation of 16 × 0.75, a rotation time of 1.0 s, and a matrix size of 512 × 512. These scans were reconstructed with varying slice thicknesses and image counts optimised for visualising either soft tissue or bone (3 millimetres × 3 millimetres, 320 images, 1 millimetres × 0.5 millimetres, 1900 images).

3D scanning was performed using a "Shining3D, EinScan-S". This method captured the external surface geometry of physical objects without providing internal structural information. The scanning procedure involved capturing 36 individual pictures while the specimen was rotated on a turntable. The turntable speed was set to 1, and a half turn was performed to capture sufficient data for reconstruction. This technique is particularly well-suited for obtaining detailed surface models of objects with accessible external features.

2.1.2 3D Reconstruction Pipelines

The transformation of raw data acquired from diverse sources, including photogrammetry, μCT, and 3D scanning, into usable 3D anatomical models necessitated the implementation of distinct computational pipelines. Each pipeline was specifically designed to process the unique characteristics of the input data, ultimately yielding digital 3D mesh models suitable for further manipulation and application, such as physical fabrication through additive manufacturing.

For data obtained via photogrammetry, the reconstruction workflow was centred around specialised software capable of processing multiple overlapping two-dimensional images to generate a dense point cloud and subsequently a mesh. This pipeline involved importing the photographic images, aligning them based on common features, defining the region of interest for reconstruction, and generating a high-detail mesh. A critical subsequent step was the application of texture derived from the original photographs onto the generated mesh, creating a visually realistic 3D model. Topological defects inherent in the initial mesh

generation, such as non-manifold geometry or holes, were identified and addressed within this pipeline to ensure model integrity.

Each protocol parameter was first set to its default value, then systematically varied by ± 50 % of that baseline, and the resulting outputs were benchmarked against the default case (Edelmers et al., 2021). The entire protocol was validated using 3D models of the foot bones.

Photogrammetry Protocol

1 Launch the "RealityCapture" program
2 Import images into the program
3 Adjust alignment settings:
  3.1 Max feature per mpx.: 20000
  3.2 Max features per image: 80000
  3.3 Preselector features: 20000
  3.4 Image overlap: low
  3.5 Force component rematch: yes
  3.6 Detector sensitivity: high
4 Launch the alignment process
5 Define the reconstruction region
6 Use reconstruction with "High detail" option to initialise the meshing process
7 Use "Clean Model" tool to remove topology defects (non-manifold vertices, non-manifold edges, holes, isolated vertices)
8 Use the "Texture" instrument with the following setting to create a texture for the model:
  8.1 Imported-model default texture resolution: 16384 × 16384
  8.2 Correct colours: Yes
9 Export the 3D model along with the texture as an .obj object.

The pipeline for processing medical imaging data, particularly from CT scans, involved a different approach. Following the initial acquisition and export of data in DICOM format, the primary step was segmentation, that is the process of isolating specific anatomical structures (for example, bones, organs) from the surrounding tissues within the volumetric data. This was achieved through various techniques, including thresholding based on voxel intensity values, manual drawing, and automated or semi-automated methods. In instances where a single anatomical structure spanned across multiple image series, an initial step of merging these series was required to create a continuous volume before segmentation could be performed. The segmented data was then used to generate a surface mesh representing the boundaries of the isolated anatomical structure.

Series Merging Protocol

Data import

1 Start the “3D Slicer” software;
2 Access the “DICOM” database;
3 Choose the appropriate patient;
4 Identify two series intended for later merging;
5 Import the identified series.

Creation of region of interest (ROI)

1 Activate the “Crop Volume” module;
2 Under “Input Volume”, choose a series;
3 Under “Input ROI”, opt for “Create ROI”. The resulting volume will be named “Crop Volume” ROI;
4 Click the “Center View” button in the 3D visualisation window;
5 Select the “Fit to Volume” option;
6 Resize the ROI to ensure both loaded volumes, presented as two individual entities, fit within this new ROI.

The process of stitching two volumes

1 Access the “Stitch Volume” module;
2 Under Stitched “Volume ROI”, select the “Crop Volume” ROI you previously created;
3 For “Original Volume 1”, choose the primary volume to which the secondary volume will be appended;
4 For “Original Volume 2”, select the other loaded volume;
5 Click the “Create Stitched Volume” button.

Manual Segmentation Protocol

1 Launch the “3D Slicer” program
2 Import CT data into the program:
  2.1 Set the image contrast to ensure better visibility.
3 Add a new segment using the tool:
  3.1 Segment Editor:
    3.1.1 Set up the “Threshold” tool
    3.1.2 Using “Scissors”, “Draw”, “Islands”, manually segment the required structure
4 When segmenting one structure is complete, proceed to the second one by adding a new segment and repeat the segmentation procedure if needed
5 Export the completed segment or segments as a 3D model in the .obj file format.

Segmentation Protocol with Total Segmentation module

1 For “Input Volume”, choose the volume you have loaded
2 In “Segmentation Tasks”, opt for “Total”
3 Click the “Apply” button. Deletion of unnecessary data
4 Remove all items, retaining only the volume used in the prior step and the desired semantic segmentations of anatomical structures:
  4.1 Masks validation and correction
5 When smoothing is necessary:
  5.1 For the “Smoothing Method”, select “Median”
  5.2 Set the “Kernel Size” to 3.00 millimetres
  5.3 Toggle the “Apply to Visible Segments” option to “Enable”
6 Verify the morphological accuracy of segmented structures using references from literature or digital platforms. If required, adjust utilising the “Draw”, “Paint” (with the “Sphere Brush” feature activated), “Erase”, and “Scissors” tools
7 If there is a segmentation error where a part of one structure is identified as a segment of another bone, follow these steps to merge and rectify:
  7.1 In the “Data” module, duplicate the segment that contains a section of the incorrect bone
  7.2 Utilise the “Scissors” tool from the “Segment Editor” module to remove everything except the mislabelled structure
  7.3 Using the “Logical Operators” tool, integrate the two segments of a single structure using the “Add” operation
  7.4 Data export
8 Save the volume in .nrrd file format
9 Save segmentation for the volume in .seg.nrrd file format.

For data acquired directly from a 3D scanner, the initial output was typically a point cloud or a preliminary mesh representing the surface geometry of the scanned object. This data then entered a processing pipeline focused on refining the mesh, aligning multiple scans if necessary, and preparing the model for subsequent stages such as optimisation and printing.

Each of these pipelines culminated in the creation of a digital 3D model, typically represented as a mesh (a collection of vertices, edges, and faces defining the shape of the object). These models then served as the basis for further processing steps aimed at optimising their geometry and preparing them for specific applications, most notably 3D printing.

2.1.3 Tools and Software for 3D Reconstruction

The execution of the 3D reconstruction pipelines, and the subsequent processing of the resulting models relied on a comprehensive suite of software tools and specialised hardware (Tables 2.1 and 2.2). The selection of these tools was driven by the specific requirements of each stage of the workflow, from data acquisition to the preparation for physical output. A notable aspect of the software utilised is the availability of several powerful programs at no cost for scientific and research purposes, enhancing the accessibility of these advanced methodologies.

Table 2.1

List of used hardware

Equipment	Manufacturer	Model	Specification / URL (access date)
Camera	Sony	ILCE-7RM2	electronics.sony.com/imaging/interchangeable-lens-cameras/full-frame/p/ilce7rm2-b (accessed 17 Aug 2022)
Lens	Sigma	70 mm F2.8 DG MACRO Art	sigma-global.com/en/lenses/a018_70_28 (accessed 17 Aug 2022)
µCT	SCANCO Medical	µCT 50	scanco.ch/microct50.html (accessed 17 Aug 2022)
Computer	Lenovo	Legion 7	windows 11 Pro; AMD Ryzen 7 5800H; NVIDIA GeForce RTX 3080 16 gigabyte; 64 gigabyte DDR4 3200 megahertz; 1 terabyte solid-state drive.
3D Scanner	Shining 3D	EinScan-S	einscan.com/desktop-3d-scanners/EinScan-Se/EinScan-Se-specs (accessed 17 Aug 2022)

Table 2.2

List of used software

Software / Platform	Version	Information / URL (access date)
EinScan-S	2.5.0.7	einscan.com/support/download/software/?scan_model=EinScan-S (accessed 17 Aug 2022)
µCT	– / –	shipped along with the µCT 50 machine
3D Slicer	5.02	slicer.org (accessed 17 Aug 2022)
MeshLab	2022.02	meshlab.net (accessed 17 Aug 2022)
Meshmixer	3.5.474	meshmixer.org (accessed 17 Aug 2022)
Ultimaker Cura	4.8	ultimaker.com/software/ultimaker-cura meshmixer.org (accessed 17 Aug 2022)
RealityCapture	1.2.0.17385	capturingreality.com/RealityCapture (accessed 17 Aug 2022)
Adobe Photoshop	23.1.1	for textures colour correction
Capture One 22 Pro	15.0.1.4	for cameras RAW-image processing
Sketchfab	– / –	sketchfab.com (accessed 17 Aug 2022)

For the reconstruction of 3D models from photographic data using photogrammetry, “RealityCapture” served as the primary software platform, which is specifically designed for creating 3D models from images and/or laser scans, offering functionalities for camera

alignment, dense point cloud generation, mesh creation, and texturing. Its graphical user interface and integrated tools facilitated the implementation of the photogrammetry protocol.

The processing and segmentation of medical imaging data, particularly CT scans, were performed using "3D Slicer" (Kikinis et al., 2014). This open-source software platform is widely recognised in the field of medical image analysis and visualisation. It provided the necessary tools for importing datasets in DICOM format, adjusting visualisation parameters such as image contrast, and performing both manual and automated segmentation of anatomical structures. The "Segment Editor" module within "3D Slicer" offered a range of tools, including "Threshold", "Scissors", "Draw", "Smooth", and "Islands", for precise segmentation. For tasks involving the merging of multiple image series, the Crop Volume and Stitch Volume modules within "3D Slicer" were employed. Additionally, the "TotalSegmentator" module (Wasserthal et al., 2023) facilitated automated semantic segmentation of numerous anatomical structures.

For the crucial processes of mesh simplification and optimisation, "MeshLab" (versions 2022.02 and 2020.12) was a key tool (Cignoni et al., 2008). This open-source software is specifically designed for processing and editing unstructured 3D meshes. It provided a comprehensive set of filters and tools for cleaning up mesh artifacts, such as duplicate faces or vertices, repairing non-manifold geometry, and simplifying the mesh (reducing the number of polygons) while striving to maintain the original shape and topological integrity.

Further model editing and optimisation capabilities were provided by "Meshmixer". This software offered intuitive tools for selecting and manipulating specific areas of the mesh, including functions for erasing, filling holes, sculpting, making solid objects, and combining multiple meshes. It was particularly useful for addressing small defects like micro-holes and for performing mesh remeshing and smoothing operations to refine the model's surface.

The final stage of preparing digital models for physical fabrication involved "Ultimaker Cura" to prepare the 3D models for printing on FDM machines. This software allowed for the configuration of numerous printing parameters, including layer height, infill density and pattern, shell thickness, support structures, and build plate adhesion. The "Auto-Orientation" extension within Cura assisted in optimally positioning the model on the build platform.

Additional software used in the data acquisition and preparation phases included "Adobe Photoshop" for texture colour correction and "Capture One 22 Pro" for processing RAW images from the camera. The "Sketchfab" platform served as a means for publishing and presenting the completed digital 3D models.

The hardware employed for data acquisition included a "Sony, ILCE-7RM2" camera with a "Sigma, 70 millimetres F2.8 DG MACRO Art" lens for photogrammetry, a "SCANCO Medical, µCT50" machine for µCT, and a "Shining3D, EinScan-S" 3D scanner for optical

scanning. The computational tasks were performed on a “Lenovo Legion 7” computer system, equipped with a “Windows 11 Pro” operating system, an “AMD, Ryzen 7 5800H” processor, an “NVIDIA, GeForce RTX3080” graphics card, 64 gigabyte of double data rate 4 small-outline dual-inline memory module 3200 megahertz random access memory, and a 1000 gigabyte solid-state drive, providing ample processing power and memory for handling large 3D datasets.

2.1.4 3D Model Optimisation, Anatomical Validation, and 3D Printing Preparation

Subsequent to the successful reconstruction of 3D anatomical models, a critical phase of optimisation and preparation was undertaken to ensure the models were suitable for their intended applications, particularly physical realisation through 3D printing. This involved refining the mesh geometry, ensuring structural integrity, and configuring parameters specific to the additive manufacturing process.

Model optimisation primarily focused on improving the mesh quality and reducing file size without compromising anatomical accuracy or essential detail. This was achieved through a series of steps utilising “MeshLab” and “Meshmixer” software. Initial optimisation in “MeshLab” involved the systematic removal of topological errors and artifacts that may arise during the reconstruction process. This included identifying and eliminating isolated mesh components, duplicate faces and vertices, zero-area faces, and repairing non-manifold edges and vertices. These cleaning operations were essential for creating a watertight and structurally sound mesh, which is a prerequisite for successful 3D printing. Mesh simplification was also performed, particularly for models intended for online platforms with file size limitations. The quadric edge collapse decimation technique in “MeshLab” was applied to reduce the polygon count while preserving the model’s boundary, normals, topology, and planar features.

Each protocol parameter was first set to its default value, then systematically varied by ± 50 % of that baseline, and the resulting outputs were benchmarked against the default case (Edelmers et al., 2021). The entire protocol was validated using 3D models of the foot bones.

Simplification and Optimisation Protocol

1 Launch the “MeshLab” program
2 Import a 3D model into the program
3 Remove artifacts, simplify, and optimise the model using tools (all the default values with modifications indicated below)
  3.1 Remove isolated pieces (wrt diameter)
  3.2 Remove duplicated faces

3.3 Remove duplicated vertex

3.4 Remove zero area faces

3.5 Repair non-manifold edges by removing faces

3.6 Repair non-manifold vertices by splitting

3.7 Remove unreferenced vertices

3.8 Simplification: quadric edge collapse decimation:

3.8.1 Preserve boundary of the mesh: on

3.8.2 Preserve normal: on

3.8.3 Preserve topology: on

3.8.4 Planar simplification: on

3.8.5 Remeshing: isotropic explicit remeshing

4 Adaptive remeshing: on

5 Collapse step: off

6 Export the completed segment or segments as a 3D model in the binary .ply file format.

Further refinement and optimisation were conducted in “Meshmixer”. This included addressing smaller geometric imperfections, such as micro-holes, by reconstructing the mesh surface in the affected areas. The “Inspector tool” with a “Smooth Fill” mode was employed for this purpose, with a small threshold value to target only minor gaps. The “Remesh tool” in “Meshmixer” was utilised to optimise the polygon distribution and density, often aiming for a more uniform mesh structure which can be beneficial for printing quality and file size management. Smoothing operations were also applied to the model surface as needed to reduce jaggedness and improve the visual appearance, using a shape-preserving smoothing type to avoid distorting the underlying anatomy.

Optimisation Protocol

1 Launch the “MeshLab” program

2 Import the 3D model into the program

3 Remove artifacts using tools:

3.1 Remove Duplicated Faces

3.2 Remove Duplicated Vertex

3.3 Remove Zero Area faces

3.4 Repair Non-Manifold Edges by removing faces

3.5 Repair Non-Manifold Vertices by Splitting

3.5.1 Vertex Displacement Ratio = 0

3.6 Remove Unreferenced Vertices

3.7 Remove Isolated Pieces (wrt Diameter)

3.7.1 Max diameter of isolated attachments (%) = 10

3.7.2 Remove Unreferenced Vertices = ON

4 Export 3D model as an OBJ file

5 Launch the “Meshmixer” program

6 Import the 3D model into the application

7 Close micro-holes (boundary edge type error) by reconstructing the mesh surface using the instrument:

7.1 Inspector

8 Hole Fill Mode = Smooth Fill

9 Small Thresh = 0.01 millimetres

10 Optimise the model polygon mesh to minimise the size of the file (3D model) using tools

11 Remesh:

11.1 Remesh Mode = Relative Density

11.2 Density (%) = 0

11.3 Regularity = 100

11.4 Iterations = 10

11.5 Transition (millimetres) = 0

11.6 Smooth Group Boundaries = ON

11.7 Boundary Mode = Refined Boundary

12 Smooth the 3D models surface if needed

13 Select

14 Deform

15 Smooth:

15.1 Smoothing Type = Shape Preserving

15.2 Smoothing = 1

15.3 Smoothing Scale = 4 (decrease or increase as needed)

15.4 Constraint Rings = 3

16 Export the 3D model as an .obj file.

A crucial aspect of the workflow was the manual validation of the digital models against anatomical literature (Motsinger, 2020). If discrepancies were identified, an editing methodology utilising “Meshmixer” was employed to make necessary adjustments to the digital model to ensure anatomical correctness. This involved using tools like “Select”, “Edit” (“Erase & Fill”, “Discard”), “Brushes”, “Make Solid”, and “Add Tube” to modify the mesh

geometry. The ability to combine multiple models within “Meshmixer” was also valuable for reconstructing complex anatomical regions from individual components.

Validation Protocol

1. Check the correctness of anatomical structures using the literature (Motsinger, 2020)
2. For 3D models whose structures do not correspond to normal human anatomy, make the necessary adjustments using the “Editing Methodology”
3. Launch the “Meshmixer” program
4. Import the 3D model (or models if there is a need to combine multiple models into a single model, such as putting a foot from individual bones) into the program
5. Use instruments to make necessary adjustments:
    - 5.1 Select
    - 5.2 Edit
    - 5.3 Erase & Fill
    - 5.4 Discard
    - 5.5 Brushes
    - 5.6 Make Solid
    - 5.7 Add Tube
6. To combine multiple models into one, select all models in the “Object Browser” section by holding the “Shift” button on the keyboard and select all the models from the list by clicking on them with a cursor; then, apply the “Combine” tool
7. Export the 3D model as an .obj file.

The final stage involved preparing the optimised digital models for physical fabrication using FDM 3D printers. This was managed through “Ultimaker Cura” slicing software. Importing the 3D model into “Ultimaker Cura” allowed for the configuration of numerous print settings that directly influence the physical properties and appearance of the printed object. A custom print profile was developed, based on a high-quality “Visual” profile with a 0.1 millimetres slice thickness, and further tailored to optimise print quality, structural durability, and dimensional precision. Key parameters included setting a wall line count of 10 for the outer shell, selecting a concentric pattern for the top and bottom layers, and randomising the Z seam alignment to minimise its visibility. The internal structure was defined by an infill density of 30 % and a gyroid infill pattern, providing a balance between material usage and structural support. Build plate adhesion was enhanced using a brim, printed with PVA material from the second extruder, to ensure the model adhered securely to the build platform during printing. The “Auto-Orientation” extension was used to automatically position the model on

the build plate in an orientation that minimised the need for support structures and optimised print quality.

3D Printing Protocol | Cura Ultimaker

1. Launch the "Ultimaker Cura" program
2. Import the 3D model into the program
3. Create a profile (based on the built-in profile "Visual" with a slice thickness of 0.1 millimetres with further modification and optimisation to maximise quality, durability, and precision); the main material for the model is PLA, in its turn for the support structures the PVA is being used
4. Shell:
   - 4.1 Wall Line Count = 10
   - 4.2 Top/Bottom Pattern = Concentric
   - 4.3 Z Seam Alignment = Random
5. Infill:
   - 5.1 Density (%) = 30
   - 5.2 Infill Pattern = Gyroid
6. Build Plate Adhesion:
   - 6.1 Build Plate Adhesion Type = Brim
   - 6.2 Build Plate Adhesion Extruder = Extruder 2 (PVA)
7. Optimise models' position using the "Auto-Orientation" extension from the "Ultimaker Cura" library (Marketplace)
8. Start the printing process
9. Remove support structures from the model by immersing it into the water (25°C) for 24 h
10. Remove the 3D model from the container with water and allow it to dry
11. Check the correctness of the 3D printed model by comparing it to the virtual original.

The physical printing was performed on two models of FDM printers: "Prusa i3 MK2" and "Ultimaker S5". The primary material for the anatomical models was PLA, a widely used biodegradable thermoplastic. For support structures, polyvinyl alcohol (PVA) was utilised due to its water-soluble properties, allowing for easy removal after printing. Post-processing of the printed models involved immersing them in water at 25°C for 24 hours to dissolve the PVA support material, followed by drying. The final step was a visual and tactile inspection of the 3D printed model, comparing it against the virtual original to verify its correctness and quality.

Figure 2.1 illustrates the complete process of 3D reconstruction through to the printed model.

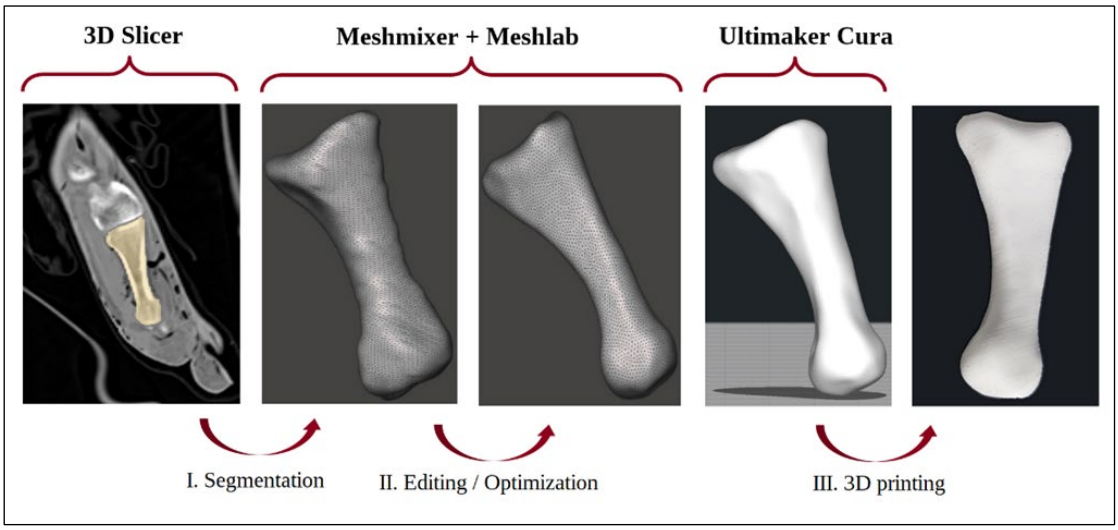

Figure 2.1. **Graphical representation of 3D reconstruction protocol**

2.2 Methodologies for AI-Driven Morphological Analysis

The methodologies for AI-driven morphological analysis were developed to automate and enhance the detection, segmentation, and quantification of anatomical and cellular structures within medical images. This involved curating specific datasets, selecting and adapting suitable deep neural network architectures, and implementing rigorous training and evaluation procedures.

2.2.1 Datasets for Development and Evaluation of AI Models

The foundation of this research relies upon comprehensive datasets appropriate for the training and evaluation of AI models in medical image analysis. Two distinct datasets were employed to address the specific objectives of adapting classification networks for segmentation and detecting spinal metastatic lesions.

The research on AI-assisted detection and localisation of spinal metastatic lesions utilised two separate datasets. The first dataset, designated for vertebra segmentation, consisted of CT scans from 115 patients presenting with polytrauma but relatively undamaged spines. These full-body CT scans were acquired at the “Riga East University Hospital” (RAKUS) hospital (2-PĒK-4/97/2022, 21 February 2022). The second dataset, focused on metastasis detection, contained CT scans from 38 patients diagnosed with spinal metastases (Edelmers, 2024). Following manual segmentation by medical professionals using “3D Slicer” software (Kikinis et al., 2014), the data were converted from DICOM format to a NRRD format to enhance input/output efficiency during model training.

For the estimation of Cajal cells in the anal canal wall, a retrospective cohort study was conducted involving forty-two patients. Forty-two formalin-fixed and paraffin-embedded (FFPE) anorectal tissue samples were collected. From whole slide images (WSIs) depicting immunohistochemically detected ICCs, 40 patches with a resolution of 2048×2048 pixels were extracted. These images were initially obtained at maximum magnification. To align with the input requirements of the YOLOv11n-obb architecture (Khanam & Hussain, 2024), each 2048×2048 patch was divided into four smaller 1024×1024 sections, resulting in a total of 160 images. All these images were annotated, yielding 1871 labelled masks for training purposes.

The datasets were specifically prepared to serve as input for the training of the AI models developed in this research. The preparation involved several crucial steps to ensure data quality, consistency, and suitability for the chosen deep neural network architectures.

In the context of spinal metastasis detection, two U-Net-based networks were trained. The first network was trained using the CT scans from 115 polytrauma patients with relatively undamaged spines for the task of spine localisation and vertebra segmentation. The second network, dedicated to the instance segmentation and classification of metastatic lesions (lytic and sclerotic), was trained on the CT scans from the 38 patients diagnosed with spinal metastases. The dataset consists of 19456 images, each with a resolution of 512×512 pixels. The nnU-Net library's built-in augmentation capabilities were utilised, which include a wide array of transformations such as rotations, scaling, Gaussian noise, Gaussian blur, adjustments in brightness and contrast, low-resolution simulation, gamma correction, and mirroring (Isensee et al., 2021). These augmentations were applied adaptively based on dataset characteristics, enhancing the model's robustness and generalizability. The dataset for metastasis detection was meticulously curated with manually created segmentation masks.

For the Cajal cell estimation using the YOLOv11n-obb architecture, a dataset comprising 160 images (derived from 40 WSIs) with 1871 labelled masks was used for training (Edelmers, 2025). The training dataset was further enhanced through rotation and flipping augmentation techniques to improve the model's robustness against variations in immunostaining intensities. The final dataset split for this task included 376 augmented images for training and 32 non-augmented images for validation.

2.2.2 Deep Neural Network Architectures

Deep neural networks constitute the core methodological framework employed in this research for medical image analysis tasks, specifically focusing on segmentation, spinal lesion detection, and cell estimation. The selection and adaptation of these networks were guided by

the specific requirements of each task, balancing performance, computational efficiency, and interpretability.

For the AI-assisted detection and localisation of spinal metastatic lesions, a multi-network approach based on the U-Net architecture was adopted. U-Net is a convolutional network architecture specifically designed for biomedical image segmentation, characterised by its symmetric encoder-decoder structure and skip connections that facilitate the transfer of spatial information from the encoder to the decoder. Two U-Net-based networks were employed: one for spine localisation and vertebra segmentation, and another for the instance segmentation and classification of metastatic lesions. This dual-stage approach allows for hierarchical processing, first localising the region of interest (the spine) and then focusing on the detailed segmentation and classification of lesions within that region. The implementation utilised the nnU-Net framework, which provides a self-configuring method for biomedical image segmentation, automating many aspects of the pipeline.

The selection of the YOLOv11n-obb architecture for the estimation of ICC was driven by the specific morphological characteristics of these cells and the computational exigencies of high-throughput digital pathology. Unlike generic object detection tasks where subjects are typically upright and compact, ICCs present as spindle-shaped or stellate structures with high aspect ratios and arbitrary orientations within the tissue matrix. Standard object detection models, such as the traditional YOLO series or Faster R-CNN, utilise horizontal bounding boxes which are axis-aligned. When applied to diagonally oriented, elongated cells, horizontal bounding boxes inevitably encompass significant background noise (non-cellular stroma) to capture the full extent of the cell, leading to a low signal-to-noise ratio that degrades classification accuracy (Ma et al., 2018).

Furthermore, the density of cellular clusters in histological samples presents a critical failure mode for HBB-based detectors. When two elongated cells lie in close proximity but at different angles, their respective horizontal bounding boxes frequently exhibit high IoU overlap. This overlap inadvertently triggers non-maximum suppression algorithms – designed to eliminate duplicate detections – to suppress valid cell instances, resulting in systematic undercounting (Neubeck & Van Gool, 2006). The YOLOv11n-obb architecture addresses this by introducing an angular parameter to the regression head, allowing the bounding box to rotate and align tightly with the cell's principal axis. This oriented approach drastically minimises background inclusion and effectively resolves the “overlapping instance” problem, ensuring that closely packed cells are distinctively recognised.

In terms of computational scale, the analysis of WSI imposes severe constraints on model complexity. A standard histological slide digitised at 40x magnification yields

gigapixel-scale data that must be tiled into thousands of patches for inference. Utilising heavy architectures with massive parameter counts, such as those based on ResNet-101 or DenseNet backbones, would introduce prohibitive latency, rendering the system impractical for clinical or large-scale research workflows (Litjens et al., 2017). The "Nano" variant of YOLOv11 was selected specifically to mitigate this bottleneck. With a highly optimised backbone containing approximately 2.6 million parameters, it enables rapid inference speeds suitable for real-time screening of massive histological datasets without necessitating specialised high-performance computing clusters (Khanam & Hussain, 2024).

Despite its compact size, the YOLOv11 architecture integrates advanced feature aggregation mechanisms that are superior to previous lightweight iterations. It employs improved Cross-Stage Partial networks and Spatial Pyramid Pooling – fast modules to enhance multi-scale feature fusion (Khanam & Hussain, 2024). This is particularly relevant for ICC detection, as the apparent size of the cells can vary depending on the sectioning plane of the tissue. By preserving high-resolution features through the network layers, the YOLOv11n-obb model maintains high sensitivity for small, thin cellular processes that are often lost in the down-sampling layers of older architectures, thus achieving a state-of-the-art balance between geometric precision and computational efficiency.

The spinal metastasis detection research employed U-Net-based architectures, implemented within the nnU-Net framework. The U-Net architecture features a contracting path (encoder) that captures context and an expansive path (decoder) that enables precise localisation. Skip connections between corresponding levels of the encoder and decoder paths are fundamental to U-Net, allowing the decoder to utilise high-resolution features from the encoder, which is vital for accurate segmentation in medical images. The specific U-Net implementation within nnU-Net included several key design choices: instance normalisation instead of batch normalisation to handle smaller batch sizes common in 3D medical imaging, leaky ReLU activation functions to introduce non-linearity and prevent dying neurons, and deep supervision with topology-adapted parameters. These choices were made to optimise the architecture for the complex and heterogeneous nature of spinal metastases and to maintain spatial precision.

2.2.3 Training Procedures, Hyperparameter Tuning, and Evaluation Metrics

The training of the deep neural networks involved carefully defined procedures and systematic hyperparameter tuning to achieve optimal performance for each specific task.

The training of the U-Net-based networks for spinal metastasis detection was managed by the nnU-Net framework, which employs an automated parameterisation approach combining fixed, rule-based, and empirical parameters to adapt to diverse datasets.

Fixed parameters included the architecture template, based on a U-Net-like structure with two convolutional blocks per resolution level and instance normalisation. Training typically ran for 1000 epochs, with 250 minibatches per epoch. The learning rate followed a polynomial decay from an initial value of 0.01 and was reduced throughout training. Optimisation was performed using stochastic gradient descent with Nesterov momentum ($\mu = 0.99$). The loss function utilised was a combined Dice and cross-entropy loss, balancing accuracy for foreground-background segmentation and boundary precision.

Rule-based parameters were determined by nnU-Net's dataset fingerprinting, which analyses characteristics such as voxel spacing and median image shape. For anisotropic datasets, anisotropic resampling was employed using the tenth percentile of the lowest resolution axis. Patch size was initially based on the median image shape and adjusted iteratively to fit within graphical processing unit memory constraints. Network topology, including the number of downsampling layers, was adapted based on target spacing and voxel size to ensure an effective receptive field size. Normalisation techniques varied by modality, with z-score normalisation for most cases and specific percentile clipping and z-scoring for CT images.

Empirical parameterisation involved testing post-processing configurations, such as largest-component suppression, to assess their impact on cross-validation performance and remove false positives. Ensemble selection evaluated the performance of different configurations (2D, full-resolution 3D, cascaded 3D U-Net) across cross-validation folds to select the best model or ensemble for predictive robustness.

Four U-Net architecture subtypes were trained: a 2D model using single slices, a 3D low-resolution model with downsampled input, a 3D full-resolution model using original resolution, and a 3D cascade full-resolution model that processed downsampled images for overall structure before refining details with full-resolution data.

For the Cajal cell estimation using YOLOv11n-obb, training was performed on the augmented dataset. Model validation was conducted at the end of each training epoch on a prepared set. During this process, the model's predictions were compared to ground truth annotations, and non-maximum suppression was applied to eliminate redundant bounding boxes. Key metrics calculated during this phase included precision, recall, and mean average precision (mAP), specifically mAP_{50} (using an intersection over union threshold of 0.5) and mAP averaged over a range of thresholds ($mAP_{50\text{-}95}$). These metrics provided a comprehensive assessment of the model's performance on unseen data, guiding hyperparameter adjustments and serving as checkpoints for selecting the best-performing model.

Results

This section reports the study's findings, emphasising the workflows and outcomes for 3D reconstruction and fabrication of anatomical structures. It also details the educational deployment of these methods and the technical procedures used for model generation and validation.

Results of 3D Anatomical Model Reconstruction and Printing

The work involved the creation of 3D digital models from various sources and their subsequent physical realisation through 3D printing. Different techniques were employed for the initial digital model creation, and a systematic approach was followed for printing and post-processing. The physical realisation of the digital anatomical models was achieved through 3D printing. Specifically, fused deposition modelling (FDM) technology was utilised for the printing process. The printing was conducted using an "Ultimaker 5S" 3D extrusion-type printer. Key parameters were meticulously controlled to ensure print quality and fidelity. These parameters included a nozzle diameter of 0.4 millimetres, a layer height of 0.1 millimetres, a print speed of 70 millimetres per second, a printing temperature of 200°C, a build plate temperature of 60°C, and a fan speed of 100 %. The printing materials comprised a polylactic acid–polyhydroxyalkanoate blend ("Semi-Matte White") for the primary model structures and "Ultimaker PVA" for the soluble support structures. Fabrication of the complete foot-bone set required 44 hours 15 minutes of print time and used 122 grams of a polylactic acid–polyhydroxyalkanoate blend for the models and 45 grams of PVA for the support structures.

Following the printing phase, a crucial post-processing methodology was implemented to prepare the physical models for use. This involved the removal of the soluble support structures. The printed models were immersed in water at 24°C for 24 hours to dissolve the PVA support material. After the dissolution process, the models were removed from the water and allowed to air dry at room temperature (24°C) for another 24 hours. The final step in the post-processing was a direct comparison between the physically printed model and its corresponding virtual 3D model to assess the outcome of the printing and post-processing steps.

3D printing methodology protocol details the steps taken from preparing the digital model for printing to the completion of the printing process, including the specific printer settings used. The outcome, depicted as a 3D printed model, is illustrated in Figure 1.

Figure 1. **Final physical output after printing and post-processing**

Assessment of Anatomical Accuracy, Print Fidelity, and Model Validation

The creation of anatomically correct and print-optimised 3D models involved a multi-step process beginning with the segmentation of relevant anatomical structures from medical imaging data. For the human foot bones, a total of 28 individual bones were segmented from 763 CT images using the "3D Slicer" application. This segmentation followed a developed methodology to isolate each bone as a separate digital model.

The initial digital models underwent a validation process to ensure anatomical correctness by comparing them against established anatomical literature. Based on this process, adjustments were made to the models using the "Meshmixer" program according to a defined editing methodology. A total of 19 models required modification to align with normal human anatomy.

Following anatomical correction, the models were optimised with the identification and correction of errors as well as artifacts that may have arisen during the segmentation phase.

The “MeshLab” program was used for this purpose, addressing issues such as duplicating points, duplicating faces, faces with zero areas, non-manifold edges and points, vertices not referenced by a face, and microparticles not forming a surface. Subsequently, the on mesh of the models was simplified to improve the visual appearance for virtual library demonstrations, make the mesh suitable for further manipulations (e. g. deformation, cutting), reduce the file size, and ensure the model’s printability on an FDM-type printer. All 28 models were optimised to correct segmentation-related errors and artifacts.

Different techniques were explored for creating bone digital 3D models from natural specimens, including 3D scanning, photogrammetry, and μCT which resulted in models with varying characteristics in terms of polygon mesh complexity and texture data (Figure 2).

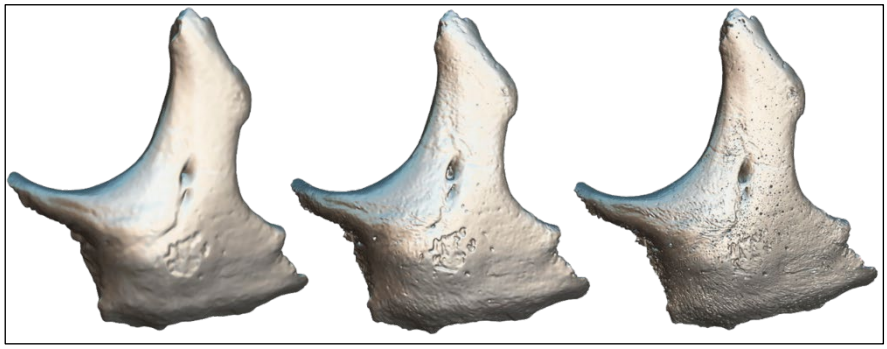

Figure 2. **3D model’s simplified and optimised polygon meshes created by using different techniques**

From left to right: 3D scanning, photogrammetry, μCT

The original number of faces and vertices before and after the application of a Simplification and Optimisation Protocol varied significantly depending on the initial reconstruction technique (Table 1).

Table 1

Number of faces and vertices of 3D models before and after application of Simplification and Optimisation Protocol

	Before Simplification		After Simplification	
Techniques	**Faces**	**Vertices**	**Faces**	**Vertices**
3D scanning	700002	350003	no simplification done	
Micro Computed Tomography	70195566	35073613	7019556	3485608
Photogrammetry	13716318	6882203	700842	350423

Similarly, the size of the obtained texture maps differed (Table 2).

Table 2

Size of obtained texture map of 3D models

Techniques	Size of Texture Map in Pixels (Width × Height)
3D scanning	766 × 998
Micro Computed Tomography	No visual data captured
Photogrammetry	16384 × 16384

Visualisation techniques, such as applying an X-ray shader, were used to reveal the internal structures of the digital models (Figure 3).

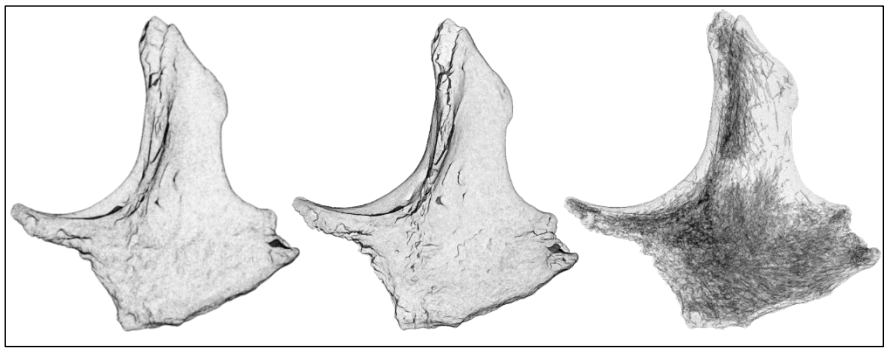

Figure 3. **3D models created by using different techniques with an X-ray shader applied**

From left to right: 3D scanning, photogrammetry, μCT

Further rendering and presentation on platforms like "Sketchfab" involved applying shaders, light sources, global illumination, ambient occlusion, and post-process filters. Models derived from 3D scanning and photogrammetry were provided with textures, while those from μCT did not have associated visual data (Figure 4).

Figure 4. **3D models with an applied shader, light sources, global illumination, ambient occlusion, and post-process filters, on "Sketchfab" platform created by using different techniques**

From left to right: 3D scanning, photogrammetry, μCT

The methodology for automatically segmenting the vertebral column was validated using a cohort of 250 patient CT scans. Under the supervision of medical expert, all 25 bones of the spine (from C1 to the coccyx) were segmented and the results were verified (Figure 5).

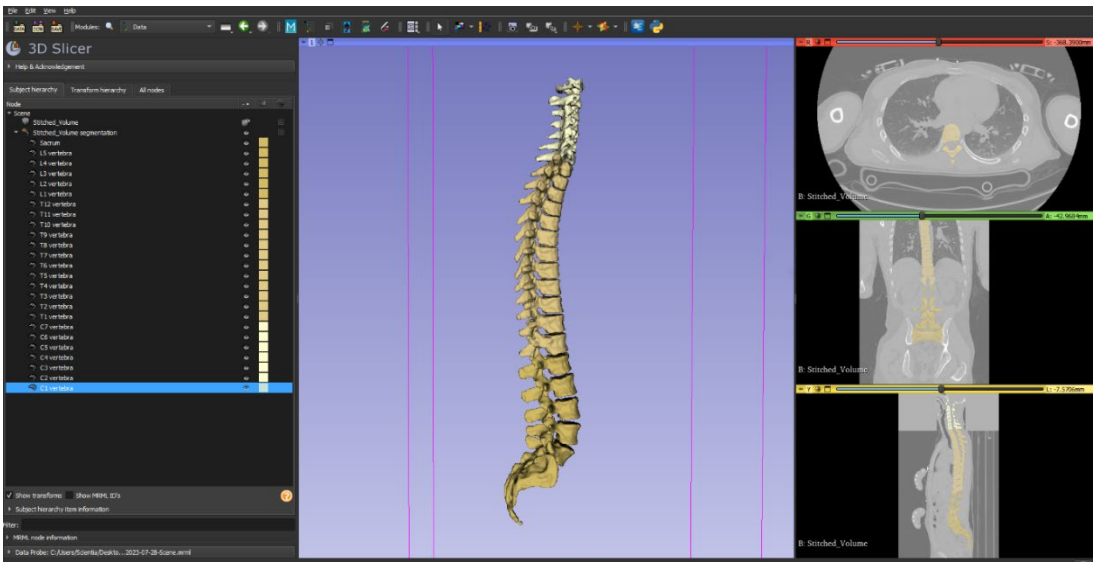

Figure 5. **Semantically segmented vertebral column serving as proof of concept of the presented methodology**

(In total, 25 bones from C1 till sacrum combined with coccyx)

The created masks were validated and corrected by comparing the segmented bones with reference anatomy from literature and software like "Complete Anatomy" (Motsinger, 2020).

Analysis of the segmentation results revealed instances of false registration anomalies (62 cases), where separate vertebrae were incorrectly identified as a single entity. Segmentation inaccuracies were also observed in all cases, where the delineated region either extended beyond or fell short of the intended anatomical boundaries, sometimes including adjacent tissues or omitting parts of the target structure (Figure 6).

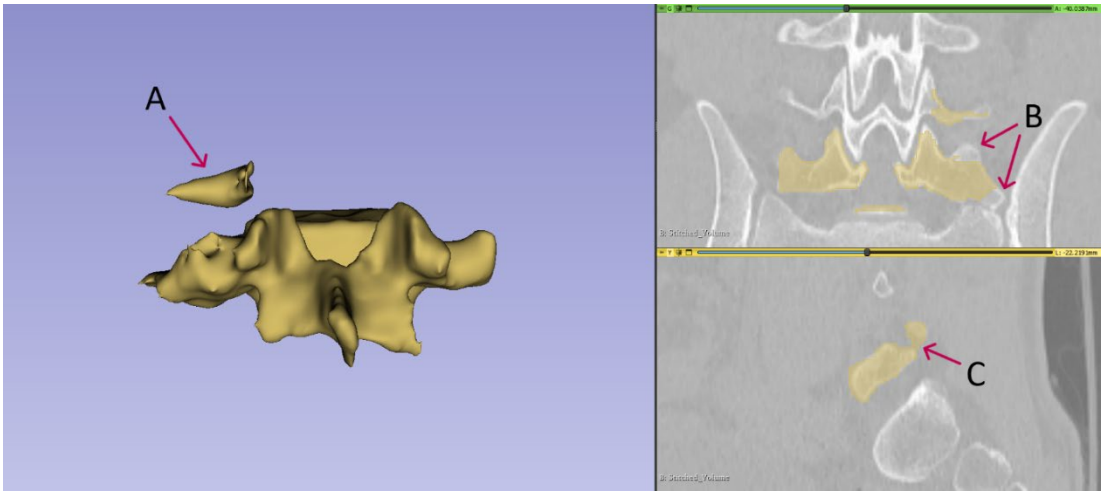

Figure 6. **Illustrative examples of artifacts in anatomical segmentation. Improper registration**

(A): A segment of the L4 vertebra is inaccurately identified as part of the L5 vertebra. Omission of critical regions (B): This artifact represents the absence of specific anatomical regions that should have been included in the segmentation. False registration (C): Soft tissues are incorrectly registered as constitutive elements of the L5 vertebra, compromising the integrity of the segmented structure.

These findings highlight the importance of rigorous validation and potential areas for improvement in automated segmentation techniques to ensure anatomical accuracy for downstream applications, including 3D printing and educational tools. The successful outcome of the automated segmentation work included the creation of a composite volume integrating cervical and thoraco-abdominal regions with corresponding segmentation masks, stored in the .NRRD file format, which offers advantages for machine learning workflows compared to the traditional DICOM format.

The integration of digital images and 3D-printed models in a Human Anatomy study course was assessed through 250 student feedback (Kazoka et al., 2021). They reported studying gross anatomy and 3D visualisations (18 % and 16 % respectively), followed by the use of 3D printed models (14 %). A small percentage (2 %) focused only on basic structures. When asked about learning from digital images and 3D printed models, students indicated a deeper understanding (19.2 %), virtual dissection (18 %), and learning about variations/abnormalities (14.8 %). Only a small number (2.8 %) mentioned the use of correct terminology (Table 3).

Table 3

Student responses to four questions in Human Anatomy study course

Question	Attitudes and Views	Students (n)	%
What did you study during the course?	Anatomical terminology	24	10
	Basic structures	5	2
	Functions of structures	25	10
	Location of structures and organs	21	8
	Topography	30	12
	Radiological anatomy	15	6
	3D visualisations of the structures	40	16
	Creation of 3D models	35	14
	Work in groups/teams	10	4
	Gross anatomy (dissection)	45	18
	More interesting learning and education	25	10
What did you study from the digital images and 3D models?	Relationships between structures	15	6
	Analysis of clinical cases	30	12
	Virtual dissection	45	18
	Different variations and/or abnormalities	37	15
	Deeper understanding of anatomy	48	19
	Simulations of clinical procedures	10	4
	Basics for clinical studies	20	8
	Overview of knowledge and skills	13	5
	Use of correct anatomical terminology	7	3
How did you solve problems or complicated situations during that time?	Including more visual aids	67	27
	Repeating material	52	21
	Help from classmates and educator	48	19
	Using more time; moving slower	32	13
	Using basic concepts	41	16
	Simplification of the information	10	4

Table 3 continued

Question	Attitudes and Views	Students (n)	%
How will the tools that you used help you in the future?	Importance of anatomy for clinical studies	65	26
	Training of some procedures	37	15
	Relationship between basic and clinical study subjects	70	28
	Basics for scientific work	13	5
	Improving clinical skills	18	7
	Success in tests/exams	47	19

Regarding problem-solving during the course, students primarily reported using more visual aids (26.8 %) and repeating material (20.8 %). Other strategies included using more time (12.8 %) and simplifying information (4 %). The tools were perceived to be helpful for future studies, particularly in understanding the relationship between basic and clinical subjects (28 %), recognising the importance of anatomy for clinical studies (26 %), and achieving success on tests and exams (18.8 %). A small group (5.2 %) related the tools to scientific work.

Overall, students expressed satisfaction with the 3D models used in the course. A significant portion (20.4 %) felt stimulated and motivated to learn more and perceived the course as more intensive due to the incorporation of digital images and 3D printed models. Students used 3D-printed models alongside digital images to study anatomy, reporting deeper understanding, opportunities for real and/or virtual dissection, and engagement with anatomical variations.

Table 4 shows the results of the students' satisfaction survey (Kazoka et al., 2021).

Table 4

Students' satisfaction using 3D models in Human Anatomy study course

Satisfaction Aspect	Students (n)	%
Reproduce taught/learned knowledge and skills	46	18
Increase motivation and intensity for learning	51	20
Develop knowledge and skills relevant to clinical needs	48	19
Improve thinking and problem-solving with respect to human-body structures	28	11
Prepare for the assessment of knowledge and skills	42	17
Provide a good background for future professional practice	35	14

Performance Evaluation of AI Models

This section outlines the experimental results derived from the application of various AI models to medical imaging datasets. The evaluation encompasses both quantitative metrics and qualitative observations, providing insights into the performance and capabilities of the developed systems in the context of image analysis.

The performance of the developed AI models was rigorously evaluated using appropriate metrics tailored to the specific tasks of segmentation in medical imaging and detection in histological slides. This subsection details the evaluation methodologies and presents the quantitative results obtained for each application area.

Performance of AI-Based Segmentation in Medical Imaging

In a study aimed at detecting and locating cancerous lesions in the spine, a U-Net model was used. The first step was to segment the entire spine, which provided the necessary context for the later analysis of the metastatic lesions. The U-Net model was trained using five-fold cross-validation and optimised with a composite loss function combining Dice loss and cross-entropy loss to enhance segmentation performance. Training was conducted on image patches extracted from the original scans, and the Dice metric was computed over these patches to assess segmentation accuracy during training. During the inference phase, a sliding window approach was utilised, which involved processing patches that might differ from those used in training, potentially leading to minor variations in the resulting Dice scores.

Validation patches were sampled using the same methodology as the training patches, ensuring consistency in the calculation of the Dice coefficient across all sampled validation data. To monitor the training progress and identify potential overfitting, a pseudo-Dice metric was employed, as depicted in Figures 7 and 8 of that study. This metric was updated iteratively throughout the training process and served as a preliminary indicator of model performance, distinct from the final Dice similarity coefficient which was computed at the conclusion of training over the entire image using a sliding window approach, providing a comprehensive evaluation of the model's accuracy on full images.

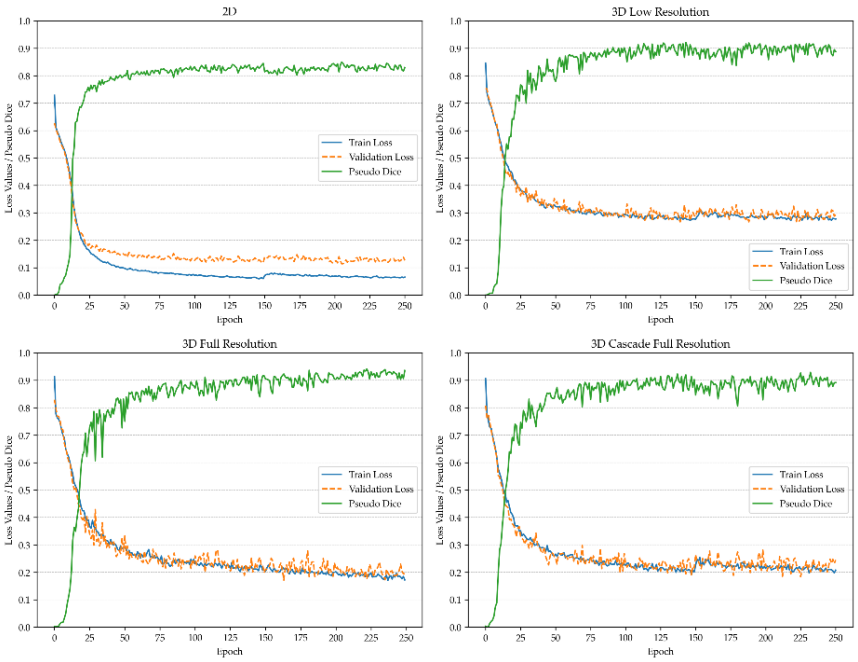

Figure 7. **Training process of the model for vertebra segmentation**

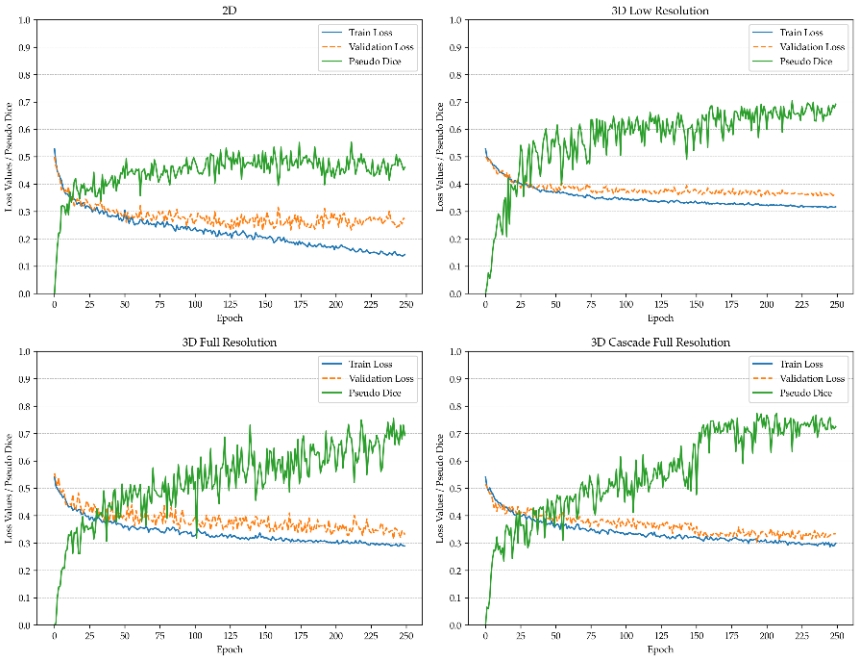

Figure 8. **Training process of the model for spinal metastasis segmentation**

Performance metrics were derived from the validation dataset using the model architecture that exhibited the highest performance during training. This structured evaluation framework facilitated a robust assessment of the U-Net model's effectiveness in both vertebra and metastasis segmentation, confirming its precision and reliability for localising and characterising metastatic regions within the vertebral column (Tables 5 and 6).

Table 5

Metrics for evaluation of "3D Cascade Full-Resolution" model for metastasis instance segmentation

Metastasis Type	Dice Similarity	F-Beta Score	Panoptic Quality
Lytic	0.71	0.68	0.45
Sclerotic	0.61	0.57	0.30

Table 6

Metrics for evaluation of "3D Full-Resolution" model for vertebrae instance segmentation

Vertebra	Dice Similarity Coefficient	F-Beta Score	Panoptic Quality
C1	0.94	0.94	0.75
C2	0.95	0.95	0.82
C3	0.93	0.93	0.75
C4	0.93	0.93	0.75
C5	0.93	0.94	0.75
C6	0.93	0.93	0.75
C7	0.94	0.93	0.79
T1	0.94	0.94	0.81
T2	0.95	0.95	0.83
T3	0.95	0.95	0.82
T4	0.95	0.95	0.83
T5	0.94	0.94	0.82
T6	0.88	0.87	0.69
T7	0.87	0.88	0.70
T8	0.91	0.92	0.75

Table 6 continued

Vertebra	Dice Similarity Coefficient	F-Beta Score	Panoptic Quality
T9	0.93	0.93	0.77
T10	0.94	0.94	0.81
T11	0.95	0.95	0.85
T12	0.95	0.94	0.84
L1	0.95	0.94	0.83
L2	0.94	0.94	0.83
L3	0.93	0.92	0.81
L4	0.94	0.89	0.84
L5	0.95	0.94	0.86
Sacrum	0.96	0.96	0.89

Figure 9 provides representative outputs from the trained 3D U-Net model for spinal metastasis segmentation. Separately, Figure 10 is dedicated to showing the masks produced by the vertebra segmentation model.

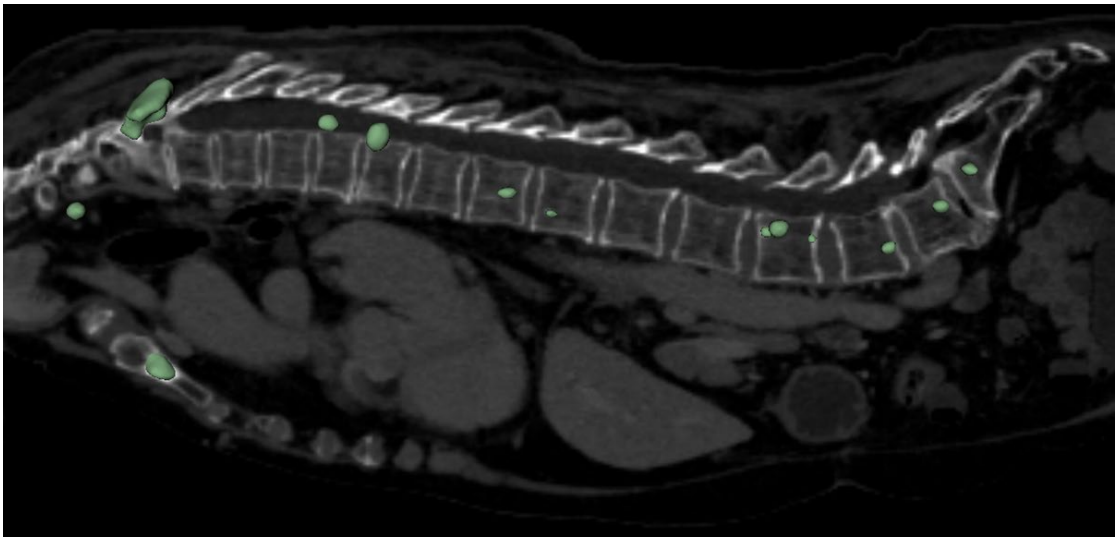

Figure 9. **Illustration of the model outputs: on the left, the predicted mask produced by the metastasis's segmentation model; on the right, the vertebra segmentation model's predicted mask with each class depicted in a distinct colour**

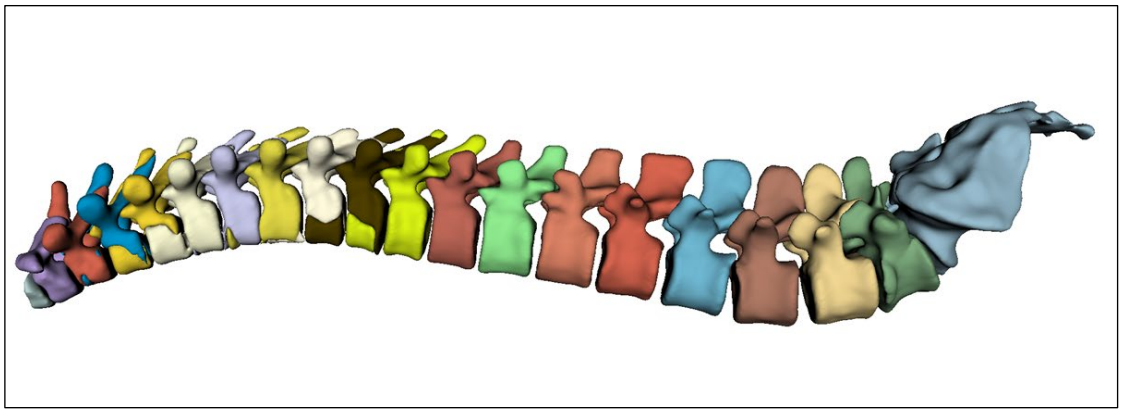

Figure 10. **Illustration of the vertebra segmentation model's predicted mask with each class depicted in a distinct colour**

Performance of AI-Based Detection in Histological Images

The primary focus of this section is on the performance of the AI models for cell detection. In the context of histological image analysis, deep neural networks were utilised for the estimation of Interstitial Cells of Cajal (ICCs) in the anal canal wall of patients with advanced haemorrhoidal disease.

Immunohistochemistry using CD117 and ANO1 was performed to identify and assess the distribution of ICCs and the membranous expression of ANO1. Immunostaining revealed ICCs as ramified cells dispersed among smooth muscle cells. The density of ICCs associated with the muscular component of the anal canal wall varied significantly among patients with haemorrhoidal disease (Figure 11). In cases with loosening of the muscular component and the presence of dilated vessels, a reduction in ICC number was observed, with cells often localised perivascularly. ANO1 immunoreactivity was primarily noted at the membrane of anal gland epithelial and smooth muscle cells, with varying expression levels across specimens.

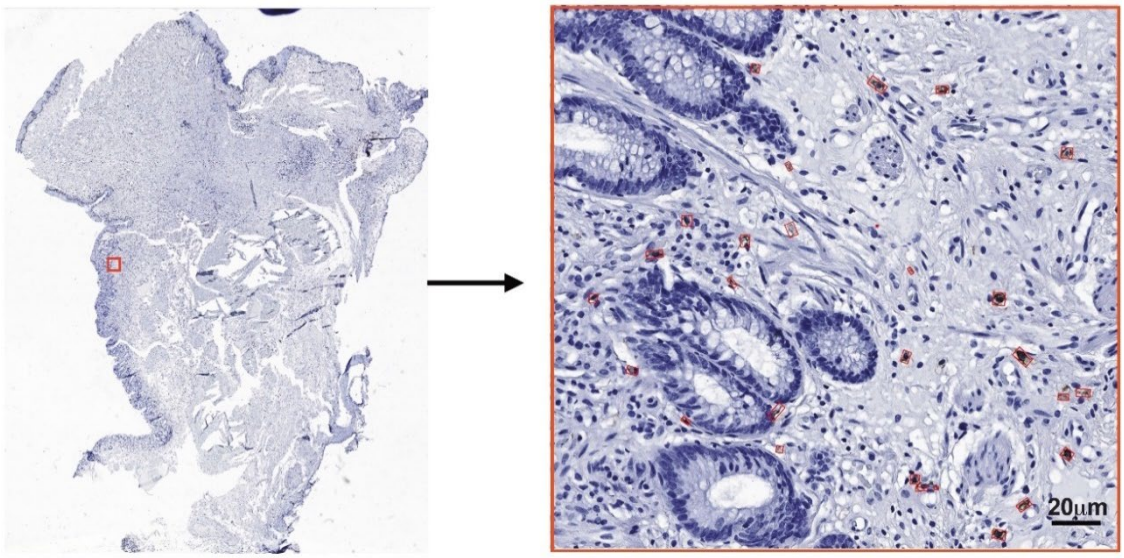

Figure 11. **Deep neural network–assisted immunohistochemical mapping of interstitial cells of Cajal in FFPE anorectal tissue**

Immunohistochemistry for ICCs was performed on formalin-fixed, paraffin-embedded anorectal specimens from haemorrhoidal disease patients. WSI were computationally segmented for regions of interest and analysed by a deep neural network to detect ICCs. Representative field showing loosening of the mucosal muscularis with irregularly oriented myocytes; brown-stained ICCs are indicated.

Several deep neural network models of different sizes were trained for ICC detection, as illustrated in Figure 12. Training was conducted over 51 epochs, and model performance was evaluated using mean Average Precision at 50 % (mAP_{50}), $mAP_{50\text{-}95}$, and F1 score. Training was halted at epoch 51, because earlier experiments that ran for up to 200 epochs showed no further performance gains beyond this point and indicated an increased risk of overfitting. All trained DNN models demonstrated comparable performance, achieving

a mAP$_{50}$ of 92 %, a recall of 86 %, and a precision of 88 %. These metrics were considered adequate for the task of cell counting. The selection of the final model for integration prioritised efficiency, balancing a low parameter count for improved performance on less powerful devices and faster inference speed. The YOLOv11n-obb model was ultimately chosen for implementation due to its optimisation for both accuracy and resource efficiency.

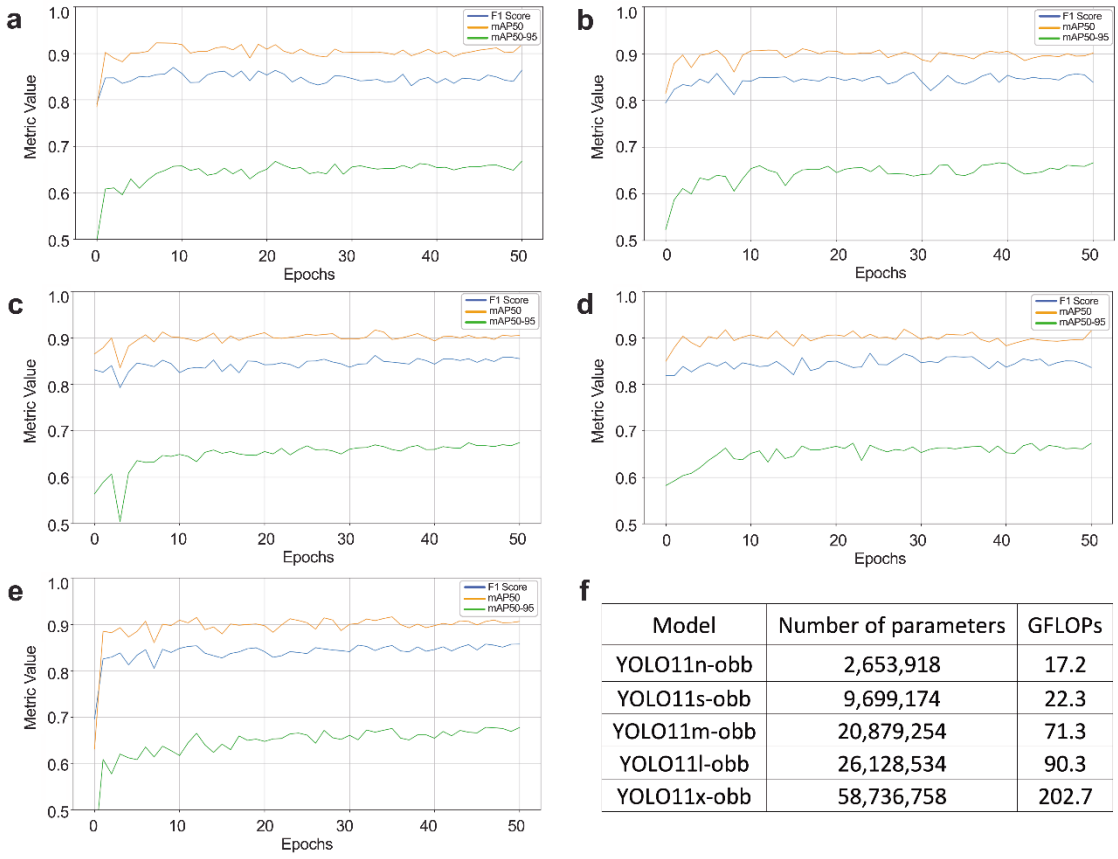

Model	Number of parameters	GFLOPs
YOLO11n-obb	2,653,918	17.2
YOLO11s-obb	9,699,174	22.3
YOLO11m-obb	20,879,254	71.3
YOLO11l-obb	26,128,534	90.3
YOLO11x-obb	58,736,758	202.7

Figure 12. **Performance of the trained models**

YOLO11n-obb (a), YOLO11s-obb (b), YOLO11m-obb (c), YOLO11l-obb (d), YOLO11x-obb (e), and parameters (f) of the trained models

A surface area quantification module was developed within the program to assess histological sections and delineate specific tissue regions. It utilises either the resolution metadata from TIFF files or a user-defined pixel size to perform pixel-to-area conversions in square millimetres. Morphological operations are applied to generate a tissue mask, enabling the computation of the tissue-occupied area relative to the entire histological slide. Following model training, the “MorpHista” (version 1.0) software was developed to efficiently process large whole slide images (WSIs) and quantify ICCs. This software integrated automated detection and post-processing steps, addressing the challenge of reassembling segmented regions after inference and consolidating detected features into a single image file with associated statistics, including ICC counts. The “MorpHista” software (Figure 13) has been

made publicly available to facilitate reproducible ICC analysis and promote research innovation in digital pathology.

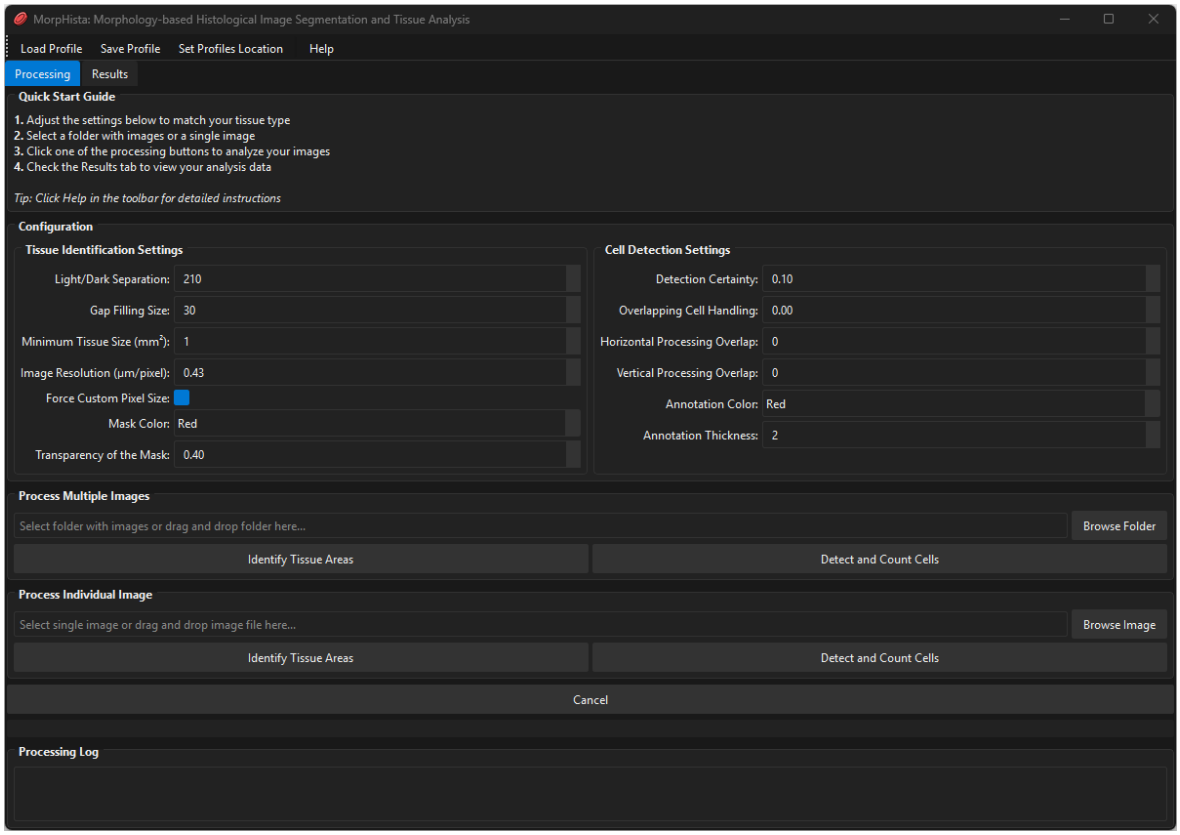

Figure 13. **User interface of "MorpHista" tool**

Building on these components, the complete MorpHista workflow operates as follows. Whole-slide immunohistochemistry images (CD117/ANO1) are imported together with resolution metadata. A tissue mask is generated by colour-based thresholding and morphological operations, enabling both exclusion of background regions and estimation of tissue area in mm². Tiles are then sampled from tissue regions and analysed by a YOLOv11n-obb detector that predicts oriented bounding boxes for interstitial cells of Cajal. Tile-level detections are mapped back to whole-slide coordinates, merged across tile borders, filtered, and intersected with the tissue mask. The final pipeline outputs per-slide ICC counts, density metrics, and visual quality-control overlays, together with machine-readable result tables for downstream statistical analysis (Figure 14).

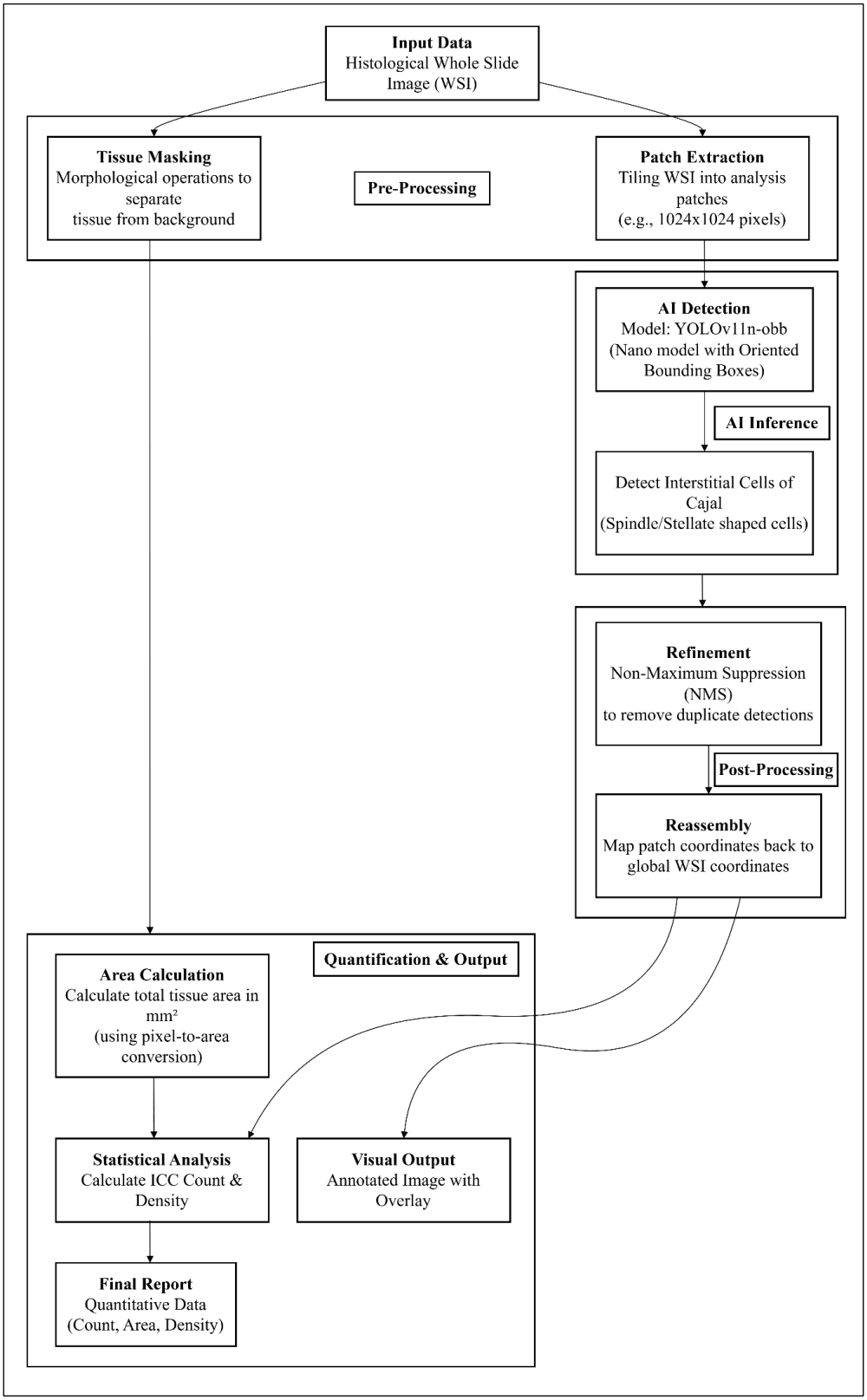

Figure 14. **Workflow of "MorpHista" software**

An attempt was made to incorporate a segmentation approach for quantifying ANO1 expression. However, the targeted Dice coefficient was not achieved. This outcome highlights the inherent complexity of pixel-level classification tasks, particularly given the variability in staining intensities and tissue morphology within the dataset. A linear regression analysis

revealed an inverse relationship between the number of ICCs and ANO1 expression in anorectal tissue from patients with advanced haemorrhoidal disease. Tissue samples exhibiting reduced ANO1 expression in myocyte membranes correlated with a higher number of ICCs, while samples with elevated ANO1 expression showed a lower number of ICCs.

To further enhance the understanding of the pathophysiology of haemorrhoidal disease, an unsupervised clustering method was applied to the research data. This analysis incorporated clinical data, immunohistochemistry data, and DNN-derived ICC quantification findings, using either five or six major factors. The clustering analysis based on six factors revealed that only 36 % of patients with Grade III haemorrhoidal disease exhibited a high density of ICCs, compared to 60 % of patients with Grade IV disease. Discomfort, pain, and bleeding were observed pre- and postoperatively in both stages. Postoperative pain was markedly reduced for both stages. A statistically significant reduction in bleeding was observed postoperatively ($p < 0.0001$). However, two patients with postoperative bleeding were diagnosed with Grade IV haemorrhoidal disease and had a high density of ICCs ($p = 0.0041$), suggesting a potential link between ICC density and disease severity.

Discussion

Interpretation of Findings: 3D Reconstruction of Morphological Structures

The integration of advanced digital technologies, particularly in the realm of 3D reconstruction of morphological structures, has profoundly impacted various fields, ranging from medical education to clinical practice and biomedical research. This section aims to provide a comprehensive analysis of the different techniques employed for 3D reconstruction, drawing upon existing literature and the specific methodologies explored in the Thesis. By examining the strengths, weaknesses, and practical considerations associated with each technique, a clearer understanding of their suitability for diverse applications can be established. Accurate segmentation and the subsequent 3D reconstruction of morphological structures form the unifying methodological axis of the Thesis, linking the 3D model-creation pipeline with the artificial intelligence workflows by providing the anatomically-grounded labels required for reconstruction, training, validation, and inference.

The creation of digital 3D models from physical specimens or imaging data can be achieved through several distinct approaches. These techniques vary in their underlying principles, required equipment, data acquisition methods, and the characteristics of the resulting 3D models.

One approach involves the use of dedicated 3D scanner. These devices capture the external geometry of an object directly, often employing technologies such as structured light, laser scanning, or photogrammetry-based systems. As demonstrated in this study (Edelmers et al., 2022), 3D scanning can capture visual data, contributing to a realistic appearance of the digital model. The choice of scanner significantly impacts the resolution and quality of the obtained texture map, with industrial-grade scanners offering higher fidelity compared to mid-level devices.

Another widely used technique is photogrammetry. This method involves taking multiple photographs of an object from different angles and using specialised software to reconstruct a 3D model based on the overlapping images. Photogrammetry is highlighted as a relatively simple and inexpensive method for creating realistic 3D digital models, capable of capturing both topological and visual data. Following specific guidelines, photogrammetry can produce metrically accurate models that are valuable for self-directed learning and understanding complex anatomical structures (Petriceks et al., 2018).

For obtaining highly detailed internal and external structural information, μCT is a powerful technique. μCT utilises X-rays to generate cross-sectional images of a specimen, which are then computationally reconstructed into a 3D volume. This method is particularly valuable for capturing the intricate inner structures of objects, such as the trabecular bone within

a bone specimen (Edelmers et al., 2022). The resulting dataset provides a high-density polygonal mesh and accurate topological data, making it suitable for applications requiring detailed structural analysis, such as implant production or biomechanical simulations.

Beyond direct scanning of physical specimens, 3D models of anatomical structures can also be generated from medical imaging data, such as CT and MRT scans (Bücking et al., 2017; Edelmers et al., 2021). These modalities provide volumetric datasets that can be processed to segment specific anatomical regions and create 3D representations. The availability of massive medical image datasets on digital platforms facilitates this approach. Differentiation of tissue density in imaging data allows for the application of segmentation techniques to isolate different anatomical structures (Van Eijnatten et al., 2018).

Increasingly, AI-driven approaches, particularly those employing machine learning and deep learning algorithms, are being integrated into the 3D reconstruction workflow, especially for the segmentation of medical images. These methods aim to automate or semi-automate the process of identifying and delineating anatomical structures within volumetric data, significantly reducing the time and effort required for manual segmentation. AI-based segmentation can be applied to a variety of anatomical structures, enhancing the efficiency of data annotation in medical imaging projects.

The application of these different techniques is often guided by the intended use of the 3D model. As categorised by this study, the main categories of implementation include visualisation, simulation, and physical replication (such as for implants or prostheses). For visualisation and educational purposes, capturing visual data and producing realistic appearances is often prioritised. For simulation and physical replication, the accuracy and density of the polygonal mesh, as well as the representation of internal structures, become more critical factors.

Methodological Challenges and Limitations in 3D Reconstruction

Despite the significant advancements in 3D reconstruction techniques, several challenges and limitations persist, impacting the accuracy, efficiency, and accessibility of this technology.

To situate the 3D reconstruction and 3D-printing protocols developed in this Thesis within the broader methodological landscape, they were compared with representative CT-based workflows described in recent reviews and implementation reports (Brumpt et al., 2023; Bücking et al., 2017; Dorweiler et al., 2021; Fedorov et al., 2012; Ferreira da-Silva et al., 2023; Flaxman et al., 2021; Leng et al., 2017). The main similarities and differences are summarised in Table 1.

Table 1

Comparison of CT-based 3D reconstruction and 3D-printing protocol developed in this Thesis with open-source workflows and commercial point-of-care 3D printing suites

Dimension	Protocols developed in this Thesis	Open-source CT→3D workflows (3D Slicer + mesh tools + slicer)	Commercial 3D modelling and printing platforms (Materialise Mimics inPrint, syngo.via)
Main purpose	Standardised CT-based bone model reconstruction and FDM printing for anatomy education and AI dataset generation	Generic patient-specific or educational models; often described as ad-hoc "how-to" case workflows	Clinical planning, device sizing, regulatory-grade models integrated in radiology workflows
Software stack	Fully open and low-cost: 3D Slicer for segmentation, MeshLab/Meshmixer for mesh editing, Cura for slicing, with explicit parameter documentation	Similar open tools (3D Slicer + mesh editor + slicer), but with more heterogeneous and less standardised parameter reporting	Proprietary integrated software (Mimics InPrint, syngo.via) with locked-in segmentation and print preparation pipelines
Segmentation & optimisation	Combines semi-automatic (and AI-assisted where applicable) segmentation with a fixed post-processing recipe tuned for FDM bone models and re-use in AI studies	Mostly thresholding, region growing and manual editing; mesh repair and smoothing described, but often without a reproducible protocol	Advanced but closed segmentation tools with presets and automated mesh optimisation for clinical use
Printing & cost	Targets affordable FDM printers, balancing anatomical fidelity and robustness; no licence costs, low per-model cost	Frequently FDM-based and low-cost, but print settings and quality assessment steps are inconsistently reported	Mix of higher-end in-house printers and external certified services; substantially higher software and implementation costs
Reproducibility & barriers	End-to-end workflow, parameters and software are fully described, facilitating replication in teaching hospitals and universities	Tools are open, but complete protocols are fragmented across reports; effective use depends on local "power users"	Highly standardised but non-transparent and expensive; adoption requires institutional budgets

A primary challenge lies in achieving and verifying the accuracy of the generated 3D models (Odeh et al., 2019; Wakjira et al., 2024). The precision of 3D printed anatomical models, for instance, is crucial for their use in education and clinical applications, but it can be influenced by the chosen printer technology. Verification of model accuracy often requires comparison with original specimens. Factors such as technical parameters, morphological variability of the specimens, and the expertise of the technical personnel can all affect the accuracy and quality of the final digital 3D models (Wendo et al., 2025).

While techniques like photogrammetry can be relatively inexpensive, high-quality 3D scanners and μCT machines represent substantial investments (Smith et al., 2018). The cost of materials and the printing process itself can also contribute to the overall expense of creating physical 3D models.

Creating a series of models through photogrammetry, for example, can be a time-consuming process (Morgan et al., 2019). Similarly, manual segmentation of anatomical structures from medical imaging data is a laborious task, although AI-driven approaches aim to mitigate this.

The process of 3D reconstruction, particularly from medical imaging, is prone to errors and artifacts. Segmentation, whether manual or semi-automated, can result in inaccuracies such as the omission of critical regions, incorrect merging of structures, and imprecise registration (Edelmers, Kazoka, et al., 2024). Pathological anomalies and anatomical variations further increase the complexity of accurate segmentation. Artifacts can also arise during the scanning process itself (Alzain et al., 2021).

The quality of the initial data is crucial as creating anatomically accurate 3D printed models requires high-resolution volumetric datasets. Low-quality input data will inevitably lead to less accurate and detailed 3D reconstructions (Edelmers et al., 2022).

Finally, the need for expert precision and validation remains crucial, even with the advent of AI-assisted methods. Manual validation of segmented structures by individuals with a high level of anatomical expertise is necessary to ensure morphological precision and methodological robustness. The lack of quantitative benchmarks for evaluating AI-segmented structures further emphasises the importance of expert oversight.

Despite these challenges, ongoing research and technological advancements continue to push the boundaries of 3D reconstruction, leading to more accurate, efficient, and accessible methods for studying and utilising morphological structures.

Interpretation of Findings: AI in Detection and Segmentation of Morphological Structures

The application of AI, particularly deep neural networks (DNNs), in the analysis of medical images for the detection and segmentation of morphological structures presents a transformative approach with significant potential to augment diagnostic capabilities. This research, building upon existing advancements in the field, demonstrates the utility of U-Net based architectures for tasks such as vertebrae segmentation and the identification of spinal metastatic lesions. The capacity of these models to process complex spatial and contextual relationships within medical imaging data is crucial for accurate identification of subtle or early-stage pathological changes. The selection of the nnU-Net architecture in

the study on spinal metastatic lesions was predicated on its demonstrated versatility and robust performance across both 2D and 3D medical image data, offering an advantage over architectures like VUNet, which is primarily designed for 3D data (Hirose et al., 2019), and the more lightweight SegNet (Badrinarayanan et al., 2017), which may not achieve comparable performance in tasks requiring high-resolution predictions and detailed boundary delineation. The automatic handling of preprocessing and architecture selection by nnU-Net further contributed to its performance edge in the context of medical segmentation where accuracy is crucial.

Beyond imaging modalities, DNNs are also proving valuable in the analysis of histopathological data. The study on the estimation of Cajal cells in the anal canal wall (Fišere et al., 2025) highlights the successful integration of DNN-based models, specifically a YOLOv11-based architecture, into the pathology workflow for the precise detection and quantification of interstitial cells of Cajal (ICCs) using immunohistochemical labelling. This represents a significant step towards utilising AI for detailed histopathological analysis, moving beyond the predominant focus on clinical and imaging modalities in previous AI studies (Patel et al., 2020). The high accuracy achieved by the YOLOv11n-obb model, with a mAP_{50} of approximately 92 %, aligns with the performance of recently developed AI systems in digital pathology, underscoring the potential of DNNs for a wide range of histopathological applications (McGenity et al., 2024). Architectures such as the U-Net and its variations, including the 3D U-Net (Çiçek et al., 2016), have been particularly successful due to their encoder-decoder structure with skip connections, which allows for the effective integration of both low-level and high-level features, crucial for precise boundary delineation.

In the domain of digital pathology, object detection models like those based on the YOLO architecture are valuable for identifying and quantifying specific cellular structures within WSIs (Debsarkar et al., 2025; Wendo et al., 2025). The application of a YOLOv11-based model for the estimation of Cajal cells demonstrates the effectiveness of this approach for cell detection tasks. The model's ability to accurately identify ICCs using the CD117 marker, achieving a mAP_{50} of 92 %, indicates its potential for automating the quantification of specific cell populations in histopathological specimens. This can significantly reduce the time and effort required for manual analysis, enabling more efficient and objective assessments.

The study on spinal metastatic lesions employed different configurations of the U-Net architecture, demonstrating that the 3D full-resolution architecture achieved the highest performance for both vertebra and metastasis segmentation (Edelmers, Ņikuļins, et al., 2024). This highlights the importance of utilising architectures capable of processing the volumetric nature of imaging data when analysing structures in 3D space. The performance metrics, including the Dice similarity coefficient (DSC), F-beta score, and panoptic quality, provide

a quantitative assessment of the models' accuracy in segmenting the target structures. The results for lytic metastases, with a DSC of 0.71 and an F-beta score of 0.68, were comparable to findings in related studies utilising U-Net based models for similar tasks (D. H. Kim et al., 2024; Liu et al., 2021).

The training process for these DNN models typically involves large datasets with expert annotations. The nnU-Net framework, for instance, incorporates automated hyperparameter selection and data augmentation to optimise model performance and generalizability. Techniques such as rotations, scaling, noise injection, and variations in brightness and contrast are applied to increase the diversity of the training data and mitigate overfitting. The use of composite loss functions, combining metrics like Dice loss and cross-entropy loss, is also common to balance the accuracy of foreground-background segmentation and the precision of boundary delineation.

Methodological Challenges and Limitations in AI-Driven Medical Image Analysis

Despite the notable successes, the application of AI, particularly DNNs, in the detection and segmentation of morphological structures in medicine faces several challenges and limitations. One significant challenge is the inherent variability and complexity of medical data. Factors such as differences in imaging protocols, equipment variations, patient anatomy, and the subtle or heterogeneous appearance of pathological structures can impact model performance.

To contextualise the contribution of the "MorpHista" pipeline within current digital pathology infrastructures, it is important to compare it directly with widely used commercial and open-source platforms. Building on recent surveys of software tools and AI-enabled workflows in digital pathology (Guerrero et al., 2022; Salo et al., 2024), Table 2 summarises key dimensions, including licensing model, algorithmic transparency and customisability, supported analytical tasks, scalability to whole-slide images, hardware requirements, regulatory status, and suitability for quantitative ICC analysis. This comparison highlights how MorpHista combines the openness and extensibility typical of research-grade tools with streamlined, task-specific workflows that lower financial and technical barriers to adoption in academic and educational settings.

Table 2

Comparison of "MorpHista" software with open-source research platforms and commercial AI digital pathology systems

Dimension	MorpHista	Open-source / research platforms (QuPath, Orbit, Cytomine, ImageJ, CellProfiler, Ilastik)	Commercial AI platforms (HALO, Visiopharm, Aiforia, Paige, PathAI, Ibex, Image-Pro)
Primary focus	Automated detection and counting of interstitial cells of Cajal (ICC) in IHC whole slide images, with domain-specific metrics (surface, density) for ENS-related research	General-purpose WSI and bioimage analysis (segmentation, IHC quantification, feature extraction, machine learning) across many tissues and biomarkers	Broad portfolio of clinical and translational applications (cancer detection and grading, biomarker scoring, toxicity, clinical trials, workflow optimisation)
Task breadth	Narrow but deep: one well-defined pipeline (ICC in CD117/ANO1 slides) with tuned pre- and post-processing (tissue masking, oriented boxes, cluster handling)	Very broad: users assemble task-specific workflows (e. g. QuPath scripts, Orbit ML pipelines, Cytomine projects, ImageJ/CellProfiler macros)	Very broad: vendor-supplied and user-trainable models for many organs, stains and study types; ICC-like tasks possible but usually not pre-packaged
AI model design	Single YOLOv11n-obb detector with oriented bounding boxes for elongated spindle cells, explicitly addressing background inclusion and NMS-driven undercounting in dense clusters	Typically provide frameworks for pixel / object classifiers and sometimes DL integration, but no built-in, ICC-specific oriented detector; geometry and post-processing must be implemented by the user	Deep learning widely used (CNNs for segmentation/classification, commercial ICC-analogous tasks), but models are proprietary and optimised for mainstream clinical endpoints (e. g. prostate, breast, colorectal cancer)
Licensing and openness	Open-source research tool; full access to code, model architecture, training dataset description and evaluation metrics, enabling reproducibility and method auditing	Mostly open-source; algorithms and scripts are inspectable and modifiable, with active developer communities (especially QuPath and ImageJ)	Proprietary, closed source; internal model details and training data are generally not disclosed, although performance and some validation studies are published
User expertise required	Minimal configuration for ICC counting (input WSI + basic parameters), but assumes understanding of IHC staining and ENS morphology; retraining requires research-level expertise	Often require considerable technical knowledge (scripting, machine learning concepts, WSI infrastructure); powerful but non-trivial to configure for robust, end-to-end ICC pipelines	Front-end users' interfaces are user-friendly for pathologists, but system deployment, integration and model governance typically demand institutional IT and vendor support

Table 2 continued

Dimension	MorpHista	Open-source / research platforms (QuPath, Orbit, Cytomine, ImageJ, CellProfiler, Ilastik)	Commercial AI platforms (HALO, Visiopharm, Aiforia, Paige, PathAI, Ibex, Image-Pro)
Deployment model	Local workstation / lab server with GPU; suited for small–medium academic cohorts	Desktop or on-prem server (QuPath, Orbit, ImageJ, CellProfiler; Cytomine often server-based); more ad-hoc, research-oriented deployments	Enterprise-grade on-prem or cloud platforms, tightly integrated with scanners, hospital networks; intended for regulated clinical and pharma environments
Cost and barriers to adoption	No license cost; main barriers are hardware (GPU), WSI file handling and moderate technical setup	No or low license cost, but configuration and maintenance are labour-intensive; effective use often requires a dedicated "power user" or image analyst	Substantial licensing, maintenance and validation costs; suitable mainly for large academic centres, reference labs and industry
Fit for ICC quantification	Direct, out-of-the-box solution tuned to ICC morphology, stain characteristics and density metrics, as described in this Thesis	Technically capable but ICC pipelines must be custom-built (tiling, annotation, model training, post-processing), which is time-consuming and requires expertise	Potentially powerful but economically and organisationally disproportionate for niche research questions; ICC-specific tools are not standard offerings

In the context of spinal metastasis segmentation, the study highlighted the comparatively lower performance for sclerotic metastases compared to lytic lesions. This is attributed to the subtle imaging characteristics of sclerotic lesions, which demand higher sensitivity to subtle density changes. This underscores a limitation in current AI models to consistently detect and segment all types of lesions with equal accuracy.

Data availability and annotation remain critical bottlenecks. Training high-performing DNN models typically requires large, diverse datasets with detailed and accurate annotations. The study on spinal metastases noted that the dataset used was drawn from a single medical centre, potentially limiting the model's generalizability across different populations and imaging environments. Furthermore, the manual creation of segmentation masks by medical professionals is a time-consuming process susceptible to inter-observer variability, which can introduce inconsistencies in the training data and affect model performance and evaluation.

Addressing this may require standardising segmentation protocols or employing semi-automated annotation tools.

Technical considerations, such as variability in CT scanning parameters, particularly resolution, can also significantly affect model accuracy. Discrepancies between the technical specifications of the training data and the data used for inference can reduce model effectiveness. The relatively small dataset for metastasis detection, especially for sclerotic

lesions, further impacted performance and highlighted the need for more extensive and diverse datasets to achieve higher reliability and generalizability.

Finally, the lack of validation in real-world clinical environments is a crucial limitation. Factors such as diverse patient anatomies, varying imaging conditions encountered in routine clinical practice, and workflow constraints can influence model performance. Clinical trials are essential to determine the actual impact of these AI models on diagnostic accuracy and patient outcomes in real-world settings.

Conclusions

The established aim and objectives of this doctoral research were successfully met, leading to the following conclusions:

1 A reproducible protocol was successfully developed to reconstruct 3D bone models from various medical imaging sources (including CT, μCT, photogrammetry, and 3D scanning) that emphasises systematic workflows using accessible software for data acquisition, segmentation, optimisation, and preparation for 3D printing, suitable for educational and research applications.

2 The reconstructed bone models were validated through fabrication with fused deposition modelling (3D printing) and subsequent physical and educational evaluation, which confirmed the fidelity of the digital-to-physical workflow and demonstrated the utility of the printed models in enhancing anatomical understanding in educational settings.

3 Annotated datasets were assembled for segmented morphological structures at two scales, including vertebrae with lytic and sclerotic lesions from computed tomography as well as intestinal Cajal cells from immunohistochemically stained whole-slide images, thus establishing efficient workflows to generate data suitable for AI model training and analysis.

4 Trained deep neural network models demonstrated high efficacy for the automated detection and segmentation of various morphological structures, including precise segmentation of spinal metastases from CT scans and accurate quantification of interstitial Cajal cells in histological images, confirming the hypothesis that these techniques can achieve reliable, accurate and reproducible results.

5 The developed AI methodologies were successfully integrated into functional software, exemplified by the “MorpHista” tool for automated quantification of interstitial cells of Cajal in whole-slide histological images, demonstrating practical applicability and potential to translate research findings into tools that improve efficiency in medical image analysis.

Publications and reports on topics of Doctoral Thesis

Publications:

1. **Edelmers, E.** (Corresponding Author), Kažoka, D., & Pilmane, M. Creation of Anatomically Correct and Optimized for 3D Printing Human Bones Models. Applied System Innovation, 2021, 4, 67. https://doi.org/10.3390/asi4030067, Q1.

   Author's personal technical and methodological contribution: conception and end to end implementation of a validated 3D reconstruction to printing workflow including data acquisition via photogrammetry, μCT and 3D scanning, DICOM processing, 3D Slicer segmentation, MeshLab and Meshmixer mesh optimization, Cura slicing with print validation, and technical optimization such as parameter sweeps, topology repair and decimation.

2. Kažoka, D. (Corresponding Author), Pilmane, M., & **Edelmers, E**. Facilitating Student Understanding through Incorporating Digital Images and 3D-Printed Models in a Human Anatomy Course. Education Sciences, 2021, 11, 380. https://doi.org/10.3390/educsci11080380, Q1.

   Author's personal technical and methodological contribution: design, fabrication, and validation of the 3D models used in the teaching intervention.

3. **Edelmers, E.** (Corresponding Author), Kazoka, D., Bolocko, K., Pilmane, M. Different Techniques of Creating Bone Digital 3D Models from Natural Specimens. Applied System Innovation, 2022, 5, 85. https://doi.org/10.3390/asi5040085, Q1.

   Author's personal technical and methodological contribution: development of comparative pipelines for 3D scanning, photogrammetry and μCT, implementation of complete software workflows including image and volume import, segmentation, meshing, optimization and texture handling, and comprehensive dataset preparation.

4. **Edelmers, E.** (Corresponding Author), Kazoka, D., Bolocko, K., Sudars, K., Pilmane, M. Automatization of CT Annotation: Combining AI Efficiency with Expert Precision. Diagnostics, 2024, 14, 185. https://doi.org/10.3390/diagnostics14020185, Q1.

   Author's personal technical and methodological contribution: design of the AI assisted CT annotation pipeline including dataset assembly and curation, preprocessing and series stitching, U Net configuration, semi-automatic mask generation with expert refinement, and quality control with anatomical validation.

5. **Edelmers, E.** (Corresponding Author), Nikulins, A., Sprudža, K. L., Stapulone, P., Saimons Pūce, N., Skrebele, E., Siņicina, E. E., Cīrule, V., Kazuša, A., & Boločko, K. AI-Assisted Detection and Localization of Spinal Metastatic Lesions. Diagnostics, 2024, 14, 2458. https://doi.org/10.3390/diagnostics14212458, Q1.

   Author's personal technical and methodological contribution: study design and data annotation, curation of vertebrae and metastasis datasets, training and evaluation of U-Net models for vertebral segmentation and metastasis instance segmentation, and specification of evaluation metrics.

6. Fišere, I., **Edelmers, E.** (Corresponding Author), Svirskis, Š., & Groma, V. (Corresponding Author). (2025). Utilisation of Deep Neural Networks for Estimation of Cajal Cells in the Anal Canal Wall of Patients with Advanced Haemorrhoidal Disease Treated by LigaSure Surgery. Cells, 14(7), 550. https://doi.org/10.3390/cells14070550, Q1.

   Author's personal technical and methodological contribution: development of the computational pipeline and software for ICC detection and quantification, including WSI patch extraction, data annotation, object detection with YOLOv11n-obb model, training and validation protocols with metric computation, and the creation of the "MorpHista" tool for whole slide post processing.

Reports and theses at international congresses and conferences:

1. **Edelmers, E.** (2023). Digitalization of Zygomatic Bone as a Part of the Orbit Wall. In P. Fedirko, M. Pilmane, O. Maksymuk, T. F. Babenko, & N. A. Garkava (Eds.), Practical Ophthalmology. Medical and Environmental Problems of our Days: Collection of Works International Scientific and Practical Interdisciplinary Conference (pp. 36-38). State Institution «National Research Center for Radiation medicine of the National Academy of Medical Sciences of Ukraine". https://science.rsu.lv/ws/portalfiles/portal/63211535/Digitalization_of_zygomatic_bone.pdf
2. Sudars, K., Namatevs, I., Nikulins, A., **Edelmers, E.**, Neimane, L., Slaidiņa, A., & Radziņš, O. (2023). Artificial Intelligence-Powered System for Identifying Bone Deterioration in Radiological Imaging. Paper presented at International Workshop on Embedded Digital Intelligence (iWoEDI"2023), Riga, Latvia. https://events.edi.lv/iwoedi2023/wp-content/uploads/sites/2/2023/06/IWoEDI-2023-Artificial-Inteligence-Powered-System-for-Identifying-Bone-Deterioration-in-Radiological-Imaging.pdf
3. **Edelmers, E.** (2024). 3D Gaussian Splatting for Real-Time Radiance Field Rendering in Anatomy Education and 3D Model Creation. 26. Abstract from 11th Baltic Morphology Meeting, Rīga, Latvia. https://doi.org/10.25143/rsu-balt-morf-11-meeting
4. **Edelmers, E.**, & Fišere, I. (2024). Deep Learning-Based Software for Automated Cell Detection and Counting in Whole-Slide Histological Image Analysis. 67. Abstract from 11th Baltic Morphology Meeting, Rīga, Latvia. https://doi.org/10.25143/rsu-balt-morf-11-meeting
5. **Edelmers, E.**, & Kažoka, D. (2021). Creation of digital bones collection with anatomically correct and optimized 3D models. 540. Abstract from RSU Research week 2021: Knowledge for Use in Practice, Rīga, Latvia.
6. **Edelmers, E.**, Kažoka, D., & Šmite, K. (2025). Automatic Segmentation of Morphological Structures, Metastasis Detection, and 3D Model Reconstruction from Medical Imaging Utilising Artificial Intelligence Based on Deep Neural Network Methodologies. 104. Abstract from Rīga Stradiņš University International Research Conference on Medical and Health Care Sciences "Knowledge for Use in Practice", Riga, Latvia. https://doi.org/10.25143/rw2025.kup.abstracts-book

References

1. Abdel-Jaber, H., Devassy, D., Al Salam, A., Hidaytallah, L., & EL-Amir, M. (2022). A Review of Deep Learning Algorithms and Their Applications in Healthcare. *Algorithms*, *15*(2), 71. https://doi.org/10.3390/a15020071
2. AbouHashem, Y., Dayal, M., Savanah, S., & Štrkalj, G. (2015). The application of 3D printing in anatomy education. *Medical Education Online*, *20*(1), 29847. https://doi.org/10.3402/meo.v20.29847
3. Ahmad, Z., Rahim, S., Zubair, M., & Abdul-Ghafar, J. (2021). Artificial intelligence (AI) in medicine, current applications and future role with special emphasis on its potential and promise in pathology: Present and future impact, obstacles including costs and acceptance among pathologists, practical and philosophical considerations. A comprehensive review. *Diagnostic Pathology*, *16*(1), 24. https://doi.org/10.1186/s13000-021-01085-4
4. Ahuja, A. S. (2019). The impact of artificial intelligence in medicine on the future role of the physician. *PeerJ*, *7*, e7702. https://doi.org/10.7717/peerj.7702
5. Aimar, A., Palermo, A., & Innocenti, B. (2019). The Role of 3D Printing in Medical Applications: A State of the Art. *Journal of Healthcare Engineering*, *2019*, 5340616. https://doi.org/10.1155/2019/5340616
6. Al-Naser, Y. A. (2023). The impact of artificial intelligence on radiography as a profession: A narrative review. *Journal of Medical Imaging and Radiation Sciences*, *54*(1), 162–166. https://doi.org/10.1016/j.jmir.2022.10.196
7. Alowais, S. A., Alghamdi, S. S., Alsuhebany, N., Alqahtani, T., Alshaya, A. I., Almohareb, S. N., Aldairem, A., Alrashed, M., Bin Saleh, K., Badreldin, H. A., Al Yami, M. S., Al Harbi, S., & Albekairy, A. M. (2023). Revolutionizing healthcare: The role of artificial intelligence in clinical practice. *BMC Medical Education*, *23*(1), 689. https://doi.org/10.1186/s12909-023-04698-z
8. Alzain, A. F., Elhussein, N., Fadulelmulla, I. A., Ahmed, A. M., Elbashir, M. E., & Elamin, B. A. (2021). Common computed tomography artifact: Source and avoidance. *Egyptian Journal of Radiology and Nuclear Medicine*, *52*(1), 151. https://doi.org/10.1186/s43055-021-00530-0
9. Antreas, K., & Piromalis, D. (2021). Employing a Low-Cost Desktop 3D Printer: Challenges, and How to Overcome Them by Tuning Key Process Parameters. *International Journal of Mechanics and Applications*, *10*(1), 11–19. https://doi.org/10.5923/j.mechanics.20211001.02
10. Archana, R., & Jeevaraj, P. S. E. (2024). Deep learning models for digital image processing: A review. *Artificial Intelligence Review*, *57*(1), 11. https://doi.org/10.1007/s10462-023-10631-z
11. Arráez-Aybar, L. A. (2025). Evolving Anatomy Education: Bridging Dissection, Traditional Methods, and Technological Innovation for Clinical Excellence. *Anatomia*, *4*(2), 9. https://doi.org/10.3390/anatomia4020009
12. Asghar, A., Naaz, S., Patra, A., Ravi, K. S., & Khanal, L. (2022). Effectiveness of 3D-printed models prepared from radiological data for anatomy education: A meta-analysis and trial sequential analysis of 22 randomized, controlled, crossover trials. *Journal of Education and Health Promotion*, *11*(1), 353. https://doi.org/10.4103/jehp.jehp_199_22
13. Backhouse, S., Taylor, D., & Armitage, J. A. (2019). Is This Mine to Keep? Three-dimensional Printing Enables Active, Personalized Learning in Anatomy. *Anatomical Sciences Education*, *12*(5), 518–528. https://doi.org/10.1002/ase.1840
14. Badrinarayanan, V., Kendall, A., & Cipolla, R. (2017). SegNet: A Deep Convolutional Encoder-Decoder Architecture for Image Segmentation. *IEEE Transactions on Pattern Analysis and Machine Intelligence*, *39*(12), 2481–2495. https://doi.org/10.1109/TPAMI.2016.2644615
15. Bajwa, J., Munir, U., Nori, A., & Williams, B. (2021). Artificial intelligence in healthcare: Transforming the practice of medicine. *Future Healthcare Journal*, *8*(2), e188–e194. https://doi.org/10.7861/fhj.2021-0095

16. Balestrini, C., & Campo-Celaya, T. (2016). With the advent of domestic 3-dimensional (3D) printers and their associated reduced cost, is it now time for every medical school to have their own 3D printer? *Medical Teacher*, *38*(3), 312–313. https://doi.org/10.3109/0142159X.2015.1060305

17. Ballard, D. H., Trace, A. P., Ali, S., Hodgdon, T., Zygmont, M. E., DeBenedectis, C. M., Smith, S. E., Richardson, M. L., Patel, M. J., Decker, S. J., & Lenchik, L. (2018). Clinical Applications of 3D Printing. *Academic Radiology*, *25*(1), 52–65. https://doi.org/10.1016/j.acra.2017.08.004

18. Bankhead, P., Loughrey, M. B., Fernández, J. A., Dombrowski, Y., McArt, D. G., Dunne, P. D., McQuaid, S., Gray, R. T., Murray, L. J., Coleman, H. G., James, J. A., Salto-Tellez, M., & Hamilton, P. W. (2017). QuPath: Open source software for digital pathology image analysis. *Scientific Reports*, *7*(1), Article 1. https://doi.org/10.1038/s41598-017-17204-5

19. Baratz, G., Wilson-Delfosse, A. L., Singelyn, B. M., Allan, K. C., Rieth, G. E., Ratnaparkhi, R., Jenks, B. P., Carlton, C., Freeman, B. K., & Wish-Baratz, S. (2019). Evaluating the Anatomage Table Compared to Cadaveric Dissection as a Learning Modality for Gross Anatomy. *Medical Science Educator*, *29*(2), 499–506. https://doi.org/10.1007/s40670-019-00719-z

20. Bell, S., Douce, C., Caeiro, S., Teixeira, A., Martín-Aranda, R., & Otto, D. (2017). Sustainability and distance learning: A diverse European experience? *Open Learning: The Journal of Open, Distance and e-Learning*, *32*(2), 95–102. https://doi.org/10.1080/02680513.2017.1319638

21. Bezek, L. B., & Williams, C. B. (2023). Process-structure-property effects of ultraviolet curing in multi-material jetting additive manufacturing. *Additive Manufacturing*, *73*, 103640. https://doi.org/10.1016/j.addma.2023.103640

22. Bharati, A. S., N, S. K., & Rani, V. S. (2018). A Study on Student Perception of Virtual Dissection Table (Anatomage) at GSL Medical College, Rajahmundry. *Academia Anatomica International*, *4*(2). https://doi.org/10.21276/aanat.2018.4.2.8

23. Bian, Y., Li, J., Ye, C., Jia, X., & Yang, Q. (2025). Artificial intelligence in medical imaging: From task-specific models to large-scale foundation models. *Chinese Medical Journal*, *138*(6), 651–663. https://doi.org/10.1097/CM9.0000000000003489

24. Bidgood, W. D., Horii, S. C., Prior, F. W., & Van Syckle, D. E. (1997). Understanding and Using DICOM, the Data Interchange Standard for Biomedical Imaging. *Journal of the American Medical Informatics Association*, *4*(3), 199–212. https://doi.org/10.1136/jamia.1997.0040199

25. Binder, J. S., Scholz, M., Ellmann, S., Uder, M., Grützmann, R., Weber, G. F., & Krautz, C. (2021). Cinematic Rendering in Anatomy: A Crossover Study Comparing a Novel 3D Reconstruction Technique to Conventional Computed Tomography. *Anatomical Sciences Education*, *14*(1), 22–31. https://doi.org/10.1002/ase.1989

26. Boykov, Y. Y., & Jolly, M.-P. (2001). Interactive graph cuts for optimal boundary & region segmentation of objects in N-D images. *Proceedings Eighth IEEE International Conference on Computer Vision. ICCV 2001*, *1*, 105–112. https://doi.org/10.1109/ICCV.2001.937505

27. Brumpt, E., Bertin, E., Tatu, L., & Louvrier, A. (2023). 3D printing as a pedagogical tool for teaching normal human anatomy: A systematic review. *BMC Medical Education*, *23*(1), Article 1. https://doi.org/10.1186/s12909-023-04744-w

28. Bücking, T. M., Hill, E. R., Robertson, J. L., Maneas, E., Plumb, A. A., & Nikitichev, D. I. (2017). From medical imaging data to 3D printed anatomical models. *PLOS ONE*, *12*(5), e0178540. https://doi.org/10.1371/journal.pone.0178540

29. Chen, L., Li, S., Bai, Q., Yang, J., Jiang, S., & Miao, Y. (2021). Review of Image Classification Algorithms Based on Convolutional Neural Networks. *Remote Sensing*, *13*(22), 4712. https://doi.org/10.3390/rs13224712

30. Chen, R. J., Ding, T., Lu, M. Y., Williamson, D. F. K., Jaume, G., Song, A. H., Chen, B., Zhang, A., Shao, D., Shaban, M., Williams, M., Oldenburg, L., Weishaupt, L. L., Wang, J. J., Vaidya, A., Le, L. P., Gerber, G., Sahai, S., Williams, W., & Mahmood, F. (2024). Towards a general-purpose foundation model for computational pathology. *Nature Medicine*, *30*(3), 850–862. https://doi.org/10.1038/s41591-024-02857-3

31. Chin, S. Y., Dikshit, V., Meera Priyadarshini, B., & Zhang, Y. (2020). Powder-Based 3D Printing for the Fabrication of Device with Micro and Mesoscale Features. *Micromachines*, *11*(7), 658. https://doi.org/10.3390/mi11070658

32. Çiçek, Ö., Abdulkadir, A., Lienkamp, S. S., Brox, T., & Ronneberger, O. (2016). 3D U-Net: Learning Dense Volumetric Segmentation from Sparse Annotation. In S. Ourselin, L. Joskowicz, M. R. Sabuncu, G. Unal, & W. Wells (Eds), *Medical Image Computing and Computer-Assisted Intervention – MICCAI 2016* (Vol. 9901, pp. 424–432). Springer International Publishing. https://doi.org/10.1007/978-3-319-46723-8_49

33. Cignoni, P., Callieri, M., Corsini, M., Dellepiane, M., Ganovelli, F., & Ranzuglia, G. (2008). MeshLab: An Open-Source Mesh Processing Tool. In *Eurographics Italian Chapter Conference* (p. 8 pages). The Eurographics Association. https://doi.org/10.2312/LOCALCHAPTEREVENTS/ITALCHAP/ITALIANCHAPCONF2008/129-136

34. Debsarkar, S. S., Aronow, B., & Prasath, V. B. S. (2025). Advancements in automated nuclei segmentation for histopathology using you only look once-driven approaches: A systematic review. *Computers in Biology and Medicine*, *190*, 110072. https://doi.org/10.1016/j.compbiomed.2025.110072

35. Dee, E. C., Alty, I. G., Agolia, J. P., Torres-Quinones, C., Van Houten, T., Stearns, D. A., Lillehei, C. W., & Shamberger, R. C. (2021). A Surgical View of Anatomy: Perspectives from Students and Instructors. *Anatomical Sciences Education*, *14*(1), 110–116. https://doi.org/10.1002/ase.1988

36. Dev Singh, D., Mahender, T., & Raji Reddy, A. (2021). Powder bed fusion process: A brief review. *Materials Today: Proceedings*, *46*, 350–355. https://doi.org/10.1016/j.matpr.2020.08.415

37. Diment, L. E., Thompson, M. S., & Bergmann, J. H. M. (2017). Clinical efficacy and effectiveness of 3D printing: A systematic review. *BMJ Open*, *7*(12), e016891. https://doi.org/10.1136/bmjopen-2017-016891

38. Dorweiler, B., Baqué, P. E., Chaban, R., Ghazy, A., & Salem, O. (2021). Quality Control in 3D Printing: Accuracy Analysis of 3D-Printed Models of Patient-Specific Anatomy. *Materials*, *14*(4), 1021. https://doi.org/10.3390/ma14041021

39. Edelmers, E. (2024). *CT Scans of Spine with Metastases (Lytic, Sclerotic)* [Data set]. Zenodo. https://doi.org/10.5281/ZENODO.13645870

40. Edelmers, E. (2025). *Segmented ICC Dataset in IHC-Stained Haemorrhoidal Disease Specimens* [Data set]. Zenodo. https://doi.org/10.5281/ZENODO.14900510

41. Edelmers, E., Kazoka, D., Bolocko, K., & Pilmane, M. (2022). Different Techniques of Creating Bone Digital 3D Models from Natural Specimens. *Applied System Innovation*, *5*(4), 85. https://doi.org/10.3390/asi5040085

42. Edelmers, E., Kazoka, D., Bolocko, K., Sudars, K., & Pilmane, M. (2024). Automatization of CT Annotation: Combining AI Efficiency with Expert Precision. *Diagnostics*, *14*(2), 185. https://doi.org/10.3390/diagnostics14020185

43. Edelmers, E., Kazoka, D., & Pilmane, M. (2021). Creation of Anatomically Correct and Optimized for 3D Printing Human Bones Models. *Applied System Innovation*, *4*(3), 67. https://doi.org/10.3390/asi4030067

44. Edelmers, E., Ņikuļins, A., Sprūdža, K. L., Stapulone, P., Pūce, N. S., Skrebele, E., Siņicina, E. E., Cīrule, V., Kazuša, A., & Boločko, K. (2024). AI-Assisted Detection and Localization of Spinal Metastatic Lesions. *Diagnostics*, *14*(21), Article 21. https://doi.org/10.3390/diagnostics14212458

45. Edgar, H., Daneshvari Berry, S., Moes, E., Adolphi, N., Bridges, P., & Nolte, K. (n.d.). *New Mexico Decedent Image Database (NMDID)*. University of New Mexico. https://doi.org/10.25827/5S8C-N515

46. Escobar Díaz Guerrero, R., Carvalho, L., Bocklitz, T., Popp, J., & Oliveira, J. L. (2022). Software tools and platforms in Digital Pathology: A review for clinicians and computer scientists. *Journal of Pathology Informatics*, *13*, 100103. https://doi.org/10.1016/j.jpi.2022.100103

47. Fan, D., Li, Y., Wang, X., Zhu, T., Wang, Q., Cai, H., Li, W., Tian, Y., & Liu, Z. (2020). Progressive 3D Printing Technology and Its Application in Medical Materials. *Frontiers in Pharmacology*, *11*, 122. https://doi.org/10.3389/fphar.2020.00122

48. Fasel, J. H. D., Aguiar, D., Kiss-Bodolay, D., Montet, X., Kalangos, A., Stimec, B. V., & Ratib, O. (2016). Adapting anatomy teaching to surgical trends: A combination of classical dissection, medical imaging, and 3D-printing technologies. *Surgical and Radiologic Anatomy*, *38*(3), 361–367. https://doi.org/10.1007/s00276-015-1588-3

49. Fedorov, A., Beichel, R., Kalpathy-Cramer, J., Finet, J., Fillion-Robin, J.-C., Pujol, S., Bauer, C., Jennings, D., Fennessy, F., Sonka, M., Buatti, J., Aylward, S., Miller, J. V., Pieper, S., & Kikinis, R. (2012). 3D Slicer as an image computing platform for the Quantitative Imaging Network. *Magnetic Resonance Imaging*, *30*(9), Article 9. https://doi.org/10.1016/j.mri.2012.05.001

50. Ferreira da-Silva, A., Donato, M. C., Oliveira da-Silva, M., Gonçalves de-Sousa, S. D., Parada Simão, T. R., Simone Kietzer, K., Liberti, E. A., & Frank, P. W. (2023). Prototyping and 3D Printing of Computed Tomography Images with an Emphasis on Soft Tissues, Especially Muscles, for Teaching Human Anatomy. *International Journal of Morphology*, *41*(1), 73–78. https://doi.org/10.4067/S0717-95022023000100073

51. Fišere, I., Edelmers, E., Svirskis, Š., & Groma, V. (2025). Utilisation of Deep Neural Networks for Estimation of Cajal Cells in the Anal Canal Wall of Patients with Advanced Haemorrhoidal Disease Treated by LigaSure Surgery. *Cells*, *14*(7), 550. https://doi.org/10.3390/cells14070550

52. Flaxman, T. E., Cooke, C. M., Miguel, O. X., Sheikh, A. M., & Singh, S. S. (2021). A review and guide to creating patient specific 3D printed anatomical models from MRI for benign gynecologic surgery. *3D Printing in Medicine*, *7*(1), 17. https://doi.org/10.1186/s41205-021-00107-7

53. Fu, Y., Liu, S., Li, H. H., & Yang, D. (2017). Automatic and hierarchical segmentation of the human skeleton in CT images. *Physics in Medicine and Biology*, *62*(7), 2812–2833. https://doi.org/10.1088/1361-6560/aa6055

54. Garas, M., Vaccarezza, M., Newland, G., McVay-Doornbusch, K., & Hasani, J. (2018). 3D-Printed specimens as a valuable tool in anatomy education: A pilot study. *Annals of Anatomy - Anatomischer Anzeiger*, *219*, 57–64. https://doi.org/10.1016/j.aanat.2018.05.006

55. Garcia, J., Yang, Z., Mongrain, R., Leask, R. L., & Lachapelle, K. (2018). 3D printing materials and their use in medical education: A review of current technology and trends for the future. *BMJ Simulation and Technology Enhanced Learning*, *4*(1), 27–40. https://doi.org/10.1136/bmjstel-2017-000234

56. Gazquez-Garcia, J., Sánchez-Bocanegra, C. L., & Sevillano, J. L. (2025). AI in the Health Sector: Systematic Review of Key Skills for Future Health Professionals. *JMIR Medical Education*, *11*, e58161–e58161. https://doi.org/10.2196/58161

57. Gilberg, L., Teodorescu, B., Maerkisch, L., Baumgart, A., Ramaesh, R., Gomes Ataide, E. J., & Koç, A. M. (2023). Deep Learning Enhances Radiologists' Detection of Potential Spinal Malignancies in CT Scans. *Applied Sciences*, *13*(14), Article 14. https://doi.org/10.3390/app13148140

58. Gon Park, S., Park, J., Rock Choi, H., Ho Lee, J., Tae Cho, S., Goo Lee, Y., Ahn, H., & Pak, S. (2024). Deep Learning Model for Real-time Semantic Segmentation During Intraoperative Robotic Prostatectomy. *European Urology Open Science*, *62*, 47–53. https://doi.org/10.1016/j.euros.2024.02.005

59. Grady, L. (2006). Random Walks for Image Segmentation. *IEEE Transactions on Pattern Analysis and Machine Intelligence*, *28*(11), 1768–1783. https://doi.org/10.1109/TPAMI.2006.233

60. Ha, J. Y., Jeon, K. N., Bae, K., & Choi, B. H. (2017). Effect of Bone Reading CT software on radiologist performance in detecting bone metastases from breast cancer. *The British Journal of Radiology*, *90*(1072), 20160809. https://doi.org/10.1259/bjr.20160809

61. Hammon, M., Dankerl, P., Tsymbal, A., Wels, M., Kelm, M., May, M., Suehling, M., Uder, M., & Cavallaro, A. (2013). Automatic detection of lytic and blastic thoracolumbar spine metastases on computed tomography. *European Radiology*, *23*(7), 1862–1870. https://doi.org/10.1007/s00330-013-2774-5

62. Hirose, N., Sadeghian, A., Xia, F., Martin-Martin, R., & Savarese, S. (2019). VUNet: Dynamic Scene View Synthesis for Traversability Estimation Using an RGB Camera. *IEEE Robotics and Automation Letters*, *4*(2), 2062–2069. https://doi.org/10.1109/LRA.2019.2894869

63. Isensee, F., Jaeger, P. F., Kohl, S. A. A., Petersen, J., & Maier-Hein, K. H. (2021). nnU-Net: A self-configuring method for deep learning-based biomedical image segmentation. *Nature Methods*, *18*(2), 203–211. https://doi.org/10.1038/s41592-020-01008-z

64. Jamróz, W., Szafraniec, J., Kurek, M., & Jachowicz, R. (2018). 3D Printing in Pharmaceutical and Medical Applications – Recent Achievements and Challenges. *Pharmaceutical Research*, *35*(9), 176. https://doi.org/10.1007/s11095-018-2454-x

65. Jeyakumar, A., Dissanayake, B., & Dissabandara, L. (2020). Dissection in the Modern Medical Curriculum: An Exploration into Student Perception and Adaptions for the Future. *Anatomical Sciences Education*, *13*(3), 366–380. https://doi.org/10.1002/ase.1905

66. Jiang, S., Hondelink, L., Suriawinata, A. A., & Hassanpour, S. (2024). Masked pre-training of transformers for histology image analysis. *Journal of Pathology Informatics*, *15*, 100386. https://doi.org/10.1016/j.jpi.2024.100386

67. Jin, C., Udupa, J. K., Zhao, L., Tong, Y., Odhner, D., Pednekar, G., Nag, S., Lewis, S., Poole, N., Mannikeri, S., Govindasamy, S., Singh, A., Camaratta, J., Owens, S., & Torigian, D. A. (2022). Object recognition in medical images via anatomy-guided deep learning. *Medical Image Analysis*, *81*, 102527. https://doi.org/10.1016/j.media.2022.102527

68. Johnson, S. M., Owens, T. L., & O'Neil, J. N. (2019). Making the clinical connection from textbook to bedside during MDY1: An integrative approach for medical physiology education employing human simulation. *Advances in Physiology Education*, *43*(2), 128–133. https://doi.org/10.1152/advan.00109.2018

69. Joseph, T. M., Kallingal, A., Suresh, A. M., Mahapatra, D. K., Hasanin, M. S., Haponiuk, J., & Thomas, S. (2023). 3D printing of polylactic acid: Recent advances and opportunities. *The International Journal of Advanced Manufacturing Technology*, *125*(3–4), 1015–1035. https://doi.org/10.1007/s00170-022-10795-y

70. Kantaros, A., & Karalekas, D. (2014). FBG Based In Situ Characterization of Residual Strains in FDM Process. In M. Rossi, M. Sasso, N. Connesson, R. Singh, A. DeWald, D. Backman, & P. Gloeckner (Eds), *Residual Stress, Thermomechanics & Infrared Imaging, Hybrid Techniques and Inverse Problems, Volume 8* (pp. 333–337). Springer International Publishing. https://doi.org/10.1007/978-3-319-00876-9_41

71. Kanumilli, S. L. D., Kosuru, B. P., Shaukat, F., & Repalle, U. K. (2024). Advancements and Applications of Three-dimensional Printing Technology in Surgery. *Journal of Medical Physics*, *49*(3), 319–325. https://doi.org/10.4103/jmp.jmp_89_24

72. Kavvadia, E.-M., Katsoula, I., Angelis, S., & Filippou, D. (2023). The Anatomage Table: A Promising Alternative in Anatomy Education. *Cureus*. https://doi.org/10.7759/cureus.43047

73. Kazoka, D., Pilmane, M., & Edelmers, E. (2021). Facilitating Student Understanding through Incorporating Digital Images and 3D-Printed Models in a Human Anatomy Course. *Education Sciences*, *11*(8), Article 8. https://doi.org/10.3390/educsci11080380

74. Khalifa, M., & Albadawy, M. (2024). AI in diagnostic imaging: Revolutionising accuracy and efficiency. *Computer Methods and Programs in Biomedicine Update*, *5*, 100146. https://doi.org/10.1016/j.cmpbup.2024.100146

75. Khanam, R., & Hussain, M. (2024). *YOLOv11: An Overview of the Key Architectural Enhancements* (Version 1). arXiv. https://doi.org/10.48550/ARXIV.2410.17725

76. Kikinis, R., Pieper, S. D., & Vosburgh, K. G. (2014). 3D Slicer: A Platform for Subject-Specific Image Analysis, Visualization, and Clinical Support. In F. A. Jolesz (Ed.), *Intraoperative Imaging and Image-Guided Therapy* (pp. 277–289). Springer New York. https://doi.org/10.1007/978-1-4614-7657-3_19

77. Kim, D. H., Seo, J., Lee, J. H., Jeon, E.-T., Jeong, D., Chae, H. D., Lee, E., Kang, J. H., Choi, Y.-H., Kim, H. J., & Chai, J. W. (2024). Automated Detection and Segmentation of Bone Metastases on Spine MRI Using U-Net: A Multicenter Study. *Korean Journal of Radiology*, *25*(4), 363. https://doi.org/10.3348/kjr.2023.0671

78. Kim, S., Bae, W. C., Masuda, K., Chung, C. B., & Hwang, D. (2018). Semi-Automatic Segmentation of Vertebral Bodies in MR Images of Human Lumbar Spines. *Applied Sciences*, *8*(9), 1586. https://doi.org/10.3390/app8091586

79. Komura, D., Ochi, M., & Ishikawa, S. (2025). Machine learning methods for histopathological image analysis: Updates in 2024. *Computational and Structural Biotechnology Journal*, *27*, 383–400. https://doi.org/10.1016/j.csbj.2024.12.033

80. Kong, X., Nie, L., Zhang, H., Wang, Z., Ye, Q., Tang, L., Huang, W., & Li, J. (2016). Do 3D Printing Models Improve Anatomical Teaching About Hepatic Segments to Medical Students? A Randomized Controlled Study. *World Journal of Surgery*, *40*(8), 1969–1976. https://doi.org/10.1007/s00268-016-3541-y

81. Lakhani, D. A., Yuan, F., & Deib, G. (2022). Photorealistic depiction of intracranial arteriovenous malformation using cinematic rendering of volumetric MRI data for presurgical planning and patient education. *Journal of NeuroInterventional Surgery*, *14*(3), 311–312. https://doi.org/10.1136/neurintsurg-2021-018281

82. Lee, J.-Y., An, J., & Chua, C. K. (2017). Fundamentals and applications of 3D printing for novel materials. *Applied Materials Today*, *7*, 120–133. https://doi.org/10.1016/j.apmt.2017.02.004

83. Lee, N. (2016). The Lancet Technology: 3D printing for instruments, models, and organs? *The Lancet*, *388*(10052), 1368. https://doi.org/10.1016/S0140-6736(16)31735-4

84. Leng, S., McGee, K., Morris, J., Alexander, A., Kuhlmann, J., Vrieze, T., McCollough, C. H., & Matsumoto, J. (2017). Anatomic modeling using 3D printing: Quality assurance and optimization. *3D Printing in Medicine*, *3*(1), 6. https://doi.org/10.1186/s41205-017-0014-3

85. Lengyel, B. C., Lumsden, A. B., & Chinnadurai, P. (2025). Cinematic Rendered Computed Tomography Imaging Enhances 3D Visualization of Upper Extremity Arteriovenous Malformation. *Methodist DeBakey Cardiovascular Journal*, *21*(1), 13–15. https://doi.org/10.14797/mdcvj.1569

86. Li, C., Cheung, T. F., Fan, V. C., Sin, K. M., Wong, C. W. Y., & Leung, G. K. K. (2017). Applications of Three-Dimensional Printing in Surgery. *Surgical Innovation*, *24*(1), 82–88. https://doi.org/10.1177/1553350616681889

87. Li, J., Dong, P., Wang, X., Zhang, J., Zhao, M., Shen, H., Cai, L., He, J., Han, M., Miao, J., Liu, H., Yang, W., Han, X., & Liu, Y. (2024). Artificial intelligence enhances whole-slide interpretation of PD-L1 CPS in triple-negative breast cancer: A multi-institutional ring study. *Histopathology*, *85*(3), 451–467. https://doi.org/10.1111/his.15205

88. Li, K. H. C., Kui, C., Lee, E. K. M., Ho, C. S., Wong, S. H., Wu, W., Wong, W. T., Voll, J., Li, G., Liu, T., Yan, B., Chan, J., Tse, G., & Keenan, I. D. (2017). The role of 3D printing in anatomy education and surgical training: A narrative review. *MedEdPublish*, *6*, 92. https://doi.org/10.15694/mep.2017.000092

89. Liang, X., Nguyen, D., & Jiang, S. B. (2021). Generalizability issues with deep learning models in medicine and their potential solutions: Illustrated with cone-beam computed tomography (CBCT) to computed tomography (CT) image conversion. *Machine Learning: Science and Technology*, *2*(1), 015007. https://doi.org/10.1088/2632-2153/abb214

90. Lim, K. H. A., Loo, Z. Y., Goldie, S. J., Adams, J. W., & McMenamin, P. G. (2016). Use of 3D printed models in medical education: A randomized control trial comparing 3D prints versus cadaveric materials for learning external cardiac anatomy. *Anatomical Sciences Education*, *9*(3), 213–221. https://doi.org/10.1002/ase.1573

91. Litjens, G., Kooi, T., Bejnordi, B. E., Setio, A. A. A., Ciompi, F., Ghafoorian, M., Van Der Laak, J. A. W. M., Van Ginneken, B., & Sánchez, C. I. (2017). A survey on deep learning in medical image analysis. *Medical Image Analysis*, *42*, 60–88. https://doi.org/10.1016/j.media.2017.07.005

92. Liu, P., Lu, L., Zhang, J., Huo, T., Liu, S., & Ye, Z. (2021). Application of Artificial Intelligence in Medicine: An Overview. *Current Medical Science*, *41*(6), 1105–1115. https://doi.org/10.1007/s11596-021-2474-3

93. Lu, M. Y., Chen, B., Williamson, D. F. K., Chen, R. J., Zhao, M., Chow, A. K., Ikemura, K., Kim, A., Pouli, D., Patel, A., Soliman, A., Chen, C., Ding, T., Wang, J. J., Gerber, G., Liang, I., Le, L. P., Parwani, A. V., Weishaupt, L. L., & Mahmood, F. (2024). A multimodal generative AI copilot for human pathology. *Nature*, *634*(8033), 466–473. https://doi.org/10.1038/s41586-024-07618-3

94. Ma, J., Shao, W., Ye, H., Wang, L., Wang, H., Zheng, Y., & Xue, X. (2018). Arbitrary-Oriented Scene Text Detection via Rotation Proposals. *IEEE Transactions on Multimedia*, *20*(11), 3111–3122. https://doi.org/10.1109/TMM.2018.2818020

95. Mahlow, C., & Hediger, A. (2019). Digital Transformation in Higher Education—Buzzword or Opportunity? *eLearn*, *2019*(5), 3329488/3331171. https://doi.org/10.1145/3329488/3331171

96. Martín, J. G. (2018). Possibilities for the use of Anatomage (the Anatomical Real Body-Size Table) for Teaching and Learning Anatomy with the Students. *Biomedical Journal of Scientific & Technical Research*, *4*(4). https://doi.org/10.26717/BJSTR.2018.04.0001094

97. McGenity, C., Clarke, E. L., Jennings, C., Matthews, G., Cartlidge, C., Freduah-Agyemang, H., Stocken, D. D., & Treanor, D. (2024). Artificial intelligence in digital pathology: A systematic review and meta-analysis of diagnostic test accuracy. *Npj Digital Medicine*, *7*(1), 114. https://doi.org/10.1038/s41746-024-01106-8

98. Memon, I. (2018). Cadaver Dissection Is Obsolete in Medical Training! A Misinterpreted Notion. *Medical Principles and Practice*, *27*(3), 201–210. https://doi.org/10.1159/000488320

99. Milletari, F., Navab, N., & Ahmadi, S.-A. (2016). V-Net: Fully Convolutional Neural Networks for Volumetric Medical Image Segmentation. *2016 Fourth International Conference on 3D Vision (3DV)*, 565–571. https://doi.org/10.1109/3DV.2016.79

100. Mogali, S. R., Yeong, W. Y., Tan, H. K. J., Tan, G. J. S., Abrahams, P. H., Zary, N., Low-Beer, N., & Ferenczi, M. A. (2018). Evaluation by medical students of the educational value of multi-material and multi-colored three-dimensional printed models of the upper limb for anatomical education. *Anatomical Sciences Education*, *11*(1), 54–64. https://doi.org/10.1002/ase.1703

101. Morgan, B., Ford, A. L. J., & Smith, M. J. (2019). Standard methods for creating digital skeletal models using structure-from-motion photogrammetry. *American Journal of Physical Anthropology*, *169*(1), 152–160. https://doi.org/10.1002/ajpa.23803

102. Motsinger, S. K. (2020). Complete Anatomy. *Journal of the Medical Library Association*, *108*(1). https://doi.org/10.5195/jmla.2020.853

103. Nair, R. R., & Lindsey, A. (2020). Student Perception on Integration of 3D Complete Anatomy Software Application in Medical Curriculum. *The FASEB Journal*, *34*(S1), 1–1. https://doi.org/10.1096/fasebj.2020.34.s1.05153

104. Najjar, R. (2023). Redefining Radiology: A Review of Artificial Intelligence Integration in Medical Imaging. *Diagnostics*, *13*(17), 2760. https://doi.org/10.3390/diagnostics13172760

105. Nath, S. I., Anuradha, B., & Dilip, B. (2021). A study on making models in anatomy. *Paripex Indian Journal of Research*, 85–87. https://doi.org/10.36106/paripex/5303381

106. Neubeck, A., & Van Gool, L. (2006). Efficient Non-Maximum Suppression. *18th International Conference on Pattern Recognition (ICPR'06)*, 850–855. https://doi.org/10.1109/ICPR.2006.479

107. Odeh, M., Levin, D., Inziello, J., Lobo Fenoglietto, F., Mathur, M., Hermsen, J., Stubbs, J., & Ripley, B. (2019). Methods for verification of 3D printed anatomic model accuracy using cardiac models as an example. *3D Printing in Medicine*, *5*(1), Article 1. https://doi.org/10.1186/s41205-019-0043-1

108. Ong, W., Zhu, L., Zhang, W., Kuah, T., Lim, D. S. W., Low, X. Z., Thian, Y. L., Teo, E. C., Tan, J. H., Kumar, N., Vellayappan, B. A., Ooi, B. C., Quek, S. T., Makmur, A., & Hallinan, J. T. P. D. (2022). Application of Artificial Intelligence Methods for Imaging of Spinal Metastasis. *Cancers*, *14*(16), 4025. https://doi.org/10.3390/cancers14164025

109. Patel, V., Khan, M. N., Shrivastava, A., Sadiq, K., Ali, S. A., Moore, S. R., Brown, D. E., & Syed, S. (2020). Artificial Intelligence Applied to Gastrointestinal Diagnostics: A Review. *Journal of Pediatric Gastroenterology and Nutrition*, *70*(1), 4–11. https://doi.org/10.1097/MPG.0000000000002507

110. Penumakala, P. K., Santo, J., & Thomas, A. (2020). A critical review on the fused deposition modeling of thermoplastic polymer composites. *Composites Part B: Engineering*, *201*, 108336. https://doi.org/10.1016/j.compositesb.2020.108336

111. Pérez, M., Carou, D., Rubio, E. M., & Teti, R. (2020). Current advances in additive manufacturing. *Procedia CIRP*, *88*, 439–444. https://doi.org/10.1016/j.procir.2020.05.076

112. Petriceks, A. H., Peterson, A. S., Angeles, M., Brown, W. P., & Srivastava, S. (2018). Photogrammetry of Human Specimens: An Innovation in Anatomy Education. *Journal of Medical Education and Curricular Development*, *5*, 2382120518799356. https://doi.org/10.1177/2382120518799356

113. Placone, J. K., & Engler, A. J. (2018). Recent Advances in Extrusion-Based 3D Printing for Biomedical Applications. *Advanced Healthcare Materials*, *7*(8), Article 8. https://doi.org/10.1002/adhm.201701161

114. Plass, M., Kargl, M., Kiehl, T., Regitnig, P., Geißler, C., Evans, T., Zerbe, N., Carvalho, R., Holzinger, A., & Müller, H. (2023). Explainability and causability in digital pathology. *The Journal of Pathology: Clinical Research*, *9*(4), 251–260. https://doi.org/10.1002/cjp2.322

115. Portuguez Castro, M., & Gómez Zermeño, M. G. (2020). Challenge Based Learning: Innovative Pedagogy for Sustainability through e-Learning in Higher Education. *Sustainability*, *12*(10), 4063. https://doi.org/10.3390/su12104063

116. Powers, M. K., Lee, B. R., & Silberstein, J. (2016). Three-dimensional printing of surgical anatomy. *Current Opinion in Urology*, *26*(3), 283–288. https://doi.org/10.1097/MOU.0000000000000274

117. Pujol, S., Baldwin, M., Nassiri, J., Kikinis, R., & Shaffer, K. (2016). Using 3D Modeling Techniques to Enhance Teaching of Difficult Anatomical Concepts. *Academic Radiology*, *23*(4), 507–516. https://doi.org/10.1016/j.acra.2015.12.012

118. Qadri, S. F., Lin, H., Shen, L., Ahmad, M., Qadri, S., Khan, S., Khan, M., Zareen, S. S., Akbar, M. A., Bin Heyat, M. B., & Qamar, S. (2023). CT-Based Automatic Spine Segmentation Using Patch-Based Deep Learning. *International Journal of Intelligent Systems*, *2023*(1), 2345835. https://doi.org/10.1155/2023/2345835

119. Raju, A. S. N., Venkatesh, K., Rajababu, M., Gatla, R. K., Eid, M. M., Ali, E., Titova, N., & Sharaf, A. B. A. (2025). A hybrid framework for colorectal cancer detection and U-Net segmentation using polynetDWTCADx. *Scientific Reports*, *15*(1), 847. https://doi.org/10.1038/s41598-025-85156-2

120. Revilla-León, M., & Özcan, M. (2019). Additive Manufacturing Technologies Used for Processing Polymers: Current Status and Potential Application in Prosthetic Dentistry. *Journal of Prosthodontics*, *28*(2), 146–158. https://doi.org/10.1111/jopr.12801

121. Rezayi, S., R Niakan Kalhori, S., & Saeedi, S. (2022). Effectiveness of Artificial Intelligence for Personalized Medicine in Neoplasms: A Systematic Review. *BioMed Research International*, *2022*, 1–34. https://doi.org/10.1155/2022/7842566

122. Ronneberger, O., Fischer, P., & Brox, T. (2015). *U-Net: Convolutional Networks for Biomedical Image Segmentation* (Version 1). arXiv. https://doi.org/10.48550/ARXIV.1505.04597

123. Rony, M. K. K., Parvin, Mst. R., Wahiduzzaman, Md., Debnath, M., Bala, S. D., & Kayesh, I. (2024). “I Wonder if my Years of Training and Expertise Will be Devalued by Machines”: Concerns About the Replacement of Medical Professionals by Artificial Intelligence. *SAGE Open Nursing*, *10*, 23779608241245220. https://doi.org/10.1177/23779608241245220

124. Saeed, M. U., Dikaios, N., Dastgir, A., Ali, G., Hamid, M., & Hajjej, F. (2023). An Automated Deep Learning Approach for Spine Segmentation and Vertebrae Recognition Using Computed Tomography Images. *Diagnostics*, *13*(16), Article 16. https://doi.org/10.3390/diagnostics13162658

125. Salo, I., Nordlund, L., Eklund, L., Ho, J., Soini, M., Kumar, D., Yeong, J., Guan, F., & Metsälä, E. (2024). Advancements and applications of AI technologies in pathology: A scoping review. *Computer Methods in Biomechanics and Biomedical Engineering: Imaging & Visualization*, *12*(1), 2396595. https://doi.org/10.1080/21681163.2024.2396595

126. Schmidt, R., & Singh, K. (2010). meshmixer: An interface for rapid mesh composition. *ACM SIGGRAPH 2010 Talks*, 1–1. https://doi.org/10.1145/1837026.1837034

127. Schutera, M., Rettenberger, L., Pylatiuk, C., & Reischl, M. (2022). Methods for the frugal labeler: Multi-class semantic segmentation on heterogeneous labels. *PLOS ONE*, *17*(2), e0263656. https://doi.org/10.1371/journal.pone.0263656

128. Sheth, R., Balesh, E. R., Zhang, Y. S., Hirsch, J. A., Khademhosseini, A., & Oklu, R. (2016). Three-Dimensional Printing: An Enabling Technology for IR. *Journal of Vascular and Interventional Radiology*, *27*(6), 859–865. https://doi.org/10.1016/j.jvir.2016.02.029

129. Shirazi, S. F. S., Gharehkhani, S., Mehrali, M., Yarmand, H., Metselaar, H. S. C., Adib Kadri, N., & Osman, N. A. A. (2015). A review on powder-based additive manufacturing for tissue engineering: Selective laser sintering and inkjet 3D printing. *Science and Technology of Advanced Materials*, *16*(3), 033502. https://doi.org/10.1088/1468-6996/16/3/033502

130. Smith, C. F., Tollemache, N., Covill, D., & Johnston, M. (2018). Take away body parts! An investigation into the use of 3D-printed anatomical models in undergraduate anatomy education. *Anatomical Sciences Education*, *11*(1), 44–53. https://doi.org/10.1002/ase.1718

131. Stefaniak, A. B., Bowers, L. N., Knepp, A. K., Luxton, T. P., Peloquin, D. M., Baumann, E. J., Ham, J. E., Wells, J. R., Johnson, A. R., LeBouf, R. F., Su, F.-C., Martin, S. B., & Virji, M. A. (2019). Particle and vapor emissions from vat polymerization desktop-scale 3-dimensional printers. *Journal of Occupational and Environmental Hygiene*, *16*(8), 519–531. https://doi.org/10.1080/15459624.2019.1612068

132. Stritt, M., Stalder, A. K., & Vezzali, E. (2020). Orbit Image Analysis: An open-source whole slide image analysis tool. *PLOS Computational Biology*, *16*(2), e1007313. https://doi.org/10.1371/journal.pcbi.1007313

133. Subedi, S., Liu, S., Wang, W., Naser Shovon, S. M. A., Chen, X., & Ware, H. O. T. (2024). Multi-material vat photopolymerization 3D printing: A review of mechanisms and applications. *Npj Advanced Manufacturing*, *1*(1), 9. https://doi.org/10.1038/s44334-024-00005-w

134. Talanki, V. R., Peng, Q., Shamir, S. B., Baete, S. H., Duong, T. Q., & Wake, N. (2022). Three-Dimensional Printed Anatomic Models Derived From Magnetic Resonance Imaging Data: Current State and Image Acquisition Recommendations for Appropriate Clinical Scenarios. *Journal of Magnetic Resonance Imaging*, *55*(4), 1060–1081. https://doi.org/10.1002/jmri.27744

135. Taylor, S. L., Ibeh, A. J., Jakus, A. E., Shah, R. N., & Dunand, D. C. (2018). NiTi-Nb micro-trusses fabricated via extrusion-based 3D-printing of powders and transient-liquid-phase sintering. *Acta Biomaterialia*, *76*, 359–370. https://doi.org/10.1016/j.actbio.2018.06.015

136. Urrea, C., Garcia-Garcia, Y., & Kern, J. (2024). Improving Surgical Scene Semantic Segmentation through a Deep Learning Architecture with Attention to Class Imbalance. *Biomedicines*, *12*(6), 1309. https://doi.org/10.3390/biomedicines12061309

137. Van Eijnatten, M., Van Dijk, R., Dobbe, J., Streekstra, G., Koivisto, J., & Wolff, J. (2018). CT image segmentation methods for bone used in medical additive manufacturing. *Medical Engineering & Physics*, *51*, 6–16. https://doi.org/10.1016/j.medengphy.2017.10.008

138. Verner, I., & Merksamer, A. (2015). Digital Design and 3D Printing in Technology Teacher Education. *Procedia CIRP*, *36*, 182–186. https://doi.org/10.1016/j.procir.2015.08.041

139. Vorontsov, E., Bozkurt, A., Casson, A., Shaikovski, G., Zelechowski, M., Severson, K., Zimmermann, E., Hall, J., Tenenholtz, N., Fusi, N., Yang, E., Mathieu, P., Van Eck, A., Lee, D., Viret, J., Robert, E., Wang, Y. K., Kunz, J. D., Lee, M. C. H., … Fuchs, T. J. (2024). A foundation model for clinical-grade computational pathology and rare cancers detection. *Nature Medicine*, *30*(10), 2924–2935. https://doi.org/10.1038/s41591-024-03141-0

140. Wakjira, Y., Kurukkal, N. S., & Lemu, H. G. (2024). Assessment of the accuracy of 3D printed medical models through reverse engineering. *Heliyon*, *10*(11), e31829. https://doi.org/10.1016/j.heliyon.2024.e31829

141. Wang, J., Lv, Y., Wang, J., Ma, F., Du, Y., Fan, X., Wang, M., & Ke, J. (2021). Fully automated segmentation in temporal bone CT with neural network: A preliminary assessment study. *BMC Medical Imaging*, *21*(1), 166. https://doi.org/10.1186/s12880-021-00698-x

142. Wang, X., Zhao, J., Marostica, E., Yuan, W., Jin, J., Zhang, J., Li, R., Tang, H., Wang, K., Li, Y., Wang, F., Peng, Y., Zhu, J., Zhang, J., Jackson, C. R., Zhang, J., Dillon, D., Lin, N. U., Sholl, L., … Yu, K.-H. (2024). A pathology foundation model for cancer diagnosis and prognosis prediction. *Nature*, *634*(8035), 970–978. https://doi.org/10.1038/s41586-024-07894-z

143. Wasserthal, J., Breit, H.-C., Meyer, M. T., Pradella, M., Hinck, D., Sauter, A. W., Heye, T., Boll, D., Cyriac, J., Yang, S., Bach, M., & Segeroth, M. (2023). TotalSegmentator: Robust Segmentation of 104 Anatomic Structures in CT Images. *Radiology: Artificial Intelligence*, e230024. https://doi.org/10.1148/ryai.230024

144. Wendo, K., Behets, C., Barbier, O., Herman, B., Schubert, T., Raucent, B., & Olszewski, R. (2025). Dimensional Accuracy Assessment of Medical Anatomical Models Produced by Hospital-Based Fused Deposition Modeling 3D Printer. *Journal of Imaging*, *11*(2), 39. https://doi.org/10.3390/jimaging11020039

145. Yakunina, G. E. (2020). Research of digital communications models within organizations and at the state level in the countries-leaders in the use of digital communication technologies. *E-Management*, *2*(4), 41–50. https://doi.org/10.26425/2658-3445-2019-4-41-50

146. Ye, Z., Dun, A., Jiang, H., Nie, C., Zhao, S., Wang, T., & Zhai, J. (2020). The role of 3D printed models in the teaching of human anatomy: A systematic review and meta-analysis. *BMC Medical Education*, *20*(1), 335. https://doi.org/10.1186/s12909-020-02242-x

147. Ye, Z., Jiang, H., Bai, S., Wang, T., Yang, D., Hou, H., Zhang, Y., & Yi, S. (2023). Meta-analyzing the efficacy of 3D printed models in anatomy education. *Frontiers in Bioengineering and Biotechnology*, *11*, 1117555. https://doi.org/10.3389/fbioe.2023.1117555

148. Yuen, J. (2020). What Is the Role of 3D Printing in Undergraduate Anatomy Education? A Scoping Review of Current Literature and Recommendations. *Medical Science Educator*, *30*(3), 1321–1329. https://doi.org/10.1007/s40670-020-00990-5

149. Yushkevich, P. A., Piven, J., Hazlett, H. C., Smith, R. G., Ho, S., Gee, J. C., & Gerig, G. (2006). User-guided 3D active contour segmentation of anatomical structures: Significantly improved efficiency and reliability. *NeuroImage*, *31*(3), 1116–1128. https://doi.org/10.1016/j.neuroimage.2006.01.015

150. Zheng, S., Cui, X., Sun, Y., Li, J., Li, H., Zhang, Y., Chen, P., Jing, X., Ye, Z., & Yang, L. (2024). Benchmarking PathCLIP for Pathology Image Analysis. *Journal of Imaging Informatics in Medicine*, *38*(1), 422–438. https://doi.org/10.1007/s10278-024-01128-4

Acknowledgments

I would like to express my heartfelt appreciation and gratitude to everyone who has supported me on this journey – whether with words or with deeds. Thank You for believing in me, for standing by me during difficult times, and for sharing your life wisdom.

Annexes

1st Publication

applied system innovation

MDPI

Technical Note

Creation of Anatomically Correct and Optimized for 3D Printing Human Bones Models

Edgars Edelmers *, Dzintra Kazoka and Mara Pilmane

Institute of Anatomy and Anthropology, Rīga Stradiņš University, LV-1010 Riga, Latvia; Dzintra.Kazoka@rsu.lv (D.K.); Mara.Pilmane@rsu.lv (M.P.)
* Correspondence: edgars.edelmers@rsu.lv

Abstract: Educational institutions in several countries state that the education sector should be modernized to ensure a contemporary, individualized, and more open learning process by introducing and developing advance digital solutions and learning tools. Visualization along with 3D printing have already found their implementation in different medical fields in Pauls Stradiņš Clinical University Hospital, and Rīga Stradiņš University, where models are being used for prosthetic manufacturing, surgery planning, simulation of procedures, and student education. The study aimed to develop a detailed methodology for the creation of anatomically correct and optimized models for 3D printing from radiological data using only free and widely available software. In this study, only free and cross-platform software from widely available internet sources has been used—"*Meshmixer*", "*3D Slicer*", and "*Meshlab*". For 3D printing, the Ultimaker 5S 3D printer along with PLA material was used. In its turn, radiological data have been obtained from the "*New Mexico Decedent Image Database*". In total, 28 models have been optimized and printed. The developed methodology can be used to create new models from scratch, which can be used will find implementation in different medical and scientific fields—simulation processes, anthropology, 3D printing, bioprinting, and education.

Keywords: medical; segmentation; 3D; printing; radiology; Meshmixer; Slicer; Meshlab

Citation: Edelmers, E.; Kazoka, D.; Pilmane, M. Creation of Anatomically Correct and Optimized for 3D Printing Human Bones Models. *Appl. Syst. Innov.* **2021**, *4*, 67. https://doi.org/10.3390/asi4030067

Academic Editor: Christos Douligeris

Received: 3 August 2021
Accepted: 10 September 2021
Published: 13 September 2021

1. Introduction

Three-dimensional (3D) printing (also known as additive manufacturing) is a process of creating physical objects from their geometrical representation in a digital file by the successive addition of different materials [1,2]. With cost-effective manufacturing for high productivity, 3D-printing technology has become more popular in medical education in recent years, and it is suitable for a variety of applications, including medical moulages or anatomical models for educational purposes [3]. The benefit of anatomical models is that they can provide educational opportunities to learners who may otherwise not have access to original specimens [4,5]. In addition, 3D printing is useful for anatomy teaching in creating anatomical models that are not available for sale or reflect real-life variability. Various created anatomical models can involve active student learning: from 3D scanning to working with a variety of 3D modeling software applications, to using 3D printers, and then preparing the final model [6]. The usage of 3D printed anatomical models is becoming not only just a tool for regular anatomical lectures and practical labs but is widely used by students and doctors in the clinical environment as well [7].

Nowadays, 3D printing is being actively used in engineering and educational fields thanks to its great flexibility and the ability to create objects with complex sophisticated structures [8]. Medical schools, hospitals, and healthcare institutions can use the 3D models to improve clinical evaluation for several pathologies as well as bring new medical devices to market. Some of the most common applications in the medical industry are preclinical medical device testing and medical training models. For example, the insertion of a central venous catheter has been improved by using anatomical training kits [9]. Additionally,

organ models play an important role in many types of major surgical procedures as well as the education and communication outside of surgery [10]. Three-dimensional (3D) models can also be used for surgical planning prior to operation, such as neurosurgery [11].

The availability of 3D printers and improved segmentation algorithms have boosted the use of 3D printing in medicine, and this has led to an interest in many potential medical applications [12]. Models can be quickly adapted to a particular patient, quickly reshaped, and 3D printed. It provides a cheap alternative to general commercially available anatomical models. Thus, 3D printing can be used to teach anatomical structures [13]. It should be noted that there are still problems making this process available to wide-ranging users.

This work describes the methodology for creating a correct and ready-to-print anatomical model for using radiological data. The whole workflow starting from the obtaining of radiological data until the physical 3D model is described in a step-by-step manner, along with programs required for the creation 3D model.

2. General Workflow

This section describes how to proceed from radiological data (CT, ultrasonography, magnetic resonance tomography) to a ready 3D-printed model. The workflow is divided into three mandatory and two additional steps:

1. Main stages:
   - 1.1 Segment the model from radiological data.
   - 1.2 Edit and optimize the model.
   - 1.3 Print the 3D model.
2. Additional stages:
   - 2.1 Validation of model correctness.
   - 2.2 Create a model library.

2.1. Model Segmentation from a Radiological Data

The first step is to acquire radiological data, which is followed by segmentation of the structure of interest. Segmentation is a process in which an image is divided into individual regions with structures of interest. It is used below to generate an exact computer model of the patient's organs. The segmentation process itself is based on the principle that each tissue type is characterized by a range of voxels with different intensities. Therefore, it is possible to distinguish different tissues and to define organ borders.

There are several commercials (for example, "*Mimics*" from "*Materialize*" company [14] or "*Synopsys Simpleware*" [15]) and free programs for image segmentation. In this work, only free and widely available software has been used while at the same time also using one internationally recognized software—"*3D Slicer*" [16].

2.2. Edit and Optimize a Model

Image segmentation is followed by editing and optimization of the 3D model to avoid potential artifacts as well as optimizing the end size of the model and improving anatomical correctness.

There are several programs for working with 3D models, but the "*Meshlab*" [17] features more advantages as it allows precise control of every program instrument, mass editing, and checking multiple models at once. The other program is "*Meshmixer*" [18], which allows you to manipulate model morphology. The main benefits of these programs are an intuitive interface and good documentation.

Errors should be corrected during the repair phase before printing (duplicating points; duplicating faces; faces with zero areas; edges with faulty geometry (*non-manifold*); points with faulty geometry (*non-manifold*); vertex not referenced by a face; microparticles that do not form a surface, etc.) and anatomical inaccuracies that may occur in the process of segmentation.

Depending on outgoing data (radiological study type, tomography settings) and segmentation, "digital noise" may occur, which may affect the quality of the model surfaces, making them uneven and with multiple artifacts. As a result, there is a need for smoothing.

In some cases, the final model can be made by combining different models.

2.3. Model Correctness Validation

To preserve the anatomical correctness of the model, it is compared with trusted literature sources. In addition, specialized as well as the certified medical virtual application can be used. A good example is the "*Complete Anatomy*" [19], which is a correct and user-friendly tool for working with anatomical models. "*Complete Anatomy*" is the world's most advanced educational three-dimensional (3D) anatomy platform created by "*3D4Medical*" from "*Elsevier*", which has been developing medical products since 2009 [20,21].

2.4. Printing a 3D Model

Special types of 3D printing technologies have been developed with different functions. This section provides an overview of the 3D printing technologies, but only some techniques are widely applied in the medical industry and most commonly used to create anatomical models. The main reasons are the specific fabrication process and raw material to meet the high-quality requirements [22]. Several researchers have been conducted aiming at studying the accumulation of residual stresses and strains during the material build-up at the end or during the fabrication process in these technologies [23]. For example, the potential advantage of fused deposition modeling (FDM) is that it offers fabricating prototypes, tooling, and functional parts without geometrical complexity limitations, but there are observed significant dimensional deviations of the model surfaces [24,25].

According to "*The American Society for Testing and Materials*" in the US (ISO/ASTM 52900), methods of 3D printing were standardized into seven groups, including the binding jetting, directed energy deposition, material extrusion, material jetting, powder bed fusion, sheet lamination, and vat photopolymerization [26,27]. The selection of the method will depend on the use and visual appearance of the replica, the properties of the materials, and the possibilities of the printer (e.g., cost, settings, print time, and volume) [28].

There are four common additive manufacturing techniques (extrusion-based printing [29], vat polymerization-based printing [30], droplet-based printing [31], and powder-based printing [32]) when it comes to printing anatomical models.

Extrusion-based printing is commonly referred to as fused deposition modeling (FDM) or fused filament fabrication (FFF) [33]. FDM is a mature technology that is based on the extrusion of thermoplastic or composite materials drawn through the hot extrusion head with one or multiple extrusion nozzles [34]. For fabricating complex devices with functional parts such as valves, lenses, and fluidic interconnects, in FDM is a widely used vat-polymerization-based printing technique [35]. It is based on light-curing resin material and light-selective hardening polymerization molding. The process, where droplets of liquid materials are ejected and polymerized throughout hundreds of jets, is a material jetting technology. By directed UV for designed structures, the polymerization occurs only selectively [36]. It includes aerosol jet printing (AJP), binder jet printing (BJP), and poly jet printing (PJP).

Powder-based 3D printing is a technique with excellent ability for customized fabrication with a variety of external shapes, internal structures, and porosities. Four common powder-based printing techniques are selective laser sintering (SLS), selective laser melting (SLM), direct metal laser sintering (DMLS), and electron beam melting (EBM) [37]. There exist differences in the printing process and product characters among these printing techniques that are based on localized heating to generate melted metallic powder. It would be used to fabricate the customized products.

These different 3D printing technologies have their benefits and disadvantages.

The most widespread is extrusion technology. The main disadvantage of this method is its low precision; in its turn, the main advantage is its low printing costs (necessary

equipment, maintenance, and material costs) as well as being the most user-friendly 3D-printing technology. Researchers have tested and concluded that several process parameters (layer thickness, extruding temperature, printing speed, retraction distance, etc.) have to be carefully tuned to accomplish the desired and successful 3D printing results, using the lower end of desktop fused filament fabrication (FFF) 3D printers, and there exist a lot of challenges [38].

In cases where high precision and quality are required, different photopolymerization technologies can be used.

3. Materials and Methods

Table 1 reflects the software that has been used in this work. It is important to highlight that all the mentioned programs can be easily downloaded at no cost; these are intended to be used solely for scientific purposes—not for clinical applications, as the programs are not certified for medical applications.

Table 1. The list of used software.

Software	Version	Source
Autodesk Meshmixer	3.5.474	meshmixer.com (accessed on 1 March 2021)
3D Slicer	4.11.20210226 r29738	slicer.org (accessed on 1 March 2021)
MeshLab	2020.12	meshlab.net (accessed on 1 March 2021)
Ultimaker Cura	4.8	ultimaker.com/software/ultimaker-cura (accessed on 1 March 2021)

The short representation of the methodology can be seen in Figure 1.

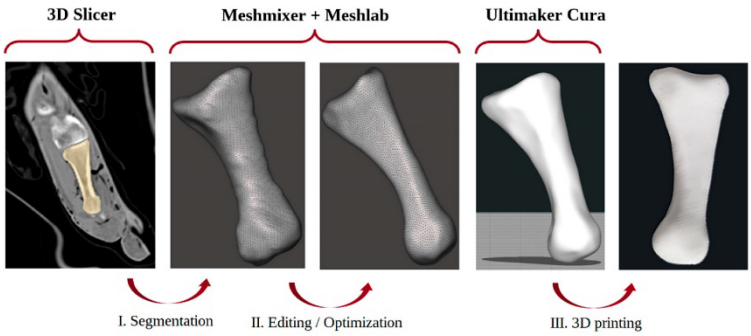

Figure 1. Graphical representation of the methodology.

3.1. Protocol for the CT Exam to Be Used

The CT scan used in this work was acquired from the *"[858158-1] Facilitating forensic research in multiple fields using a unique compilated tomography dataset"* (*"New Mexico Decedent Image Database"*) project [39].

The protocol for the CT scan was obtained from the *"New Mexico Decedent Image Database"* homepage (Table 2).

Table 2. Computed tomography protocol.

Parameter	Value
kVp	kVp 120
mAs	mAs 200
Scan length	Scan length 800–1000 mm
Scan FOV	Scan FOV 500 mm
Pitch	Pitch 0.942
Collimation	Collimation 16 × 0.75
Rotation Time	Rotation Time 1.0 s
Matrix	Matrix 512 × 512

After the scan, the reconstruction was performed with the following technical parameters:

- 3 mm × 3 mm soft tissue = 320 images.
- 3 mm × 3 mm bone = 320 images.
- 1 mm × 0.5 mm soft tissue = 1900 images.
- 1 mm × 0.5 mm bone = 1900 images.

3.2. Segmentation Methodology | 3D Slicer

1. Launch the *3D Slicer* program.
2. Import CT data into the program.
    - Set image contrast to ensure better visibility.
3. Use the instrument:
    - *"Volume Rendering"*
        - Using the *region of interest* tool separate the segmentation region from any other structures.
4. Add a new segment using the tool:
    - *Segment Editor*
        - Set up the *Threshold* tool.
        - Using the *Scissors*, *Smooth*, *Draw*, manually segment the required structure.
5. When completed segmentizing one structure, proceed to the second one by adding a new segment and repeat the segmentation procedure.
6. Export the completed segment or segments as a 3D model in the OBJ file format.

3.3. Validation Methodology | Literature

1. Check the correctness of anatomical structures using the literature [19–21].
2. For 3D models whose structures do not correspond to normal human anatomy, make the necessary adjustments using the editing methodology.

3.4. Editing Methodology | Meshmixer

1. Launch the *"Meshmixer"* program.
2. Import the 3D model (or models if there is a need to combine multiple models into a single model, such as putting a foot from individual bones) into the program.
3. Use instruments to make necessary adjustments:
    - *Select*
        - *Edit*
            - *Erase & Fill*
            - *Discard*
    - *Discard*
    - *Brushes*
    - *Make Solid*
    - *Add Tube*
4. To combine multiple models into one, select all models in the *"Object Browser"* section by holding the *"Shift"* button on the keyboard and select all the models from the list by clicking on them with a cursor; then, apply the *"Combine"* tool.
5. Export the 3D model as an OBJ file.

3.5. Optimization Methodology | MeshLab + Meshmixer

1. Launch the *"MeshLab"* program.
2. Import the 3D model into the program.
3. Remove artifacts using tools:
    - *Remove duplicated faces*

- *Remove duplicated vertex*
- *Remove Zero Area faces*
- *Repair Non-Manifold Edges by removing faces*
- *Repair Non-Manifold Verticles by Splitting*
  - *Vertex Displacement Ration* = 0
- *Remove Unreported Vertex*
- *Remove Solved Attachments* (*wrt Diameter*)
  - *Max diameter of isolated attachments* (%) = 10
  - *Remove Unreported Vertex* = ON

4. Export 3D model as an OBJ file.
5. Launch the "*Meshmixer*" program.
6. Import the 3D model into the application.
7. Close micro-holes (*Boundary edge* type error) by reconstructing the mesh surface using the instrument:
   - *Inspector*
     - *Hole Fill Mode* = *Smooth Fill*
     - *Small Thresh* = 0.01 mm
8. Optimize the model polygon mesh to minimize the size of the file (3D model) using the tool:
   - *Remesh*
     - *Remesh Mode* = *Relative Density*
     - *Density* (%) = 0
     - *Regularity* = 100
     - *Iterations* = 10
     - *Transition* (mm) = 0
     - *Smooth Group Boundaries* = ON
     - *Boundary Mode* = *Refined Boundary*
9. Smooth the 3D models surface if needed:
   - *Select*
     - *Deform*
       - *Smooth*
         - *Smoothing Type* = *Shape Preserving*
         - *Smoothing* = 1
         - *Smoothing Scale* = 4 (decrease or increase as needed)
         - *Constraint Rings* = 3
10. Export the 3D model as an OBJ file.

3.6. Validation Methodology | Literature

1. Check the correctness of anatomical structures using literature [19–21].
2. For 3D models whose structures do not correspond to normal human anatomy, make the necessary adjustments using the editing methodology.

3.7. 3D Printing | Cura Ultimaker

1. Launch the "*Ultimaker Cura*" program.
2. Import the 3D model into the program.
3. Create a profile (based on the built-in profile "*Visual*" with a slice thickness of 0.1 mm with further modification and optimization to maximize quality, durability, and precision); the main material for the model is PLA, in it's turn for the support structures the PVA is being used.
   - *Shell*

- *Wall Line Count* = 10
- *Top/Bottom Pattern* = *Concentric*
- *Z Seam Alignment* = *Random*

- *Infill*
  - *Density* (%) = 30
  - *Infill Pattern* = *Gyroid*
- *Build Plate Adhesion*
  - *Build Plate Adhesion Type* = *Brim*
  - *Build Plate Adhesion Extruder* = *Extruder* 2 (*PVA*)

4. Optimize models' position using the "*Auto—Orientation*" extension from the "*Ultimaker Cura*" library (*Marketplace*).
5. Start the printing process.
6. Remove support structures from the model by immersing the model in water (25 °C) for 24 h.
7. Remove the 3D model from the container with water and allow it to dry.
8. Check the correctness of the 3D printed model by comparing it to the virtual original.

4. Results

All 28 foot bones were segmented using the "*3D Slicer*" application following the developed segmentation methodology. Each bone was segmented, processed, and 3D printed separately.

A total of 28 anatomical 3D models were created by segmenting the relevant structures from 763 CT images.

The validation of 28 models' anatomical correction with the help of the literature [19–21] was performed. At this stage, it is necessary to decide whether additional model editing is required. In case of a positive result, adjustments are made by the editing methodology in the "*Meshmixer*" program.

A total of 19 models were modified by "*Meshmixer*" to retain anatomical correctness according to normal human anatomy.

The next step is the optimization of the models, which begins with the correction of errors and artifacts in the "*Meshlab*" program (duplicating points; duplicating faces; faces with zero areas; edges with faulty geometry (*non-manifold*); points with faulty geometry (*non-manifold*); vertex not referenced by a face; microparticles that do not form a surface).

This is followed by the optimization (simplification) of a polygon mesh (Figure 2) to improve the visual aspect of the model (for demonstration in a virtual library during classes), make the mesh suitable for further manipulation (deformation, cutting, modeling, etc.), reduce the model size as well as ensure printability of the model on an FDM-type printer.

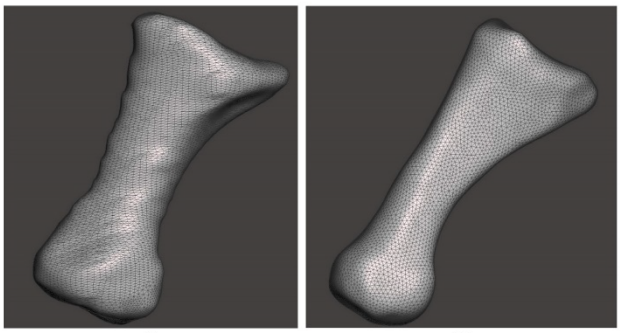

(**a**) (**b**)

Figure 2. *Os metatarsus primus* 3D model original polygon mesh (**a**) and model with edited and optimized polygon mesh (**b**).

A total of 28 models were optimized to correct the errors and artifacts that occurred during the segmentation process (Figure 3).

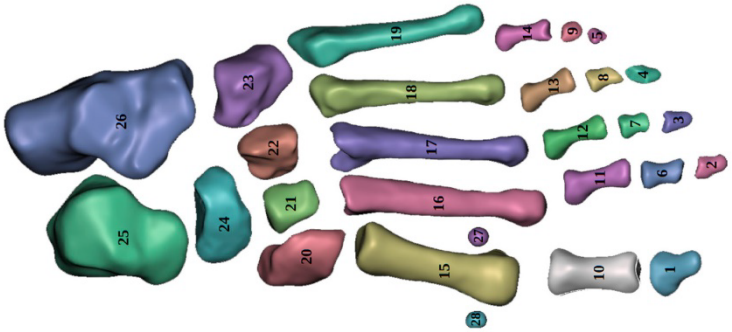

Figure 3. The structure of human foot 3D model. *1—Phalanx distalis hallucis, 2—Phalanx distalis digiti pedis secundi, 3—Phalanx distalis digiti pedis tertii, 4—Phalanx distalis digiti pedis quarti, 5—Phalanx distalis digiti pedis minimi, 6—Phalanx media digiti pedis secundi, 7—Phalanx media digiti pedis tertii, 8—Phalanx media digiti pedis quarti, 9—Phalanx media digiti pedis minii, 10—Phalanx proximalis hallucis, 11—Phalanx proximalis digiti pedis secundi, 12—Phalanx proximalis pedis digiti tertii, 13—Phalanx proximalis digiti pedis quarti, 14—Phalanx proximalis digiti pedis minimi, 15—Os metatarsus primus, 16—Os metatarsus secundus, 17—Os metatarsus tertius, 18—Os metatarsus quartus, 19—Os metatarsus quintus, 20—Os cuneiforme mediale, 21—Os cuneiforme intermedium, 22—Os cuneiforme laterale, 23—Os cuboideum, 24—Os naviculare, 25—Talus, 26—Calcaneus, 27/28—Os sesamoideum.*

The next step is the validation of models' anatomical correction with the help of the literature [19–21]. At this stage, it is necessary to decide whether additional model editing is required. In case of a positive result, adjustments are made following the editing methodology in the "*Meshmixer*" program.

The final step is 3D printing, which takes place in accordance with the 3D printing methodology (partly shown in Figure 4), while the printing process itself uses a 5S 3D extrusion-type printer from *Ultimaker* company with the following parameters:

Nozzle diameter: 0.4 mm,
Layer Height: 0.1 mm,
Print Speed: 70 mm/s,
Temperature: 200 °C,
Build Plate Temperature: 60 °C,
Fans Speed: 100%.

The printing process took 44 h and 15 min; during the process, 122 g of "*PLA/PHA Semi-Matte White*" and 45 g of "*Ultimaker PVA*" were used.

During the post-process, all models were immersed in water (24 °C) for 24 h to dissolve support structures. After removal from the water, the models were left to dry for 24 h at room temperature (24 °C). The final stage is to compare the 3D printed model to the virtual one. The final result is shown in Figure 5.

In total, 723 radiological images have been used, 28 models from segmented areas have been created, 28 models have been checked, 19 models have been modified, and 28 models have been optimized and printed.

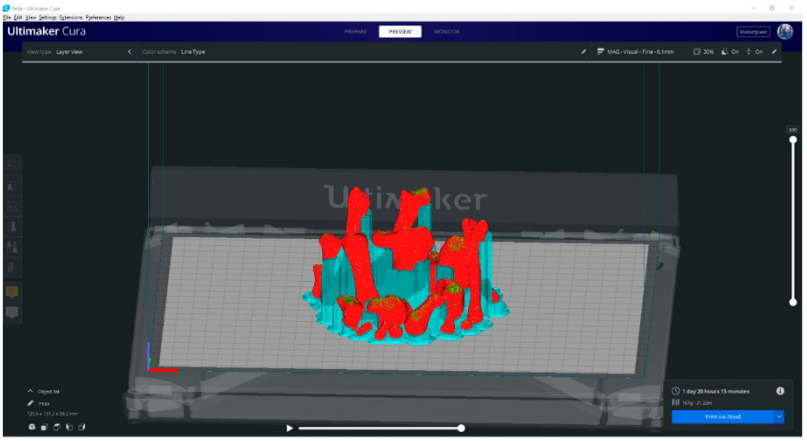

Figure 4. The graphical user interface of the "*Ultimaker Cura*" program. Individually positioned bones of the foot 3D model are shown in red color, supporting structures are shown in turquoise color.

Figure 5. Three-dimensional (3D) printed model of human foot bones.

5. Discussion

Today, using 3D printers especially for medical applications is a challenging task, as it involves special knowledge about human anatomy and the structures. New materials, technologies, and segmentation techniques require regular testing to be integrated effectively in the education, engineering, and clinical environment. Nowadays, for the creation and transplantation of different tissues, 3D bioprinting has been used in the scientific and medical fields [40]. Different materials and fabrication methods (traditional and free-form) have been investigated for use in other medical fields or regenerative tissue engineering (TE), for example for creating scaffolds in bone tissue [41]. The 3D-printed tissue scaffolds can be constructed with a very high level of accuracy and repeatability of predetermined forms and structures, and these designs can be used for the comparison of their mechanical properties [42]. In addition, scaffold structures must be related to several important criteria, for example, the case-specific internal geometry design with a controlled porosity percentage [43]. In addition, 3D technology has shown great potential as an educational tool in areas such as anatomical modeling and images, and it can be used to scan the human body with magnetic resonance imaging or with computed tomography scans [44,45].

Several models can be replicated in large quantities for students to be used during practical classes. A range of human body models has already been developed for different

applications in both educational and medical fields. Our study states that 3D human anatomical models can support the study process in the absence of cadaveric material, for example during remote classes with students. Knowledge of skeletal anatomy is a basic educational component for every medical student [46]. Bones are very important parts of the human body and provide structural support to the system, and due to this fact, the bone system has been chosen as the first system that shall be digitalized. Different studies report how 3D printing allows the creation of reproductions of dissected human cadavers and different anatomical specimens for teaching purposes and surgical training [47,48].

Three-dimensional (3D) printing creates opportunities for integrating science, engineering, technology, and mathematics (STEM) with other disciplines [49]. The integration of 3D technology, in different forms, allows for the visualization of new creative possibilities that the STEM field has to offer. Therefore, many teachers are focused on using 3D printing, including it at all school levels, from primary through to secondary (high school). When learners can engage with STEM concepts from a young age, STEM education aims to adopt a new learning approach, and it goes beyond the ability to remember facts and procedures [50]. At the third level of education, there are greater possibilities to teach students how 3D printing technology works. Nowadays, many third-level universities or technical colleges incorporate 3D printing modules and projects into applied sciences, engineering, and other courses [51].

It is believed that this technology will be more integrated into undergraduate anatomy education [52]. At the same time, the creation of anatomical models to fully understand the anatomical relationships between different structures will be important for studying normal and pathological anatomy [53]. These models can be manufactured as functional multi-layered units and offer rich possibilities for sectional and/or reduced anatomy [54].

To assess the quality of these innovative resources as anatomy educational tools, the accuracy of all printed models should be compared with original specimens. It seems that some of the available 3D printed products cannot be used in work with students due to the bad precision and different anatomical inaccuracies. Many studies describe the experience of the use of such teaching techniques as a pre-test, live tests, and post-test surveys [55,56]. Nevertheless, the implementation of 3D models in anatomy education shows promising outcomes [57].

The 3D model search includes special requirements including the quality of structures, high resolution, and accurate color reproductions. This process can be very complicated, and it can take a lot of time.

Furthermore, anatomically correct models can be computer-generated from medical image data. Computational modeling is common in many areas of science and engineering, only recently have advances in experimental techniques and medical imaging allowed this tool to be applied in cardiac surgery [58]. A computational heart model can provide additional information that is not easily measurable in experiments [59]. Forces are applied to any specific spot on the extrapolated 3D model to calculate stresses and strains in different areas of the model. For example, in vivo evaluation of the aortic wall strain was simple, fast, and it could be used to develop a rupture potential criterion based on the aortic aneurysm extensibility [60]. Furthermore, wall shear stress (WSS) has an important implication on bicuspid aortopathy, and computational flow analyses were used to estimate this parameter and aortic geometry with comparison to standard geometric reconstructions obtained by computed-tomography angiography (CTA) scans [61].

The creation of the online 3D model database may encourage educators to easily manufacture these models for specific educational purposes [62]. Most of these databases provide the function of a text-based model search for keywords. The most crucial part of the fabrication of a qualitative 3D model is to obtain high-resolution CT data of the organ [63]. Unfortunately, the segmentation process leads to the creation of different kinds of errors and artifacts (non-manifold objects, duplicated vertex, etc.). Verification of all printed models' accuracy is an essential step in 3D model creation. Full-reference image visual quality metrics are widely used at different stages of digital image processing [64].

Once the model is finished, it can be explored in 3D, measured, formatted, and manipulated to gain an all-encompassing understanding of the anatomy.

Further, the possibility to manipulate with models in three-dimensional space is important for medical students, clinicians, and surgeons [65–67] to better understand anatomical structures. Different patient-specific 3D printed models can allow specialists to review both normal and abnormal anatomical structures. In addition, the interpretation of complex three-dimensional spatial relationships in cross-sectional and radiological images can enhance student's interpretation of cross-sectional anatomy [68–70].

Nowadays, 3D objects that are based on actual image data of human bodies are more and more used to teach human anatomy, but some authors report that to efficiently create 3D-printed anatomic models and later use them safely for medical purposes, professionals and radiologists have to understand the methodology and process of converting medical imaging data into digital models [71–73].

6. Conclusions

The creation of anatomically accurate reproductions of human bones offers many advantages as it allows the rapid production of multiple copies at any size scale and should be suitable for any teaching facility. Three-dimensional (3D)-printed bones can be successfully applied in anatomy education at Rīga Stradiņš University.

During this study, a methodology for transforming, segmenting, and processing human bone Digital Imaging and Communications in Medicine (DICOM) images has been developed that allows the creation (segment) of 3D models from radiological data. Only free and widely available programs have been used to ensure results reproducibility and allow students as well as medical and education specialists to allow access to this innovative method of medical 3D model creation. The application of 3D anatomical models will further ramify and expand into other study courses. Moreover, the 3D printing of the human bones will soon involve other anatomical structures, particularly those that are difficult to detect and manipulate. It is planned that created models of the bones will also be utilized in the pathology field of human anatomy.

Furthermore, alternative printers and techniques will be explored, and our proposed methods will be improved and used in work with students and incorporated in a new direction—education science at the Rīga Stradiņš University. This technique can enrich the medical education process, support specialists in the clinical field in complicated cases and with limited resources, and in the end boost the research in an interdisciplinary field where medicine meets computed sciences. The mentioned methodology can be enhanced in terms of visual quality and precision by replacing the FDM-type printer with a vat polymerization (SLA or DLP) 3D printer.

Author Contributions: Conceptualization, E.E.; methodology, E.E.; investigation, E.E. and D.K.; writing—original draft preparation, E.E.; writing—review and editing, E.E., M.P. and D.K. All authors have read and agreed to the published version of the manuscript.

Funding: This research received no external funding.

Institutional Review Board Statement: Not applicable.

Informed Consent Statement: The approval from RSU Ethics Committee has been received Nr. 2-3/217.

Data Availability Statement: Data are contained within the article.

Conflicts of Interest: The authors declare no conflict of interest.

References

1. Shahrubudin, N.; Lee, T.C.; Ramlan, R. An Overview on 3D Printing Technology: Technological, Materials, and Applications. *Procedia Manuf.* **2019**, *35*, 1286–1296. [CrossRef]
2. Thomas, D.B.; Hiscox, J.D.; Dixon, B.J.; Potgieter, J. 3D Scanning and Printing Skeletal Tissues for Anatomy Education. *J. Anat.* **2016**, *229*, 473–481. [CrossRef] [PubMed]
3. Lim, K.H.A.; Loo, Z.Y.; Goldie, S.J.; Adams, J.W.; McMenamin, P.G. Use of 3D Printed Models in Medical Education: A Randomized Control Trial Comparing 3D Prints versus Cadaveric Materials for Learning External Cardiac Anatomy: Use of 3D Prints in Medical Education. *Am. Assoc. Anat.* **2016**, *9*, 213–221. [CrossRef]
4. Pujol, S.; Baldwin, M.; Nassiri, J.; Kikinis, R.; Shaffer, K. Using 3D Modeling Techniques to Enhance Teaching of Difficult Anatomical Concepts. *Acad. Radiol.* **2016**, *23*, 507–516. [CrossRef]
5. Ngo, T.D.; Kashani, A.; Imbalzano, G.; Nguyen, K.T.Q.; Hui, D. Additive Manufacturing (3D Printing): A Review of Materials, Methods, Applications and Challenges. *Compos. Part B Eng.* **2018**, *143*, 172–196. [CrossRef]
6. AbouHashem, Y.; Dayal, M.; Savanah, S.; Štrkalj, G. The Application of 3D Printing in Anatomy Education. *Med. Educ. Online* **2015**, *20*, 29847. [CrossRef]
7. Kazoka, D.; Pilmane, M.; Edelmers, E. Facilitating Student Understanding through Incorporating Digital Images and 3D-Printed Models in a Human Anatomy Course. *Educ. Sci.* **2021**, *11*, 380. [CrossRef]
8. Li, K.H.C.; Kui, C.; Lee, E.K.M.; Ho, C.S.; Wong, S.H.; Wu, W.; Wong, W.T.; Voll, J.; Li, G.; Liu, T.; et al. The Role of 3D Printing in Anatomy Education and Surgical Training: A Narrative Review. *MedEdPublish* **2017**, *6*. [CrossRef]
9. Ford, S.; Minshall, T. Invited Review Article: Where and How 3D Printing Is Used in Teaching and Education. *Addit. Manuf.* **2019**, *25*, 131–150. [CrossRef]
10. Evans, L.V.; Dodge, K.L.; Shah, T.D.; Kaplan, L.J.; Siegel, M.D.; Moore, C.L.; Hamann, C.J.; Lin, Z.; D'Onofrio, G. Simulation Training in Central Venous Catheter Insertion: Improved Performance in Clinical Practice. *Acad. Med.* **2010**, *85*, 1462–1469. [CrossRef] [PubMed]
11. Müller, A.; Krishnan, K.G.; Uhl, E.; Mast, G. The Application of Rapid Prototyping Techniques in Cranial Reconstruction and Preoperative Planning in Neurosurgery. *J. Craniofacial Surg.* **2003**, *14*, 899–914. [CrossRef]
12. Trace, A.P.; Ortiz, D.; Deal, A.; Retrouvey, M.; Elzie, C.; Goodmurphy, C.; Morey, J.; Hawkins, C.M. Radiology's Emerging Role in 3-D Printing Applications in Health Care. *J. Am. Coll. Radiol.* **2016**, *13*, 856–862.e4. [CrossRef]
13. Rengier, F.; Mehndiratta, A.; von Tengg-Kobligk, H.; Zechmann, C.M.; Unterhinninghofen, R.; Kauczor, H.-U.; Giesel, F.L. 3D Printing Based on Imaging Data: Review of Medical Applications. *Int. J. CARS* **2010**, *5*, 335–341. [CrossRef] [PubMed]
14. Materialise Mimics. Available online: https://www.materialise.com (accessed on 27 August 2021).
15. Synopsys Simpleware. Available online: https://www/simpleware.com (accessed on 27 August 2021).
16. Giannopoulos, A.A.; Mitsouras, D.; Yoo, S.-J.; Liu, P.P.; Chatzizisis, Y.S.; Rybicki, F.J. Applications of 3D Printing in Cardiovascular Diseases. *Nat. Rev. Cardiol.* **2016**, *13*, 701–718. [CrossRef] [PubMed]
17. Cignoni, P.; Ranzuglia, M.; Corsini, G. MeshLab: An Open—Source 3D Mesh Proceeding System. European Association for Computer Graphics. In *Eurographics Italian Chapter Proceedings, Proceedings of the Sixth Eurographics Italian Chapter Conference, Salerno, Italy, 2–4 July 2008*; Scarano, V., Ed.; Eurographics Association: Aire-la-Ville, Switzerland, 2008; pp. 129–136.
18. Qin, Y.; Qi, Q.; Scott, P.J.; Jiang, X. Status, Comparison, and Future of the Representations of Additive Manufacturing Data. *Comput. Aided Des.* **2019**, *111*, 44–64. [CrossRef]
19. Motsinger, S.K. Complete Anatomy. *JMLA* **2020**, *108*. [CrossRef]
20. Nair, R.R.; Lindsey, A. Student Perception on Integration of 3D Complete Anatomy Software Application in Medical Curriculum. *FASEB J.* **2020**, *34* (Suppl. S1), 1. [CrossRef]
21. 3D4Medical. Complete Anatomy. 3D4Medical. Available online: https://3d4medical.com (accessed on 27 August 2021).
22. Fan, D.; Li, Y.; Wang, X.; Zhu, T.; Wang, Q.; Cai, H.; Li, W.; Tian, Y.; Liu, Z. Progressive 3D Printing Technology and Its Application in Medical Materials. *Front. Pharmacol.* **2020**, *11*, 122. [CrossRef] [PubMed]
23. Kantaros, A.; Karalekas, D. FBG Based In Situ Characterization of Residual Strains in FDM Process. In *Residual Stress, Thermomechanics & Infrared Imaging, Hybrid Techniques and Inverse Problems*; Rossi, M., Sasso, M., Connesson, N., Singh, R., DeWald, A., Backman, D., Gloeckner, P., Eds.; Conference Proceedings of the Society for Experimental Mechanics Series; Springer International Publishing: Cham, Switzerland, 2014; Volume 8, pp. 333–337. [CrossRef]
24. Boschetto, A.; Bottini, L. Design for Manufacturing of Surfaces to Improve Accuracy in Fused Deposition Modeling. *Robot. Comput. Integr. Manuf.* **2016**, *37*, 103–114. [CrossRef]
25. Kantaros, A.; Karalekas, D. Fiber Bragg Grating Based Investigation of Residual Strains in ABS Parts Fabricated by Fused Deposition Modeling Process. *Mater. Des.* **2013**, *50*, 44–50. [CrossRef]
26. Hodgdon, T.; Danrad, R.; Patel, M.J.; Smith, S.E.; Richardson, M.L.; Ballard, D.H.; Ali, S.; Trace, A.P.; DeBenedectis, C.M.; Zygmont, M.E.; et al. Logistics of Three-Dimensional Printing. *Acad. Radiol.* **2018**, *25*, 40–51. [CrossRef]
27. Horn, T.J.; Harrysson, O.L.A. Overview of Current Additive Manufacturing Technologies and Selected Applications. *Sci. Prog.* **2012**, *95*, 255–282. [CrossRef] [PubMed]
28. Aimar, A.; Palermo, A.; Innocenti, B. The Role of 3D Printing in Medical Applications: A State of the Art. *J. Healthc. Eng.* **2019**, *2019*, 1–10. [CrossRef] [PubMed]

29. Taylor, S.L.; Ibeh, A.J.; Jakus, A.E.; Shah, R.N.; Dunand, D.C. NiTi-Nb Micro-Trusses Fabricated via Extrusion-Based 3D-Printing of Powders and Transient-Liquid-Phase Sintering. *Acta Biomater.* **2018**, *76*, 359–370. [CrossRef] [PubMed]
30. Stefaniak, A.B.; Bowers, L.N.; Knepp, A.K.; Luxton, T.P.; Peloquin, D.M.; Baumann, E.J.; Ham, J.E.; Wells, J.R.; Johnson, A.R.; LeBouf, R.F.; et al. Particle and Vapor Emissions from Vat Polymerization Desktop-Scale 3-Dimensional Printers. *J. Occup. Environ. Hyg.* **2019**, *16*, 519–531. [CrossRef]
31. Graham, A.D.; Olof, S.N.; Burke, M.J.; Armstrong, J.P.K.; Mikhailova, E.A.; Nicholson, J.G.; Box, S.J.; Szele, F.G.; Perriman, A.W.; Bayley, H. High-Resolution Patterned Cellular Constructs by Droplet-Based 3D Printing. *Sci. Rep.* **2017**, *7*, 7004. [CrossRef] [PubMed]
32. Shirazi, S.F.S.; Gharehkhani, S.; Mehrali, M.; Yarmand, H.; Metselaar, H.S.C.; Adib Kadri, N.; Osman, N.A.A. A Review on Powder-Based Additive Manufacturing for Tissue Engineering: Selective Laser Sintering and Inkjet 3D Printing. *Sci. Technol. Adv. Mater.* **2015**, *16*, 033502. [CrossRef]
33. Placone, J.K.; Engler, A.J. Recent Advances in Extrusion-Based 3D Printing for Biomedical Applications. *Adv. Healthc. Mater.* **2018**, *7*, 1701161. [CrossRef]
34. Paxton, N.; Smolan, W.; Böck, T.; Melchels, F.; Groll, J.; Jungst, T. Proposal to Assess Printability of Bioinks for Extrusion-Based Bioprinting and Evaluation of Rheological Properties Governing Bioprintability. *Biofabrication* **2017**, *9*, 044107. [CrossRef] [PubMed]
35. Carve, M.; Wlodkowic, D. 3D-Printed Chips: Compatibility of Additive Manufacturing Photopolymeric Substrata with Biological Applications. *Micromachines* **2018**, *9*, 91. [CrossRef]
36. Revilla-León, M.; Özcan, M. Additive Manufacturing Technologies Used for Processing Polymers: Current Status and Potential Application in Prosthetic Dentistry: Polymer Additive Manufacturing for Prosthodontics. *J. Prosthodont.* **2019**, *28*, 146–158. [CrossRef]
37. Brunello, G.; Sivolella, S.; Meneghello, R.; Ferroni, L.; Gardin, C.; Piattelli, A.; Zavan, B.; Bressan, E. Powder-Based 3D Printing for Bone Tissue Engineering. *Biotechnol. Adv.* **2016**, *34*, 740–753. [CrossRef]
38. Antreas, K.; Piromalis, D. Employing a Low-Cost Desktop 3D Printer: Challenges, and How to Overcome Them by Tuning Key Process Parameters. *Mechanics* **2021**, *10*, 11–19. [CrossRef]
39. Edgar, H.J.H.; Berry, S.D.; Moes, E.; Adolphi, N.L.; Bridges, P.; Nolte, K.B. *New Mexico Decedent Image Database*; Office of the Medical Investigator, University of New Mexico: Albuquerque, NM, USA, 2020. [CrossRef]
40. Murphy, S.V.; Atala, A. 3D Bioprinting of Tissues and Organs. *Nat. Biotechnol.* **2014**, *32*, 773–785. [CrossRef]
41. Wubneh, A.; Tsekoura, E.K.; Ayranci, C.; Uludağ, H. Current state of fabrication technologies and materials for bone tissue engineering. *Acta Biomater.* **2018**, *80*, 1–30. [CrossRef]
42. Kantaros, A.; Chatzidai, N.; Karalekas, D. 3D Printing-Assisted Design of Scaffold Structures. *Int. J. Adv. Manuf. Technol.* **2016**, *82*, 559–571. [CrossRef]
43. Kantaros, A.; Piromalis, D. Fabricating Lattice Structures via 3D Printing: The Case of Porous Bio-Engineered Scaffolds. *Appl. Mech.* **2021**, *2*, 289–302. [CrossRef]
44. Ye, Z.; Dun, A.; Jiang, H.; Nie, C.; Zhao, S.; Wang, T.; Zhai, J. The Role of 3D Printed Models in the Teaching of Human Anatomy: A Systematic Review and Meta-Analysis. *BMC Med. Educ.* **2020**, *20*, 335. [CrossRef]
45. Vaccarezza, M.; Papa, V. 3D Printing: A Valuable Resource in Human Anatomy Education. *Anat. Sci. Int.* **2015**, *90*, 64–65. [CrossRef]
46. Wu, A.-M.; Wang, K.; Wang, J.-S.; Chen, C.-H.; Yang, X.-D.; Ni, W.-F.; Hu, Y.-Z. The Addition of 3D Printed Models to Enhance the Teaching and Learning of Bone Spatial Anatomy and Fractures for Undergraduate Students: A Randomized Controlled Study. *Ann. Transl. Med.* **2018**, *6*, 403. [CrossRef]
47. McMenamin, P.G.; Quayle, M.R.; McHenry, C.R.; Adams, J.W. The Production of Anatomical Teaching Resources Using Three-Dimensional (3D) Printing Technology: 3D Printing in Anatomy Education. *Am. Assoc. Anat.* **2014**, *7*, 479–486. [CrossRef]
48. Langridge, B.; Momin, S.; Coumbe, B.; Woin, E.; Griffin, M.; Butler, P. Systematic Review of the Use of 3-Dimensional Printing in Surgical Teaching and Assessment. *J. Surg. Educ.* **2018**, *75*, 209–221. [CrossRef] [PubMed]
49. Lin, K.-Y.; Hsiao, H.-S.; Chang, Y.-S.; Chien, Y.-H.; Wu, Y.-T. The Effectiveness of Using 3D Printing Technology in STEM Project-Based Learning Activities. *EURASIA J. Math. Sci. Technol. Educ.* **2018**, *14*, em1633. [CrossRef]
50. Fleer, M. Working Technologically: Investigations into How Young Children Design and Make During Technology Education. *Int. J. Technol. Des. Educ.* **2000**, *10*, 43–59. [CrossRef]
51. Cohen, B. Teaching STEM after School: Correlates of Instructional Comfort. *J. Educ. Res.* **2018**, *111*, 246–255. [CrossRef]
52. Keenan, I.; Awadh, A.B. Integrating 3D Visualisation Technologies in Undergraduate Anatomy Education. *Adv. Exp. Med. Biol.* **2019**, *1120*, 39–53. [CrossRef] [PubMed]
53. Smith, C.F.; Tollemache, N.; Covill, D.; Johnston, M. Take Away Body Parts! An Investigation into the Use of 3D-Printed Anatomical Models in Undergraduate Anatomy Education. *Am. Assoc. Anat.* **2018**, *11*, 44–53. [CrossRef]
54. Smith, M.L.; Jones, J.F.X. Dual-Extrusion 3D Printing of Anatomical Models for Education: Two Materials 3D Printing in Anatomy. *Am. Assoc. Anat.* **2018**, *11*, 65–72. [CrossRef]
55. Garas, M.; Vaccarezza, M.; Newland, G.; McVay-Doornbusch, K.; Hasani, J. 3D-Printed Specimens as a Valuable Tool in Anatomy Education: A Pilot Study. *Ann. Anat. Anat. Anz.* **2018**, *219*, 57–64. [CrossRef]

56. Chen, S.; Pan, Z.; Wu, Y.; Gu, Z.; Li, M.; Liang, Z.; Zhu, H.; Yao, Y.; Shui, W.; Shen, Z.; et al. The Role of Three-Dimensional Printed Models of Skull in Anatomy Education: A Randomized Controlled Trail. *Sci. Rep.* **2017**, *7*, 575. [CrossRef] [PubMed]
57. Chytas, D.; Johnson, E.O.; Piagkou, M.; Tsakotos, G.; Babis, G.C.; Nikolaou, V.S.; Markatos, K.; Natsis, K. Three-Dimensional Printing in Anatomy Teaching: Current Evidence. *Surg. Radiol. Anat.* **2020**, *42*, 835–841. [CrossRef]
58. Lee, L.C.; Genet, M.; Dang, A.B.; Ge, L.; Guccione, J.M.; Ratcliffe, M.B. Applications of Computational Modeling in Cardiac Surgery: Computational Modeling of cardiac mechanics. *J. Card. Surg.* **2014**, *29*, 293–302. [CrossRef]
59. Pellikka, P.A.; Arruda-Olson, A.; Chaudhry, F.A.; Chen, M.H.; Marshall, J.E.; Porter, T.R.; Sawada, S.G. Guidelines for Performance, Interpretation, and Application of Stress Echocardiography in Ischemic Heart Disease: From the American Society of Echocardiography. *J. Am. Soc. Echocardiogr.* **2020**, *33*, 1–41.e8. [CrossRef] [PubMed]
60. Pasta, S.; Agnese, V.; Di Giuseppe, M.; Gentile, G.; Raffa, G.M.; Bellavia, D.; Pilato, M. In Vivo Strain Analysis of Dilated Ascending Thoracic Aorta by ECG-Gated CT Angiographic Imaging. *Ann. Biomed. Eng.* **2017**, *45*, 2911–2920. [CrossRef] [PubMed]
61. Pasta, S.; Gentile, G.; Raffa, G.M.; Scardulla, F.; Bellavia, D.; Luca, A.; Pilato, M.; Scardulla, C. Three-Dimensional Parametric Modeling of Bicuspid Aortopathy and Comparison with Computational Flow Predictions: 3D Anatomic Representations of Bicuspid Aortopathy. *Artif. Organs* **2017**, *41*, E92–E102. [CrossRef] [PubMed]
62. Yuen, J. What Is the Role of 3D Printing in Undergraduate Anatomy Education? A Scoping Review of Current Literature and Recommendations. *Med. Sci. Educ.* **2020**, *30*, 1321–1329. [CrossRef]
63. Mendonca, D.; Deraje, V.; Gujjalanavar, R.; Gopal, S. Case Series of Three-Dimensional Printing Technology Applied in Complex Craniofacial Deformity Surgery. *J. Cleft Lip Palate Craniofac. Anomal.* **2016**, *3*, 88. [CrossRef]
64. Ponomarenko, M.; Ieremeiev, O.; Lukin, V.; Egiazarian, K. An Expandable Image Database for Evaluation of Full-Reference Image Visual Quality Metrics. *Electron. Imaging* **2020**, *2020*, 137-1–137-6. [CrossRef]
65. Azer, S.A.; Azer, S. 3D Anatomy Models and Impact on Learning: A Review of the Quality of the Literature. *Health Prof. Educ.* **2016**, *2*, 80–98. [CrossRef]
66. Peeler, J.; Bergen, H.; Bulow, A. Musculoskeletal Anatomy Education: Evaluating the Influence of Different Teaching and Learning Activities on Medical Students Perception and Academic Performance. *Ann. Anat. Anat. Anz.* **2018**, *219*, 44–50. [CrossRef] [PubMed]
67. Kim, J.W.; Lee, Y.; Seo, J.; Park, J.H.; Seo, Y.M.; Kim, S.S.; Shon, H.C. Clinical Experience with Three-Dimensional Printing Techniques in Orthopedic Trauma. *J. Orthop. Sci.* **2018**, *23*, 383–388. [CrossRef]
68. Ben Awadh, A.; Clark, J.; Clowry, G.; Keenan, I.D. Multimodal Three-Dimensional Visualization Enhances Novice Learner Interpretation of Basic Cross-Sectional Anatomy. *Anat. Sci. Educ.* **2021**, ase.2045. [CrossRef] [PubMed]
69. Çeri, N.G. Effect of Non-Cadaveric Methods on the Anatomy Education of Medical Students. *Meandros* **2021**, *22*, 105–115. [CrossRef]
70. Hoyek, N.; Rienzo, F.D.; Guillot, A.; Collet, C. The Role of Mental and Motor Processes in Conceiving, Developing and Validating 3D Interactive Human Anatomy Learning Tools. *FASEB J.* **2020**, *34* (Suppl. S1), 1. [CrossRef]
71. Bücking, T.M.; Hill, E.R.; Robertson, J.L.; Maneas, E.; Plumb, A.A.; Nikitichev, D.I. From Medical Imaging Data to 3D Printed Anatomical Models. *PLoS ONE* **2017**, *12*, e0178540. [CrossRef]
72. Flaxman, T.E.; Cooke, C.M.; Miguel, O.X.; Sheikh, A.M.; Singh, S.S. A Review and Guide to Creating Patient Specific 3D Printed Anatomical Models from MRI for Benign Gynecologic Surgery. *3D Print. Med.* **2021**, *7*, 17. [CrossRef] [PubMed]
73. Byrne, N.; Velasco Forte, M.; Tandon, A.; Valverde, I.; Hussain, T. A Systematic Review of Image Segmentation Methodology, Used in the Additive Manufacture of Patient-Specific 3D Printed Models of the Cardiovascular System. *JRSM Cardiovasc. Dis.* **2016**, *5*, 204800401664546. [CrossRef] [PubMed]

2md Publication

education sciences

MDPI

Article

Facilitating Student Understanding through Incorporating Digital Images and 3D-Printed Models in a Human Anatomy Course

Dzintra Kazoka *, Mara Pilmane and Edgars Edelmers

Institute of Anatomy and Anthropology, Rīga Stradiņš University, LV-1007 Riga, Latvia; Mara.Pilmane@rsu.lv (M.P.); Edgars.Edelmers@rsu.lv (E.E.)
* Correspondence: Dzintra.Kazoka@rsu.lv

Abstract: Combining classical educational methods with interactive three-dimensional (3D) visualization technology has great power to support and provide students with a unique opportunity to use them in the study process, training, and/or simulation of different medical procedures in terms of a Human Anatomy course. In 2016, Rīga Stradiņš University (RSU) offered students the 3D Virtual Dissection Table "Anatomage" with possibilities of virtual dissection and digital images at the Department of Morphology. The first 3D models were printed in 2018 and a new printing course was integrated into the Human Anatomy curriculum. This study was focused on the interaction of students with digital images, 3D models, and their combinations. The incorporation and use of digital technologies offered students great tools for their creativity, increased the level of knowledge and skills, and gave them a possibility to study human body structures and to develop relationships between basic and clinical studies.

Keywords: human anatomy; digital images; printed models; students; learning; perspectives

Citation: Kazoka, D.; Pilmane, M.; Edelmers, E. Facilitating Student Understanding through Incorporating Digital Images and 3D-Printed Models in a Human Anatomy Course. *Educ. Sci.* **2021**, *11*, 380. https://doi.org/10.3390/educsci11080380

Academic Editors: Jon Mason, Christian M. Stracke, Daniel Burgos, Cleo Sgouropoulou and Jin Gon Shon

Received: 29 June 2021
Accepted: 22 July 2021
Published: 26 July 2021

1. Introduction

A variety of methods and models are typically required when addressing educational challenges [1]. Some authors underline that higher education institutions with their various roles and responsibilities can make a significant impact on the advancement of Sustainable Development (SD) [2,3]. Moreover, the nature of SD is complicated and multidisciplinary at many levels. Education for sustainability is described by different models and ways. Higher education should support students in developing their capacity for recognizing and understanding the complexity of sustainability issues [4].

Nowadays, political, economic, and social situations, facing the changes described below, make the issues of SD more pressing than before [5]. Thus, sustainability is compared to a never-ending staircase that step-by-step must be moved in the right direction [6]. According to this, we need special skills and a relevant attitude for the transformation of our knowledge-centered education into the educational process that is based on our experience.

In the last years, the institutions of higher education have been experiencing a lot of changes in classical teaching and learning methods, induced by modern technologies, socio-economic trends, and situations. Development and incorporation of 3D digital technologies into the Human Anatomy course at Rīga Stradiņš University (RSU) has led to great results of current students' level of knowledge, skills, as well as their performance. By studying anatomy, students learn not only about the general structures and composition of the human body, but it also provides the basics for understanding clinical subjects. The best methods of teaching and learning anatomy are still widely debated, but some innovations represent general trends in this direction [7–9]. Nevertheless, Human Anatomy is one of the main study subjects for all medical professionals. In addition to known

traditional methods such as dissections, lectures, and practical labs, a lot of digital images and new three-dimensional-printed (3Dp) models have been incorporated at the Department of Morphology in RSU. In 2016, students were offered the 3D Virtual Dissection Table "Anatomage" with possibilities of virtual dissection and digital images. The first 3D models were printed in 2018 and a new printing course was integrated into the Human Anatomy curriculum.

In this article, we describe the materials and methods that were incorporated in our educational process and highlight that these tools can be perspective elements of SD. We also underline that medical education must be a part of education on sustainability.

Section 2.1 of this article provides an overview of the digital images and 3Dp models' roles and challenges that have been published in the literature. Two following subsections will look at how some of the digital images and 3Dp models are used by educators and students in the Human Anatomy course at the Department of Morphology. The third section will focus on the materials and methods of this study. The fourth section shows the results of this study. The next section introduces some discussions about digital tools in the educational process. Finally, the sixth section concludes with some directions and trends for the future role of digital images and 3Dp models in teaching and learning.

2. Background

2.1. Roles of Digital Images and 3Dp Models

2.1.1. Digital Images

The Human Anatomy course in medical education includes different methods and tools, each with different teaching and learning goals [10]. In our experience, these tools include lectures, practical labs, and real and/or virtual dissections. Practical labs include different topics of study about the human body, where theory from lectures is combined with information from anatomical textbooks, electronic sources, and specially prepared cadaveric materials.

There are many benefits to using digital images or virtual human anatomy in comparison with traditional anatomical studies [11]. Digital images and cross-sections are of high quality and rich content. It is clear that dissections are often time-demanding in terms of preparing hours of the human body. With virtual dissection and digital images, where all of the images can be displayed on a screen simultaneously, the study process can be more compact in comparison with traditional dissection. Digital images can be easily stored on a computer disk.

If the current trends continue, the incorporation of virtual dissection and digital images will make the teaching and learning process more interesting, active, and creative [12].

Moreover, these tools have also been shown to develop students' and/or educators' cooperation and communication, and improve student–educator interactions [13]. However, some students still find traditional methods and real dissection crucial for them in the study process.

2.1.2. 3Dp Models

According to the technique of 3Dp, including digital images, many fields of life have started to develop and improve in ways that we never imagined up to now [14,15]. Medical education, as one of those, has kept with the times, and during recent years, there have been new possibilities and trends created for the modern study process [16]. One of the major directions is a combination of classical, traditional teaching methods with currently popular methods. In the Human Anatomy course, the use of digital images and 3Dp models have been appreciated by educators and students since they were implemented in the lectures and practical labs. Both of them are effective and very beneficial tools for teaching anatomy to students [17,18].

During recent years, the development of 3Dp and the use of printed products have been growing at a progressive rate for many different specialists, companies, governments,

schools, and universities [19]. Every year, in the medical field, 3Dp and new possibilities help to save and/or change the lives of people [20,21].

There exist special plans about investment into preparing educators in the basics of 3Dp for different educational institutions in the future [22]. However, still, only a few schools and universities use 3Dp as an educational tool across the world [23,24]. Additionally, educators have to detect, through their communication with students, what kind of methods and used materials work best for them. Now, with the new challenges of study courses arising, it will be very likely to see medical educators using 3Dp and digital images on a daily basis.

3Dp technology is still growing in popularity and use in everyday life. In the education sector, it is very important to invest money into 3D technologies and teaching personnel as that is the most effective way to develop the study process [25]. There are many possibilities for using 3Dp to create anatomical models for students. There is no doubt that in the next few years, we will see how useful this technology can be for the rapid development of knowledge and skills of students in the Human Anatomy course. This is a great possibility to study the human body in a step-by-step manner, including structures on micro- and macro-levels.

It is clear that 3Dp can be used in conjunction with different methods and materials, mostly because of the costs, for several advantages. One of the major advantages is the preparation of anatomical models for regular lectures and practical labs. Based on the creation of solid objects layer-by-layer, students can study normal anatomy and/or several variations, defects, and congenital diseases not only in one organ but also in complex organs or systems, and using this information, they can gain a better understanding about their relationships within the human body.

According to this, students can plan different methods of treatment at the clinical level and consider applying to clinical courses during their studies. This involves training before any procedure, surgery, or patient care. It provides the possibility to combine anatomical knowledge and skills with practical experience. There is no doubt that these accurate 3D anatomical models with the possibility to see anatomical structures from different angles improve practical skills in terms of different procedures [26,27].

3Dp models have a great significance for medical specialists for various approaches, experience, and methods. 3Dp models can be used before real treatment or during the process. They can shorten the time of treatment significantly, provide more positive results, and improve the outcome of any procedure. In addition, 3Dp technology and models are capable of visualizing complex structures for substitution of them from high-resolution Computer Tomography (CT) images. This process allows to prepare different anatomical structures and/or organs in special sizes, with accurate details and many copies, and it is a great advantage for study and training processes.

2.2. Accessibility of Digital Images and 3Dp Models

2.2.1. Teaching/Learning Environments with Digital Images

The Human Anatomy course is under a digital revolution enabled by virtual dissection. Several publications show that "Anatomage" table-based education has proven to be effective [28,29]. Virtual Dissection Table "Anatomage" (developed by a 3D medical technology company located in San José (California) in conjunction with Stanford University's Clinical Anatomy Division) is one of the most advanced visualization systems that is used as an instrument in anatomy education [30].

Dissection Table is a computerized table that allows students and educators to visualize anatomical structures exactly as they would on a fresh cadaver. All digital images are taken from real cadavers, which are frozen and cut into sections to allow for virtual dissection and reconstruction of the human body. Students can follow the instructions of the educators and study the parts, structures, and details that are located in different regions of the human body. There are a lot of possibilities to cut in different places and

directions, and to combine the view at one level with a view of structures in other levels and planes.

This computerized full-size human body table offers the possibilities to use and study high-speed and high-resolution digital cross-sections, X-rays, CT scans, ultrasound, and MRI images in a format that allows them to be viewed by students and educators on a fully interactive touch screen. Students and educators are enabled to quickly find answers to any anatomy structures through thousands of annotations, use drawing and dissection tools, and adding and removing special medical devices.

The digital library of the "Anatomage" can be used for the study of cases and pathologies of human or veterinary anatomy (Figure 1).

Figure 1. Prepared Virtual Dissection Table "Anatomage" with opened digital library in the practical lab.

The "Anatomage" Table is a very powerful tool for the educators and students in our department. Based on our experience, an increase in working activities of students with "Anatomage" showed an increase in their results of tests, colloquiums, and exam scores. Some students used the accurate details and rich content of this technology for their scientific activities and projects. The "Anatomage" Table can be used for training of residency, clinical staff, and skills training, pre- and post-surgical planning, as well as the development of collaboration between medical specialists.

2.2.2. Teaching/Learning Environments with 3Dp Models

There are two ways of incorporating teaching tools such as 3D models in the education process. One of them is to order and buy them from specialist companies that produce these models [31].

The second way of obtaining educational 3D models is to create them on site, where is it is possible to adapt models for the needs of educators and students in specific educational institutions [32–34]. It is possible with access to 3D printers, some of which are safe and relatively easy to use for students and educators. Additionally, students find 3Dp very useful, interesting, and modern, and a creative way to learn human anatomy.

Printing files are publicly available from different free and open sources on the Internet. Some files can be downloaded and printed directly, while some 3D objects can be modified before printing. According to the preparation of 3D anatomical models, the dualization can be adjusted, and it is also possible to add or remove different anatomical structures from the final model. The possibility to use different materials during the printing process of anatomical modes makes a regular study of the human body more effective. Materials for 3D printing such as PLA (polylactic acid) are the easiest to use (especially for beginners), and this material is relatively cheap. It is clear that there exist many possibilities for printing time reduction. Some detailed models can be printed in a few minutes, while others require many hours to finish only one model. Fast printed models are useful for educators to better explain some anatomical structures, without any additional tools. More expensive materials can be useful for the printing of more complex structures of the human body [35].

The possibility to use the 3Dp method provides a lot of different benefits in the Human Anatomy course. Apart from medical plastic models that could be used daily in educators'

work, students can work on creating their 3D anatomical models for personal use during their practical lab.

However, more research needs to be performed measuring the effectiveness of the 3D model's incorporation into the anatomy teaching processes and on assessment of the level of knowledge and skills of students. Young people will be able to precisely describe the quality of their model, its conditions, and develop an understanding of problems that can affect structures of the organs inside the human body. After acquiring such knowledge, students will be able to develop further steps for modification of their created models or to solve different clinical problems regarding a patient's treatment.

2.3. Creation of Anatomical Models

There exist different strategies for creating 3D anatomical models [36,37]. Structures, shapes, and sizes of models can be prepared manually by using computer software.

However, it is up to the educators and/or students how detailed these models should be. For example, when creating a bone model, we could decide only to present the actual structures without any attachment places of muscles, or we could choose for the model to be more detailed and display major muscles on bone surfaces. A more complicated way of preparing realistic and highly detailed anatomical models is creating models from radiological medical images with the help of the computer segmentation technique, which allows identification of any anatomical structures and their variations, pathological processes, and conditions of separate organs. For this reason, for creating 3D models in our practical labs, we use medical digital images with the help of CT (Computed Tomography) and MRI (Magnetic Resonance Imaging) techniques.

Structures are identified and prepared step-by-step for segmentation with the help of specialized computer software, and afterward, they are converted into a special 3D file format, such as stereolithographic (STL) or OBJ file format. Created models can be printed in different sizes with different levels of detail [38]. It is clear that in medicine, a few millimeters can be very important in some cases.

This can provide a deeper understanding for students and our future specialists about structures and their conditions in the human body. Additionally, during lectures and practical labs, qualified educators can use real, increased, or decreased in size 3Dp models and combine their own or students' knowledge and skills for exploration of anatomy during other basic study courses, such as embryology, histology, physiology, chemistry, and biology. These topics can be separated into several systems of the body: skeletal, muscular, respiratory, digestive, urinary, genital, nervous, circulatory, endocrine and immune, and sense organs.

According to our experience, the easiest system for 3Dp anatomical models is the skeletal system. Some bones and their structures are simple, and students can prepare these models very easily. Moreover, in the creation process of these models, the cross-sections and segmentation from any of the medical images can be used. Nonetheless, 3Dp technology can provide a lot of new options and possibilities, such as printing single bones or several bones in different sizes.

When students would like to try to prepare more complicated models, they can choose to print models from the muscular system. There are different possibilities, for example students can separate muscles one by one, or combine them into groups.

At the end of the first semester of the first study year, some of the students prepare for printing combinations of the bones together with muscles.

When it comes to the other systems of organs, students are able to prepare and print 3D models of the heart, brain, kidneys, or some specific structures that can be used for a better understanding of their location and functions. In later study semesters, some students come back to the 3Dp process, but in these cases, students have a strong motivation to prepare and print more complicated and specific things. At the Department of Morphology exists the possibility to study and obtain knowledge about bioprinting, a field of medicine

that offers new ways to use human cells to print tissues, organs, or any other structures for research purposes.

3D models can help students' understanding and evaluation of health status and risk factors, including pain location and irradiation, injuries, traumas, primary or secondary developed processes, variations, and levels of damages.

3. Materials and Methods

3.1. Participants and First Practical Procedures

This study was a small-scale study focusing on anatomy education processes, and it was conducted at the Department of Morphology, RSU, in Latvia. The department provides general education requirements for basic study as well as a few specific study courses. The study was carried out based on the Human Anatomy course that is compulsory and is taken by all students. For the time being, several modern, digital methods are implemented in our medical study courses, which are based on traditional as well as innovative educational models.

This study includes information about students' knowledge and skills, regarding the incorporation of new educational instruments which are related to sustainable education.

Therefore, this study aimed to incorporate and use digital images and 3Dp models as innovative tools for medical students. Additionally, one of the objectives was to determine the level of knowledge and skills for students' improvement and perspectives on SD.

In 2019–2020, 250 students of the first study year at the Faculty of Medicine, RSU, were included in this study. The mean age of participants ranged from 18 to 25 years. We chose this group because 3D printing is only part of the anatomy course at the beginning of studies at the Faculty of Medicine. There were no other students, study years, or Faculties with this option.

The selection of students was based on an open and voluntary invitation, and the study did not include any tests of significant importance on the subjects involved. According to this, the study did not require the Ethical committees' permission. The participants were informed about their right to opt out from the study at any time. To ensure confidentiality and anonymity, the principle of secrecy was preserved. Besides this, the gathered data were intended for the purposes of this study.

In practical labs, educators used teacher- and student-centered methods.

Our selected students used 3D tools such as digital images and 3Dp models that were supported for learning about anatomy. All students were instructed on how to use the digital images and how to work with 3D printers to create models.

Students learned to identify several anatomical structures in digital images using the 3D Virtual Dissection Table "Anatomage" (USA). More than 100 cross-sections were used and studied from 4 prepared specimens of the "Anatomage" (Table Application software from Anatomage, Inc. (Table EDU 6.0)) database for 4 male and female cadavers, and over 50 clinical cases from a digital library with a variety of visualization options (X-rays, CT, MRI, etc.) of the body.

The basic procedures for the anatomical 3Dp model creation consisted of the following steps: introduction to 3Dp technology, an overview of 3D printing materials, preparation for the creation and downloading of the 3D file of the model, modeling, printing, and post-processing. We used 4 Fused Filament Fabrication (FFF) printers, and all anatomical models were produced using 2 "Prusa i3 MK2" (Prusa Research) and 2 "Ultimaker S5" 3D printers.

3.2. Data Collection Tool and Analysis

For gathering information, we used interviews as a qualitative data collection tool [39,40]. The open-ended questions were designed for the needs of this study to find out about students' experiences (self-assessment) using digital images and 3Dp models, their perspectives for a level of knowledge, and skills after taking this course. Students answered these questions at the end of the practical lab. In the beginning, four structured

questions were asked: Q1: What did you study during the course? Q2: What did you study from digital images and 3Dp models? Q3: How did you solve the problems or complicated situations during that time? Q4: How will the tools that you used help you in the future? At the end of the interview, a fifth question was asked: Q5: How satisfied were you with the use of the 3D tools during the course?

All answers were recorded and transcribed by one educator of the Human Anatomy course. Afterward, the data were processed, coded, and analyzed using content analysis [41,42]. Coding categories were derived directly from the answers. Categories were grouped into subcategories. In order to provide internal validity of the qualitative study, the texts of the interviews, codes, and reproduced categories were evaluated by the first author.

The data acquired were expressed with numbers and percentages. The approach used in this analysis was conventional [43].

Lastly, we also used content analysis of qualitative interview data, by categorizing and interpreting the data for assessing the level of participants' satisfaction with the use of the 3D tools (digital images and 3Dp models) in the study course.

4. Results

In this section, we present the results of the study, aiming to answer the 4 questions mentioned above (Table 1).

Table 1. Students' answers to the 4 study questions in the Human Anatomy course.

Question	Attitudes and Views	Number of Students and %
What did you study during the course?	anatomical terminology	24 (10%)
	basic structures	5 (2%)
	functions of structures	25 (10%)
	location of structures and organs	21 (8.4%)
	topography	30 (12%)
	radiological anatomy	15 (6%)
	3D visualizations of the structures	40 (16%)
	using 3Dp models and their creation	35 (14%)
	work in groups, teams	10 (4%)
	gross anatomy (dissection)	45 (18%)
What did you study from the digital images and 3Dp models?	more interesting learning and education	25 (10%)
	relationships between structures	15 (6%)
	analysis of clinical cases	30 (12%)
	virtual dissection	45 (18%)
	different variations and/or abnormalities	37 (14.8%)
	more deep understanding of anatomy	48 (19.2%)
	several simulations of clinical procedures	10 (4%)
	basics for clinical studies	20 (8%)
	overview of knowledge and skills	13 (5.2%)
	the use of correct anatomical terminology	7 (2.8%)
How did you solve the problems or complicated situations during that time?	including more visual aids	67 (26.8%)
	repeating material	52 (20.8%)
	help from classmates and educator	48 (19.2%)
	using more time, moving slower	32 (12.8%)
	using basic concepts	41 (16.4%)
	simplification of the information	10 (4%)

Table 1. *Cont.*

Question	Attitudes and Views	Number of Students and %
How will the tools that you used help you in the future?	importance of anatomy for clinical studies	65 (26%)
	training of some procedures	37 (14.8%)
	relationship between basic and clinical study subjects	70 (28%)
	basics for scientific work	13 (5.2%)
	improving clinical skills	18 (7.2%)
	success in tests, exams	47 (18.8%)

For the question "What did you study during the course?", 45 out of 250 (18%) students answered that they studied gross anatomy (dissections) and 3D visualizations of the structures (40, or 16%), followed by the use of 3Dp models (35 or 14%), while 5 out of 250 (2%) students answered that they studied only basic structures.

The question "What did you study from digital images and 3Dp models?" was asked to students, and 48 (19.2%) out of 250 students answered that they studied a deeper understanding of human anatomy, while 45 (18%) students indicated virtual dissection, followed by different variations/abnormalities (37 or 14.8%). Only 7 (2.8%) students mentioned the use of correct terminology in this question.

Regarding the question "How did you solve the problems or complicated situations during that time?", 67 (26.8%) students stated using more visual aids and 52 (20.8%) students used repeating of material. Using more time and moving slower were solutions for 32 (12.8%) students. Very few students (10, or 4%) indicated that they used a simplification of information.

Finally, for the question "How will the tools that you used help you in the future?", the answers varied from ideas about the relationship between basic and clinical study subjects (70, or 28%), the importance of anatomy for clinical studies (65, or 26%), and success on tests, exams (47, or 18.8%). For 13 (5.2%) students, these tools were indicated as related to scientific work.

It was discovered that the students were satisfied with the 3D tools that were used for their teaching during the course (Table 2).

Table 2. The satisfaction of students with the 3D tools used in the study course.

The Use of 3D Tools for Students' Satisfaction	Number of Students and %
reproduce taught/learned knowledge and skills	46 (18.4%)
increase motivation and intensity for learning	51 (20.4%)
develop knowledge and skills relevant to clinical needs	48 (19.2%)
improve their thinking and solution of problems with understanding of structures of the human body	28 (11.2%)
prepare for the assessment of knowledge and skills	42 (16.8%)
provide a good background for the future	35 (14%)

The majority (51, or 20.4%) of students were stimulated and motivated to learn more materials and felt that this course was more intensive through the use of digital images and 3Dp models during these activities (Figure 2).

Figure 2. A few 3Dp models of the human skeletal system from plastic materials and in different sizes.

5. Discussion

Today, some classical educational methods are replaced, transformed, or modified by multiple digital technologies [44–46].

In the Human Anatomy course, dissection has been the primary teaching tool for a long time at RSU. With recent scientific progress, a lot of created technological innovations and their possibilities have developed new trends in medical education and led to curriculum changes. Nowadays, in our department and laboratory, we underline the fundamental necessity of cadaveric dissection and continuation of it for the future in combination with new and modern directions. We consider that students and tutors should use both traditional and progressive technological tools for anatomy education, theoretical knowledge, and practical skills. In this article, we analyzed the role of perspectives of digital images and 3Dp models, but we did not exclude or replace dissection from the anatomy curriculum. We also note that anatomy teaching excluded dissections in the time of COVID-19. To support the students and continue the teaching and learning processes of human anatomy in this situation, we implemented and used different digital tools and 3Dp models.

The transition from traditional anatomy to virtual anatomy presents certain challenges for both educators and students, and the methods of preparing and delivering the topics of lectures or practical labs change. Contents of lectures and practical labs can be prepared by educators, and students can learn all study materials at home on a personal computer. The accessibility of digital images makes it easier to present them in seminars, conferences, scientific works, and other activities, including the use of these tools in the distant education process. Finally, digital images can be utilized in other study courses and incorporated into online study platforms. In this new digital age, all parts of information and/or sources transform into digital language and format. Nowadays, a lot of educational resources are available in digital format and computers occupy a central place in the teaching and learning process [47–49]. Each institution and department have their own educational methods [50]. Some authors state that students must better understand the environments of their intended professions [51,52]. Educators should promote the students to understand their roles in SD and, according to this, collaborate in multi-disciplinary ways to share knowledge [53,54].

With increasing numbers of students, there is an increase in the need for different methods, materials, and resources. New methods of the educational process in the anatomy field have faced numerous challenges to their incorporation and widespread implementation. Different authors have written about curricular changes in the anatomical courses, many of which directly underlined the need to move away from the traditional educational styles [55,56]. Several authors described a re-thinking about how education should be implemented nowadays; however, they indicated to transition to more student-centered teaching [57,58].

Modern didactic processes should enable the use of different forms of teaching, and according to this, there is a need to revise the existing guidelines of the educational process. Teaching applies modern didactic methods. It is proposed that multi-methods are recommended for the modern medical anatomy study processes [59]. Different teaching

techniques can be combined into Human Anatomy courses, depending on what teaching effects we expect. Nowadays, possibilities for the use of 3D tools may lead to better learning outcomes with more active roles for students during these types of practical labs. In our study process, active practical labs were perceived by students and educators as an effective study process.

Our traditional teaching methods include lectures, video lectures, practical labs, e-studies, cadaveric dissection, and anatomical models. Approaches concerning topographical anatomy are also included in the teaching/learning course, while digital simulation tools such as Virtual Dissection "Anatomage" Table and digital images are also used as major educational instruments. Highly accurate 3Dp models such as visual and interactive aids concerning normal and abnormal structures are used in the Human Anatomy study course, providing educational processes, clinical discussions, and training in some medical procedures.

All 3Dp models and digital images represent special anatomical information. According to this, an analysis of each structure and detail was very interesting from the detection of students' knowledge and skills points of view.

The assessment process of the use of new innovations by students provides an opportunity to identify and address any field in which improvement may be made and to identify those directions that reflect effective educational practice in the Human Anatomy course. Evaluation of any innovations or changes in the study curriculum or teaching methods from the perspectives of the educators is very important for the development of the educational environment. In addition, in the education system, satisfaction of students is an indicator of the quality. The assessment of the current possibilities in Human Anatomy course education must provide educators with periodic information in order to continue, change, or correct the learning process accordingly. However, it is understood from various studies on teaching methodologies that the proper utilization of newer technologies along with the traditional teaching methods will certainly lead to better understanding of Human Anatomy and will eventually improve students' performance.

The satisfaction of students with the use of 3D tools in the learning of Human Anatomy is demonstrated in several studies, though with some differences between them [60,61]. Students highly agreed that these tools helped them improve their ability to better study the Human Anatomy course and to develop their level of knowledge and skills for other basic and clinical studies. Students ranked teaching/learning with the use of digital images and 3Dp models as some of the best methods for understanding topics. Digitalization of different educational materials has a considerable impact on the environment in which medical students learn [62].

Thanks to advancements in technologies, 3D products have achieved great progress with new directions [63]. At present, the incorporation of digital images and 3D anatomical models into the Human Anatomy course offers new opportunities and possibilities for students and educators, for creative, innovative teaching/learning, and for increasing students' results in their knowledge and skills. The assessment of the effectiveness of the anatomical education process is multi-factorial. As established by several studies, students' obtainment of knowledge in the short-term and long-term retention must be evaluated [64,65].

It is widely mentioned that the use and role of medical images has increased drastically during recent years [66,67]. Medical education has rapidly upgraded under the influence of various factors, including this forced down-time during the COVID-19 pandemic [68]. According to the current needs, technologies have facilitated anatomists to develop several digital and creative solutions. It is a vital step to prepare the educators and students to cope with the modern technological innovations [69]. The world of anatomists has been disrupted by COVID-19, and these disruptions require that educators reimagine their role [70]. Virtual anatomy education is the only way to continue learning and teaching processes in the current pandemic situation [71].

Digital images and 3Dp models allow students to work on any topic in groups, create and exchange ideas between each other and the educator, and increase knowledge and show better results in a short period of time. Digital technologies with different possibilities help students and educators to reduce paperwork, developing new possibilities in the study process [72,73]. According to the literature sources, the technologies should also develop communication skills and logical thinking, including improvement of competencies [74,75]. In summary, we observed that this study can lead to modern anatomical education for SD.

6. Conclusions

There exist several directions and strategies that can develop the teaching and learning of the Anatomy course now and in the future. The usage of digital images and 3Dp models is becoming not only just a tool for anatomical lectures and practical labs, but it is also widely used by students in clinical studies. In the near future, these tools will be incorporated not only in the Human Anatomy curriculum but also in other courses requiring anatomical knowledge, as a new digital revolution in the educational sphere is approaching, changing the way that new things are learned and new skills are obtained.

During the 3D course, all of these challenges are related to SD, but more work is required to learn how to continue to improve SD skills in students' education environment.

Author Contributions: Conceptualization, D.K. and M.P.; methodology, D.K. and M.P.; investigation, D.K. and E.E.; writing—original draft preparation, D.K.; writing—review and editing, D.K., M.P. and E.E. All authors have read and agreed to the published version of the manuscript.

Funding: This research received no external funding.

Institutional Review Board Statement: Not applicable.

Informed Consent Statement: Informed Consent was obtained from all subjects involved in the study.

Data Availability Statement: Data are contained within the article.

Acknowledgments: The authors are grateful to medical students of the Human Anatomy course for participating in this study and for the help, support, and guidance of the team of educators of 3Dp at the Department of Morphology.

Conflicts of Interest: The authors declare no conflict of interest.

References

1. Mahlow, C.; Hediger, A. Digital Transformation in Higher Education—Buzzword or Opportunity? *eLearn* **2019**, *5*. [CrossRef]
2. Abad-Segura, E.; Cortés-García, F.J.; Belmonte-Ureña, L.J. The Sustainable Approach to Corporate Social Responsibility: A Global Analysis and Future Trends. *Sustainability* **2019**, *11*, 5382. [CrossRef]
3. Bell, S.; Douce, C.; Caeiro, S.; Teixeira, A.; Martín-Aranda, R.; Otto, D. Sustainability and Distance Learning: A Diverse European Experience? *Open Learn. J. Open Distance e-Learn.* **2017**, *32*, 95–102. [CrossRef]
4. Nölting, B.; Molitor, H.; Reimann, J.; Skroblin, J.-H.; Dembski, N. Transfer for Sustainable Development at Higher Education Institutions-Untapped Potential for Education for Sustainable Development and for Societal Transformation. *Sustainability* **2020**, *12*, 2925. [CrossRef]
5. Portuguez Castro, M.; Gómez Zermeño, M.G. Challenge Based Learning: Innovative Pedagogy for Sustainability through e-Learning in Higher Education. *Sustainability* **2020**, *12*, 4063. [CrossRef]
6. Hasan, S.M.; Khan, E.A.; Nabi, M.N.U. Entrepreneurial Education at University Level and Entrepreneurship Development. *Educ. Train.* **2017**, *59*, 888–906. [CrossRef]
7. Jeyakumar, A.; Dissanayake, B.; Dissabandara, L. Dissection in the Modern Medical Curriculum: An Exploration into Student Perception and Adaptions for the Future. *Anat. Sci. Educ.* **2020**, *13*, 366–380. [CrossRef]
8. Memon, I. Cadaver Dissection Is Obsolete in Medical Training! A Misinterpreted Notion. *Med. Princ. Pract.* **2018**, *27*, 201–210. [CrossRef]
9. Garas, M.; Vaccarezza, M.; Newland, G.; McVay-Doornbusch, K.; Hasani, J. 3D-Printed Specimens as a Valuable Tool in Anatomy Education: A Pilot Study. *Ann. Anat. Anat. Anz.* **2018**, *219*, 57–64. [CrossRef]
10. Fasel, J.H.D.; Aguiar, D.; Kiss-Bodolay, D.; Montet, X.; Kalangos, A.; Stimec, B.V.; Ratib, O. Adapting Anatomy Teaching to Surgical Trends: A Combination of Classical Dissection, Medical Imaging, and 3D-Printing Technologies. *Surg. Radiol. Anat.* **2016**, *38*, 361–367. [CrossRef]

11. Martín, J.G. Possibilities for the Use of Anatomage (the Anatomical Real Body-Size Table) for Teaching and Learning Anatomy with the Students. *Biomed. J. Sci. Tech. Res.* **2018**, *4*. [CrossRef]
12. Bücking, T.M.; Hill, E.R.; Robertson, J.L.; Maneas, E.; Plumb, A.A.; Nikitichev, D.I. From Medical Imaging Data to 3D Printed Anatomical Models. *PLoS ONE* **2017**, *12*, e0178540. [CrossRef] [PubMed]
13. Yakunina, G.E. Research of Digital Communications Models within Organizations and at the State Level in the Countries-Leaders in the Use of Digital Communication Technologies. *E-Management* **2020**, *2*, 41–50. [CrossRef]
14. Lee, J.-Y.; An, J.; Chua, C.K. Fundamentals and Applications of 3D Printing for Novel Materials. *Appl. Mater. Today* **2017**, *7*, 120–133. [CrossRef]
15. Jamróz, W.; Szafraniec, J.; Kurek, M.; Jachowicz, R. 3D Printing in Pharmaceutical and Medical Applications—Recent Achievements and Challenges. *Pharm. Res.* **2018**, *35*, 176. [CrossRef] [PubMed]
16. Yuen, J. What Is the Role of 3D Printing in Undergraduate Anatomy Education? A Scoping Review of Current Literature and Recommendations. *Med. Sci. Educ.* **2020**, *30*, 1321–1329. [CrossRef]
17. Backhouse, S.; Taylor, D.; Armitage, J.A. Is This Mine to Keep? Three-dimensional Printing Enables Active, Personalized Learning in Anatomy. *Anat. Sci. Educ.* **2019**, *12*, 518–528. [CrossRef]
18. Dee, E.C.; Alty, I.G.; Agolia, J.P.; Torres-Quinones, C.; Houten, T.; Stearns, D.A.; Lillehei, C.W.; Shamberger, R.C. A Surgical View of Anatomy: Perspectives from Students and Instructors. *Anat. Sci. Educ.* **2021**, *14*, 110–116. [CrossRef]
19. Verner, I.; Merksamer, A. Digital Design and 3D Printing in Technology Teacher Education. *Procedia CIRP* **2015**, *36*, 182–186. [CrossRef]
20. Lee, N. The Lancet Technology: 3D Printing for Instruments, Models, and Organs? *Lancet* **2016**, *388*, 1368. [CrossRef]
21. Marconi, S.; Pugliese, L.; Botti, M.; Peri, A.; Cavazzi, E.; Latteri, S.; Auricchio, F.; Pietrabissa, A. Value of 3D Printing for the Comprehension of Surgical Anatomy. *Surg. Endosc.* **2017**, *31*, 4102–4110. [CrossRef] [PubMed]
22. Abou Hashem, Y.; Dayal, M.; Savanah, S.; Štrkalj, G. The Application of 3D Printing in Anatomy Education. *Med. Educ. Online* **2015**, *20*, 29847. [CrossRef]
23. Smith, C.F.; Tollemache, N.; Covill, D.; Johnston, M. Take Away Body Parts! An Investigation into the Use of 3D-Printed Anatomical Models in Undergraduate Anatomy Education. *Am. Assoc. Anat.* **2018**, *11*, 44–53. [CrossRef] [PubMed]
24. Balestrini, C.; Campo-Celaya, T. With the Advent of Domestic 3-Dimensional (3D) Printers and Their Associated Reduced Cost, Is It Now Time for Every Medical School to Have Their Own 3D Printer? *Med. Teach.* **2016**, *38*, 312–313. [CrossRef] [PubMed]
25. Garcia, J.; Yang, Z.; Mongrain, R.; Leask, R.L.; Lachapelle, K. 3D Printing Materials and Their Use in Medical Education: A Review of Current Technology and Trends for the Future. *BMJ STEL* **2018**, *4*, 27–40. [CrossRef] [PubMed]
26. Diment, L.E.; Thompson, M.S.; Bergmann, J.H.M. Clinical Efficacy and Effectiveness of 3D Printing: A Systematic Review. *BMJ Open* **2017**, *7*, e016891. [CrossRef] [PubMed]
27. Ballard, D.H.; Trace, A.P.; Ali, S.; Hodgdon, T.; Zygmont, M.E.; DeBenedectis, C.M.; Smith, S.E.; Richardson, M.L.; Patel, M.J.; Decker, S.J.; et al. Clinical Applications of 3D Printing. *Acad. Radiol.* **2018**, *25*, 52–65. [CrossRef]
28. Baratz, G.; Wilson-Delfosse, A.L.; Singelyn, B.M.; Allan, K.C.; Rieth, G.E.; Ratnaparkhi, R.; Jenks, B.P.; Carlton, C.; Freeman, B.K.; Wish-Baratz, S. Evaluating the Anatomage Table Compared to Cadaveric Dissection as a Learning Modality for Gross Anatomy. *Med. Sci. Educ.* **2019**, *29*, 499–506. [CrossRef]
29. Bharati, A.S.; Rani, V.S. A Study on Student Perception of Virtual Dissection Table (Anatomage) at GSL Medical College, Rajahmundry. *Acad. Anat. Int.* **2018**, *4*. [CrossRef]
30. Tsoucalas, G. Technology, Imaging, History and Anatomy the Future of Learning Techniques. *Biomed. J. Sci. Tech. Res.* **2018**, *8*. [CrossRef]
31. Sheth, R.; Balesh, E.R.; Zhang, Y.S.; Hirsch, J.A.; Khademhosseini, A.; Oklu, R. Three-Dimensional Printing: An Enabling Technology for IR. *J. Vasc. Interv. Radiol.* **2016**, *27*, 859–865. [CrossRef] [PubMed]
32. Lim, K.H.A.; Loo, Z.Y.; Goldie, S.J.; Adams, J.W.; McMenamin, P.G. Use of 3D Printed Models in Medical Education: A Randomized Control Trial Comparing 3D Prints versus Cadaveric Materials for Learning External Cardiac Anatomy: Use of 3D Prints in Medical Education. *Am. Assoc. Anat.* **2016**, *9*, 213–221. [CrossRef] [PubMed]
33. Kong, X.; Nie, L.; Zhang, H.; Wang, Z.; Ye, Q.; Tang, L.; Huang, W.; Li, J. Do 3D Printing Models Improve Anatomical Teaching About Hepatic Segments to Medical Students? A Randomized Controlled Study. *World J. Surg.* **2016**, *40*, 1969–1976. [CrossRef] [PubMed]
34. Li, C.; Cheung, T.F.; Fan, V.C.; Sin, K.M.; Wong, C.W.Y.; Leung, G.K.K. Applications of Three-Dimensional Printing in Surgery. *Surg. Innov.* **2017**, *24*, 82–88. [CrossRef] [PubMed]
35. Powers, M.K.; Lee, B.R.; Silberstein, J. Three-Dimensional Printing of Surgical Anatomy. *Curr. Opin. Urol.* **2016**, *26*, 283–288. [CrossRef] [PubMed]
36. Chen, S.; Pan, Z.; Wu, Y.; Gu, Z.; Li, M.; Liang, Z.; Zhu, H.; Yao, Y.; Shui, W.; Shen, Z.; et al. The Role of Three-Dimensional Printed Models of Skull in Anatomy Education: A Randomized Controlled Trail. *Sci. Rep.* **2017**, *7*, 575. [CrossRef]
37. Nath, S.I.; Anuradha, B.; Dilip, B. A Study on Making Models in Anatomy. *PIJR* **2021**, 85–87. [CrossRef]
38. Mogali, S.R.; Yeong, W.Y.; Tan, H.K.J.; Tan, G.J.S.; Abrahams, P.H.; Zary, N.; Low-Beer, N.; Ferenczi, M.A. Evaluation by Medical Students of the Educational Value of Multi-Material and Multi-Colored Three-Dimensional Printed Models of the Upper Limb for Anatomical Education: 3D Printed Upper Limb in Anatomical Education. *Am. Assoc. Anat.* **2018**, *11*, 54–64. [CrossRef]

39. Cohen, L.; Manion, L.; Morrison, K. *Research Methods in Education*, 6th ed.; Routledge: London, UK; New York, NY, USA, 2007; pp. 461–495.
40. Strauss, A.L.; Corbin, J.M. *Basics of Qualitative Research: Techniques and Procedures for Developing Grounded Theory*, 4th ed.; Sage Publications: Thousand Oaks, CA, USA, 2015; pp. 85–105.
41. Elo, S.; Kääriäinen, M.; Kanste, O.; Pölkki, T.; Utriainen, K.; Kyngäs, H. Qualitative Content Analysis: A Focus on Trustworthiness. *SAGE Open* **2014**, *4*, 215824401452263. [CrossRef]
42. Ahmady, S.; Khajeali, N.; Kalantarion, M.; Amini, M. A Qualitative Content Analysis of "Problem Students": How Can We Identify and Manage Them? *BMC Res. Notes* **2020**, *13*, 566. [CrossRef]
43. Hsieh, H.-F.; Shannon, S.E. Three Approaches to Qualitative Content Analysis. *Qual. Health Res.* **2005**, *15*, 1277–1288. [CrossRef] [PubMed]
44. Ghemawat, P. Strategies for Higher Education in the Digital Age. *Calif. Manag. Rev.* **2017**, *59*, 56–78. [CrossRef]
45. Hill, C.; Lawton, W. Universities, the Digital Divide and Global Inequality. *J. High. Educ. Policy Manag.* **2018**, *40*, 598–610. [CrossRef]
46. Beghetto, V.; Agostinis, L.; Taffarello, R.; Samiolo, R. Innovative Technology for Sustainable New Materials. *Eur. J. Sustain. Dev.* **2016**, *5*. [CrossRef]
47. Maffey, G.; Homans, H.; Banks, K.; Arts, K. Digital Technology and Human Development: A Charter for Nature Conservation. *Ambio* **2015**, *44* (Suppl. S4), 527–537. [CrossRef] [PubMed]
48. Jääskelä, P.; Häkkinen, P.; Rasku-Puttonen, H. Teacher Beliefs Regarding Learning, Pedagogy, and the Use of Technology in Higher Education. *J. Res. Technol. Educ.* **2017**, *49*, 198–211. [CrossRef]
49. Crittenden, W.F.; Biel, I.K.; Lovely, W.A. Embracing Digitalization: Student Learning and New Technologies. *J. Mark. Educ.* **2019**, *41*, 5–14. [CrossRef]
50. Mintz, K.; Tal, T. The Place of Content and Pedagogy in Shaping Sustainability Learning Outcomes in Higher Education. *Environ. Educ. Res.* **2018**, *24*, 207–229. [CrossRef]
51. González-Zamar, M.-D.; Ortiz Jiménez, L.; Sánchez Ayala, A.; Abad-Segura, E. The Impact of the University Classroom on Managing the Socio-Educational Well-Being: A Global Study. *Int. J. Environ. Res. Public Health* **2020**, *17*, 931. [CrossRef]
52. López Meneses, E.; Vázquez-Cano, E.; Jaén Martínez, A. Los Portafolios Digitales Grupales: Un Estudio Diacrónico En La Universidad Pablo Olavide (2009–2015) = The Group e-Portfolio: A Diachronic Study at University Pablo de Olavide in Spain (2009–2015). *Rev. Humanid.* **2017**, 123. [CrossRef]
53. Testov, V.A. On Some Methodological Problems of Digital Transformation of Education. *Inf. Obraz.* **2019**, 31–36. [CrossRef]
54. Hilty, L.M.; Huber, P. Motivating Students on ICT-Related Study Programs to Engage with the Subject of Sustainable Development. *Int. J. Sustain. High. Educ.* **2018**, *19*, 642–656. [CrossRef]
55. Mahmoud, A.; Bennett, M. Introducing 3-Dimensional Printing of a Human Anatomic Pathology Specimen: Potential Benefits for Undergraduate and Postgraduate Education and Anatomic Pathology Practice. *Arch. Pathol. Lab. Med.* **2015**, *139*, 1048–1051. [CrossRef]
56. Moore, C.W.; Wilson, T.D.; Rice, C.L. Digital Preservation of Anatomical Variation: 3D-Modeling of Embalmed and Plastinated Cadaveric Specimens Using UCT and MRI. *Ann. Anat. Anat. Anz.* **2017**, *209*, 69–75. [CrossRef] [PubMed]
57. Altomonte, S.; Logan, B.; Feisst, M.; Rutherford, P.; Wilson, R. Interactive and Situated Learning in Education for Sustainability. *Int. J. Sustain. High. Educ.* **2016**, *17*, 417–443. [CrossRef]
58. Takala, A.; Korhonen-Yrjänheikki, K. A Decade of Finnish Engineering Education for Sustainable Development. *Int. J. Sustain. High. Educ.* **2019**, *20*, 170–186. [CrossRef]
59. Sagun, L.; Arias, R. Digital Pathology: An Innovative Approach to Medical Education. *Philipp. J. Pathol.* **2018**, *3*, 7–11. [CrossRef]
60. Berney, S.; Bétrancourt, M.; Molinari, G.; Hoyek, N. How Spatial Abilities and Dynamic Visualizations Interplay When Learning Functional Anatomy with 3D Anatomical Models: Interplay of Spatial Ability and Dynamic Visualization. *Am. Assoc. Anat.* **2015**, *8*, 452–462. [CrossRef]
61. Hackett, M.; Proctor, M. Three-Dimensional Display Technologies for Anatomical Education: A Literature Review. *J. Sci. Educ. Technol.* **2016**, *25*, 641–654. [CrossRef]
62. Alkhowailed, M.S.; Rasheed, Z.; Shariq, A.; Elzainy, A.; El Sadik, A.; Alkhamiss, A.; Alsolai, A.M.; Alduraibi, S.K.; Alduraibi, A.; Alamro, A.; et al. Digitalization Plan in Medical Education during COVID-19 Lockdown. *Inform. Med. Unlocked* **2020**, *20*, 100432. [CrossRef]
63. Wright, N.; Wrigley, C. Broadening Design-Led Education Horizons: Conceptual Insights and Future Research Directions. *Int. J. Technol. Des. Educ.* **2019**, *29*, 1–23. [CrossRef]
64. Biberhofer, P.; Lintner, C.; Bernhardt, J.; Rieckmann, M. Facilitating Work Performance of Sustainability-Driven Entrepreneurs through Higher Education: The Relevance of Competencies, Values, Worldviews and Opportunities. *Int. J. Entrepr. Innov.* **2019**, *20*, 21–38. [CrossRef]
65. Brown, B.J.; Hanson, M.E.; Liverman, D.M.; Merideth, R.W. Global Sustainability: Toward Definition. *Environ. Manag.* **1987**, *11*, 713–719. [CrossRef]
66. Ammanuel, S.; Brown, I.; Uribe, J.; Rehani, B. Creating 3D Models from Radiologic Images for Virtual Reality Medical Education Modules. *J. Med. Syst.* **2019**, *43*, 166. [CrossRef]

67. Jang, H.W.; Oh, C.-S.; Choe, Y.H.; Jang, D.S. Use of Dynamic Images in Radiology Education: Movies of CT and MRI in the Anatomy Classroom. *Am. Assoc. Anat.* **2018**, *11*, 547–553. [CrossRef] [PubMed]
68. Byrnes, K.G.; Kiely, P.A.; Dunne, C.P.; McDermott, K.W.; Coffey, J.C. Communication, Collaboration and Contagion: "Virtualisation" of Anatomy during COVID-19. *Clin. Anat.* **2021**, *34*, 82–89. [CrossRef] [PubMed]
69. Singal, A.; Bansal, A.; Chaudhary, P.; Singh, H.; Patra, A. Anatomy Education of Medical and Dental Students during COVID-19 Pandemic: A Reality Check. *Surg. Radiol. Anat.* **2021**, *43*, 515–521. [CrossRef]
70. Sadeesh, T.; Prabavathy, G.; Ganapathy, A. Evaluation of Undergraduate Medical Students' Preference to Human Anatomy Practical Assessment Methodology: A Comparison between Online and Traditional Methods. *Surg. Radiol. Anat.* **2021**, *43*, 531–535. [CrossRef] [PubMed]
71. Jones, D.G. Anatomy in a Post-Covid-19 World: Tracing a New Trajectory. *Anat. Sci. Educ.* **2021**, *14*, 148–153. [CrossRef]
72. Frey, C.B.; Osborne, M.A. The Future of Employment: How Susceptible Are Jobs to Computerisation? *Technol. Forecast. Soc. Chang.* **2017**, *114*, 254–280. [CrossRef]
73. Hara, C.Y.N.; Aredes, N.D.A.; Fonseca, L.M.M.; de Campos Pereira Silveira, R.C.; Camargo, R.A.A.; de Goes, F.S.N. Clinical Case in Digital Technology for Nursing Students' Learning: An Integrative Review. *Nurse Educ. Today* **2016**, *38*, 119–125. [CrossRef] [PubMed]
74. Hesrcu-Kluska, R. The Interaction between Learners and Learner-Facilitator in an Online Learning Environment. *Creat. Educ.* **2019**, *10*, 1713–1730. [CrossRef]
75. Carter, J.; Bababekov, Y.J.; Majmudar, M.D. Training for Our Digital Future: A Human-Centered Design Approach to Graduate Medical Education for Aspiring Clinician-Innovators. *NPJ Digit. Med.* **2018**, *1*, 26. [CrossRef] [PubMed]

3rd Publication

applied system innovation

MDPI

Article

Different Techniques of Creating Bone Digital 3D Models from Natural Specimens

Edgars Edelmers [1,*], Dzintra Kazoka [1], Katrina Bolocko [2] and Mara Pilmane [1]

[1] Institute of Anatomy and Anthropology, Rīga Stradiņš University, LV-1010 Riga, Latvia
[2] Department of Computer Graphics and Computer Vision, Riga Technical University, LV-1048 Riga, Latvia
* Correspondence: edgars.edelmers@rsu.lv

Abstract: The choice of technique for the creation of a 3D digital human bone model from natural specimens has a critical impact on the final result and usability of the obtained model. The cornerstone factor in 3D modeling is the number of faces of polygon mesh, along with topological accuracy, as well as resolution and level of detail of the texture map. Three different techniques (3D scanning, photogrammetry, and micro-computed tomography) have been used to create a digital 3D model of the human zygomatic bone. As implementation and use of 3D models can be divided into three main categories—visualization, simulation, and physical replication to obtain a functioning model (implant or prothesis)—the obtained models have been evaluated by the density and topological accuracy of the polygonal mesh, as well as by visual appearance by inspecting the obtained texture map. The obtained data indicate that for biomedical applications and computer biomechanical simulation the most appropriate technique of 3D model obtainment is micro-computed tomography, in its turn for visualization and educational purposes, the photogrammetry technique is a more preferable choice.

Keywords: micro-CT; 3D scanning; photogrammetry; anatomy; 3D printing; 3D modeling; bone; image processing; 3D model; medicine

Citation: Edelmers, E.; Kazoka, D.; Bolocko, K.; Pilmane, M. Different Techniques of Creating Bone Digital 3D Models from Natural Specimens. *Appl. Syst. Innov.* **2022**, *5*, 85. https://doi.org/10.3390/asi5040085

Academic Editors: Teen-Hang Meen and Chun-Yen Chang

Received: 29 July 2022
Accepted: 18 August 2022
Published: 22 August 2022

1. Introduction

Today, three-dimensional (3D) printing technology and models play an irreplaceable and significant role in different areas of medicine, including the education process, anatomical images and modeling, preclinical, and clinical studies [1]. 3D printing technology offers researchers the opportunity to create patient-specific models from medical images that represent anatomical structures in complex cases of congenital or multiple anomalies [2]. This allows a more accurate assessment of different and unique surgical procedures, their preintervention, or planning. 3D printing with various possibilities, materials, and challenges, allows it to become increasingly popular in the fields of medical implant design, manufacturing, tissue engineering, and biomedicine, including the fabrication of scaffolds called patient-specific tissue regeneration lattice structures [3]. Therefore, the new industrial revolution of 3D printing technologies requires a high level of expertise to achieve acceptable results, notably in modern STEM educational practices (Science, Technology, Engineering, Arts, and Mathematics) [4]. In addition, an essential part of the medical field is the development of the fourth industrial revolution, or Industry 4.0, with technologies that perform special functions, solve various medical problems with the interdisciplinary approach, increase the precision of surgical procedures, and create high-quality medical devices and components using advanced manufacturing technique [5]. In conjunction with autonomous, interconnected, and intelligent systems, portability, and a wide variety of materials, 3D printing has become one of the leading emerging technologies with a rapidly expanding market, where different innovative products are being created, from prototypes to fully functional complexes [6].

Annex 3 continued

It is difficult to imagine teaching and learning human anatomy without any visualization tools to understand complex details, their dislocations, and relationships. Several authors recommend the integration of 3D models into teaching and evaluation for educational alignment, anatomical knowledge, and selection of a model for specific purposes [7–9]. 3D printed anatomical models are excellent tools that can be used for training and developing practical skills, not only for students, but also for medical professionals. Related to this, these models can also increase the potential interest and attention of different specialists in the development of new techniques, methods, and printing materials. Models can be replicated in varied sizes, colors, and quantities, according to the demand. It should be noted that the quality of models can be affected by thermal deformation of materials, removal of support structures, or other factors [10]. Today, the use of 3D models by educators in basic medical studies, practitioners in hospitals, and clinics, has exciting potential and should continue with a focus on sustainability. Furthermore, 3D computer-assisted reconstruction may improve treatment results, increase safety, and education, and improve surgeons' ability to perform complex operations [11]. At the same time, there are many challenges in adopting this process [12]. Medical students can also emphasize the artistic role of 3D models in education, and the positive impact they have on their observation skills [13]. Another advantage of 3D models is the possibility of recreating different anatomical variations of any complexity, preoperative planning, development, and simulation of specific procedures [14]. 3D printed models, especially bones, can also make the necessity of natural human bones obsolete, encouraging virtual and remote education, helping to plan surgical interventions, and stimulating the implementation of cutting-edge technologies [15]. In addition to this, traditional anatomy teaching that incorporates 3D models is more involving and modern than the use of only computed tomography (CT) and/or magnetic resonance imaging (MRI) data, which can improve an understanding of the specific clinical manipulations and improve patient outcomes [16]. In the future, novel anatomical models can offer many possibilities for sectional anatomy, due to their nature as a multilayered and functional dissectible unit, as well as the ability to publish/share them for free access for educators, scientists, and students [17].

In anatomy education, 3D printed anatomical models can be used as a teaching tool as well as additional content to the curriculum and complement established learning methods, such as dissection-based teaching [18]. Furthermore, 3D models can offer new online teaching possibilities, reshaping teaching and learning spaces and providing a new experience for tutors and students [19]. The design of specific models for more complicated anatomical topics and microstructures is a major step in the development of modern study courses. In this research, we used three different techniques (3D scanning, photogrammetry, and micro-computed tomography) to produce a digital 3D model of zygomatic bone from a natural specimen. As zygomatic bone poses an intricate structure in terms of morphology, as well as its well-established protocol of replacement by an implant in case of severe injury, this makes zygomatic bone an ideal candidate for the creation of a precise and accurate human bone 3D digital model. Three techniques have been chosen as the most effective approaches in 3D model creation from natural specimens, which are being actively used at the Department of Morphology of Rīga Stradiņš University (RSU).

2. Materials and Methods

The photo images used for the photogrammetry technique were acquired with the help of a Sony ILCE-7RM2 camera and a Sigma 70 mm F2.8 DG MACRO Art lens (image capture parameters: f/8.0, 1/640s, ISO 100). The most important characteristic of the camera in terms of photogrammetry is the sensors' pixel count (the used model has 42.3 megapixels; Table 1).

Table 1. The list of used technical equipment.

Equipment	Manufacturer	Model	Specification
Camera	Sony	ILCE-7RM2	electronics.sony.com/imaging/interchangeable-lens-cameras/full-frame/p/ilce7rm2-b (accessed on 17 August 2022)
Lens	Sigma	70 mm F2.8 DG MACRO Art	sigma-global.com/en/lenses/a018_70_28 (accessed on 17 August 2022)
X-ray micro-computed tomography	SCANCO Medical	µCT50	scanco.ch/microct50.html (accessed on 17 August 2022)
Computer	Lenovo	Legion 7	Windows 11 Pro, AMD Ryzen 7 5800H, NVIDIA GeForce RTX 3080 16 GB, 64 GB DDR4 3200 MHz, 1000 GB solid-state drive.
3D Scanner	Shining3D	EinScan-S	einscan.com/desktop-3d-scanners/einscan-se/einscan-se-specs (accessed on 17 August 2022)

The higher the pixel count, the higher the quality/resolution of the obtained texture of the 3D model. Related to photogrammetry, the most crucial factor is the sharpness and clearness of the images, which require the use of a tripod and additional light sources. For the final image postprocessing (RAW data conversion, saturation, contrast), Adobe Photoshop and Capture One software have been used, followed by processing in RealityCapture (Table 2).

Table 2. The list of software used.

Software | Platform	Version	Information
EinScan-S	2.5.0.7	einscan.com/support/download/software/?scan_model=einscan-s (accessed on 17 August 2022).
Micro-CT	-//-	Was shipped along with the µCT50 micro-CT machine.
3D Slicer	5.02	slicer.org (accessed on 17 August 2022)
MeshLab	2022.02	meshlab.net (accessed on 17 August 2022)
RealityCapture	1.2.0.17385	capturingreality.com/realitycapture (accessed on 17 August 2022)
Adobe Photoshop	23.1.1	For textures' color correction.
Capture One 22 Pro	15.0.1.4	For cameras' RAW images procession.
Sketchfab	-//-	sketchfab.com (accessed on 17 August 2022)

For micro-computed tomography scanning the µCT50 machine (Table 2) has been used, along with the following parameters:

Dimensions of the scanned area (cylinder): diameter = 48 mm, height= 110 mm;
Energy: 90 kVp;
Intensity: 88 uA;
Filter: Al 0.5 mm;
Preset: High resolution,
Field of view (FOV): 49.6 mm;
Voxel size: 24.2 um;
Integration time: 1500.

The software for raw data processing has been shipped along with the machine. The post-processed data have been exported in a form of DICOM (Digital Imaging and Communications in Medicine) files, and then imported into 3D Slicer (Table 1) software for the creation of a 3D model according to the *Segmentation Protocol*.

For mesh simplification and optimization, MeshLab software has been used (Table 1) according to the *Simplification and Optimization Protocol*.

The acquired photo images were post-processed with the help of RealityCapture software (Table 1). The program requires purchasing a license, but for academic and research staff is being provided free of charge. The process is quite straightforward and

intuitive, due to the simple GUI (graphical user interface) of the software, as well as the built-in 'Quick Start' tool, which guides you through the entire creation process of the textured 3D model. The standard settings have been changed according to *Photogrammetry Protocol* to maximize the quality and precision of the final result. The obtained texture has been corrected with the help of Adobe Photoshop software (Table 1) to make it isotropic in terms of contrast, brightness, saturation, and shadow presence. The model was then simplified and optimized according to the *Simplification and Optimization Protocol* (to reduce the file size, since the Sketchfab platform, which is being used to publish and present the model, has a limitation of 100 MB per model (for a base account)). Simplification has been carried out, while keeping the original models' topology and level of detail of the original models.

For 3D scanning, EinScan-S (Table 2) has been used, along with the following parameters:
Picture number: 36
Turntable Speed: 1
Turntable turns: half turn

The obtained 3D model has been optimized according to the Simplification and Optimization Protocol (the *Simplification: quadric edge collapse decimation* step has been skipped due to the low number of faces, in comparison to models created by other techniques).

2.1. Photogrammetry Protocol | Reality Capture

1. Launch the RealityCapture program.
2. Import images into the program.
3. Adjust alignment settings:
   - Max feature per mpx.: 20,000;
   - Max features per image: 80,000;
   - Preselector features: 20,000;
   - Image overlap: low;
   - Force component rematch: yes;
   - Detector sensitivity: high.
4. Launch the alignment process.
5. Define the reconstruction region.
6. Use reconstruction with *High detail* option to initialize the meshing process.
7. Use *Clean Model* tool to remove topology defects (non-manifold vertices, non-manifold edges, holes, isolated vertices).
8. Use the Texture instrument with the following setting to create a texture for the model:
   - Imported-model default texture resolution: 16,384 × 16,384;
   - Correct colors: Yes.
9. Export the 3D model along with the texture as an OBJ (file format) object.

2.2. Segmentation Protocol | 3D Slicer

1. Launch the 3D Slicer program.
2. Import CT data into the program:
   - Set the image contrast to ensure better visibility.
3. Add a new segment using the tool:
   - Segment Editor:
     - Set up the Threshold tool;
     - Using Scissors, Draw, Islands, manually segment the required structure.
4. When segmentizing one structure is complete, proceed to the second one by adding a new segment and repeat the segmentation procedure if needed.
5. Export the completed segment or segments as a 3D model in the OBJ (file format) file format.

2.3. Simplification and Optimization Protocol | MeshLab

1. Launch the MeshLab program.
2. Import a 3D model into the program.
3. Remove artifacts, simplify, and optimize the model using tools (all the default values with modifications indicated below):
   - Remove isolated pieces (wrt diameter);
   - Remove duplicated faces;
   - Remove duplicated vertex;
   - Remove zero area faces;
   - Repair non-manifold edges by removing faces;
   - Repair non-manifold vertices by splitting;
   - Remove unreferenced vertices;
   - Simplification: quadric edge collapse decimation:
     - Preserve boundary of the mesh: on;
     - Preserve normal: on;
     - Preserve topology: on;
     - Planar simplification: on.
   - Remeshing: isotropic explicit remeshing:
     - Adaptive remeshing: on;
     - Collapse step: off.
4. Export the completed segment or segments as a 3D model in the binary PLY file format.

3. Results

Three models have been created in total using different techniques—3D scanning, photogrammetry, and micro-computed tomography (Figure 1).

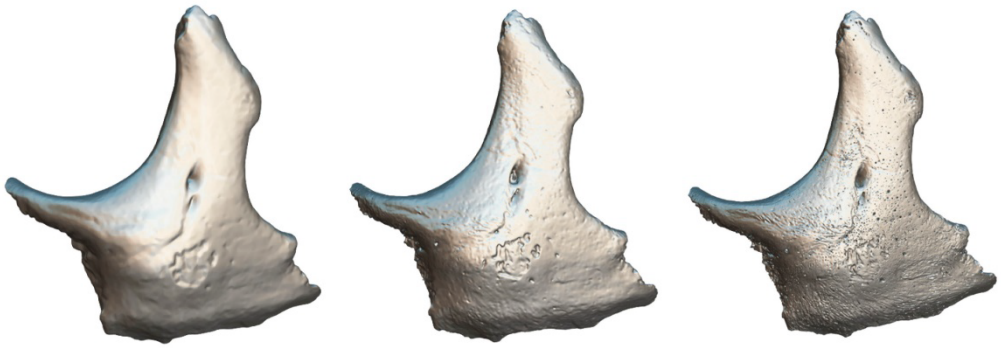

Figure 1. 3D model's simplified and optimized polygon meshes created by using different techniques. (**A**) 3D scanning, (**B**) photogrammetry, (**C**) micro-computed tomography.

All models have been simplified and optimized except the model created by the 3D scanning technique, which was only optimized.

The original number of faces and vertices for 3D models before and after the application of the *Simplification and Optimization Protocol* can be observed in Table 3.

The size of an obtained texture map of 3D models can be observed in Table 4.

In Figure 2, models with an applied X-ray shader allowing to see the inner structures can be observed.

Next, Figure 3, presents the 3D models with an applied shader, light sources, global illumination, ambient occlusion, and post-process filters, on the Sketchfab platform. All

the models, except the one obtained with the help of the micro-computed tomography technique, are provided with textures.

Table 3. The number of faces and vertices of 3D models before and after application of the *Simplification and Optimization Protocol*.

Techniques	Before Simplification (Faces | Vertices)	After Simplification (Faces | Vertices)
3D scanning	700,002 350,003	*Has not been simplified*
Micro Computed Tomography	70,195,566 35,073,613	7,019,556 3 485,608
Photogrammetry	13,716,318 6,882,203	700,842 350,423

Table 4. The size of an obtained texture map of 3D models.

Techniques	Size of the Texture Map (Pixels; Width × Height)
3D scanning	766 × 998
Micro Computed Tomography	*No visual data havebeen captured*
Photogrammetry	16,384 × 16,384

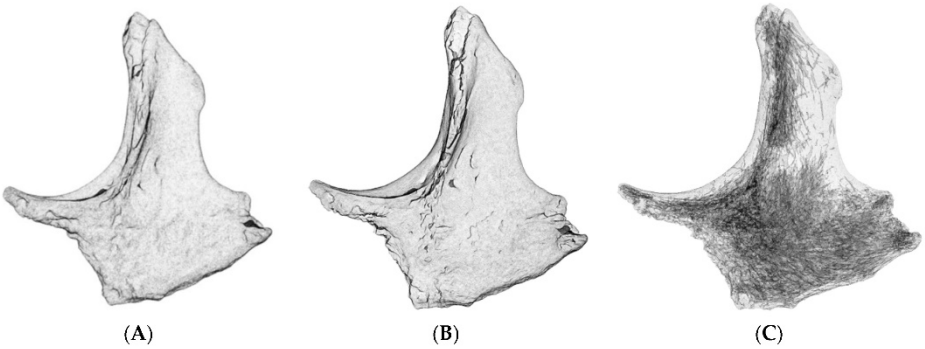

Figure 2. 3D models were created by using different techniques with an X-ray shader applied. (**A**) 3D scanning, (**B**) photogrammetry, (**C**) micro-computed tomography.

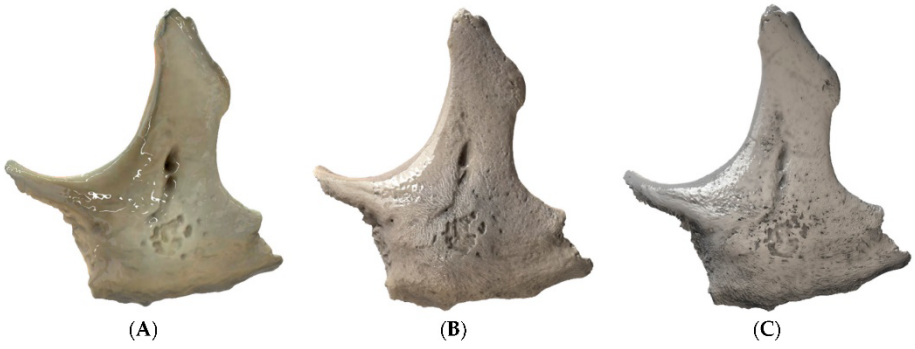

Figure 3. 3D models with an applied shader, light sources, global illumination, ambient occlusion, and post-process filters, on Sketchfab platform created by using different techniques. (**A**) 3D scanning, (**B**) photogrammetry, (**C**) micro-computed tomography.

All the models can be observed in 3D, downloaded, and used under the Attribution 4.0 International (CC BY 4.0) license at the Sketchfab platform—https://sketchfab.com/edler/models (accessed on 17 August 2022).

4. Discussion

Different techniques for the creation of 3D models allow their greater application in medical training and biomedical sciences [20]. Without a doubt, digital technologies have revolutionized anatomy education through 3D visual reconstruction of the human body, and have stimulated the teaching/learning experience of clinicians in different fields and levels [21]. Following an overview of new technological developments for anatomy education, this process raises several ethical and technical questions, at the same time providing proof in favor of 3D printing, and its advantages over other teaching resources [22,23]. Some studies have demonstrated the benefits of using 3D printed models in complex cases in gynecology, orthopedics, neuroanatomy, and radiology [24–27]. Researchers underline the potential of 3D printing to create more detailed and complex models, including regional, vascular, and nervous system structures [28]. Therefore, various materials may be needed to reproduce particular anatomical structures, or precise physical properties of human tissue, especially in scaffold engineering [29]. Furthermore, different anatomical structures have different mechanical properties, and they need special materials to meet the required performance of the printed object. Related to this, the most important factor is the correct selection of materials which is related to the selection of the 3D printing process, printer, and the mechanical properties of the model [30]. Widely used 3D printing technologies and specially designed models allow students to study complex anatomical regions and areas that are difficult for them to comprehend, requiring various levels of expertise [31,32]. In the medical field, 3D printed models serve as a great visualization tool that can represent the anatomy of patients, with great potential in presurgical planning and surgery [33–36]. A realistic 3D printed anatomical model can increase the effectiveness of surgery, can be used for determining the safest treatment strategy, and for designing patient-specific surgical instruments [37]. The process of developing a bone prototype with the help of modern 3D technologies can be an alternative to conventional model manufacturing [38].

The construction of 3D models from two-dimensional (2D) images depends on the user's needs, possibilities, the time needed to create the models, and costs. In the process of anatomical models, the cornerstone is the methodology used for their development [39]. Using inexpensive materials and/or low-cost equipment can decrease the quality of the models. The choice of the 3D printing technique is the most crucial step that affects the accuracy and quality [40]. Moreover, early detection of errors and flaws during the design creation and fabrication processes of 3D printed products can reduce waste, manufacturing time, and cost [41]. Several studies report that the accuracy of 3D printed bones is key in the production of representative prints, but it can be affected by printer technology [42,43]. Visualization of 3D anatomic structures offers different interactive tools for teaching students, or patients, about the anatomy of the body; however, it requires a knowledgeable specialist in both teaching and anatomy [44,45]. Students should develop an understanding of complex anatomical structures after a limited time of practical classes. In these cases, access to 3D models can help them better prepare for tests and exams, improve anatomical knowledge, and prepare for clinical study courses. It is important to mention that our students can study the basic steps of 3D printing in the first study year of the Human Anatomy course at RSU. Based on our experience, we believe that created and printed anatomical models are especially useful in the teaching and learning of anatomy for undergraduate students [46]. Several studies show that models can serve not only as an addition to cadaver dissection but also can serve as a valuable alternative to natural specimens when access to the cadaveric material is limited [47,48]. Some authors reported that different medical specialists have focused on 3D scanning and printing technologies to enrich the medical education process with modern technologies [49,50]. All 3D technologies complement each other, and their

integration can open new possibilities for the creation of new, valuable, and revolutionizing products [51,52].

The implementation and application of 3D models can be divided into three main categories: visualization, simulation, and physical replication to obtain a functioning model (implant or prosthesis). The visualization aspect prioritizes the overall appearance over the topological accuracy of the model. There are different areas, such as education, where the original look of a scanned bone is significant for the education process. Such an application requires a 3D model creation technique to capture not only the topological data, but also the visual ones. As can be seen in Figure 3, no texture is captured during microcomputed tomography scanning, and the final result consists only of topological data. Two other techniques, photogrammetry, and 3D scanning can capture visual data; however, their capabilities differ. As the camera image sensor is important for the photogrammetry process, it is for 3D scanning. In this study, a mid-level 3D scanner was used, which negatively impacted the resolution of the obtained texture map; it cannot compete with the texture map obtained with the help of the photogrammetry technique (Table 4). More advanced, industrial-grade 3D scanners capable of competing with photogrammetry in terms of the resolution of 3D model texture maps, are far more expensive and can cost up to 30,000 euros. In its turn, the equipment for photogrammetry can be obtained for less than 3000 euros. Photogrammetry is a relatively simple and inexpensive method of creating realistic 3D digital models that can be used in almost any setting to produce digital models [53]. Following special guidelines, these models can be metrically accurate, promoting self-directed learning and a greater understanding of complex anatomical structures [54]. However, creating a series of models through photogrammetry can be time-consuming [55,56].

In relation to the simulation and physical replication aspects, the density and accuracy of the polygonal mesh are more important factors than the resolution, or presence of the texture map. The data from Table 3 demonstrate that the microcomputed tomography technique is the most preferable way to obtain high density polygonal mesh, as well as this technique produces the most accurate results in terms of topology. Another crucial aspect is the presence of inner structures that are impossible to capture using any other technique (Figure 2). These data are necessary for implant production, or correct computer biomechanical simulation.

It is important to note that the first requirement for the creation of an anatomically accurate 3D printed model is a high-resolution volumetric dataset. Most models are created from computed tomography (CT) data, but it is possible to create models from datasets with modalities such as magnetic resonance imaging (MRI) and ultrasound [57]. Today, digital platforms and data storage include many massive medical image datasets [58]. Access to high-quality virtual images can offer a unique possibility for acquiring information about normal anatomy and/or anatomical variations. Differentiation of tissue density (from low to high) allows the segmentation technique to be used for different anatomical structures [59]. Depending on the imaging modality, different features can be observed, and different image segmentation algorithms can be applied. These segmentation algorithms and the availability of 3D printers stimulated the development of 3D printing in medical education and research, which had a positive impact on the precision of 3D printing technology and the costs of patient-specific 3D printed implants and prostheses [60,61]. Our experience and practice do not stand aside from these processes. In practical classes, 3D printed specimens help academic personnel and students to explain and/or understand anatomical structures.

Despite the many advantages of the use of 3D anatomical structures, the results of some studies were inconsistent in their effectiveness in improving anatomical knowledge and expertise for students with low spatial visualization ability, knowledge acquisition, and knowledge retention in a long-term perspective [62,63]. More research and analysis are necessary to better assess the role of anatomical models in the educational process. Although several models can be suitable for simple teaching/learning purposes, special

3D prints should be prepared for detailed topographical anatomy, and for a wide range of human anatomy pathologies [64]. Furthermore, every model should be morphologically accurate and qualitative. Some authors recommend using high-quality 3D scanners only because techniques such as photogrammetry are more time consuming and possess an increased risk of the occurrence of different artifacts in the 3D models [65].

Different technical parameters and the morphological variability of each model should also be considered. High-resolution and geometrically accurate medical images have been recommended in the literature [66]. Many studies have focused on best practices, optimal methodologies for conversion of patient radiographic scans to printable 3D models, specific software, and mathematical algorithms for optimization of 3D models' polygonal mesh [67,68].

According to our research, it is important to note that the results can be affected by several factors in the 3D model creation process. Due to the possible errors in each step of the creation and/or printing of the anatomical 3D model, the choice of size and verification techniques depends on unique and specific requirements, guidelines, preferences, and the expertise of technical personnel [69]. Finally, the accuracy of printed models should be compared with that of the original samples [70]. In this study, one of the limitations is the choice of the bones from natural specimens, and their complicity and sizes because of the type and specifications of the 3D scanner/micro-computed tomography machine. In this case, it was only possible to use bones of a small size. Some technical difficulties and artifacts during scanning occurred, thus several steps were repeated several times as a countermeasure to presume the morphological accuracy and quality of the texture map. Furthermore, the choice of techniques and software used depends on the available equipment and possibilities available in the Department of Morphology. Finally, the background, anatomical, and technical expertise of researchers has a significant impact on the accuracy and quality of bone digital 3D models.

5. Conclusions

In this study, three different techniques have been presented and compared for the creation of the digital 3D zygomatic bone model from natural specimens. The results demonstrate that these techniques varied in their precision, complexity, quality, and accuracy, which distinguishes the techniques in terms of possible applications of the created 3D model. For morphological accuracy, the most preferable technique is micro-computed tomography; for visualization and demonstration of the original texture, the photogrammetry technique is the most optimal choice. The 3D scanning technique requires a professional, advanced 3D scanner to be able to compete with the other two techniques.

In addition, we have provided an improved strategy for the creation of digital 3D bone models from natural specimens and their assessment, in terms of practical use for educational purposes in the Human Anatomy course at Rīga Stradiņš University, also underlining the scientific and practical potential of digital models within the medical field in future work.

Author Contributions: Conceptualization, E.E.; methodology, E.E.; software, E.E.; validation, E.E. and K.B.; formal analysis, E.E.; investigation, E.E.; resources, K.B. and E.E.; writing—original draft preparation, E.E. and D.K.; writing—review and editing, E.E., D.K., K.B. and M.P.; visualization, E.E.; supervision, E.E. All authors have read and agreed to the published version of the manuscript.

Funding: This research received no external funding.

Institutional Review Board Statement: The study was conducted in accordance with the Declaration of Helsinki, and the protocol was approved by the Ethics Committee of Rīga Stradiņš University (2-PĒK-4/97/2022).

Informed Consent Statement: Not applicable.

Data Availability Statement: The simplified models are published on the Sketchfab platform—https://sketchfab.com/edler/models (accessed on 17 August 2022).

Acknowledgments: Authors acknowledge the support and assistance of Janis Locs and Marika Mosina from Riga Technical University.

Conflicts of Interest: The authors declare no conflict of interest.

References

1. Ye, Z.; Dun, A.; Jiang, H.; Nie, C.; Zhao, S.; Wang, T.; Zhai, J. The role of 3D printed models in the teaching of human anatomy: A systematic review and meta-analysis. *BMC Med. Educ.* **2020**, *20*, 335. [CrossRef] [PubMed]
2. Schrot, J.; Pietila, T.; Sahu, A. State of the art: 3D printing for creating compliant patient-specific congenital heart defect models. *J. Cardiovasc. Magn. Reason.* **2014**, *16* (Suppl. 1), W19. [CrossRef]
3. Kantaros, A.; Piromalis, D. Fabricating lattice structures via 3d printing: The case of porous bio-engineered scaffolds. *Appl. Mech.* **2021**, *2*, 289–302. [CrossRef]
4. Kantaros, A.; Diegel, O.; Piromalis, D.; Tsaramirsis, G.; Khadidos, A.O.; Khadidos, A.O.; Khan, F.Q.; Jan, S. 3D printing: Making an innovative technology widely accessible through makerspaces and outsourced services. *Mater. Today Proc.* **2022**, *49*, 2712–2723. [CrossRef]
5. Javaid, M.; Haleem, A. Industry 4.0 applications in medical field: A brief review. *Curr. Med. Res. Pract.* **2019**, *9*, 102–109. [CrossRef]
6. Tsaramirsis, G.; Kantaros, A.; Al-Darraji, I.; Piromalis, D.; Apostolopoulos, C.; Pavlopoulou, A.; Alrammal, M.; Ismail, Z.; Buhari, S.M.; Stojmenovic, M.; et al. A modern approach towards an industry 4.0 model: From driving technologies to management. *J. Sens.* **2022**, *2022*, 5023011. [CrossRef]
7. Hammerton, C.; Yip, S.W.L.; Manobharath, N.; Myers, G.; Sturrock, A. Are 3D printed models acceptable in assessment? *Clin. Teach.* **2022**, *19*, 221–228. [CrossRef]
8. Yuen, J. What is the role of 3d printing in undergraduate anatomy education? A scoping review of current literature and recommendations. *Med. Sci. Edu.* **2020**, *30*, 1321–1329. [CrossRef]
9. Garas, M.; Vaccarezza, M.; Newland, G.; McVay-Doornbusch, K.; Hasani, J. 3D-Printed specimens as a valuable tool in anatomy education: A pilot study. *Ann. Anat.* **2018**, *219*, 57–64. [CrossRef]
10. Zou, Y.; Han, Q.; Weng, X.; Zou, Y.; Yang, Y.; Zhang, K.; Yang, K.; Xu, X.; Wang, C.; Qin, Y.; et al. The precision and reliability evaluation of 3-dimensional printed damaged bone and prosthesis models by stereo lithography appearance. *Medicine* **2018**, *97*, e9797. [CrossRef]
11. Day, K.M.; Kelley, P.K.; Harshbarger, R.J.; Dorafshar, A.H.; Kumar, A.R.; Steinbacher, D.M.; Patel, P.; Combs, P.D.; Levine, J.P. Advanced three-dimensional technologies in craniofacial reconstruction. *Plast. Reconstr. Surg.* **2021**, *148*, 94e–108e. [CrossRef] [PubMed]
12. Bastawrous, S.; Wu, L.; Liacouras, P.C.; Levin, D.B.; Ahmed, M.T.; Strzelecki, B.; Amendola, M.F.; Lee, J.T.; Coburn, J.; Ripley, B. Establishing 3d printing at the point of care: Basic principles and tools for success. *Radiographics* **2022**, *42*, 451–468. [CrossRef] [PubMed]
13. Bell, L.T.O.; Evans, D.J.R. Art, anatomy, and medicine: Is there a place for art in medical education? Art, Anatomy, and Medical Education. *Anat. Sci. Edu.* **2014**, *7*, 370–378. [CrossRef] [PubMed]
14. Govsa, F.; Yagdi, T.; Ozer, M.A.; Eraslan, C.; Alagoz, A.K. Building 3D anatomical model of coiling of the internal carotid artery derived from CT angiographic data. *Eur. Arch. Otorhinolaryngol.* **2017**, *274*, 1097–1102. [CrossRef] [PubMed]
15. Pugalendhi, A.; Arumugam, S.; Ranganathan, R.; Ganesan, S. 3D printed patient-specific bone models for anatomy education from medical imaging. *J. Eng. Res.* **2021**, 1–12. [CrossRef]
16. Xie, Y.; Wu, G.; Liang, Y.; Fan, G. Three-dimensional physical model in urologic cancer. *Front. Surg.* **2022**, *9*, 757337. [CrossRef] [PubMed]
17. Smith, M.L.; Jones, J.F.X. Dual-extrusion 3D printing of anatomical models for education: Two Materials 3D Printing in Anatomy. *Anat. Sci. Edu.* **2018**, *11*, 65–72. [CrossRef]
18. Smith, C.F.; Tollemache, N.; Covill, D.; Johnston, M. Take away body parts! An investigation into the use of 3D-printed anatomical models in undergraduate anatomy education. *Anat. Sci. Edu.* **2018**, *11*, 44–53. [CrossRef]
19. Diaz, C.M.; Linden, K.; Solyali, V. Novel and innovative approaches to teaching human anatomy classes in an online environment during a pandemic. *Med. Sci. Edu.* **2021**, *31*, 1703–1713. [CrossRef]
20. Ugidos Lozano, M.T.; Blaya Haro, F.; Ruggiero, A.; Manzoor, S.; Nuere Menendez-Pidal, S.; Juanes Méndez, J.A. Different digitalization techniques for 3d printing of anatomical pieces. *J. Med. Syst.* **2018**, *42*, 46. [CrossRef]
21. Wickramasinghe, N.; Thompson, B.R.; Xiao, J. The opportunities and challenges of digital anatomy for medical sciences: Narrative review. *JMIR Med. Educ.* **2022**, *8*, e34687. [CrossRef] [PubMed]
22. Al-Mosawe, A.; Agha, H.; Al-Hadeethi, L.; Al-Mahaidi, R. Efficiency of image correlation photogrammetry technique in measuring strain. *Aust. J. Struct. Eng.* **2018**, *19*, 207–213. [CrossRef]
23. Jones, D.G. Three-dimensional printing in anatomy education: Assessing potential ethical dimensions. *Anat. Sci. Educ.* **2019**, *12*, 435–443. [CrossRef]
24. Flaxman, T.E.; Cooke, C.M.; Miguel, O.X.; Sheikh, A.M.; Singh, S.S. A review and guide to creating patient specific 3D printed anatomical models from MRI for benign gynecologic surgery. *3D Print Med.* **2021**, *7*, 17. [CrossRef]

25. Lima, L.F.; Barros, A.J.; Martini, A.D.; Stocco, M.B.; Kuczmarski, A.H.; Souza, R.L. Photogrammetry and 3D prototyping: A low-cost resource for training in veterinary orthopedics. *Cienc. Rural* **2019**, *49*, e20180929. [CrossRef]
26. Sikes, R.W.; Sniezek, C.M.; Clancey, B.T.; Johnson, C.J. Virtual 3d brain slices: Improving learning of cross-sectional neuroanatomy by expanding access to human brain cross-sections through photogrammetric 3d scanning. *FASEB J.* **2018**, *32* (Suppl. 1), 635-17. [CrossRef]
27. Tashiro, M.; Minohara, S.; Yusa, K.; Sakurai, H.; Kanai, T.; Baba, M.; Miyamoto, T.; Nakano, T. 242 Quantitative evaluation of 3d lung motion with anatomical feature tracking technique for precise particle radiotherapy. *Radiother. Oncol.* **2006**, *78*, S85–S86. [CrossRef]
28. Bartikian, M.; Ferreira, A.; Gonçalves-Ferreira, A.; Neto, L.L. 3D printing anatomical models of head bones. *Surg. Radiol. Anat.* **2019**, *41*, 1205–1209. [CrossRef]
29. Ratinam, R.; Quayle, M.; Crock, J.; Lazarus, M.; Fogg, Q.; McMenamin, P. Challenges in creating dissectible anatomical 3D prints for surgical teaching. *J. Anat.* **2019**, *234*, 419–437. [CrossRef]
30. Aimar, A.; Palermo, A.; Innocenti, B. The role of 3d printing in medical applications: A state of the art. *J. Healthc. Eng.* **2019**, *2019*, 5340616. [CrossRef]
31. Schmidt, R.; Gartrell, R.; Yeung, J.M. A pipeline for generating interactive, schematic 3d surgical anatomy models. *J. Surg. Educ.* **2021**, *78*, 1419–1424. [CrossRef] [PubMed]
32. Shahrubudin, N.; Lee, T.C.; Ramlan, R. An overview on 3d printing technology: Technological, materials, and applications. *Procedia Manuf.* **2019**, *35*, 1286–1296. [CrossRef]
33. Betancourt, M.C.; Araújo, C.; Marín, S.; Buriticá, W. The quantitative impact of using 3d printed anatomical models for surgical planning optimization: Literature review. *3D Print Addit. Manuf.* **2022**, 3dp.2021.0188. [CrossRef]
34. Formisano, M.; Iuppariello, L.; Mirone, G.; Cinalli, G.; Casaburi, A.; Guida, P.; Clemente, F. 3d printed anatomical model for surgical planning: A pediatric hospital experience. In Proceedings of the International Conference on E-Health and Bioengineering (EHB), Iasi, Romania, 18–19 November 2021. [CrossRef]
35. Cornejo, J.; Cornejo-Aguilar, J.A.; Vargas, M.; Helguero, C.G.; Milanezi de Andrade, R.; Torres-Montoya, S.; Asensio-Salazar, J.; Rivero Calle, A.; Martínez Santos, J.; Damon, A.; et al. Anatomical engineering and 3d printing for surgery and medical devices: International review and future exponential innovations. *Biomed. Res. Int.* **2022**, *2022*, 6797745. [CrossRef] [PubMed]
36. Fasel, J.H.D.; Malis, D.D.; Wiederer, C.; Hagenbuch, N. 3D printing of anatomical models for surgeons: An investigation on repeatability. *IJIDeM* **2018**, *12*, 621–627. [CrossRef]
37. Osti, F.; Santi, G.; Neri, M.; Liverani, A.; Frizziero, L.; Stilli, S.; Maredi, E.; Zarantonello, P.; Gallone, G.; Stallone, S.; et al. Ct conversion workflow for intraoperative usage of bony models: From dicom data to 3d printed models. *Appl. Sci.* **2019**, *9*, 708. [CrossRef]
38. Narayan, Y.S.; Prakash, K.J.; Rajashekhar, S.; Narendra, P. 3D printed human humerus bone with proximal implant prototype for arthroplasty. *Int. J. Health Sci.* **2022**, *6* (Suppl. 4). [CrossRef]
39. Salazar, D.A.; Cramer, J.; Markin, N.W.; Hunt, N.H.; Linke, G.; Siebler, J.; Zuniga, J. Comparison of 3D printed anatomical model qualities in acetabular fracture representation. *Ann. Transl. Med.* **2022**, *10*, 391. [CrossRef]
40. Saleh, Y.; Piper, R.; Richard, M.; Jeyaretna, S.; Cosker, T. Designing a 3d printed model of the skull-base: A collaboration between clinicians and industry. *J. Med. Educ. Curric. Dev.* **2022**, *9*, 238212052210807. [CrossRef]
41. Martinez-Marquez, D.; Mirnajafizadeh, A.; Carty, C.P.; Stewart, R.A. Application of quality by design for 3D printed bone prostheses and scaffolds. *PLoS ONE* **2018**, *13*, e0195291. [CrossRef]
42. Rungrojwittayakul, O.; Kan, J.Y.; Shiozaki, K.; Swamidass, R.S.; Goodacre, B.J.; Goodacre, C.J.; Lozada, J.L. Accuracy of 3d printed models created by two technologies of printers with different designs of model base. *J. Prosthodont.* **2020**, *29*, 124–128. [CrossRef] [PubMed]
43. Carew, R.M.; Iacoviello, F.; Rando, C.; Moss, R.M.; Speller, R.; French, J.; Morgan, R.M. A multi-method assessment of 3D printed micromorphological osteological features. *Int. J. Leg. Med.* **2022**, *136*, 1391–1406. [CrossRef] [PubMed]
44. Ammanuel, S.; Brown, I.; Uribe, J.; Rehani, B. Creating 3d models from radiologic images for virtual reality medical education modules. *J. Med. Syst.* **2019**, *43*, 166. [CrossRef] [PubMed]
45. Silén, C.; Karlgren, K.; Hjelmqvist, H.; Meister, B.; Zeberg, H.; Pettersson, A. Three-dimensional visualisation of authentic cases in anatomy learning–An educational design study. *BMC Med. Educ.* **2022**, *22*, 477. [CrossRef]
46. Edelmers, E.; Kazoka, D.; Pilmane, M. Creation of Anatomically Correct and Optimized for 3D Printing Human Bones Models. *Appl. Syst. Innov.* **2021**, *4*, 67. [CrossRef]
47. Hochman, J.B.; Rhodes, C.; Wong, D.; Kraut, J.; Pisa, J.; Unger, B. Comparison of cadaveric and isomorphic three-dimensional printed models in temporal bone education. *Laryngoscope* **2015**, *125*, 2353–2357. [CrossRef]
48. McMenamin, P.G.; Quayle, M.R.; McHenry, C.R.; Adams, J.W. The production of anatomical teaching resources using three-dimensional (3d) printing technology: 3D Printing in Anatomy Education. *Anat. Sci. Educ.* **2014**, *7*, 479–486. [CrossRef]
49. Blahuta, R.I.; Blikhar, V.S.; Dufeniuk, O.M. Transfer of 3d scanning technologies into the field of criminal proceedings. *Sci. Innov.* **2020**, *16*, 84–91. [CrossRef]
50. Higueras, M.; Calero, A.I.; Collado-Montero, F.J. Digital 3D modeling using photogrammetry and 3D printing applied to the restoration of a Hispano-Roman architectural ornament. *DAACH* **2021**, *20*, e00179. [CrossRef]

51. Baltsavias, E.P. A comparison between photogrammetry and laser scanning. *ISPRS J. Photogramm. Remote Sens.* **1999**, *54*, 83–94. [CrossRef]
52. Bridger, C.A.; Reich, P.D.; Caraça Santos, A.M.; Douglass, M.J.J. A dosimetric comparison of CT- and photogrammetry- generated 3D printed HDR brachytherapy surface applicators. *Phys. Eng. Sci. Med.* **2022**, *45*, 125–134. [CrossRef] [PubMed]
53. Morgan, B.; Ford, A.L.J.; Smith, M.J. Standard methods for creating digital skeletal models using structure-from-motion photogrammetry. *Am. J. Phys. Anthropol.* **2019**, *169*, 152–160. [CrossRef] [PubMed]
54. Wesencraft, K.M.; Clancy, J.A. Using Photogrammetry to Create a Realistic 3D Anatomy Learning Aid with Unity Game Engine. *Adv. Exp. Med. Biol.* **2019**, *1205*, 93–104. [CrossRef] [PubMed]
55. Carew, R.M.; Morgan, R.M.; Rando, C. Experimental assessment of the surface quality of 3D printed bones. *Aust. J. Forensic Sci.* **2021**, *53*, 592–609. [CrossRef]
56. Petriceks, A.H.; Peterson, A.S.; Angeles, M.; Brown, W.P.; Srivastava, S. Photogrammetry of human specimens: An innovation in anatomy education. *J. Med. Educ. Curric. Dev.* **2018**, *5*, 238212051879935. [CrossRef]
57. Ripley, B.; Levin, D.; Kelil, T.; Hermsen, J.L.; Kim, S.; Maki, J.H.; Wilson, G.J. 3d printing from mri data: Harnessing strengths and minimizing weaknesses: 3d printing from mri data. *J. Magn. Reason. Imaging* **2017**, *45*, 635–645. [CrossRef]
58. Bois, M.C.; Morris, J.M.; Boland, J.M.; Larson, N.L.; Scharrer, E.F.; Aubry, M.-C.; Maleszewski, J.J. Three-dimensional surface imaging and printing in anatomic pathology. *J. Pathol. Inform.* **2021**, *12*, 22. [CrossRef]
59. Bücking, T.M.; Hill, E.R.; Robertson, J.L.; Maneas, E.; Plumb, A.A.; Nikitichev, D.I. From medical imaging data to 3D printed anatomical models. *PLoS ONE* **2017**, *12*, e0178540. [CrossRef]
60. Andreß, S.; Achilles, F.; Bischoff, J.; Kußmaul, A.C.; Böcker, W.; Weidert, S. A method for finding high accuracy surface zones on 3D printed bone models. *Comput. Biol. Med.* **2021**, *135*, 104590. [CrossRef]
61. van Eijnatten, M.; van Dijk, R.; Dobbe, J.; Streekstra, G.; Koivisto, J.; Wolff, J. CT image segmentation methods for bone used in medical additive manufacturing. *Med. Eng. Phys.* **2018**, *51*, 6–16. [CrossRef]
62. Labranche, L.; Wilson, T.D.; Terrell, M.; Kulesza, R.J. Learning in stereo: The relationship between spatial ability and 3d digital anatomy models. *Anat. Sci. Educ.* **2022**, *15*, 291–303. [CrossRef]
63. Lau, I.; Sun, Z. The role of 3D printed heart models in immediate and long-term knowledge acquisition in medical education. *Rev. Cardiovasc. Med.* **2022**, *23*, 1. [CrossRef] [PubMed]
64. McMenamin, P.G.; Hussey, D.; Chin, D.; Alam, W.; Quayle, M.R.; Coupland, S.E.; Adams, J.W. The reproduction of human pathology specimens using three-dimensional (3d) printing technology for teaching purposes. *Med. Teach.* **2021**, *43*, 189–197. [CrossRef] [PubMed]
65. Douglass, M.J.J. Can optical scanning technologies replace CT for 3D printed medical devices in radiation oncology? *J. Med. Radiat. Sci.* **2022**, *69*, 139–142. [CrossRef] [PubMed]
66. Crowe, S.; Luscombe, J.; Maxwell, S.; Simpson-Page, E.; Poroa, T.; Wilks, R.; Li, W.; Cleland, S.; Chan, P.; Lin, C.; et al. Evaluation of optical 3D scanning system for radiotherapy use. *J. Med. Radiat. Sci.* **2022**, *69*, 218–226. [CrossRef]
67. Fogarasi, M.; Coburn, J.C.; Ripley, B. Algorithms used in medical image segmentation for 3D printing and how to understand and quantify their performance. *3D Print Med.* **2022**, *8*, 18. [CrossRef]
68. Brouwers, L.; Teutelink, A.; van Tilborg, F.A.J.B.; de Jongh, M.A.C.; Lansink, K.W.W.; Bemelman, M. Validation study of 3D-printed anatomical models using 2 PLA printers for preoperative planning in trauma surgery, a human cadaver study. *Eur. J. Trauma Emerg. Surg.* **2019**, *45*, 1013–1020. [CrossRef]
69. Paramasivam, V.; Sindhu; Singh, G.; Santhanakrishnan, S. 3d printing of human anatomical models for preoperative surgical planning. *Procedia Manuf.* **2020**, *48*, 684–690. [CrossRef]
70. Odeh, M.; Levin, D.; Inziello, J.; Lobo Fenoglietto, F.; Mathur, M.; Hermsen, J.; Stubbs, J.; Ripley, B. Methods for verification of 3D printed anatomic model accuracy using cardiac models as an example. *3D Print Med.* **2019**, *5*, 6. [CrossRef]

4th Publication

diagnostics

MDPI

Technical Note

Automatization of CT Annotation: Combining AI Efficiency with Expert Precision

Edgars Edelmers [1,*], Dzintra Kazoka [1], Katrina Bolocko [2], Kaspars Sudars [3] and Mara Pilmane [1]

[1] Institute of Anatomy and Anthropology, Rīga Stradiņš University, LV-1010 Riga, Latvia; dzintra.kazoka@rsu.lv (D.K.); mara.pilmane@rsu.lv (M.P.)
[2] Department of Computer Graphics and Computer Vision, Riga Technical University, LV-1048 Riga, Latvia; katrina.bolocko@rtu.lv
[3] Institute of Electronics and Computer Science, LV-1006 Riga, Latvia; sudars@edi.lv
* Correspondence: edgars.edelmers@rsu.lv

Abstract: The integration of artificial intelligence (AI), particularly through machine learning (ML) and deep learning (DL) algorithms, marks a transformative progression in medical imaging diagnostics. This technical note elucidates a novel methodology for semantic segmentation of the vertebral column in CT scans, exemplified by a dataset of 250 patients from Riga East Clinical University Hospital. Our approach centers on the accurate identification and labeling of individual vertebrae, ranging from C1 to the sacrum–coccyx complex. Patient selection was meticulously conducted, ensuring demographic balance in age and sex, and excluding scans with significant vertebral abnormalities to reduce confounding variables. This strategic selection bolstered the representativeness of our sample, thereby enhancing the external validity of our findings. Our workflow streamlined the segmentation process by eliminating the need for volume stitching, aligning seamlessly with the methodology we present. By leveraging AI, we have introduced a semi-automated annotation system that enables initial data labeling even by individuals without medical expertise. This phase is complemented by thorough manual validation against established anatomical standards, significantly reducing the time traditionally required for segmentation. This dual approach not only conserves resources but also expedites project timelines. While this method significantly advances radiological data annotation, it is not devoid of challenges, such as the necessity for manual validation by anatomically skilled personnel and reliance on specialized GPU hardware. Nonetheless, our methodology represents a substantial leap forward in medical data semantic segmentation, highlighting the potential of AI-driven approaches to revolutionize clinical and research practices in radiology.

Keywords: radiology; artificial intelligence; computer vision; semantic segmentation; annotation

Citation: Edelmers, E.; Kazoka, D.; Bolocko, K.; Sudars, K.; Pilmane, M. Automatization of CT Annotation: Combining AI Efficiency with Expert Precision. *Diagnostics* **2024**, *14*, 185. https://doi.org/10.3390/diagnostics14020185

Academic Editors: Xuan V. Nguyen, Engin Dikici and Ali Gholamrezanezhad

Received: 8 November 2023
Revised: 12 January 2024
Accepted: 13 January 2024
Published: 15 January 2024

1. Introduction

Recent advancements in artificial intelligence (AI) have revolutionized numerous sectors, including automotive engineering, economics, finance, and particularly medical diagnostics and treatment planning. AI, a pivotal branch of computer science, involves designing algorithms capable of mimicking human tasks, thereby facilitating in-depth learning, remote teaching, prompt feedback, innovative assessment, and efficient data storage in education [1]. According to Saga et al. [2], AI's precision and wide-ranging benefits have attracted extensive research interest. In medical contexts, AI has proven invaluable in managing large datasets, aiding in clinical decision-making, and enhancing the accuracy of medical practice [3–9]. Specifically, AI-powered tools have become integral in image-guided systems for surgical planning and simulation, leveraging advanced visualization technologies [10].

Moreover, the evolution of imaging techniques has markedly improved the visualization and identification of anatomical structures. AI's application in anatomy education

Annex 4 continued

promises significant advancements, potentially enhancing both student learning and instructor teaching methodologies [11,12]. The scalability and speed of AI technologies offer unprecedented opportunities in educational settings [13]. In medical data analysis, AI's precision is instrumental in CT and MRI scans, enabling the detailed detection of complex anatomical structures. This precision aids in various medical applications, from surgery planning to patient care. AI also plays a crucial role in developing and utilizing 3D anatomical models for educational purposes, enhancing students' comprehension of human anatomy [14,15]. Visual representations in medical imaging are vital for professionals, researchers, educators, students, and patients. AI has significantly advanced medical data annotation methods, including in the study of human bone structures. AI algorithms efficiently process and update large datasets, creating detailed and accurate images for medical analysis [14,15].

This paper presents a semi-automatic workflow for the semantic segmentation of human spine CT data using AI tools. This method greatly reduces the time and resources required for manual segmentation, thereby offering significant benefits in AI and healthcare applications and proving effective upon testing. The workflow includes volume stitching for multiple series, AI-driven semantic segmentation, validation of anatomical correctness, and practical applications of segmented radiological data. Section 2 details the materials and methods, Section 3 presents the results, Section 4 analyzes the methodology and concludes the paper, discussing potential future research directions.

1.1. Performance Semantic Segmentation

This section outlines a method for performing semi-automatic semantic segmentation of computed tomography (CT) data, utilizing AI-based tools. The workflow is methodically structured into four distinct stages, two of which are mandatory and two optional, depending on the specific requirements of the dataset.

Volume Stitching (Mandatory in Certain Cases): This step is essential in instances where multiple series are involved, such as when the CT data encompasses separate scans of the cervical region and thoraco-abdominal areas. The stitching process integrates these series into a cohesive volume, facilitating a more comprehensive analysis.

Semantic Segmentation with AI (Mandatory): At this core stage, AI-driven instruments are employed to segment the CT data semantically. The AI tools identify and delineate various anatomical structures within the scans, streamlining the segmentation process.

Validation of Segmentation Anatomical Correctness (Mandatory): This critical step involves the verification of the AI-segmented data for anatomical accuracy. It ensures that the segmentation aligns correctly with established anatomical standards, thereby maintaining the precision and reliability of the results.

Post-Processing (Optional): In cases where further refinement or adjustments are necessary, post-processing can be applied. This step allows for the fine-tuning of the segmented data, addressing any specific needs or discrepancies that may arise from the initial AI segmentation.

1.2. Volume Stitching

In radiological imaging, particularly for semantic segmentation, the integration of individual volumes is paramount. This is especially true for complex anatomical structures like the spine, where a comprehensive and uninterrupted view is essential. The vertebral column extends from the cervical region at the top to the thoraco-abdominal region at the bottom. If these areas are scanned separately, the resulting images may be fragmented, failing to provide a holistic view of the spine's anatomy.

Semantic segmentation, a process where each pixel in an image is classified into specific categories such as different tissues or structures [16], relies heavily on the completeness of the data. By stitching together separate volumes from cervical and thoraco-abdominal scans, we ensure that the segmentation algorithms have a full representation of the spine. This holistic view is crucial for achieving accurate and reliable segmentation outcomes.

Furthermore, different scanning protocols for cervical and thoraco-abdominal regions often lead to variations in image quality, resolution, or contrast [17]. By merging these distinct volumes, we create a uniform dataset, which is critical for consistent analysis. This uniformity significantly reduces the likelihood of errors or inconsistencies that can arise during the segmentation process. Moreover, working with a single, unified dataset, as opposed to multiple disjointed ones, greatly streamlines the analysis process, enhancing efficiency and accuracy.

1.3. Semantic Segmentation with AI

Semantic segmentation, a critical process in medical radiology, involves classifying each pixel in an image into specific classes, thereby extracting detailed anatomical and pathological information. This technique is instrumental in diagnosing diseases, planning treatments, and monitoring disease progression. Despite its importance, the implementation of semantic segmentation in medical radiology encounters several significant challenges.

One primary challenge is the inherent complexity of medical images. Modalities like MRIs, CT scans, and X-rays reveal detailed internal structures, where the diverse appearances of tissues and overlapping structures can complicate the segmentation process. Additionally, images are often subject to noise, artifacts, and distortions due to factors like patient movement, limitations of imaging devices, or specific scanning parameters [18,19]. These imperfections can lead to inaccurate segmentations. Another obstacle is the variability among patients. Factors such as age, genetics, and health conditions result in wide anatomical differences, often necessitating extensive customization or manual adjustments in standardized segmentation models. Further complexity arises from the high dimensionality of medical imaging; CTs and MRIs produce volumetric, 3D data, adding to the segmentation challenges.

A significant hurdle in semantic segmentation is the scarcity of accurately annotated data. Supervised learning models require extensive labeled datasets for training [20]. However, obtaining precise annotations from experienced radiologists is a resource-intensive and time-consuming task. Class imbalance in medical images, where crucial features like tumors may occupy a small portion of the image, can skew algorithms towards more dominant classes, leading to segmentation inaccuracies [21].

Inter-rater variability in medical image annotations poses another challenge. Even among expert radiologists, discrepancies in image interpretation and annotation are common [22]. This variability complicates the establishment of a consistent ground truth for training models. In certain applications, such as image-guided surgeries, real-time semantic segmentation is required, adding to the complexity.

Lastly, the issue of model generalization is a significant concern. Models trained with data from one medical institution or a specific imaging device may not perform well with data from different sources, due to variations in imaging protocols, patient demographics, or device characteristics [23]. This highlights the need for adaptable and robust models capable of handling diverse datasets.

The recent advancements in machine learning (ML) and deep learning (DL) algorithms have markedly increased the adoption of artificial intelligence (AI) in the medical field [24]. These developments, coupled with powerful new imaging modalities provided by advanced scanners, present unique challenges in visualization. Future healthcare technologies, driven by these advancements, are expected to enhance the quality of medical imaging while reducing associated costs, thereby simplifying the extraction and optimal combination of individual data [25].

Computer-aided platforms, leveraging these technological advancements, assist medical professionals in making critical clinical decisions related to diagnosis, disease tracking, and prognosis [26–28]. Medical image creation, tailored to individual patients' medical data, enables professionals to visualize and detect specific manifestations of diseases, enhancing personalized medical care. AI algorithms play a crucial role in diagnosing diseases, planning effective treatment strategies, and monitoring treatment outcomes. These algorithms can analyze medical imaging data to create detailed illustrations of bone dislocations, frac-

tures, or tumors, specifying their location, size, shape, and characteristics. Moreover, AI has demonstrated its capability to surpass human performance in certain tasks, such as image segmentation [29]. It can process a wide array of data types in the medical context, including outputs from imaging scanners, sensor data, or patient metadata. Modern computers, equipped with DL algorithms, are adept at semantic labeling and image classification. In medical data analysis, these algorithms focus on identifying anatomical landmarks, geometric descriptors, centerlines of structures, shape, deformation, and fiber orientation, thereby providing remarkable diagnostic accuracy for various diseases [30].

New methodologies in AI have been developed for the identification and classification of objects in medical images [31,32]. The creation of better methods and standards for designing, implementing, and evaluating clinical AI-enabled instruments is crucial to ensure their effectiveness and value to end users [33]. These algorithms, trained on large datasets, can predict outcomes on new data without explicit programming [34]. Current computer vision algorithms excel at identifying patterns in digital data, achieving human-level accuracy in object detection.

Image segmentation, a fundamental procedure in many medical imaging applications, involves delineating regions within images that are occupied by objects of interest [35]. Traditional segmentation methods, which often rely on areas and edges, face limitations due to factors such as non-uniform grayscale, individual differences, and the presence of artifacts and noise in images [36]. The advent of deep learning (DL) has brought about advanced architectures and feature extraction mechanisms that significantly enhance the segmentation of deformed anatomy [37], thereby improving the accuracy of disease diagnosis and minimizing redundant computations. Automatic segmentation of bones is a crucial step in deriving quantitative markers for accurate clinical diagnosis and in developing computer-aided decision support systems. In modalities like computed tomography (CT) and magnetic resonance imaging (MRI), understanding the pathology and observing changes in the anatomical structures, shape, size, and texture of bones are vital for initial disease diagnosis and monitoring its progression. For instance, in spine image analysis and 3D spine reconstruction applications, accurately locating and segmenting vertebrae from CT spinal images is fundamental [38]. Accurate bone segmentation provides a stable structural reference for both inter and intra-patient registration and internal organ localization, facilitating the automatic segmentation of internal organs [39]. However, despite the relative ease of visual observation of bones in CT images, challenges such as low signal-to-noise ratio, insufficient spatial resolution, and indistinct image intensity between spongy bones and soft tissues make the precise segmentation of individual bones a complex task [40]. Accurately segmenting the spine into individual vertebrae is crucial for diagnosing spine-related illnesses, especially for detecting and classifying bone damage, fractures, lesions, and tumors [41–43].

1.4. Validation of Segmentation Anatomical Correctness

To maintain the anatomical accuracy of the model, it is cross-referenced with credible academic references. Furthermore, the use of expert and accredited medical virtual applications is recommended. Complete Anatomy serves as a prime example of such tools, providing an accurate and intuitive interface for manipulating anatomical models. Developed by 3D4Medical under the aegis of Elsevier, Complete Anatomy stands as a sophisticated educational 3D anatomy platform, with the company's expertise in the development of medical products dating back to 2009 [44,45].

1.5. Practical Use of Segmented Radiological Data

Semantically segmented medical datasets have become fundamental in advancing medical research and technology. Their integration into artificial intelligence (AI) and 3D technologies heralds a new era of opportunities and breakthroughs.

In medical AI, these datasets are indispensable. AI algorithms, trained on semantically segmented data, have transformed diagnostic processes by precisely identifying and classi-

fying abnormalities [46]. This advancement aids radiologists and clinicians in early and accurate diagnosis, paving the way for personalized medicine. Furthermore, AI models utilizing these datasets can perform predictive analyses, anticipating disease progression, patient outcomes, and treatment efficacy [47]. Automated segmentation, another critical application, allows AI to process intricate medical images efficiently, reducing manual labor and ensuring uniformity in results [48–50].

Three-dimensional technologies have significantly benefited from these datasets, enabling the creation of detailed anatomical reconstructions [51]. Surgeons utilize these 3D models for meticulous procedural planning, enhancing patient outcomes and optimizing surgical times. Additionally, the integration of these datasets into virtual and augmented reality platforms enhances medical training and patient education, providing immersive experiences and real-time surgical guidance [52].

Beyond AI and 3D applications, semantically segmented datasets are pivotal in telemedicine [53]. They facilitate real-time sharing and analysis, ensuring access to expert care regardless of location. These datasets are at the forefront of contemporary medical innovation, enhancing current practices and setting the stage for future advancements.

In clinical contexts, computer-aided and semi-automated segmentation techniques are crucial for interpreting CT and MRI images for bone pathologies. Correct vertebra segmentation allows for monitoring the progression of diseases under treatment. Traditional manual segmentation is time-consuming, requiring an in-depth understanding of anatomy and extensive effort; for instance, segmenting a vertebral column can take up to 24 h, depending on data quality and scanning protocols. This duration may double for novices. Our proposed methodology enables non-specialists to perform initial segmentation of general, non-pathological structures semi-automatically. This process provides a basis for adjustments, allowing initial segmentation by AI, followed by manual validation and refinement against literature sources and anatomical standards.

2. Materials and Methods

The 3D Slicer software (version: 5.4; slicer.org (accessed on 30 August 2023) [54] was used in this work. It is important to highlight that the program can be easily downloaded and used at no cost, being an open-source software.

The dataset used in this research comprised 250 patient CT scans sourced from Riga East Clinical University Hospital.

In cases where it is necessary to merge multiple series in order to segment the whole anatomical structure, the steps below should be followed.

2.1. Methodology for Series Merging (Optional)

Data import

1. Start the 3D Slicer software.;
2. Access the DICOM database;
3. Choose the appropriate patient;
4. Identify two series intended for later merging;
5. Import the identified series.

Creation of region of interest (ROI)

1. Activate the Crop Volume module;
2. Under Input Volume, choose a series;
3. Under Input ROI, opt for Create ROI. The resulting volume will be named Crop Volume ROI;
4. Click the Center View button in the 3D visualization window;
5. Select the Fit to Volume option;
6. Resize the ROI to ensure both loaded volumes, presented as two individual entities, fit within this new ROI.

The process of stitching two volumes

1. Access the Stitch Volume module;
2. Under Stitched Volume ROI, select the Crop Volume ROI you previously created;
3. For Original Volume 1, choose the primary volume to which the secondary volume will be appended;
4. For Original Volume 2, select the other loaded volume;
5. Click the Create Stitched Volume button.

The Stitch Volume function is designed to create a unified composite image from multiple image volumes. It operates by selecting specific images and merging them within a user-defined rectangular region of interest (ROI). This function meticulously handles the trimming and fusion of overlapping areas in the volumes, dividing each area based on its proximity to the midpoint of the overlap.

Key to the process is the preservation of image resolution. The function precisely adopts the resolution of the initial input volume. To maintain image fidelity, nearest-neighbor interpolation is applied, which accounts for minor shifts in voxel placement. In situations where the image volumes have varying resolutions, windowed sync interpolation is utilized to achieve a uniform resolution across the merged image.

For areas outside the scope of the original volumes, the function assigns a default voxel value of zero. This assignment ensures clear demarcation of the merged areas from the non-covered regions. The process concludes with the generation of a consolidated image, confined within the defined ROI and matching the resolution of the first input volume.

2.2. Methodology for Segmentation

The creation of semantic mask | TotalSegmentator module

1. For Input Volume, choose the volume you have loaded;
2. In Segmentation Tasks, opt for Total;
3. Click the Apply' button.

Deletion of unnecessary data

4. Remove all items, retaining only the volume used in the prior step and the desired semantic segmentations of anatomical structures.

Masks validation and correction

5. When smoothing is necessary:
    1. For the Smoothing Method, select Median;
    2. Set the Kernel Size to 3.00 mm;
    3. Toggle the Apply to Visible Segments option to Enable.
6. Verify the morphological accuracy of segmented structures using references from literature or digital platforms. If required, make adjustments utilizing the Draw, Paint (with the Sphere Brush feature activated), Erase, and Scissors tools.
7. If there is a segmentation error where a part of one structure is identified as a segment of another bone, follow these steps to merge and rectify:
    1. In the Data module, duplicate the segment that contains a section of the incorrect bone;
    2. Utilize the Scissors tool from the Segment Editor module to remove everything except the mislabeled structure;
    3. Using the Logical Operators tool, integrate the two segments of a single structure using the Add operation.

Data export

8. Save the volume in *.nrrd* file format;
9. Save segmentation for the volume in *seg.nrrd* file format.

3. Results

The methodology we discuss has been rigorously validated by applying it to a dataset of 250 patient CT scans from Riga East Clinical University Hospital. This validation

specifically involved the semantic segmentation of the vertebral column, with a keen focus on accurately registering and naming each individual vertebra.

In selecting our patient cohort, we implemented a meticulously designed criterion to ensure a demographically balanced sample in terms of age and sex, thus enhancing the generalizability of our study's findings. A pivotal inclusion criterion was the structural integrity of the vertebral column. We exclusively analyzed scans where the vertebrae were free from severe dispositions or deformities to minimize potential confounding factors that could bias our results.

The core of our workflow, aside from the optional step of volume stitching to create a single comprehensive volume, was the segmentation of the vertebral column. This involved the detailed semantic segmentation of all 25 bones in the vertebral column, including C1 to C7 (cervical), T1 to T12 (thoracic), L1 to L5 (lumbar), and the sacrum combined with the coccyx. An illustrative example of a semantically segmented vertebral column, as executed following our presented methodology, is depicted in Figure 1.

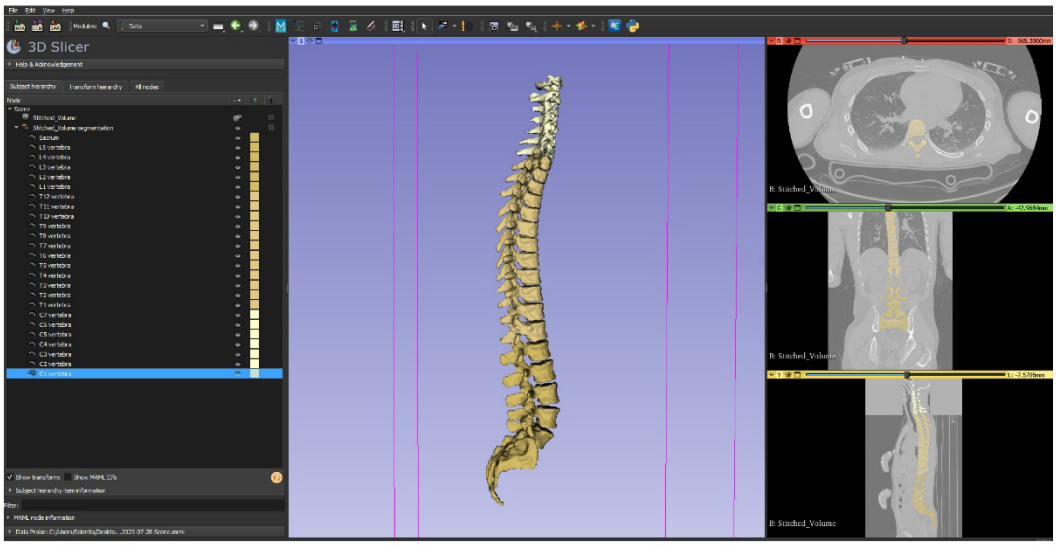

Figure 1. Semantically segmented vertebral column serving as proof of concept of the presented methodology (in total, 25 bones from C1 till sacrum combined with coccyx).

The segmentation was conducted under the supervision of an experienced radiologist and an anatomy professor, ensuring accuracy and adherence to established medical standards. All the created masks have been validated and corrected according to the methodology by comparing all the semantically segmented bones with the reference anatomy from the literature (Figure 2).

In our analysis, we identified instances of false registration anomalies (in 62 cases), a significant error in which two separate vertebrae were mistakenly identified and registered as a single anatomical entity. This misregistration presents a considerable source of error, adversely affecting both the qualitative and quantitative assessments of spinal structure.

Moreover, we observed segmentation inaccuracies where the delineated region either exceeded or fell short of the intended anatomical limits (in all cases). In some cases, the segmentation extended into adjacent tissues, while in others, it failed to include parts of the target structure. Such deviations result in a misrepresented portrayal of the spine's true morphology, as exemplified in Figure 3.

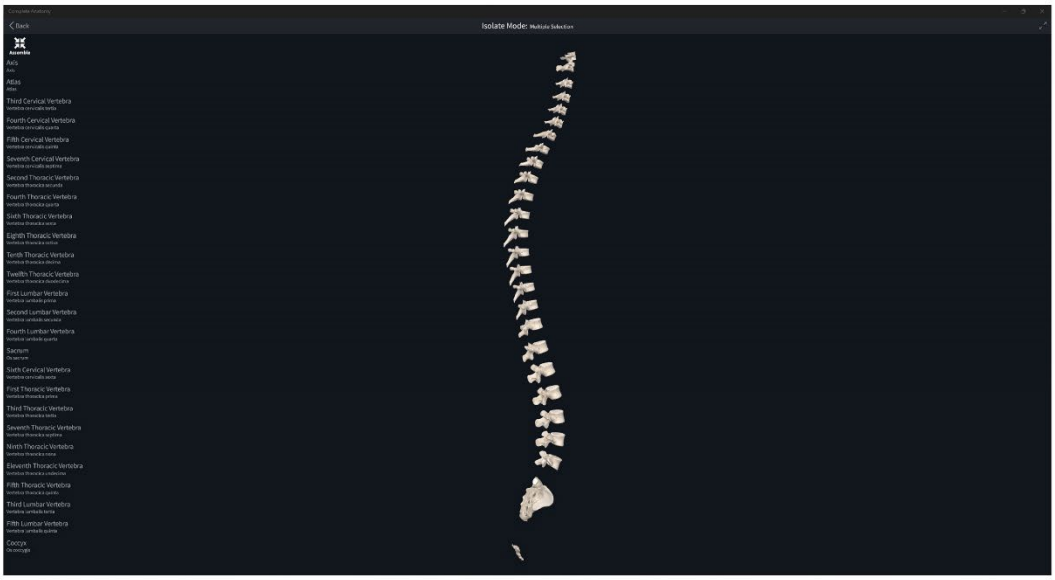

Figure 2. Reference digital models of vertebras used during the validation methodology from Complete Anatomy software (ver. 10.0.1) [44].

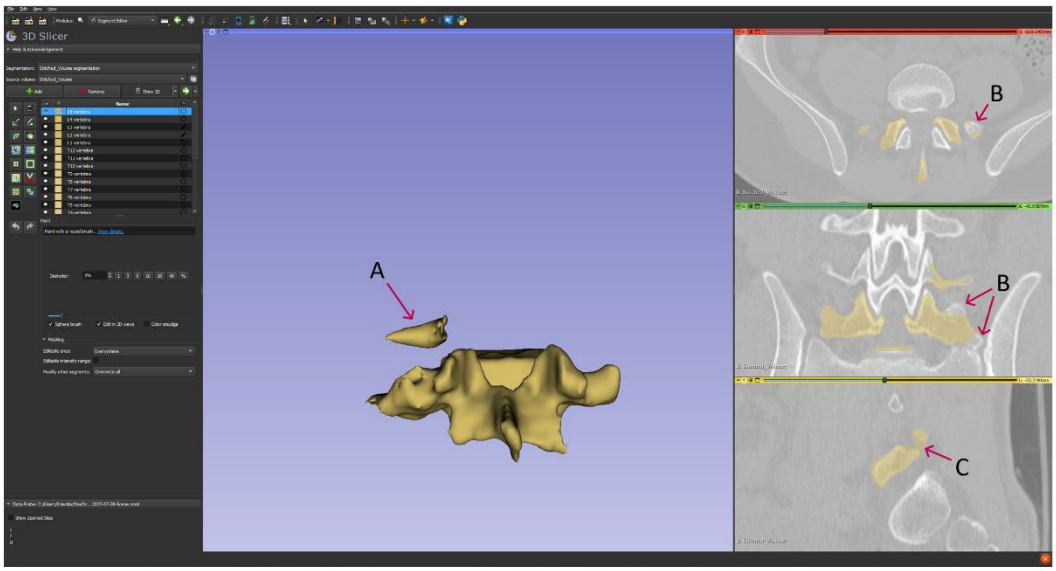

Figure 3. Illustrative examples of artifacts in anatomical segmentation. (A) Improper registration: A segment of the L4 vertebra is inaccurately identified as part of the L5 vertebra. (B) Omission of critical regions: This artifact represents the absence of specific anatomical regions that should have been included in the segmentation. (C) False registration: Soft tissues are incorrectly registered as constitutive elements of the L5 vertebra, compromising the integrity of the segmented structure.

These artifacts not only undermine the data's accuracy but also present substantial challenges in clinical or research contexts that depend on precise anatomical demarcation. Ensuring the correctness of vertebral identification and maintaining the integrity of anatomical boundaries are crucial for the reliability and applicability of our findings in subsequent medical analyses and applications.

The successful conclusion of our study resulted in the creation of a composite volume, which effectively integrated two critical anatomical regions: the cervical and the thoracoabdominal areas. This integration was complemented by their corresponding segmentation masks. A notable aspect of our data storage approach was the adoption of the Nearly Raw Raster Data (.NRRD) file format, diverging from the traditional Digital Imaging and Communications in Medicine (DICOM) format.

This deliberate choice to utilize the .NRRD format was driven by its several advantages, particularly in the context of machine learning applications. The .NRRD format facilitates faster data loading speeds, a crucial factor in efficiently processing large datasets in AI-driven research. This efficiency is especially beneficial when dealing with the complex, multi-region datasets like ours, where streamlined data handling can significantly enhance computational performance and analysis throughput.

4. Discussion

Our methodology employs AI in an easy-to-use format, providing operators with a graphical user interface (GUI). All necessary components related to different Slicer modules are pre-installed within the program, eliminating the need for external downloads.

However, a significant limitation of this methodology is the need for manual validation of all segmented anatomical structures. This process requires a high level of anatomical expertise and introduces potential sources of error and subjectivity. The segmentation process is prone to inaccuracies such as the omission of critical regions, incorrect merging of different anatomical regions, and imprecise registration of structures. For example, two adjacent vertebrae might be inaccurately registered as a single entity, affecting data integrity. Pathological anomalies and anatomical variations add complexity to the segmentation task, requiring both AI and human validators to uphold morphological precision and methodological robustness. The lack of quantitative benchmarks and metric evaluation for AI-segmented structures further complicates the validation process.

Additionally, the segmentation capabilities are limited by the TotalSegmentator software (ver. 2.0.4), which supports only a specific range of anatomical structures, thereby restricting the method's applicability in broader anatomical studies [55,56].

This methodology introduces an enhanced approach to the annotation of radiological data. Its distinct advantage lies in its broad applicability to a variety of anatomical structures, making it a valuable tool in AI-driven projects, especially in the area of medical data segmentation. A notable feature of this methodology is its inclusive design, which expands the range of annotators beyond traditional radiological professionals. This inclusivity accelerates the data annotation process, enabling quicker completion of projects and resulting in efficient use of resources. Furthermore, for specialists in segmentation tasks, this approach offers a significant reduction in the time required, enhancing overall productivity.

Author Contributions: Conceptualization, E.E.; methodology, E.E.; software, E.E.; validation, E.E. and K.B.; formal analysis, E.E.; investigation, E.E.; resources, K.B. and E.E.; writing—original draft preparation, E.E. and D.K.; writing—review and editing, E.E., D.K., K.B., K.S. and M.P.; visualization, E.E.; supervision, E.E. All authors have read and agreed to the published version of the manuscript.

Funding: This research received no external funding.

Institutional Review Board Statement: The study was conducted in accordance with the Declaration of Helsinki and approved by the Ethics Committee of Rīga Stradiņš University (2-PĒK-4/97/2022, 21 February 2022).

Informed Consent Statement: Not applicable.

Conflicts of Interest: The authors declare no conflicts of interest.

References

1. Abdellatif, H.; Al Mushaiqri, M.; Albalushi, H.; Al-Zaabi, A.A.; Roychoudhury, S.; Das, S. Teaching, Learning and Assessing Anatomy with Artificial Intelligence: The Road to a Better Future. *Int. J. Environ. Res. Public Health* **2022**, *19*, 14209. [CrossRef] [PubMed]
2. Saga, R. AI and Visualization with Medical Data: Medical Image and Deep Learning. *J. Vis.* **2018**, *38*, 19–22. [CrossRef]
3. Minopoulos, G.M.; Memos, V.A.; Stergiou, K.D.; Stergiou, C.L.; Psannis, K.E. A Medical Image Visualization Technique Assisted with AI-Based Haptic Feedback for Robotic Surgery and Healthcare. *Appl. Sci.* **2023**, *13*, 3592. [CrossRef]
4. Choudhry, P. Use of Artificial Intelligence in Healthcare Applications. *Acta Sci. Neuro* **2021**, *4*, 73–74. [CrossRef]
5. Botwe, B.O.; Akudjedu, T.N.; Antwi, W.K.; Rockson, P.; Mkoloma, S.S.; Balogun, E.O.; Elshami, W.; Bwambale, J.; Barare, C.; Mdletshe, S.; et al. The Integration of Artificial Intelligence in Medical Imaging Practice: Perspectives of African Radiographers. *Radiography* **2021**, *27*, 861–866. [CrossRef]
6. Zhuang, Y.; Jiang, N.; Xu, Y. Progressive Distributed and Parallel Similarity Retrieval of Large CT Image Sequences in Mobile Telemedicine Networks. *Wirel. Commun. Mob. Comput.* **2022**, *2022*, 1–13. [CrossRef]
7. Zhang, Z.; Wang, L.; Zheng, W.; Yin, L.; Hu, R.; Yang, B. Endoscope Image Mosaic Based on Pyramid ORB. *Biomed. Signal Process Control* **2022**, *71*, 103261. [CrossRef]
8. Lu, S.; Yang, B.; Xiao, Y.; Liu, S.; Liu, M.; Yin, L.; Zheng, W. Iterative Reconstruction of Low-Dose CT Based on Differential Sparse. *Biomed. Signal Process Control* **2023**, *79*, 104204. [CrossRef]
9. Lu, S.; Liu, S.; Hou, P.; Yang, B.; Liu, M.; Yin, L.; Zheng, W. Soft Tissue Feature Tracking Based on Deep Matching Network. *Comput. Model. Eng. Sci.* **2023**, *136*, 363–379. [CrossRef]
10. Golland, P.; Kikinis, R.; Halle, M.; Umans, C.; Grimson, W.E.L.; Shenton, M.E.; Richolt, J.A. AnatomyBrowser: A Novel Approach to Visualization and Integration of Medical Information. *Comput. Aided Surg.* **1999**, *4*, 129–143. [CrossRef]
11. Liu, M.; Zhang, X.; Yang, B.; Yin, Z.; Liu, S.; Yin, L.; Zheng, W. Three-Dimensional Modeling of Heart Soft Tissue Motion. *Appl. Sci.* **2023**, *13*, 2493. [CrossRef]
12. Shen, X.; Du, S.-C.; Sun, Y.-N.; Sun, P.Z.H.; Law, R.; Wu, E.Q. Advance Scheduling for Chronic Care Under Online or Offline Revisit Uncertainty. *IEEE Trans. Automat. Sci. Eng.* **2023**, 1–14. [CrossRef]
13. Lazarus, M.D.; Truong, M.; Douglas, P.; Selwyn, N. Artificial Intelligence and Clinical Anatomical Education: Promises and Perils. *Anat. Sci. Educ.* 2022; *Early View*. [CrossRef]
14. Potočnik, J.; Foley, S.; Thomas, E. Current and Potential Applications of Artificial Intelligence in Medical Imaging Practice: A Narrative Review. *J. Med Imaging Radiat. Sci.* **2023**, *54*, 376–385. [CrossRef]
15. Deng, Y.; Wang, L.; Zhao, C.; Tang, S.; Cheng, X.; Deng, H.-W.; Zhou, W. A Deep Learning-Based Approach to Automatic Proximal Femur Segmentation in Quantitative CT Images. *Med. Biol. Eng. Comput.* **2022**, *60*, 1417–1429. [CrossRef] [PubMed]
16. Krithika Alias AnbuDevi, M.; Suganthi, K. Review of Semantic Segmentation of Medical Images Using Modified Architectures of UNET. *Diagnostics* **2022**, *12*, 3064. [CrossRef]
17. Trattner, S.; Pearson, G.D.N.; Chin, C.; Cody, D.D.; Gupta, R.; Hess, C.P.; Kalra, M.K.; Kofler, J.M.; Krishnam, M.S.; Einstein, A.J. Standardization and Optimization of CT Protocols to Achieve Low Dose. *J. Am. Coll. Radiol.* **2014**, *11*, 271–278. [CrossRef]
18. Alzain, A.F.; Elhussein, N.; Fadulelmulla, I.A.; Ahmed, A.M.; Elbashir, M.E.; Elamin, B.A. Common Computed Tomography Artifact: Source and Avoidance. *Egypt. J. Radiol. Nucl. Med.* **2021**, *52*, 151. [CrossRef]
19. Noda, C.; Ambale Venkatesh, B.; Wagner, J.D.; Kato, Y.; Ortman, J.M.; Lima, J.A.C. Primer on Commonly Occurring MRI Artifacts and How to Overcome Them. *RadioGraphics* **2022**, *42*, E102–E103. [CrossRef]
20. Ahmad, Z.; Rahim, S.; Zubair, M.; Abdul-Ghafar, J. Artificial Intelligence (AI) in Medicine, Current Applications and Future Role with Special Emphasis on Its Potential and Promise in Pathology: Present and Future Impact, Obstacles Including Costs and Acceptance among Pathologists, Practical and Philosophical Considerations. A Comprehensive Review. *Diagn. Pathol.* **2021**, *16*, 24. [CrossRef]
21. Schutera, M.; Rettenberger, L.; Pylatiuk, C.; Reischl, M. Methods for the Frugal Labeler: Multi-Class Semantic Segmentation on Heterogeneous Labels. *PLoS ONE* **2022**, *17*, e0263656. [CrossRef]
22. Brady, A.; Laoide, R.Ó.; McCarthy, P.; McDermott, R. Discrepancy and Error in Radiology: Concepts, Causes and Consequences. *Ulster Med. J.* **2012**, *81*, 3–9.
23. Liang, X.; Nguyen, D.; Jiang, S. Generalizability Issues with Deep Learning Models in Medicine and Their Potential Solutions: Illustrated with Cone-Beam Computed Tomography (CBCT) to Computed Tomography (CT) Image Conversion. *Mach. Learn. Sci. Technol.* **2020**, *2*, 015007. [CrossRef]
24. Sapci, A.H.; Sapci, H.A. Artificial Intelligence Education and Tools for Medical and Health Informatics Students: Systematic Review. *JMIR Med. Educ.* **2020**, *6*, e19285. [CrossRef] [PubMed]
25. Diaz, O.; Kushibar, K.; Osuala, R.; Linardos, A.; Garrucho, L.; Igual, L.; Radeva, P.; Prior, F.; Gkontra, P.; Lekadir, K. Data Preparation for Artificial Intelligence in Medical Imaging: A Comprehensive Guide to Open-Access Platforms and Tools. *Phys. Med.* **2021**, *83*, 25–37. [CrossRef]

26. Shi, F.; Wang, J.; Shi, J.; Wu, Z.; Wang, Q.; Tang, Z.; He, K.; Shi, Y.; Shen, D. Review of Artificial Intelligence Techniques in Imaging Data Acquisition, Segmentation, and Diagnosis for COVID-19. *IEEE Rev. Biomed. Eng.* **2021**, *14*, 4–15. [CrossRef] [PubMed]
27. Yin, G.; Zhang, L.; Dai, T. Application and Visualization of Human 3D Anatomy Teaching for Healthy People Based on a Hybrid Network Model. *J. Healthc. Eng.* **2022**, *2022*, 1–6. [CrossRef]
28. Xia, Q.; Du, M.; Li, B.; Hou, L.; Chen, Z. Interdisciplinary Collaboration Opportunities, Challenges, and Solutions for Artificial Intelligence in Ultrasound. *Curr. Med Imaging Rev.* **2022**, *18*, 1046–1051. [CrossRef]
29. Gillmann, C.; Smit, N.N.; Groller, E.; Preim, B.; Vilanova, A.; Wischgoll, T. Ten Open Challenges in Medical Visualization. *IEEE Comput. Grap. Appl.* **2021**, *41*, 7–15. [CrossRef]
30. Al-Naser, Y.A. The Impact of Artificial Intelligence on Radiography as a Profession: A Narrative Review. *J. Med Imaging Radiat. Sci.* **2023**, *54*, 162–166. [CrossRef]
31. Kawamoto, M.; Kamiya, N.; Zhou, X.; Kato, H.; Hara, T.; Fujita, H. Simultaneous Learning of Erector Spinae Muscles for Automatic Segmentation of Site-Specific Skeletal Muscles in Body CT Images. *IEEE Access* **2023**, 1. [CrossRef]
32. Kamiya, N.; Kume, M.; Zheng, G.; Zhou, X.; Kato, H.; Chen, H.; Muramatsu, C.; Hara, T.; Miyoshi, T.; Matsuo, M.; et al. Automated Recognition of Erector Spinae Muscles and Their Skeletal Attachment Region via Deep Learning in Torso CT Images. In *Computational Methods and Clinical Applications in Musculoskeletal Imaging*; Vrtovec, T., Yao, J., Zheng, G., Pozo, J.M., Eds.; Lecture Notes in Computer Science; Springer International Publishing: Cham, Switzerland, 2019; Volume 11404, pp. 1–10. ISBN 978-3-030-11165-6.
33. Tulk Jesso, S.; Kelliher, A.; Sanghavi, H.; Martin, T.; Henrickson Parker, S. Inclusion of Clinicians in the Development and Evaluation of Clinical Artificial Intelligence Tools: A Systematic Literature Review. *Front. Psychol.* **2022**, *13*, 830345. [CrossRef] [PubMed]
34. Madani, A.; Namazi, B.; Altieri, M.S.; Hashimoto, D.A.; Rivera, A.M.; Pucher, P.H.; Navarrete-Welton, A.; Sankaranarayanan, G.; Brunt, L.M.; Okrainec, A.; et al. Artificial Intelligence for Intraoperative Guidance: Using Semantic Segmentation to Identify Surgical Anatomy During Laparoscopic Cholecystectomy. *Ann. Surg.* **2022**, *276*, 363–369. [CrossRef] [PubMed]
35. Jin, C.; Udupa, J.K.; Zhao, L.; Tong, Y.; Odhner, D.; Pednekar, G.; Nag, S.; Lewis, S.; Poole, N.; Mannikeri, S.; et al. Object Recognition in Medical Images via Anatomy-Guided Deep Learning. *Med. Image Anal.* **2022**, *81*, 102527. [CrossRef] [PubMed]
36. Song, Y.; Ren, S.; Lu, Y.; Fu, X.; Wong, K.K.L. Deep Learning-Based Automatic Segmentation of Images in Cardiac Radiography: A Promising Challenge. *Comput. Methods Programs Biomed.* **2022**, *220*, 106821. [CrossRef]
37. Wang, J.; Lv, Y.; Wang, J.; Ma, F.; Du, Y.; Fan, X.; Wang, M.; Ke, J. Fully Automated Segmentation in Temporal Bone CT with Neural Network: A Preliminary Assessment Study. *BMC Med. Imaging* **2021**, *21*, 166. [CrossRef] [PubMed]
38. Cheng, P.; Yang, Y.; Yu, H.; He, Y. Automatic Vertebrae Localization and Segmentation in CT with a Two-Stage Dense-U-Net. *Sci. Rep.* **2021**, *11*, 22156. [CrossRef] [PubMed]
39. Kim, S.; Bae, W.; Masuda, K.; Chung, C.; Hwang, D. Semi-Automatic Segmentation of Vertebral Bodies in MR Images of Human Lumbar Spines. *Appl. Sci.* **2018**, *8*, 1586. [CrossRef]
40. Fu, Y.; Liu, S.; Li, H.H.; Yang, D. Automatic and Hierarchical Segmentation of the Human Skeleton in CT Images. *Phys. Med. Biol.* **2017**, *62*, 2812–2833. [CrossRef]
41. Jakubicek, R.; Chmelik, J.; Jan, J. Vertebrae Segmentation in 3D CT Data: A Review of Methods and Evaluation Approaches. *Curr. Med Imaging Rev.* **2018**, *14*, 853–866. [CrossRef]
42. Qadri, S.F.; Lin, H.; Shen, L.; Ahmad, M.; Qadri, S.; Khan, S.; Khan, M.; Zareen, S.S.; Akbar, M.A.; Bin Heyat, M.B.; et al. CT-Based Automatic Spine Segmentation Using Patch-Based Deep Learning. *Int. J. Intell. Syst.* **2023**, *2023*, 1–14. [CrossRef]
43. Saeed, M.U.; Dikaios, N.; Dastgir, A.; Ali, G.; Hamid, M.; Hajjej, F. An Automated Deep Learning Approach for Spine Segmentation and Vertebrae Recognition Using Computed Tomography Images. *Diagnostics* **2023**, *13*, 2658. [CrossRef] [PubMed]
44. Motsinger, S.K. Complete Anatomy. Available online: https://3d4medical.com/ (accessed on 30 August 2023).
45. Nair, R.R.; Lindsey, A. Student Perception on Integration of 3D Complete Anatomy Software Application in Medical Curriculum. *FASEB J.* **2020**, *34*, 1. [CrossRef]
46. Mekov, E.; Miravitlles, M.; Petkov, R. Artificial Intelligence and Machine Learning in Respiratory Medicine. *Expert. Rev. Respir. Med.* **2020**, *14*, 559–564. [CrossRef] [PubMed]
47. Rezayi, S.; R Niakan Kalhori, S.; Saeedi, S. Effectiveness of Artificial Intelligence for Personalized Medicine in Neoplasms: A Systematic Review. *BioMed Res. Int.* **2022**, *2022*, 1–34. [CrossRef] [PubMed]
48. Kart, T.; Fischer, M.; Küstner, T.; Hepp, T.; Bamberg, F.; Winzeck, S.; Glocker, B.; Rueckert, D.; Gatidis, S. Deep Learning-Based Automated Abdominal Organ Segmentation in the UK Biobank and German National Cohort Magnetic Resonance Imaging Studies. *Investig. Radiol.* **2021**, *56*, 401–408. [CrossRef]
49. Lenchik, L.; Heacock, L.; Weaver, A.A.; Boutin, R.D.; Cook, T.S.; Itri, J.; Filippi, C.G.; Gullapalli, R.P.; Lee, J.; Zagurovskaya, M.; et al. Automated Segmentation of Tissues Using CT and MRI: A Systematic Review. *Acad. Radiol.* **2019**, *26*, 1695–1706. [CrossRef]
50. Thomas, M.F.; Kofler, F.; Grundl, L.; Finck, T.; Li, H.; Zimmer, C.; Menze, B.; Wiestler, B. Improving Automated Glioma Segmentation in Routine Clinical Use Through Artificial Intelligence-Based Replacement of Missing Sequences With Synthetic Magnetic Resonance Imaging Scans. *Investig. Radiol.* **2022**, *57*, 187–193. [CrossRef]
51. Bücking, T.M.; Hill, E.R.; Robertson, J.L.; Maneas, E.; Plumb, A.A.; Nikitichev, D.I. From Medical Imaging Data to 3D Printed Anatomical Models. *PLoS ONE* **2017**, *12*, e0178540. [CrossRef]

52. Frajhof, L.; Borges, J.; Hoffmann, E.; Lopes, J.; Haddad, R. Virtual Reality, Mixed Reality and Augmented Reality in Surgical Planning for Video or Robotically Assisted Thoracoscopic Anatomic Resections for Treatment of Lung Cancer. *J. Vis. Surg.* **2018**, *4*, 143. [CrossRef]
53. Hwang, S.; Song, Y.; Kim, J. Evaluation of AI-Assisted Telemedicine Service Using a Mobile Pet Application. *Appl. Sci.* **2021**, *11*, 2707. [CrossRef]
54. Kikinis, R.; Pieper, S.D.; Vosburgh, K.G. 3D Slicer: A Platform for Subject-Specific Image Analysis, Visualization, and Clinical Support. In *Intraoperative Imaging and Image-Guided Therapy*; Jolesz, F.A., Ed.; Springer: New York, NY, USA, 2014; pp. 277–289. ISBN 978-1-4614-7656-6.
55. Wasserthal, J.; Breit, H.-C.; Meyer, M.T.; Pradella, M.; Hinck, D.; Sauter, A.W.; Heye, T.; Boll, D.; Cyriac, J.; Yang, S.; et al. Total Segmentator: Robust Segmentation of 104 Anatomic Structures in CT Images. *Radiol. Artif. Intell.* **2023**, *5*, e230024. [CrossRef] [PubMed]
56. Wasserthal, J. TotalSegmentator. 2023. Available online: https://github.com/wasserth/TotalSegmentator (accessed on 12 January 2024).

5th Publication

diagnostics

MDPI

Technical Note

AI-Assisted Detection and Localization of Spinal Metastatic Lesions

Edgars Edelmers [1,2,*], Artūrs Ņikuļins [2], Klinta Luīze Sprūdža [1], Patrīcija Stapulone [1], Niks Saimons Pūce [2], Elizabete Skrebele [3], Everita Elīna Siņicina [4], Viktorija Cīrule [5], Ance Kazuša [1] and Katrina Boločko [6]

[1] Faculty of Medicine, Rīga Stradiņš University, LV-1010 Riga, Latvia; 040214@rsu.edu.lv (K.L.S.); 040230@rsu.edu.lv (P.S.); 032155@rsu.edu.lv (A.K.)
[2] Faculty of Computer Science, Information Technology and Energy, Riga Technical University, LV-1048 Riga, Latvia; arturs.nikulins@edu.rtu.lv (A.Ņ.); niks-saimons.puce@edu.rtu.lv (N.S.P.)
[3] Faculty of Civil and Mechanical Engineering, Riga Technical University, LV-1048 Riga, Latvia; elizabete.skrebele@edu.rtu.lv
[4] Faculty of Biology, University of Latvia, LV-1004 Riga, Latvia; everita.elina@biomed.lu.lv
[5] Department of Radiology, Faculty of Medicine, Rīga Stradiņš University, LV-1010 Riga, Latvia; vikdem@rsu.lv
[6] Department of Computer Graphics and Computer Vision, Riga Technical University, LV-1048 Riga, Latvia; katrina.bolocko@rtu.lv
* Correspondence: edgars.edelmers@rsu.lv

Abstract: Objectives: The integration of machine learning and radiomics in medical imaging has significantly advanced diagnostic and prognostic capabilities in healthcare. This study focuses on developing and validating an artificial intelligence (AI) model using U-Net architectures for the accurate detection and segmentation of spinal metastases from computed tomography (CT) images, addressing both osteolytic and osteoblastic lesions. Methods: Our methodology employs multiple variations of the U-Net architecture and utilizes two distinct datasets: one consisting of 115 polytrauma patients for vertebra segmentation and another comprising 38 patients with documented spinal metastases for lesion detection. Results: The model demonstrated strong performance in vertebra segmentation, achieving Dice Similarity Coefficient (DSC) values between 0.87 and 0.96. For metastasis segmentation, the model achieved a DSC of 0.71 and an F-beta score of 0.68 for lytic lesions but struggled with sclerotic lesions, obtaining a DSC of 0.61 and an F-beta score of 0.57, reflecting challenges in detecting dense, subtle bone alterations. Despite these limitations, the model successfully identified isolated metastatic lesions beyond the spine, such as in the sternum, indicating potential for broader skeletal metastasis detection. Conclusions: The study concludes that AI-based models can augment radiologists' capabilities by providing reliable second-opinion tools, though further refinements and diverse training data are needed for optimal performance, particularly for sclerotic lesion segmentation. The annotated CT dataset produced and shared in this research serves as a valuable resource for future advancements.

Keywords: artificial intelligence; spinal metastases; vertebrae segmentation; computer tomography; medical imaging; instance segmentation; radiomics

Citation: Edelmers, E.; Ņikuļins, A.; Sprūdža, K.L.; Stapulone, P.; Pūce, N.S.; Skrebele, E.; Siņicina, E.E.; Cīrule, V.; Kazuša, A.; Boločko, K. AI-Assisted Detection and Localization of Spinal Metastatic Lesions. *Diagnostics* **2024**, *14*, 2458. https://doi.org/10.3390/diagnostics14212458

Academic Editor: Jae-Ho Han

Received: 26 September 2024
Revised: 29 October 2024
Accepted: 2 November 2024
Published: 3 November 2024

1. Introduction

1.1. Machine Learning in Healthcare

Radiomics has emerged as a novel discipline within artificial intelligence, focusing on the extraction of malignancy-associated information from medical images by integrating pathophysiologically significant data into mathematical parameters [1]. Clinical integration of radiomics necessitates several key steps. Initially, a clearly defined target population must be established, utilizing radiomics to achieve improvements over standard-of-care diagnostic examinations. Secondly, technical considerations regarding statistical methodologies are paramount; minimizing variability through image stratification and addressing machine

Annex 5 continued

learning aspects such as potential biases and computational parameters—illustrated by techniques like Bayesian updating—are essential. Thirdly, the reproducibility of experimental test performance must be ensured to validate findings [2]. Additionally, adherence to regulations such as the European Union's General Data Protection Regulation ensures transparency and ethical compliance in clinical applications [1].

Deep residual convolutional neural networks have been employed for the detection of metastatic bone lesions through automatically segmented regions. Deep-learning segmentation techniques can be adapted for use in computed tomography (CT) scans and magnetic resonance imaging (MRI) [3]. CT scans offer a sensitivity of up to 74% and a specificity of 56%, providing comprehensive assessment of the skeletal system and systemic staging, while minimizing patient exposure to radioactivity. MRI, on the other hand, delivers superior resolution for both bone and soft tissue, with proposed sensitivity and specificity rates of 95% and 90%, respectively [1].

Bone metastases can be diagnosed using a variety of imaging modalities, each presenting specific advantages and limitations. Plain radiographs (X-rays) are typically the initial imaging method for patients presenting with bone pain; however, they have limited utility in asymptomatic patients and in evaluating bones with a high cortex-to-marrow ratio, such as the ribs, due to their low sensitivity in detecting subtle or early-stage metastases [4]. In such cases, CT scans are preferred, offering superior resolution for cortical and trabecular bone structures and allowing for adjustments in window width and level. CT provides detailed multiplanar views, enhancing diagnostic sensitivity and specificity. A recent study reported a pooled sensitivity of 72.9% and a specificity of 94.8% for CT in detecting bone metastases, particularly in areas like the ribs [5]. In oncology, CT scans are commonly utilized for staging and follow-up in cancers affecting the thorax and abdomen, covering extensive portions of the axial skeleton. This enables clinicians to assess the spread of metastatic disease and differentiate between metastatic and degenerative changes. CT also assists in evaluating structural abnormalities identified using other modalities such as MRI and scintigraphy [6]. Although other imaging techniques like MRI, positron emission tomography/computed tomography (PET/CT), single-photon emission computed tomography (SPECT), and bone scintigraphy offer higher sensitivities (91% for MRI, 90% for PET/CT, and 86% for scintigraphy), their routine use is limited by higher costs and reduced availability, especially in countries with constrained healthcare resources [7]. MRI is typically reserved for cases requiring detailed soft-tissue contrast or assessment of bone marrow involvement, while PET/CT and scintigraphy are employed in specific scenarios but are less common for general screening, due to their expense and logistical challenges [8].

Selecting the appropriate imaging modality based on clinical needs is crucial for optimizing diagnostic accuracy. CT remains an accessible and reliable choice for detecting bone metastases, especially in complex anatomical regions like the ribs, where other imaging techniques may have limited utility. Artificial intelligence is a rapidly advancing technology demonstrating significant potential across various domains, including medicine. AI is poised to transform numerous aspects of the medical field such as patient care, administrative processes, diagnostics, treatment planning, and scientific research. In radiology, AI is often combined with radiomics to extract quantitative features from medical images, uncovering patterns not visible to the human eye. These radiomic features, when integrated with AI methodologies like machine learning and deep learning, enhance diagnostic accuracy, prognostic predictions, and personalized treatment strategies. AI technologies—including machine learning, natural language processing, and robotics—can be applied independently or synergistically to analyze clinical data, generate reports, assist in diagnosing conditions, and predict treatment outcomes based on patient-specific variables. The integration of radiomics and AI holds the potential to refine medical imaging analysis, offering deeper insights into disease characterization and treatment efficacy [9].

Higher diagnostic accuracy not only improves patient outcomes but also prevents unnecessary tests that consume time and financial resources, pose psychological burdens, and may expose patients to ionizing radiation and toxic contrast media. Research indicates

that artificial intelligence shows promise, with a high accuracy in diagnostics across various specializations:

- Radiology: Recognition of tuberculosis in chest X-ray images, differentiation of benign and malignant lung nodules based on CT data, detection of breast cancer lesions in mammography, and classification of other tumors.
- Pathology: Differentiation of melanocytic lesions, classification of gastric cancer types, prediction of gene mutations associated with cancer, and determination of kidney function from biopsy results.
- Ophthalmology: Diagnosis of retinal diseases, glaucoma, keratoconus, and grading of cataracts.
- Cardiology: Improvement in cardiovascular risk prediction and patient outcome prediction accuracy in pulmonary hypertension.
- Gastroenterology: Endoscopic detection of colorectal polyps, gastric and esophageal cancer, Barrett's esophagus, squamous cell carcinoma, and other lesions.

The growing need for healthcare services and the advancement of artificial intelligence have led to the creation of conversational agents—chatbots and speech recognition screening systems—that can assist with various health-related tasks such as behavioral change, treatment support, health monitoring, training, triage, and screening. Studies have generally shown that these conversational agents are effective and satisfactory [10]. While AI has the potential to automate certain tasks in healthcare specialties involving digital information, such as radiology and pathology, it is not expected to replace healthcare specialists. Instead, AI aims to augment their skills, allowing them to focus more on patient care and tasks requiring uniquely human abilities such as empathy, persuasion, and holistic integration of information. The integration of AI into healthcare presents ethical, legal, and practical challenges that must be carefully addressed. Further research is necessary to fully understand the long-term effects and ensure the safe and effective incorporation of AI-based technologies into healthcare systems [11].

1.2. Vertebral Metastases

Vertebral metastases represent the secondary involvement of the vertebral spine by hematogenously disseminated metastatic cells [12]. They constitute the third most common site of metastasis, after the lungs and liver, and are a major cause of morbidity, characterized by severe pain, impaired mobility, and pathological fractures [13]. Remarkably, vertebral metastases are asymptomatic in 90% of cases and are present in 60–70% of patients with systemic cancer. Approximately 80% of primary tumors give rise to bone metastases [13], which are classified as osteolytic, osteoblastic, or mixed, according to their primary mechanism of interference with normal bone remodeling. Osteolytic lesions are characterized by the destruction of normal bone, while osteoblastic (sclerotic) lesions involve the deposition of new bone [14].

Primary tumors with predominantly osteolytic metastases include breast cancer (65–75%), thyroid cancer (65–75%), urothelial cancer (20–25%), renal cell carcinoma (20–25%), melanoma (14–45%), non-Hodgkin lymphoma, and multiple myeloma. Types with predominantly sclerotic metastases include prostate cancer (60–80%), small cell lung cancer (30–40%), and Hodgkin lymphoma [12–14]. Mixed-type lesions are present in breast cancer (15–20%), gastrointestinal cancers, and squamous cell carcinomas [14]. The incidence of spinal metastatic disease is increasing, due to improved patient survival and advanced diagnostic techniques [15]. Median survival from the diagnosis of bone metastasis varies among different cancers: 6 months in melanoma; 6–7 months in lung cancer; 6–9 months in bladder cancer; 12 months in renal cell carcinoma; 12–53 months in prostate cancer; 19–25 months in breast cancer; and up to 48 months in thyroid cancer [14].

Unfortunately, no treatment has been proven to increase the life expectancy of patients with spinal metastases. The primary goals of therapy are pain control and functional preservation [16]. Therefore, it is crucial, not only to diagnose spinal metastases, but also to monitor disease progression, evaluate the stability of the vertebral column, and

identify patients who may benefit from surgical consultation or intervention. Multiple scoring systems are available for evaluating different aspects of well-being in patients with metastatic spine disease. One such system is the Spinal Instability Neoplastic Score (SINS), which is used to assess spinal instability and acts as a prognostic tool for surgical decision-making [17].

The SINS is based on one clinical factor (pain) and five radiographic parameters: location, bone lesion quality, spinal alignment, vertebral body collapse, and involvement of posterolateral spinal elements. Each component is assigned a score reflecting its contribution to the overall instability of the spinal segment. The six individual scores are summed to yield a cumulative score ranging from 0 to 18, with higher total scores indicating more severe instability [18]. In the evaluation of 131 surgically stabilized spine metastasis patients, the SINS demonstrated near-perfect inter- and intra-observer reliability in determining three clinically relevant categories of stability. Patients with a SINS ≥ 7 who underwent surgical stabilization showed significant improvements in quality of life [15].

The presented research serves as a proof of concept for an upcoming project in which we plan to create a representative cohort group with even age, sex, and oncology stage distribution within the dataset. Our main objective is to locate metastases in patient computed tomography (CT) scans, when present. On a daily basis, small, barely visible occurrences of metastases in CT scans can be easily missed by healthcare professionals. A well-tuned artificial intelligence (AI) system that can indicate regions of possible disease could be crucial for patient outcomes. If there is any deformation of the bone morphology, an AI could detect and record it. Tasks that have been performed manually by professionals could be accomplished faster and with greater precision by AI. After the identification of deformation regions, healthcare professionals could determine whether these are metastases.

The U-Net segmentation architecture was initially developed for medical imaging data analysis. Its architecture provides segmentation masks with the same size as the input, which is ideal for indicating possible metastases. For this project, we utilized a 3D version of the U-Net architecture to work with the three-dimensional nature of CT data, along with the 2D version [19,20]. One study demonstrated that a deep-learning algorithm (DLA) could assist radiologists in detecting possible spinal cancers in CT scans. The system, which used a U-Net-like architecture, achieved a sensitivity of 75% in identifying potentially malignant spinal bone lesions, significantly boosting radiologists' ability to detect incidental lesions that might otherwise go unnoticed due to scan focus or diagnostic bias. In this context, AI serves as a second reader, significantly increasing detection sensitivity, without leading to excessive false positives [21].

Another important component of AI in spinal metastatic imaging is its involvement in early detection and therapy, which is key for avoiding complications and enhancing patient quality of life. Recent research has explored the use of AI approaches in image processing, diagnosis, decision support, and therapeutic assistance, summarizing the current applications of AI applications in spinal metastasis care. These technologies have shown promising results in boosting work productivity and reducing adverse events, but further study is needed to evaluate clinical performance and enable adoption into routine practice [22]. A similar study introduced a deep learning (DL) algorithm designed for diagnosing lumbar spondylolisthesis using lateral radiographs. This research aimed to improve the accuracy of medical diagnostics by assisting doctors in reducing errors in disease detection and treatment. The study was retrospective, involving multiple institutions, and focused on patients with lumbar spondylolisthesis. The DL models utilized included Faster R-CNN and RetinaNet for spondylolisthesis detection, demonstrating the potential of AI to significantly enhance diagnostic accuracy in spinal conditions [23].

2. Materials and Methods

Our research was organized into two distinct stages, utilizing a previously validated methodology for the preprocessing of radiological data to enhance precision in detecting spinal metastases [24]. The first stage centers on the localization of the patient's spine, a

critical step for identifying regions potentially impacted by metastatic disease. In this stage, each vertebra is individually isolated and segmented, starting from the cervical spine and extending through to the lower spine, inclusive of the sacrum and coccyx. This meticulous segmentation allows for a detailed anatomical mapping, which is essential for subsequent identification of metastases.

The second stage targets the identification and classification of metastases by applying segmentation masks to identify lytic and sclerotic metastatic lesions within the spine. Our approach leverages two U-Net-based neural networks: the first network is specifically trained for spine localization and segmentation, ensuring each vertebra is accurately detected. The second network is dedicated to the instance segmentation of metastatic lesions, where it not only identifies the lesions but also categorizes them by type, distinguishing between lytic and sclerotic metastases. This structured, multi-network approach ensures highly accurate localization and identification of spinal metastases, thereby supporting targeted clinical interventions.

For this study, we utilized two distinct datasets. The first dataset, intended for vertebra segmentation, comprises CT scans from 115 patients diagnosed with polytrauma but presenting relatively undamaged spines. These full-body CT scans were acquired at the RAKUS (Rīgas Austrumu klīniskā universitātes slimnīca) hospital. The second dataset, focused on metastasis detection, includes CT scans from 38 patients diagnosed with spinal metastases, with the detailed information outlined in Table 1 [25]. This dual-dataset structure allowed for both a robust segmentation framework and reliable identification of metastatic patterns across diverse patient presentations.

In this study, we leveraged the nnU-Net library's comprehensive, built-in data augmentation capabilities to enhance the model performance and generalizability across diverse imaging scenarios. These augmentation techniques are an integral part of nnU-Net's adaptive framework and include a wide array of transformations, such as rotations, scaling, Gaussian noise, Gaussian blur, adjustments in brightness and contrast, low-resolution simulation, gamma correction, and mirroring. By utilizing nnU-Net's robust and automated augmentation pipeline, our model benefited from consistent, optimized data transformations across all training subsets, significantly increasing the data diversity and minimizing overfitting risks. This built-in augmentation framework allowed for seamless integration of complex augmentation strategies, without additional external code, thus ensuring reproducibility and alignment with nnU-Net's standardized approach.

The augmentation process in nnU-Net is designed to adaptively balance transformation intensity and type based on dataset characteristics, which aligns well with our dual-stage segmentation approach. In the initial stage, the augmentations enhanced the training of the neural network tasked with isolating individual vertebrae from the cervical to the lower spine, including the sacrum and coccyx. In the subsequent stage, augmentations strengthened the model's capability to distinguish between and accurately segment lytic and sclerotic metastases, particularly given the subtle differences in appearance between these lesion types.

The model architecture itself is based on an encoder–decoder structure with skip connections, facilitating the integration of high-level, semantic features with detailed spatial information. This architecture, optimized for segmentation, employed instance normalization to enhance the data consistency across batches, leaky ReLU activation to introduce non-linearity, and deep supervision with topology-adapted parameters. These architectural choices were specifically designed to accommodate the complex, heterogeneous nature of spinal metastases. Skip connections enabled the network to retain high-resolution information across encoding and decoding paths, which is crucial in medical imaging, where spatial precision directly impacts diagnostic utility.

Table 1. Descriptive statistics of the dataset utilized for training the vertebra segmentation model.

Sex	Age	Metastasis Type	Primary Metastatic Site
Female	57	Sclerotic	Melanoma
Female	72	Sclerotic	Lungs
Female	72	Sclerotic	Lungs
Female	68	Lytic	Ovary
Female	39	Sclerotic	Breast
Male	74	Lytic	Prostate
Female	82	Sclerotic	Breast
Female	82	Sclerotic	Breast
Female	64	Sclerotic	Breast
Female	65	Sclerotic	Breast
Female	65	Sclerotic	Breast
Female	61	Sclerotic	Breast
Female	45	Sclerotic	Breast
Female	45	Sclerotic	Breast
Female	70	Sclerotic	Breast
Male	66	Sclerotic	Lungs
Female	52	Sclerotic	Breast
Male	53	Lytic	Kidney
Female	60	Sclerotic	Breast
Male	74	Sclerotic	Blader
Female	79	Lytic	Kidney
Female	48	Lytic	Ovary
Male	66	Sclerotic	Large intestine
Female	73	Lytic	Multiple myeloma
Male	66	Lytic	Multiple myeloma
Female	61	Sclerotic	Breast
Female	73	Lytic	Breast
Female	79	Lytic	Kidney
Female	48	Lytic	Ovary
Male	75	Lytic	Stomach
Male	75	Lytic	Stomach
Male	64	Lytic	Kidney
Female	39	Lytic	Ovary
Male	55	Lytic	Multiple myeloma
Female	60	Lytic	Multiple myeloma
Female	70	Lytic	Breast
Female	32	Lytic	Multiple myeloma
Female	61	Lytic	Kidney

Furthermore, the training data were meticulously curated with segmentation masks, manually created by medical professionals at Riga Stradiņš University using 3D Slicer software (v5.6.0). This software, known for its capabilities in medical image informatics, image processing, and three-dimensional visualization, allowed for precise segmentation, essential for training accuracy. [26] Following segmentation, the data were converted from DICOM into a "nearly raw raster data" format to optimize input/output operations during model training, allowing for efficient handling of the large image volumes typical in medical imaging.

The nnU-Net framework for hyperparameter selection in biomedical image segmentation utilizes a systematic approach to mitigate the complexities associated with manual configuration, as described in the article by Isensee et al. [27]. The automated parameterization in nnU-Net combines fixed, rule-based, and empirical parameters to achieve optimal adaptability across diverse datasets with minimal human intervention.

Fixed Parameters:

Architecture Template: nnU-Net follows a U-Net-like architecture, based on the hypothesis that a well-configured U-Net remains challenging to surpass in performance. This template employs a plain encoder–decoder structure, with two convolutional blocks

per resolution level and instance normalization instead of batch normalization to handle smaller batch sizes (usually 2 for 3D models due to GPU constraints). Patch sizes are large enough to capture contextual information, optimized through an iterative reduction process for efficient GPU utilization.

Training Configuration: Training typically ran for 1000 epochs across 250 minibatches per epoch, employing a learning rate that followed a polynomial decay (initial value 0.01) and was reduced throughout training. The optimization was performed using stochastic gradient descent with Nesterov momentum ($\mu = 0.99$).

Loss Function: nnU-Net utilizes a combined Dice and cross-entropy loss to balance between foreground–background class segmentation accuracy and boundary precision, making it well-suited for various biomedical segmentation tasks.

Rule-Based Parameters:

Dataset Fingerprinting and Target Spacing: For each new dataset, nnU-Net analyzes specific characteristics like voxel spacing and median image shape. For anisotropic datasets (e.g., those with a spacing ratio greater than 3 between axes), nnU-Net employs anisotropic resampling strategies, using the tenth percentile of the lowest resolution axis to maintain structural integrity in resampled images (s41592-020-01008-z).

Patch Size and Network Topology: The initial patch size is determined by the median image shape, and iteratively adjusted to meet GPU memory constraints. Network topology, including the number and configuration of downsampling layers, is adapted according to the target spacing and voxel size, ensuring that the effective receptive field size matches the patch size and contextual requirements (s41592-020-01008-z).

Normalization and Augmentation: nnU-Net applies different normalization techniques based on the modality, with z-score normalization for most cases, but using specific percentile clipping and z-scoring for CT images to retain tissue properties. Data augmentation encompasses a variety of transformations, such as rotations, scaling, noise addition, and mirroring, enhancing the model's generalization ability across various tasks (s41592-020-01008-z).

Empirical Parameterization:

Post-Processing Configuration: Post-processing decisions, such as the inclusion of largest-component suppression, are empirically tested, to assess whether they improve cross-validation performance. This step ensures that nnU-Net achieves optimal accuracy by removing false-positive predictions in multi-class segmentation tasks.

Ensemble Selection: nnU-Net evaluates the performance of different configurations, including 2D, full-resolution 3D U-Net, and a cascaded 3D U-Net, across cross-validation folds. It then selects the best-performing model or an ensemble of configurations to enhance the predictive robustness.

Following data preparation, four U-Net architecture subtypes were trained: 2D images in the form of single slices from CT scans; 3D low-resolution with downsampled input image data; 3D full-resolution utilizing the original resolution of the CT scans; and 3D cascade full-resolution, which used downsampled images to understand the overall structure at a large scale, before learning details from the full-resolution image data, as stated in the utilized library [27].

3. Results

In the first stage, the spine was segmented to support the subsequent analysis of metastatic lesions. The U-Net architecture, trained with five cross-validations, employed a composite loss function that combined Dice loss and cross-entropy loss for optimal segmentation performance. Training was conducted on patches extracted from the original images, and the Dice metric was calculated over these patches to evaluate the segmentation accuracy. During inference, a sliding window approach was utilized, introducing patches that may have differed from those encountered in training, which could have contributed to minor fluctuations in the Dice score.

Validation patches were sampled following the same methodology as during training, enabling a consistent calculation of the Dice coefficient across all sampled validation patches. To monitor the progression of the training and detect potential overfitting, a pseudo-Dice metric was applied, as depicted in Figures 1 and 2. This metric, updated iteratively throughout the training process, served as a preliminary indicator of model performance and differed from the final Dice similarity coefficient, which was computed at the end of training. Unlike the patch-based pseudo-Dice metric, the final Dice similarity coefficient was calculated over the entire image using a sliding window approach, providing a comprehensive assessment of model accuracy on full images.

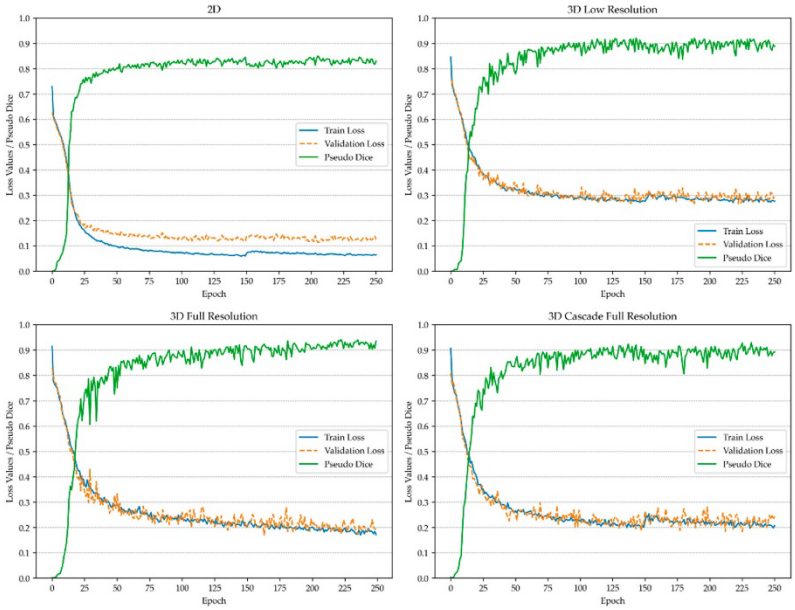

Figure 1. Training process of the model for vertebra detection and instance segmentation.

Performance metrics were derived from validation data using the network architecture that demonstrated the highest performance during training. Metrics related to vertebra segmentation are provided in Table 2, while those for the segmentation of metastatic lesions are detailed in Table 3. This evaluation framework allowed for a robust assessment of model effectiveness in both vertebra and metastasis segmentation, confirming the precision and reliability of the U-Net-based approach for localizing and characterizing metastatic regions within the vertebral column.

Table 2. Metrics for the evaluation of the "3D Full-Resolution" model for vertebra detection and instance segmentation.

Vertebra	Dice Similarity Coefficient	F-Beta Score	Panoptic Quality
C1	0.94	0.94	0.75
C2	0.95	0.95	0.82
C3	0.93	0.93	0.75
C4	0.93	0.93	0.75
C5	0.93	0.94	0.75

Table 2. *Cont.*

Vertebra	Dice Similarity Coefficient	F-Beta Score	Panoptic Quality
C5	0.93	0.94	0.75
C6	0.93	0.93	0.75
C7	0.94	0.93	0.79
T1	0.94	0.94	0.81
T2	0.95	0.95	0.83
T3	0.95	0.95	0.82
T4	0.95	0.95	0.83
T5	0.94	0.94	0.82
T6	0.88	0.87	0.69
T7	0.87	0.88	0.70
T8	0.91	0.92	0.75
T9	0.93	0.93	0.77
T10	0.94	0.94	0.81
T11	0.95	0.95	0.85
T12	0.95	0.94	0.84
L1	0.95	0.94	0.83
L2	0.94	0.94	0.83
L3	0.93	0.92	0.81
L4	0.94	0.89	0.84
L5	0.95	0.94	0.86
Sacrum	0.96	0.96	0.89

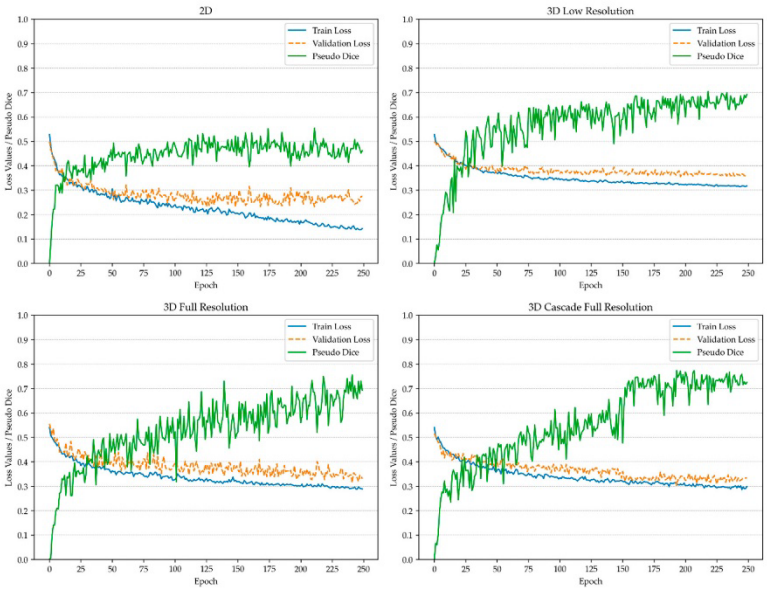

Figure 2. Training process of the model for spinal metastasis detection and instance segmentation.

Table 3. Metrics for the evaluation of the "3D Cascade Full-Resolution" model for metastasis instance segmentation.

Metastasis Type	Dice Similarity Coefficient	F-Beta Score	Panoptic Quality
Lytic	0.71	0.68	0.45
Sclerotic	0.61	0.57	0.30

4. Discussion

Predicting metastasis involves complex spatial and contextual relationships in medical images, which require deep learning models capable of capturing these intricacies. We evaluated several candidate architectures to determine the best performance for our task. VUNet is designed for volumetric (3D) medical data and works well for tasks like organ segmentation in 3D MRI or CT scans [28]. However, our task may involve both 2D and 3D data, and nnU-Net's versatility in handling both 2D and 3D images with minimal modifications made it more appropriate. SegNet is more lightweight and efficient, making it ideal for real-time segmentation [29]. However, it cannot match the performance of nnU-Net on medical image data, particularly in tasks requiring detailed boundary delineation and high-resolution predictions. nnU-Net's ability to automatically handle preprocessing and architecture selection gave it a substantial performance edge over SegNet for our medical segmentation task, where accuracy was more critical than speed.

In discussing the model performance, it is essential to address the limitations and suitability of commonly used metrics, such as the Dice similarity coefficient (DSC), particularly in tasks involving small structures like metastases. The DSC, while widely used, may not be an ideal metric for metastasis segmentation, due to its tendency to overemphasize large structures, potentially undervaluing the segmentation accuracy of smaller lesions. Recent literature have suggested that metrics such as F-beta score and panoptic quality offer more reliable performance assessments for instance segmentation tasks [30]. However, the panoptic quality metric, as presented in Table 3, has been criticized for tasks with a high frequency of small, variably shaped segmentations, as it often treats the background as a separate class, complicating its applicability to metastasis segmentation [31].

Given the specific requirements of oncological diagnostics, the F-beta score was customized to better emphasize recall, thereby reducing the risk of false negatives, which are particularly consequential in cancer detection. For this purpose, we adjusted the F-beta score with a beta value of 2, which prioritized recall while maintaining sensitivity to false positives—striking a balance that is critical in detecting metastases, where both false positives and negatives hold clinical significance.

Our findings indicate that the 3D full-resolution architecture achieved the highest performance for vertebra segmentation, as illustrated by the predicted mask in Figure 3. Similarly, this architecture demonstrated superior performance for metastasis segmentation, with the results shown in Figure 4. Notably, the model successfully detected and segmented metastases, not only in the spine, but also in other skeletal structures, such as the sternum, as depicted in Figure 4. This capability aligns with recent advancements in deep learning applications for metastasis segmentation, particularly in MRI studies focused on spinal metastases. Our model contributed valuable performance metrics for both lytic and sclerotic metastases, supporting the broader trend of AI-assisted segmentation in oncology.

For lytic metastases, our model achieved a Dice similarity coefficient (DSC) of 0.71, an F-beta score of 0.68, and a panoptic quality of 0.45. These results are comparable to those reported by Kim et al. (2024), who achieved a mean per-lesion sensitivity of 0.746 and a positive predictive value of 0.701 with a U-Net-based model [32]. Additionally, Liu et al. (2021) reported similar segmentation results for pelvic bone metastases, achieving a precision of 0.76 and a recall of 0.67 [33]. Our model's F-beta score and DSC values indicate a robust capacity for detecting and segmenting lytic lesions, reinforcing the findings from these related studies.

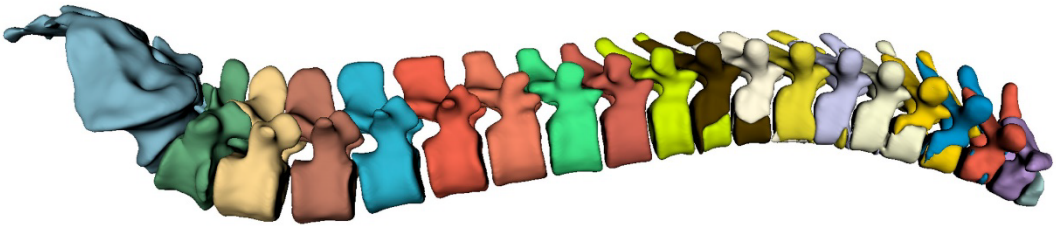

Figure 3. The predicted mask generated by the vertebra segmentation model, with different classes represented in various colors.

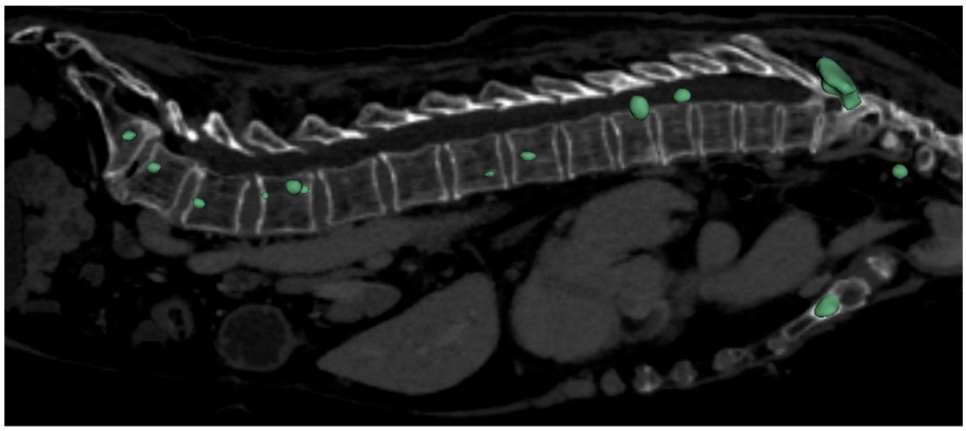

Figure 4. The predicted mask utilizing metastases segmentation model.

However, the segmentation performance for sclerotic metastases was comparatively lower, with a DSC of 0.61, an F-beta score of 0.57, and a panoptic quality of 0.30. This outcome is consistent with reports in the literature; for example, Ong et al. (2022) achieved a DSC of up to 0.78, with sensitivity rates of 78.9% for sclerotic spinal metastases, highlighting the inherent difficulties posed by the subtle imaging characteristics of sclerotic lesions [22]. Our lower scores for sclerotic metastases reflect these challenges, as the detection and segmentation of sclerotic lesions demand higher sensitivity to subtle density changes, which remains a limitation in current AI models for metastasis detection.

In summary, our research illustrates both the strengths and limitations of a U-Net-based model in detecting and segmenting spinal metastases, providing a balanced assessment across relevant metrics. While lytic lesions were identified and segmented with a high degree of accuracy, sclerotic metastases continued to present challenges. These findings suggest the need for further development of specialized architectures or training strategies tailored to the nuanced imaging characteristics of sclerotic metastases, to improve overall diagnostic accuracy in metastatic spinal disease.

A noteworthy benchmark in vertebrae segmentation is provided by the VerSe: Large Scale Vertebrae Segmentation Challenge, where the state-of-the-art models achieved a mean vertebrae identification rate of 96.6% and a Dice coefficient of 91.7%. This challenge has made a substantial contribution to the field by offering a comprehensive dataset of 374 multi-detector CT scans, catalyzing advancements in vertebrae segmentation research [34]. In comparison, our study utilized a significantly smaller dataset, and the model was trained for a shorter duration (250 epochs). Despite these constraints, our model demonstrated competitive performance, particularly in the segmentation of lytic metastases. However,

segmentation of more complex lesion types, such as sclerotic metastases, highlighted areas where further refinement is needed. This comparison underscores the effectiveness of our approach, even within the constraints of limited computational resources and data availability, suggesting its potential for scalability and broader applications.

While our findings are promising, several limitations must be considered. Primarily, the dataset used for training was drawn from a single medical center, which could limit the model's generalizability across different populations and imaging environments. Expanding the dataset to include a wider array of imaging conditions and patient demographics would likely enhance the model's robustness and adaptability, contributing to more consistent performance across varied clinical settings. Additionally, the segmentation masks used in training were created manually by medical professionals, a process susceptible to inter-observer variability. This variability could have introduced inconsistencies in the training data, potentially affecting both the model's learning and the evaluation of its performance. Addressing these issues may involve standardizing segmentation protocols or employing semi-automated segmentation tools to reduce observer-related discrepancies.

Another important limitation is that the model has not yet been validated in real-world clinical environments, where factors such as diverse patient anatomies, varying imaging conditions, and clinical workflow constraints could influence its performance. To ensure the model's utility and effectiveness in clinical practice, further validation through clinical trials is essential. Such trials would help determine its actual impact on diagnostic accuracy and patient outcomes, providing a more comprehensive assessment of its clinical applicability.

Technical considerations related to CT scanning protocols also play a critical role in model performance. Variability in scanning parameters, particularly resolution, can significantly affect model accuracy. For optimal inference results, the radiological data used should ideally match the technical specifications of the training data, as discrepancies in resolution or imaging quality may reduce model effectiveness. The relatively small dataset for metastasis detection impacted the model's performance, particularly for sclerotic lesions, underscoring the need for a more extensive dataset to achieve higher reliability. By incorporating a larger, more diverse set of cases with varying patient demographics and imaging characteristics, we could improve both the model's robustness and its generalizability, ultimately leading to enhanced accuracy in detecting and segmenting metastases across diverse clinical scenarios. This dataset expansion is crucial for increasing the model's diagnostic effectiveness and realizing its full potential in real-world healthcare applications [35,36].

5. Conclusions

This study developed and validated two AI-based models for vertebra and spinal metastasis segmentation, leveraging advanced U-Net architectures to achieve high accuracy across these tasks. Vertebra segmentation demonstrated robust performance, with an F-beta score ranging from 0.88 to 0.96 across vertebra classes, underscoring the model's precision in anatomical localization. For spinal metastasis detection, the model achieved an F-beta score of 0.68 for lytic metastases and 0.57 for sclerotic metastases, showcasing a strong capacity for identifying lytic lesions, while indicating the greater challenges posed by sclerotic lesion segmentation, due to subtler imaging characteristics.

A significant outcome of this study is the publication of a dataset with annotated CT images containing metastases, which can serve as a valuable resource for future research in metastasis detection and segmentation. This annotated dataset contributes essential information for developing and validating models aimed at metastatic disease, offering a foundational source for further advancements in AI-driven medical imaging.

Notably, the model demonstrated the ability to detect isolated metastatic lesions beyond the spine, such as in the sternum, underscoring its adaptability for broader skeletal metastasis detection and supporting its potential utility across varied clinical scenarios. This capability is crucial for early and accurate metastasis detection, potentially improving patient outcomes by enabling more precise targeting of affected regions.

Author Contributions: Conceptualization, E.E.; methodology, E.E.; software, E.E., A.Ņ.; validation, E.E.; formal analysis, E.E.; investigation, E.E.; resources, E.E., K.B., V.C.; data curation, E.E., A.Ņ., K.L.S., P.S., N.S.P., E.S., E.S., E.E.S., A.K.; writing—original draft preparation, E.E., A.Ņ.; writing—review and editing, E.E.; visualization, E.E.; supervision, E.E.; project administration, E.E.; funding acquisition, E.E. All authors have read and agreed to the published version of the manuscript.

Funding: This research was funded by the Development Fund of Riga Technical University.

Institutional Review Board Statement: The study was conducted in accordance with the Declaration of Helsinki, and approved by the Research Ethics Committee of Rīga Stradiņš University (2-PĒK-4/584/2023 at 20 October 2023).

Data Availability Statement: CT Scans of Spine with Metastases (Lytic, Sclerotic). https://doi.org/10.5281/zenodo.13645871 (accessed on 25 September 2024).

Acknowledgments: We express our gratitude to the "INNO HEALTH HUB" program which is implemented by the Design Factory of the Riga Technical University's Science and Innovation Centre and the Riga Technical University's Development Fund with the support of "Mikrotīkls" Ltd.

Conflicts of Interest: The authors declare no conflicts of interest.

References

1. Dong, X.; Chen, G.; Zhu, Y.; Ma, B.; Ban, X.; Wu, N.; Ming, Y. Artificial Intelligence in Skeletal Metastasis Imaging. *Comput. Struct. Biotechnol. J.* **2024**, *23*, 157–164. [CrossRef] [PubMed]
2. Huang, E.P.; O'Connor, J.P.B.; McShane, L.M.; Giger, M.L.; Lambin, P.; Kinahan, P.E.; Siegel, E.L.; Shankar, L.K. Criteria for the Translation of Radiomics into Clinically Useful Tests. *Nat. Rev. Clin. Oncol.* **2023**, *20*, 69–82. [CrossRef] [PubMed]
3. Liu, S.; Feng, M.; Qiao, T.; Cai, H.; Xu, K.; Yu, X.; Jiang, W.; Lv, Z.; Wang, Y.; Li, D. Deep Learning for the Automatic Diagnosis and Analysis of Bone Metastasis on Bone Scintigrams. *Cancer Manag. Res.* **2022**, *14*, 51–65. [CrossRef] [PubMed]
4. Heindel, W.; Gübitz, R.; Vieth, V.; Weckesser, M.; Schober, O.; Schäfers, M. The Diagnostic Imaging of Bone Metastases. *Dtsch. Ärzteblatt Int.* **2014**, *111*, 741–747. [CrossRef] [PubMed]
5. Woo, S.; Suh, C.H.; Kim, S.Y.; Cho, J.Y.; Kim, S.H. Diagnostic Performance of Magnetic Resonance Imaging for the Detection of Bone Metastasis in Prostate Cancer: A Systematic Review and Meta-Analysis. *Eur. Urol.* **2018**, *73*, 81–91. [CrossRef]
6. Ellmann, S.; Beck, M.; Kuwert, T.; Uder, M.; Bäuerle, T. Multimodal Imaging of Bone Metastases: From Preclinical to Clinical Applications. *J. Orthop. Transl.* **2015**, *3*, 166–177. [CrossRef]
7. Liu, F.; Dong, J.; Shen, Y.; Yun, C.; Wang, R.; Wang, G.; Tan, J.; Wang, T.; Yao, Q.; Wang, B.; et al. Comparison of PET/CT and MRI in the Diagnosis of Bone Metastasis in Prostate Cancer Patients: A Network Analysis of Diagnostic Studies. *Front. Oncol.* **2021**, *11*, 736654. [CrossRef]
8. Orcajo-Rincon, J.; Muñoz-Langa, J.; Sepúlveda-Sánchez, J.M.; Fernández-Pérez, G.C.; Martínez, M.; Noriega-Álvarez, E.; Sanz-Viedma, S.; Vilanova, J.C.; Luna, A. Review of Imaging Techniques for Evaluating Morphological and Functional Responses to the Treatment of Bone Metastases in Prostate and Breast Cancer. *Clin. Transl. Oncol.* **2022**, *24*, 1290–1310. [CrossRef]
9. Davenport, T.; Kalakota, R. The Potential for Artificial Intelligence in Healthcare. *Future Healthc. J.* **2019**, *6*, 94–98. [CrossRef]
10. Milne-Ives, M.; De Cock, C.; Lim, E.; Shehadeh, M.H.; De Pennington, N.; Mole, G.; Normando, E.; Meinert, E. The Effectiveness of Artificial Intelligence Conversational Agents in Health Care: Systematic Review. *J. Med. Internet Res.* **2020**, *22*, e20346. [CrossRef]
11. Ahuja, A.S. The Impact of Artificial Intelligence in Medicine on the Future Role of the Physician. *PeerJ* **2019**, *7*, e7702. [CrossRef] [PubMed]
12. Rasuli, B.; Dawes, L. Vertebral Metastases. 2008. Available online: https://radiopaedia.org/ (accessed on 25 September 2024).
13. Shah, L.M.; Salzman, K.L. Imaging of Spinal Metastatic Disease. *Int. J. Surg. Oncol.* **2011**, *2011*, 769753. [CrossRef] [PubMed]
14. Macedo, F.; Ladeira, K.; Pinho, F.; Saraiva, N.; Bonito, N.; Pinto, L.; Gonçalves, F. Bone Metastases: An Overview. *Oncol. Rev.* **2017**, *11*, 321. [CrossRef]
15. Mossa-Basha, M.; Gerszten, P.C.; Myrehaug, S.; Mayr, N.A.; Yuh, W.T.; Jabehdar Maralani, P.; Sahgal, A.; Lo, S.S. Spinal Metastasis: Diagnosis, Management and Follow-Up. *Br. J. Radiol.* **2019**, *92*, 20190211. [CrossRef] [PubMed]
16. Wibmer, C.; Leithner, A.; Hofmann, G.; Clar, H.; Kapitan, M.; Berghold, A.; Windhager, R. Survival Analysis of 254 Patients After Manifestation of Spinal Metastases: Evaluation of Seven Preoperative Scoring Systems. *Spine* **2011**, *36*, 1977–1986. [CrossRef] [PubMed]
17. Fox, S.; Spiess, M.; Hnenny, L.; Fourney, D.R. Spinal Instability Neoplastic Score (SINS): Reliability Among Spine Fellows and Resident Physicians in Orthopedic Surgery and Neurosurgery. *Glob. Spine J.* **2017**, *7*, 744–748. [CrossRef]
18. Murtaza, H.; Sullivan, C.W. Classifications in Brief: The Spinal Instability Neoplastic Score. *Clin. Orthop. Relat. Res.* **2019**, *477*, 2798–2803. [CrossRef]
19. Ronneberger, O.; Fischer, P.; Brox, T. U-Net: Convolutional Networks for Biomedical Image Segmentation. In *Medical Image Computing and Computer-Assisted Intervention–MICCAI 2015, Proceedings of the MICCAI 2015, 18th International Conference, Munich, Germany, 5–9 October 2015*; Springer: Cham, Switzerland, 2015. [CrossRef]

20. Çiçek, Ö.; Abdulkadir, A.; Lienkamp, S.S.; Brox, T.; Ronneberger, O. 3D U-Net: Learning Dense Volumetric Segmentation from Sparse Annotation. In *Medical Image Computing and Computer-Assisted Intervention–MICCAI 2016, Proceedings of the 19th International Conference, Athens, Greece, 17–21 October 2016*; Springer: Cham, Switzerland, 2016.
21. Gilberg, L.; Teodorescu, B.; Maerkisch, L.; Baumgart, A.; Ramaesh, R.; Gomes Ataide, E.J.; Koç, A.M. Deep Learning Enhances Radiologists' Detection of Potential Spinal Malignancies in CT Scans. *Appl. Sci.* **2023**, *13*, 8140. [CrossRef]
22. Ong, W.; Zhu, L.; Zhang, W.; Kuah, T.; Lim, D.S.W.; Low, X.Z.; Thian, Y.L.; Teo, E.C.; Tan, J.H.; Kumar, N.; et al. Application of Artificial Intelligence Methods for Imaging of Spinal Metastasis. *Cancers* **2022**, *14*, 4025. [CrossRef]
23. Zhang, J.; Lin, H.; Wang, H.; Xue, M.; Fang, Y.; Liu, S.; Huo, T.; Zhou, H.; Yang, J.; Xie, Y.; et al. Deep Learning System Assisted Detection and Localization of Lumbar Spondylolisthesis. *Front. Bioeng. Biotechnol.* **2023**, *11*, 1194009. [CrossRef]
24. Edelmers, E.; Kazoka, D.; Bolocko, K.; Sudars, K.; Pilmane, M. Automatization of CT Annotation: Combining AI Efficiency with Expert Precision. *Diagnostics* **2024**, *14*, 185. [CrossRef] [PubMed]
25. Edelmers, E. CT Scans of Spine with Metastases (Lytic, Sclerotic). 2024. [CrossRef]
26. Fedorov, A.; Beichel, R.; Kalpathy-Cramer, J.; Finet, J.; Fillion-Robin, J.-C.; Pujol, S.; Bauer, C.; Jennings, D.; Fennessy, F.; Sonka, M.; et al. 3D Slicer as an Image Computing Platform for the Quantitative Imaging Network. *Magn. Reson. Imaging* **2012**, *30*, 1323–1341. [CrossRef] [PubMed]
27. Isensee, F.; Jaeger, P.F.; Kohl, S.A.A.; Petersen, J.; Maier-Hein, K.H. nnU-Net: A Self-Configuring Method for Deep Learning-Based Biomedical Image Segmentation. *Nat. Methods* **2021**, *18*, 203–211. [CrossRef] [PubMed]
28. Hirose, N.; Sadeghian, A.; Xia, F.; Martin-Martin, R.; Savarese, S. VUNet: Dynamic Scene View Synthesis for Traversability Estimation Using an RGB Camera. *IEEE Robot. Autom. Lett.* **2019**, *4*, 2062–2069. [CrossRef]
29. Badrinarayanan, V.; Kendall, A.; Cipolla, R. SegNet: A Deep Convolutional Encoder-Decoder Architecture for Image Segmentation. *IEEE Trans. Pattern Anal. Mach. Intell.* **2017**, *39*, 2481–2495. [CrossRef]
30. Maier-Hein, L.; Reinke, A.; Godau, P.; Tizabi, M.D.; Buettner, F.; Christodoulou, E.; Glocker, B.; Isensee, F.; Kleesiek, J.; Kozubek, M.; et al. Metrics Reloaded: Recommendations for Image Analysis Validation. *Nat. Methods* **2024**, *21*, 195–212. [CrossRef]
31. Foucart, A.; Debeir, O.; Decaestecker, C. Panoptic Quality Should Be Avoided as a Metric for Assessing Cell Nuclei Segmentation and Classification in Digital Pathology. *Sci. Rep.* **2023**, *13*, 8614. [CrossRef] [PubMed]
32. Kim, D.H.; Seo, J.; Lee, J.H.; Jeon, E.-T.; Jeong, D.; Chae, H.D.; Lee, E.; Kang, J.H.; Choi, Y.-H.; Kim, H.J.; et al. Automated Detection and Segmentation of Bone Metastases on Spine MRI Using U-Net: A Multicenter Study. *Korean J. Radiol.* **2024**, *25*, 363. [CrossRef]
33. Liu, P.; Lu, L.; Zhang, J.; Huo, T.; Liu, S.; Ye, Z. Application of Artificial Intelligence in Medicine: An Overview. *Curr. Med. Sci.* **2021**, *41*, 1105–1115. [CrossRef]
34. Sekuboyina, A.; Husseini, M.E.; Bayat, A.; Löffler, M.; Liebl, H.; Li, H.; Tetteh, G.; Kukačka, J.; Payer, C.; Štern, D.; et al. VerSe: A Vertebrae Labelling and Segmentation Benchmark for Multi-Detector CT Images. *Med. Image Anal.* **2021**, *73*, 102166. [CrossRef]
35. Papalia, G.F.; Brigato, P.; Sisca, L.; Maltese, G.; Faiella, E.; Santucci, D.; Pantano, F.; Vincenzi, B.; Tonini, G.; Papalia, R.; et al. Artificial Intelligence in Detection, Management, and Prognosis of Bone Metastasis: A Systematic Review. *Cancers* **2024**, *16*, 2700. [CrossRef] [PubMed]
36. Koike, Y.; Yui, M.; Nakamura, S.; Yoshida, A.; Takegawa, H.; Anetai, Y.; Hirota, K.; Tanigawa, N. Artificial Intelligence-Aided Lytic Spinal Bone Metastasis Classification on CT Scans. *Int. J. Comput. Assist. Radiol. Surg.* **2023**, *18*, 1867–1874. [CrossRef] [PubMed]

6th Publication

cells

MDPI

Article

Utilisation of Deep Neural Networks for Estimation of Cajal Cells in the Anal Canal Wall of Patients with Advanced Haemorrhoidal Disease Treated by LigaSure Surgery

Inese Fišere [1,2], Edgars Edelmers [3,4,5,*], Šimons Svirskis [6] and Valērija Groma [7,*]

[1] Department of Doctoral Studies, Rīga Stradiņš University, Dzirciema Street 16, LV-1007 Riga, Latvia; inese_fisere@inbox.lv
[2] Surgery Clinic, Pauls Stradins Clinical University Hospital, Pilsonu Street 13, LV-1002 Riga, Latvia
[3] Medical Education Technology Centre, Rīga Stradiņš University, Dzirciema Street 16, LV-1007 Riga, Latvia
[4] Faculty of Computer Science Information Technology and Energy, Riga Technical University, LV-1048 Riga, Latvia
[5] Institute of Electronics and Computer Science, Dzerbenes Street 14, LV-1006 Riga, Latvia
[6] Institute of Microbiology and Virology, Rīga Stradiņš University, Ratsupītes Street 5, LV-1067 Riga, Latvia; simons.svirskis@rsu.lv
[7] Institute of Anatomy and Anthropology, Rīga Stradiņš University, Dzirciema Street 16, LV-1007 Riga, Latvia
* Correspondence: edgars.edelmers@rsu.lv (E.E.); valerija.groma@rsu.lv (V.G.)

Abstract: Interstitial cells of Cajal (ICCs) play a key role in gastrointestinal smooth muscle contractions, but their relationship with anal canal function in advanced haemorrhoidal disease (HD) remains poorly understood. This study uses deep neural network (DNN) models to estimate ICC presence and quantity in anal canal tissues affected by HD. Haemorrhoidectomy specimens were collected from patients undergoing surgery with the LigaSure device. A YOLOv11-based machine learning model, trained on 376 immunohistochemical images, automated ICC detection using the CD117 marker, achieving a mean average precision (mAP50) of 92%, with a recall of 86% and precision of 88%. The DNN model accurately identified ICCs in whole-slide images, revealing that one-third of grade III HD patients and 60% of grade IV HD patients had a high ICC density. Preoperatively, pain was reported in 35% of grade III HD patients and 41% of grade IV patients, with a significant reduction following surgery. A significant decrease in bleeding ($p < 0.0001$) was also noted postoperatively. Notably, patients with postoperative bleeding, diagnosed with stage IV HD, had high ICC density in their anorectal tissues ($p = 0.0041$), suggesting a potential link between ICC density and HD severity. This AI-driven model, alongside clinical data, may enhance outcome prediction and provide insights into HD pathophysiology.

Keywords: interstitial cells of Cajal; deep neural networks; advanced haemorrhoidal disease; LigaSure surgery; anoctamin 1

Academic Editor: Yu Xue

Received: 13 March 2025
Revised: 31 March 2025
Accepted: 3 April 2025
Published: 5 April 2025

Citation: Fišere, I.; Edelmers, E.; Svirskis, Š.; Groma, V. Utilisation of Deep Neural Networks for Estimation of Cajal Cells in the Anal Canal Wall of Patients with Advanced Haemorrhoidal Disease Treated by LigaSure Surgery. *Cells* **2025**, *14*, 550. https://doi.org/10.3390/cells14070550

1. Introduction

The current understanding of haemorrhoidal development suggests that it results from a multifaceted interplay of anatomical and physiological alterations, including the displacement of the anal cushions due to disruption of the fixation network, complex changes within the vascular structures of the anorectal region such as venous distension and altered haemodynamic profiles, distension and subsequent vascular congestion caused by excess tissue, and increased intra-abdominal pressure, which places heightened strain on the anorectal vascular plexus [1].

Annex 6 continued

The prevalence of haemorrhoids ranges from 38.9% to 44.7% in colonoscopy screening, whereas the incidence is around 55% [2–5]. The recurrence rate with nonsurgical techniques is 10–50% over a five-year period, whereas with haemorrhoidectomy, it is less than 5% [3]. A haemorrhoidectomy is the gold-standard treatment for patients with grade III or grade IV haemorrhoidal disease (HD), offering the lowest recurrence rate [3,4,6–10]. The most serious complication is faecal incontinence due to damage to the sphincter, although haemorrhoidectomy can cause changes in continence without direct sphincter injury [6,11]. After excisional haemorrhoidectomy, patients typically have linear wounds that may lead to internal anal sphincter (IAS) hypertonia [10]. Postoperative pain and tenesmus are commonly attributed to increased muscle spasms caused by the surgical wound, often necessitating physiotherapist-led interventions or the addition of neurostimulation for neuromuscular therapy [12].

LigaSure haemorrhoidectomy (LH) is a closed procedure without sutures, using the instrumental sealing of mucosal edges and dividing the pedicle [3]. It reduces reflex anal spasm, allows for bloodless haemorrhoidectomy, accelerates healing, and reduces postoperative pain, often caused by injury or sutures to the IAS [3,6,10]. In LH, the advanced system identifies tissue type between the instrument's jaws, applying the right pressure and energy to seal the vessel wall with minimal tissue damage, proving more effective in reducing postoperative pain and complications than traditional haemorrhoidectomy [3,7,13].

In the gastrointestinal (GI) tract, interstitial cells of Cajal (ICCs) act as natural pacemakers, generating bioelectrical slow waves that trigger electrical activity and regulate gut motility [14–16]. This pacemaker function, involving the generation of calcium waves, triggering rhythmic contractions, and establishing basal tone, has been previously proven for the IAS [17]. ICC pacemaker activity is thought to arise from intracellular Ca^{2+} release from the smooth endoplasmic reticulum, activating anoctamin 1 (ANO1), a calcium-activated chloride channel [17,18].

The substantial progress made in artificial intelligence (AI) over the past decade has the potential to significantly impact clinical practice. Furthermore, recent AI-guided applications have been developed to enhance the morphological analysis of various upper and lower GI tract pathologies, including inflammatory conditions and tumours [19–23]. Moving beyond these well-recognised and explored pathologies, we propose applying AI to a specific anatomical region of the GI tract—the anal canal. In our study, the use of an artificial neural network structured as a deep neural network (DNN) aimed to map the tissue distribution of ICCs, thereby improving the understanding of the underlying ICC pacemaker function and coupling these findings with the investigation of clinical data and LH surgical outcomes using extensive bioinformatics. This novel approach specifically targets the results of LH surgery, emphasising the need for an in-depth analysis of the pathobiology of HD, particularly when addressing the major complaints and treatment strategies.

The primary objective of this study was to determine the capacity of AI, specifically the integration of DNN into the pathology workflow, and its application in the IHC analysis of anal canal tissues removed during LH intervention. Additionally, it aimed to link these data to the assessment of surgical outcomes in patients with advanced stages of HD.

2. Materials and Methods

2.1. Study Design

In this retrospective cohort study, forty-two patients were included who underwent excisional haemorrhoidectomies with the LH device at Pauls Stradiņš Clinical University Hospital, Riga, Latvia, from January 2021 to December 2022. The database used for patient selection was comprehensive and included HD patients from a regional medical centre, thus enhancing the representativeness of the study population. This study was approved

by the Ethics Committee of Riga Stradiņš University (Decision No. 22-2/264/2021) and conducted in accordance with the Declaration of Helsinki. All sensitive information was excluded, and informed consent was obtained from all study participants.

The inclusion criteria for the study cohort were patients over 18 years of age with haemorrhoidal disease grade III or IV, with indications for excisional haemorrhoidectomy, identified with an American Society of Anaesthesiologists (ASA) score of I or II. The exclusion criteria were patients with concomitant pathologies of the anal region (sphincter defect, rectal prolapse, polyps, inflammatory diseases, etc.), previous operations for anal incontinence, existing incontinence for solid stool, identified with an ASA score of III, or a planned duration of hospitalisation due to general illnesses exceeding three days. The rationale for excluding these pathologies was to obtain more objective data on the healing process in conjunction with LigaSure surgery for HD and to ensure a proper understanding of the postoperative clinical manifestations that occur thereafter.

The following clinical parameters were recorded, collected, and analysed: age, sex, presenting symptoms, complaints, surgery description, immediate postoperative complications, and visit conclusions. Pain intensity was assessed using the Visual Analogue Scale (VAS). Postoperative digital and anoscope examinations were carried out during follow-up visits for six weeks, with a final control visit 9 months after surgery.

2.2. Surgical Procedure

The procedure was performed using an LH device. Excisional haemorrhoidectomies were carried out for symptomatic prolapsed haemorrhoids, with an optimised combination of pressure and radiofrequency at positions 5, 7, and 11 o'clock. The patient received premedication, analgesia, and 500 mg of metronidazole preoperatively. Under regional anaesthesia, in the lithotomy position, a 5 mm "V" incision was made with scalpel No. 11 at the border of the anal canal and the skin using an anoscope. The nodule was retracted, and the LH was placed 3 mm above the sphincter at the base of the haemorrhoidal nodule and resected without any sutures. Haemostasis control was then carried out, if necessary, using electrocoagulation. A swab with lidocaine-containing gel was inserted into the rectum for up to 24 h after surgery. Patients were discharged the next day after wound control, with analgesic and flavonoids, and analgesia and granulation-enhancing ointments.

2.3. Immunohistochemistry Procedure

Forty-two formalin-fixed and paraffin-embedded (FFPE) HD anorectal tissue samples were collected retrospectively, sectioned, and mounted on SuperFrost Plus slides (Gerhard Menzel GmbH, Braunschweig, Germany). Haematoxylin and eosin staining confirmed the diagnosis of HD and identified the tissue site relative to the dentate line and mucosal epithelial type. CD117, used as the primary protein marker of ICCs in pathology specimens, and ANO1, also known as TMEM16A, expressions were assessed immunohistochemically according to the manufacturer's guidelines. Deparaffinised sections were incubated overnight at 4 °C with a rabbit monoclonal antibody against CD117 (c-kit) (YR145) (Cell Marque, Rocklin, CA, USA, 1:300 dilution) and a rabbit polyclonal antibody against TMEM16A (Abcam, Cambridge, UK, 1:100 dilution, ab201980). The IHC reactions were visualised using a HiDef Detection HRP Polymer system and a diaminobenzidine substrate kit (Cell Marque, Rocklin, CA, USA), with Mayer's haematoxylin counterstaining cell nuclei. Negative controls omitted the primary antibodies. The immunostaining was conducted on all tissue slides at once to achieve objective results from IHC performance, avoiding multiple repetitions. The evaluation of the results was performed by two experienced morphologists who were blinded to the clinical and histopathological data. Images were captured with a Glissando Slide Scanner (Objective Imaging Ltd., Cambridge, UK). ANO1 expression

was assessed using semiquantitative scoring: 0 for negative expression, 1 for 1–10%, 2 for 11–50%, and 3 for over 50%, in both epithelial cells of the crypt and myocytes.

2.4. Training and Validation Cohorts

Models of varying architecture sizes were trained and optimised to enhance performance and efficiency. Through careful simplification, each model was refined to balance accuracy with computational demands. A total of 40 patches, each with a resolution of 2048 × 2048, were extracted from whole slide images (WSIs), depicting immunohistochemically detected ICCs. These images were initially obtained at maximum magnification. To align with the recommended patch size of the YOLOv11n-obb architecture, each image was subsequently divided into smaller 1024 × 1024 sections, producing a total of 160 images. All images were annotated, resulting in 1871 labelled masks for training purposes.

YOLOv11 is among the newest architectures offering oriented object detection capabilities. Oriented object detection extends conventional methods by incorporating an additional angular parameter, which enables the more precise localization of objects within an image. Moreover, it has been demonstrated to achieve state-of-the-art performance in terms of mAP50 and processing speed on the standard COCO dataset [24].

The rotation and flipping augmentation techniques were employed to enhance the trained model's robustness and mitigate potential performance variations due to differing immunostaining intensities. The final dataset comprised 376 images for training, with an additional set of 32 non-augmented images used for validation. Images representing all possible variations in the anorectal tissue, including mucosal epithelium, connective tissue, as well as both compact and loose muscular components, tissue regions distorted by dilated and disrupted vessels, and images depicting diverse distributions of ICCs, were selected. This selection process was consistently applied to both the training and validation sets.

The validation was performed by evaluating the model on a held-out validation set at the end of each training epoch. During this phase, the model performs inference on all validation images, and its predictions are compared to the corresponding ground truth annotations. Non-maximum suppression is applied to eliminate redundant bounding boxes, ensuring that each object is detected only once. The evaluation process calculates key metrics such as precision, recall, and mean average precision (mAP), specifically mAP50—where an Intersection over Union (IoU) threshold of 0.5 is used—and mAP averaged over a range of thresholds (mAP50-95). These metrics are aggregated across the entire validation set to provide a comprehensive assessment of the model's performance on unseen data, guiding adjustments in hyperparameters and serving as a checkpoint for selecting the best-performing model.

2.5. Statistics

Data analysis and visualisation were executed utilising GraphPad Prism 9.0 for MacOS (GraphPad Software, San Diego, CA, USA), Jamovi (version 2.4.12, The Jamovi Project, Sydney, Australia), and JMP 17 (SAS, Cary, NC, USA). Descriptive statistics for clinical parameters were represented as median values accompanied by their corresponding interquartile ranges (IQRs). For the comparative analysis of immunostaining values within HD patient groups, the non-parametric Wilcoxon signed-rank test was employed. The distribution of variables in the anorectal tissue of male and female patients with HD was assessed using Chi-squared analysis. To explore potential associations between patient symptomatology and demographic correlations with sex, Spearman's rank correlation coefficient was calculated. Multivariate pattern recognition was performed through hierarchical cluster analysis using Ward's minimum variance method, enabling the identification of distinct subgroups, the exploration of data similarities and differences, and the detection

of latent data structures. The threshold for statistical significance was set at $p < 0.05$ for all analytical procedures.

3. Results

The median age was 53 years for women and 46 years for men, with a range of 24 to 72 years. Three women (15%) and seven men (31.81%) were under 40. Of the patients, 50% of women and 45.45% of men had HD stage III, while 50% of women and 54.55% of men had HD stage IV. Bleeding was the main preoperative complaint in both genders for HD stage III (75%), followed by prolapsed tissue (45%) with no significant gender differences. Men reported more faecal spotting (20%) and formations (20%) than women (10%). For HD stage IV, bleeding (72.7%) and formations (40.9%) were most common, with pain more frequent in women (38.4%) than men (4.5%). Males complained more of faecal spotting (18.2%) and discomfort (18.2%), while women reported itching and burning (18.2%). There were no significant gender differences in preoperative complaints across age groups. The average HD symptom duration was 4.6 years for women and 7.8 years for men. While women had more nodes excised, this was not associated with patient complaints.

At the first postoperative visit, 1–2 weeks after LH, discomfort and maceration were more pronounced in males (15%), with 25% reporting bleeding without defecation after haemorrhoidectomy for grade III HD compared to none after grade IV HD. Faecal incontinence occurred in 10% of males after LH for HD III but not in those with HD IV. Both grades provoked tenesmus in males, more so after grade IV (13.6%). In contrast, females showed fewer postoperative complaints, with 10% experiencing faecal incontinence after LH for HD III. After grade IV surgery, 13.6% of women had bleeding without defecation. Maximum pain (VAS score of 8) was reported by six (30%) women aged 43–66 years (mean age 56.8), one of whom had reduced anal sphincter tone preoperatively. In males, only two (9.09%) patients reported maximum pain, aged 30 and 52, with abnormal anal sphincter tone. Three males aged 27, 29, and 44 had persistent complaints beyond 6 weeks, including discomfort, oedema, and previous issues such as bleeding, tissue prolapse, faecal incontinence, discomfort/itching, peri-anal formations, and obstructive defecation. The research data regarding the complaints of study participants and the stage of HD have been summarised and are presented in Figure 1.

In the postoperative period, analgesia was administered to all patients, with Ultracod 500 mg/30 mg tablets (up to 4× daily) or Ketanov 10 mg tablets (up to 2× daily) being the most common. Flavonoids were prescribed in 76.2% of cases, while antibacterial therapy was indicated in 19%. Topical granulation-stimulating creams were used in 42.9% of patients, and diltiazem was applied topically in 28.6% of patients, with men receiving it twice as often. Physiotherapist supervision for pelvic muscle coordination was required in 16.7% of cases, with no significant gender difference. Neurostimulation for correct neuromuscular therapy was needed in 14.3% of patients, equally distributed across both sexes (Supplementary Figure S1).

In the "All" columns, dark red ovals represent the most pronounced complaints (>30%) in terms of percentage, while brown ovals indicate less pronounced complaints (20–30%). Orange ovals highlight complaints that are dominant in either women or men, whereas red ovals denote significant differences between the sexes, as determined by Fisher's exact test ($p < 0.05$).

CD117 and ANO1 immunohistochemistry were employed to detect the presence and distribution of ICCs and to assess the membranous expression of ANO1, a calcium-activated chloride channel found in anal glandular and smooth muscle cells, respectively. Immunostaining revealed ICCs as ramified cells, dispersed among the smooth muscle cells. The density of ICCs associated with the muscular component of the anal canal wall, as

estimated in the study cohort of patients with HD, varied significantly (Figure 2a–c). With the loosening of the muscular component of the anal canal wall and the appearance of large, dilated vessels, the ICCs demonstrated a reduction in number and were often localised perivascularly.

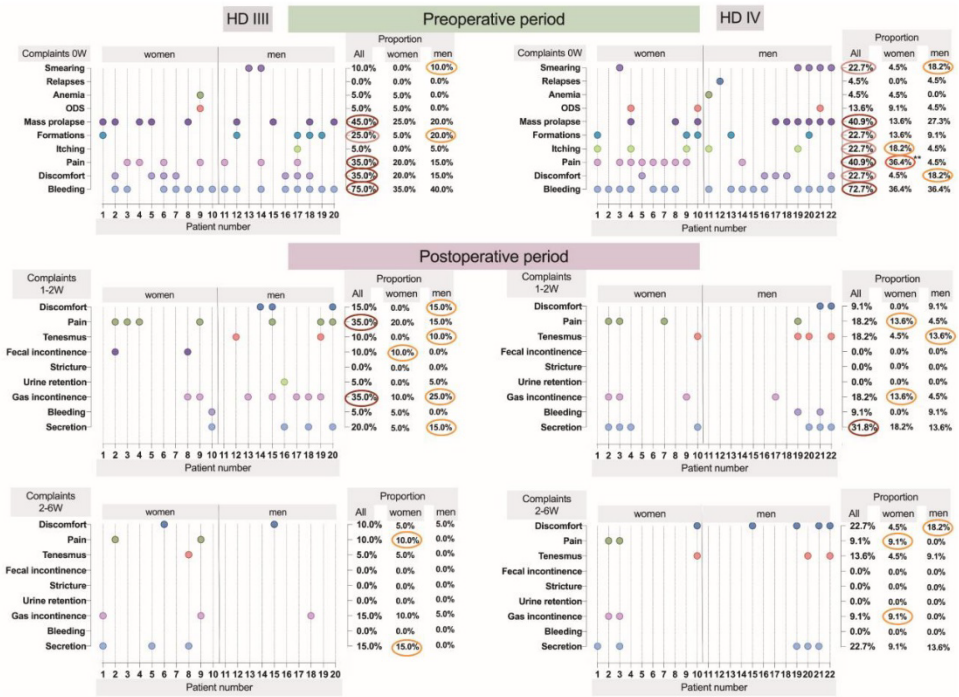

Figure 1. Dynamics of preoperative and postoperative complaints of study participants, along with disease characteristics.

ANO1 immunoreactivity was predominantly observed at the membrane of anal gland epithelial and smooth muscle cells (Supplementary Figure S2). The expression of ANO1 across the specimens in the study cohort varied considerably, with some membranes showing no expression, while others were assessed semiquantitatively with a score of "3", indicating appropriate expression in more than 50% of the structures.

Several models of varying sizes were trained to detect ICCs, as shown in Figure 3. Training was conducted over 51 epochs, evaluating model performance using three primary metrics: mAP50, mAP50-95, and F1 score. All DNN models exhibited similar performance, achieving a mean average precision at 50% (mAP50) of 92%, with a recall of 86% and a precision of 88%, which is deemed adequate for cell-counting tasks. The model selected for integration prioritised efficiency, balancing low parameter count for improved performance on low-powered devices and faster inference speed. The final model chosen for implementation was YOLOv11n-obb, optimised for both accuracy and resource efficiency [24]. The surface area quantification module within the programme provided a method for assessing histological sections and delineating specific tissue regions. Utilising either the resolution metadata embedded within TIFF files or a user-defined pixel size, the algorithm performs pixel-to-area conversions in square millimetres. Through the application of morphological operations, the programme generates a tissue mask, facilitating the computation of the tissue-occupied area relative to the entire histological slide. Following model training, the

"MorpHista" (1.0) software was developed to efficiently process large WSIs and quantify ICCs. It integrated automated detection and post-processing, addressing the challenge of reassembling segmented regions after inference to consolidate all detected features into a single image file while compiling relevant statistics, including ICC counts. The tool has been made publicly available, enabling reproducible ICC analysis and fostering broader research innovation in digital pathology.

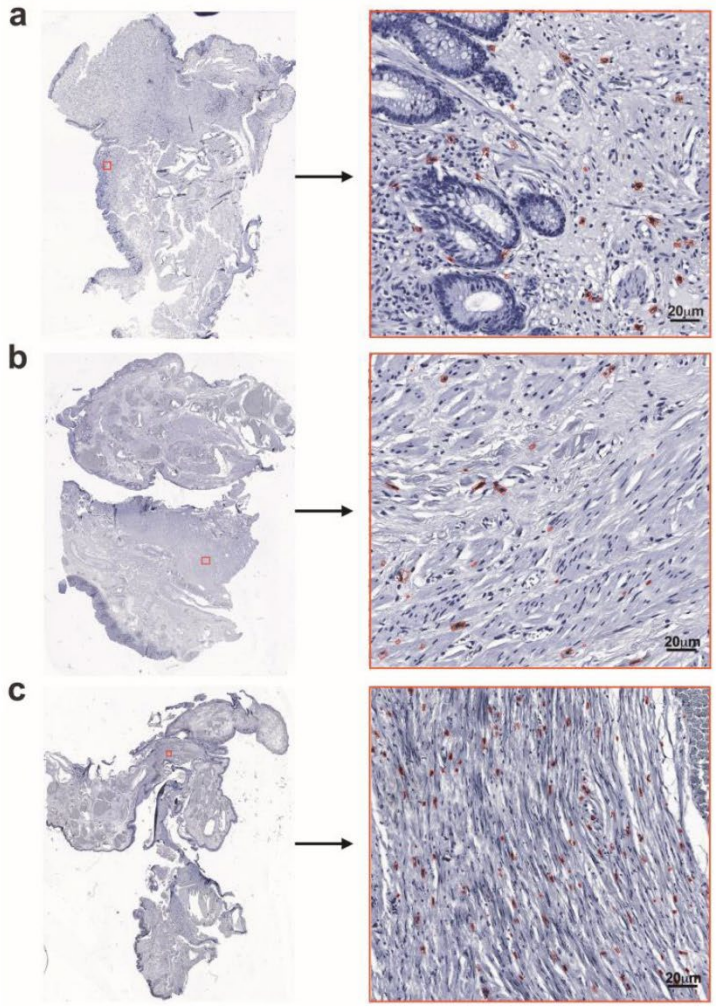

Figure 2. ICC IHC performed on FFPE HD anorectal tissue samples, processed from whole slide images with region selection and detection using DNN. (**a**) A representative image demonstrating the loosening of the mucosal muscular component with haphazard orientation of myocytes, with some ICCs displaying brown coloration. (**b**) A small number of ICCs in the muscularis externa, corresponding to DNN detection. (c) Densely distributed ICCs in the muscularis externa, as detected by DNN. Scale bars: 20 µm.

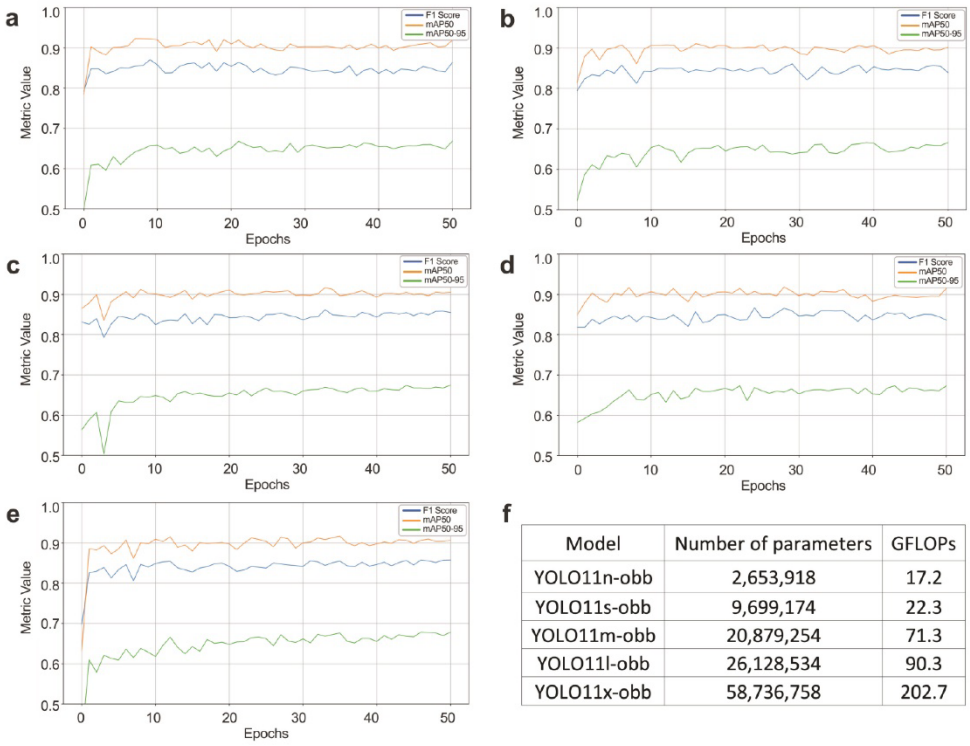

Model	Number of parameters	GFLOPs
YOLO11n-obb	2,653,918	17.2
YOLO11s-obb	9,699,174	22.3
YOLO11m-obb	20,879,254	71.3
YOLO11l-obb	26,128,534	90.3
YOLO11x-obb	58,736,758	202.7

Figure 3. Performance of the trained models. (**a**) YOLO11n-obb, (**b**) YOLO11s-obb, (**c**) YOLO11m-obb, (**d**) YOLO11l-obb, (**e**) YOLO11x-obb, and (f) parameters of the trained models.

Despite the efforts to incorporate a segmentation approach for quantifying ANO1 expression, we did not achieve our targeted Dice coefficient. This shortfall highlights the complexity inherent in pixel-level classification tasks, especially given the variability in staining intensities and tissue morphology within our dataset. A robust linear regression analysis simultaneously confirmed an inverse relationship between the number of ICCs and ANO1 expression in anorectal tissue of patients with advanced HD. Tissue samples with reduced ANO1 expression in myocyte membranes showed a higher number of ICCs, whereas samples with elevated ANO1 expression exhibited a lower number of ICCs (Supplementary Figure S3). However, further hierarchical clustering analysis revealed other important trends (Supplementary Figure S5). It confirmed that HD patients in the green cluster, as well as most in the blue cluster, exhibited low to moderate ICC density in their samples, which corresponded with low ANO1 expression. In contrast, patients in the orange cluster predominantly displayed high ICC density alongside elevated ANO1 expression. Finally, patients in the red cluster demonstrated highly heterogeneous patterns for both ICC density and ANO1 expression, including both similar and inverse correlations. Collectively, these findings, coupled with the inherent complexity of HD biology and the influence of individual patient characteristics identified in this analysis, provide an important context for understanding the results.

To gain a deeper understanding of the contribution of ICCs to the development of HD, we performed a correlation analysis of the estimations obtained using the AI-driven approach with surgically removed anal canal tissues, exploring the association between the

number of counted ICCs and the tissue area of the anal canal wall. The estimated density of ICCs across surgical samples of various shapes and sizes is presented in Supplementary Figure S4. A 95% confidence interval (CI) for the mean calculated from the sample ranged from 0.3900 to 0.7849 ($p < 0.0001$).

Finally, in conducting an in-depth analysis of ICC estimation across the study samples, we aimed to enhance the understanding of the pathophysiology of HD. To this end, we applied an unsupervised clustering method to the research data, incorporating clinical data, IHC data, and DNN-derived findings related to the quantification of ICCs, which constituted either five (Supplementary Figure S5) or six (Figure 4) major factors included in the analysis. Of the patients, 43% of women and 57% of men had HD stage III, while 52% of women and 48% of men had HD stage IV. The ICCs appeared to be almost equally densely distributed across two large clusters of HD patients, characterised by disease grades III and IV, constituting 58% and 57%, respectively, of the anorectal tissues obtained from patients with HD grades III and IV (Supplementary Figure S5). Upon conducting the cluster analysis based on the exploration of six factors, only one-third (36%) of patients with HD grade III exhibited a high density of ICCs in their surgical specimens. In contrast, 60% of patients with HD grade IV showed a high density of these cells. For both stages of HD, discomfort, pain, and bleeding were observed both pre- and postoperatively. Specifically, preoperatively, pain was reported in 35% of patients with grade III HD and 41% of those with grade IV; however, it was markedly reduced following surgical treatment for stages III and IV HD. Regarding bleeding, a statistically significant reduction ($p < 0.0001$) in this symptom was observed postoperatively. However, two patients who experienced postoperative bleeding were diagnosed with stage IV HD and exhibited a high density of ICCs in their anorectal tissues ($p = 0.0041$), suggesting a potential association between ICC density and the severity of HD.

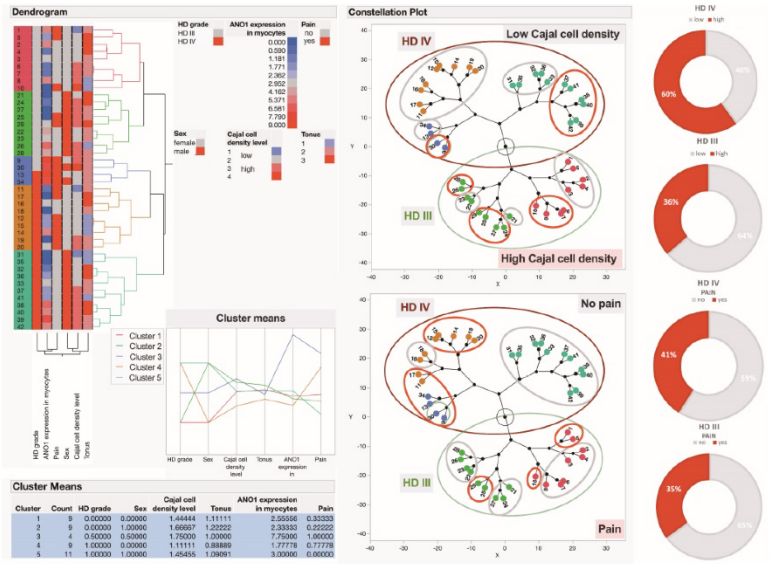

Figure 4. Hierarchical clustering of HD patients and visual representation of ICC density, pain manifestation, and disease severity in the study cohort. The dendrogram, as the output of the hierarchical clustering algorithm, represents a two-dimensional tree structure that depicts the order

of nested clusters within the studied HD patient cohort, with respect to ICC density, pain manifestations, muscular tone, ANO1 expression levels in myocytes, patient sex, and disease severity. Variables are colour-scaled from blue to red, representing a gradient from the lowest to the highest observed values. The dendrogram demonstrates that distinct clusters of HD patients were identified primarily based on disease grade, patient sex, as well as ICC density and the presence of pain. Patients in the red, yellow-green, and one half of the blue-coloured clusters presented with HD grade III, whereas the remainder of the study cohort had grade IV. Notably, HD patients grouped in the blue-green-coloured cluster and most of the red-coloured cluster presented without pain, whereas HD patients in the blue-coloured cluster and half of the orange-coloured cluster manifested with pain. All HD males identified in the blue-green-coloured cluster, and almost all females in the red-coloured cluster, presented without pain.

Using hierarchical clustering analysis, groups with similar characteristics were identified, with characteristics within a specific cluster being more like each other than those across the five clusters recognised in this study. The hierarchical clustering dendrogram shown in Figure 4 illustrates the formation of distinct patient clusters within the HD cohort. The constellation plots further illustrate the clustering of HD patients based on the varying levels of the respective variables. Additionally, the pie charts provide a visual representation of the disparities between patients with grade III and IV HD, categorised by low and high ICC density, alongside the differentiation between those manifesting with and without pain.

4. Discussion

HD is one of the most prevalent anorectal conditions encountered in general practice, affecting approximately one-third of the global population [6,25]. It is a leading contributor to lower GI bleeding and is recognised as a significant cause of morbidity [26]. It is a multifaceted condition that often carries significant emotional strain, necessitates daily adjustments, and has a considerable social impact. Common symptoms such as bleeding and pain frequently cause patients to experience fear and embarrassment, leading them to limit or avoid social activities. While some patients manage to adjust their daily routines to cope with the condition, many seek medical advice for treatment. Modern advanced surgical techniques for managing haemorrhoids, such as stapled haemorrhoidopexy, LigaSure excision, and haemorrhoidal artery ligation, generally yield positive outcomes. However, these procedures have become increasingly costly compared to traditional interventions, resulting in economic and social challenges within the community [27,28]. Therefore, research into surgical interventions that reduce tissue trauma, minimise incontinence, and improve wound healing without complications has been conducted.

Modern treatment methods for HD typically reduce both the duration of surgery and the recovery time required for patients to return to normal daily activities, compared to conventional surgical techniques. LH and Doppler-guided ligation of the haemorrhoidal arteries each have their own advantages and disadvantages. The reported length of hospital stays, postoperative bleeding time, and post-defecation pain score are significantly higher with LH. In contrast, the amount of bleeding during the operation is greater with vascular ligation [29]. As a bipolar electrosurgical instrument, the LigaSure device meets these requirements by achieving local tissue haemostasis through the denaturation of collagen and elastin within the vascular wall and surrounding connective tissue [30,31]. Haemorrhoidectomy performed with a vascular sealing device and the use of topical calcium channel blockers have demonstrated excellent results in reducing postoperative pain [32,33].

The complication rate following haemorrhoidectomy is generally proportional to the grade of the disease and the invasiveness of the surgery [34]. Postoperative pain presents a

significant challenge after haemorrhoidectomy. In our study cohort, 35% of patients with grade III HD and 41% of patients with grade IV HD reported pain preoperatively, but this symptom was alleviated after surgery, suggesting the success of the applied treatment. The causes of post-haemorrhoidectomy pain are multifactorial, including the choice of surgical technique, the wound healing process, spasm of the anal sphincters, spasm of the *musculus puborectalis*, the administration of postoperative analgesia, stool consistency, and other factors [11,32,35]. While external sphincter spasms are typically mild and transient, IAS spasms can persist for longer. These spasms may result from exposure of the IAS myocytes during surgery, irritation by faeces, or involvement in suture bites. If the IAS spasm persists after the excised area heals, it may lead to an anal fissure, causing long-term pain following haemorrhoidectomy [36].

Several approaches can help reduce post-haemorrhoidectomy pain, such as the selection of the most suitable yet least traumatic surgical technique, the use of intraoperative adjuncts, anaesthetic methods, and postoperative interventions. Analgesics have been reported to provide the effective management of post-haemorrhoidectomy pain, regardless of whether they are administered locally or systemically [32,36]. These were applied to all study participants in our research (100% of cases). The second most used medication during the postoperative period was the application of phlebotonics, administered in two-thirds of all HD cases. These findings align with the results reported by other authors [37,38]. The topical application of diltiazem has been reported to effectively relieve pain after haemorrhoidectomy [32,33]. It acts by inhibiting the flow of extracellular calcium ions into the cisternae of the smooth endoplasmic reticulum in IAS myocytes, thereby preserving oxygen, which results in muscle relaxation and pain relief [33]. Previous studies have demonstrated that calcium channel blockers induce the relaxation of smooth muscle cells in the GI tract, and oral diltiazem has been shown to reduce resting anal pressure [32,33]. Almost one-third of all HD patients included in this study were treated with diltiazem.

Pain in HD implicates spasm of the IAS and the functioning of ICCs; however, it does not establish causality for this association. These are ubiquitous cells found between and within the smooth muscle layers of the digestive tract, from the oesophagus to the IAS in humans [39]. They exhibit CD117 (c-kit) immunopositivity and display morphological heterogeneity [40]. Previous studies have demonstrated that, in patients with obstructed defecation syndrome, ICCs are more densely distributed in the anterior wall of the rectum compared to the posterior wall and are more abundant than those in the controls, where ICCs are more evenly distributed, with their density being lower in the IAS [41,42]. In gastrointestinal inflammatory conditions, the number of ICCs is reduced, and ICCs exhibit abnormal ultrastructure and impaired function, which strongly suggests that gastrointestinal dysmotility in these diseases is partly due to ICC injury [43]. Furthermore, a link between ICCs and gastrointestinal stromal tumours (GISTs), which share similar markers indicating a common origin, has been suggested. ICCs, undergoing genetic alterations similar to those in GISTs, may act as precursors or provide a supportive microenvironment for GIST growth [44]. ICCs are electrically active cells that generate and transmit slow waves along the digestive tract, coordinating smooth muscle contractions and peristalsis [45,46]. However, under the influence of local tissue factors activating paracrine mechanisms, this pacemaker function can become excessive, leading to the creation of an ectopic pacemaker site that may initiate abnormal contractions [47–50]. ANO1, a Ca^{2+}-activated Cl^{-} channel associated with the pacemaker function of ICCs, is an important molecule responsible for the mechanism of slow waves [47–49]. Unfortunately, under the conditions set in this investigation, we were unable to demonstrate significant associations between the expression of this plasma membrane protein and the ICC marker. Further research, incorporating individual features of HD patients and involving a larger cohort, may provide deeper

insights into the complex biology of the disease [51,52]. Distributed within the smooth muscle layers, ICCs play a key role in regulating rhythmic muscle contractions [53]. This function is also facilitated by their mechanosensitive properties and the functioning of sodium channels, which enable the transduction of inhibitory and excitatory motor neuron inputs [54,55]. ICC dysfunction can cause motor abnormalities in conditions such as slow transit constipation, chronic idiopathic pseudo-obstruction, Hirschsprung's disease, diverticular disease, and faecal incontinence [51,52]. The decline in ICC numbers, mainly due to the suppression of the signal-regulated kinase 1/2 signalling pathway, has also been observed alongside the ageing process and contributes to impaired fundic relaxation and decreased gastric compliance [56]. However, the specific role of ICCs in disease is not fully understood, highlighting the need for their detailed characterisation.

ICCs and their function have received significant attention from researchers across various medical subfields, with a range of methodologies, including computational approaches and mathematical modelling, employed for the precise quantification of these cells [57,58]. So far, most AI studies have focused predominantly on clinical and imaging modalities rather than on biological tissue data exploration [59]. AI-based methods have demonstrated considerable success in detecting various tumours and inflammatory conditions of the GI tract, contributing to the development of objective scoring systems for risk stratification, and being used to predict disease prognosis, including patient survival and treatment response [60,61]. However, to our knowledge, no research to date has employed a DNN-based model specifically to detect and quantify ICCs using tissue characteristics observed after immunohistochemical labelling. Notably, the recent systematic review and meta-analysis by McGenity et al. synthesised findings from 100 AI-driven pathology studies (48 included in the meta-analysis) and reported mean sensitivities and specificities of 96.3% (95% CI 94.1–97.7) and 93.3% (95% CI 90.5–95.4), respectively [31]. Our detection approach, characterised by an mAP50 of approximately 92%, falls within this high-accuracy range. These findings suggest that our model achieves performance comparable to recently developed AI systems in digital pathology, highlighting the versatility and diagnostic potential of DNN-based approaches for a wide range of histopathological applications.

In this research, we demonstrate that morphologically based DNN models can effectively integrate with clinical patient assessments to accurately predict surgical outcomes for HD patients. The models were trained and validated to identify the specific immunohistochemical marker CD117, which is characteristic of ICCs. This focus on ICCs is crucial due to its significant role in the pathophysiology of HD. We emphasised that a deeper understanding of the pathogenetic mechanisms of the disease, facilitated using AI, in conjunction with the appropriately selected and applied surgical technique, along with the use of appropriate pharmacological therapy and interventions during the postoperative period, can contribute to achieving better clinical outcomes.

The strengths of this study lie in our integration of DNN-based actions into the pathology workflow, particularly in relation to efficient WSI analysis. Additionally, we focused on cells that contribute to various GI tract diseases, enhancing the relevance and impact of our approach.

A primary limitation of our study is the moderate sample size of the cohort. Nevertheless, individuals with advanced haemorrhoidal disease (HD) were equally represented in grades III and IV, and the study included both sexes, as assigned at birth. Despite this constraint, the findings adequately reflect the characteristics of the investigated cohort, satisfying internal validity criteria through validation by a single evaluator. Another limitation is the narrow range of staining variability, as the current model was optimised for a specific local laboratory staining protocol. This constraint could be addressed by retraining the model with additional augmentation techniques—such as adjustments to

hue, intensity, brightness, and contrast—to enhance its generalisability. Furthermore, compiling a training dataset that incorporates images from multiple sources, and then validating against both internal and external datasets, would further mitigate issues related to interobserver variability.

5. Conclusions

Surgical excision remains the most effective treatment for grade III and IV HD, offering the best long-term patient satisfaction despite an increased risk of initial side effects and complications. The AI-driven model employed in this study, focused on the histological features of HD with a particular emphasis on ICCs, when integrated with clinical data, proves to be a valuable tool for enhancing the understanding of disease pathophysiology. This approach also facilitates more accurate estimations of patient outcomes, thereby holding significant potential for both diagnostic and prognostic applications in clinical practice.

Furthermore, a dedicated application was introduced for WSI analysis and automated ICC quantification, seamlessly integrating tissue segmentation, cell- and tissue-level measurements, and the efficient handling of large TIFF files within a single platform. This software automatically generates annotated images, tissue masks, and summary reports, providing a thorough yet flexible tool for pathologists and researchers engaged in histopathological imaging.

Supplementary Materials: The following supporting information can be downloaded at: https://www.mdpi.com/article/10.3390/cells14070550/s1, Figure S1: Overview of postoperative medication regiments and interventions in patients with HD. Figure S2: ANO1 IHC performed on FFPE anorectal tissue samples from patients with HD. Figure S3: Association between the number of detected ICCs and ANO1 expression in anal canal wall myocytes. Figure S4: Association between the number of detected ICCs and the tissue area of anal canal wall specimens. Figure S5: Hierarchical clustering of HD patients and visual representation of ICC density, patient sex, and disease severity in the study cohort.

Author Contributions: Conceptualization, I.F. and V.G.; methodology, I.F. and V.G.; software, E.E.; validation, V.G.; formal analysis, Š.S.; investigation, V.G.; resources, I.F.; data curation, V.G. and E.E.; writing—original draft preparation, I.F., V.G., E.E. and Š.S.; writing—review and editing, I.F., V.G., E.E. and Š.S.; visualisation, Š.S.; supervision, V.G.; project administration, V.G.; funding acquisition, I.F. All authors have read and agreed to the published version of the manuscript.

Funding: This research and APC were funded by the Riga Stradiņš University Department of Doctoral studies, decision number Nr. 6-DN-20/3/2024.

Institutional Review Board Statement: This study was conducted in accordance with the Declaration of Helsinki and approved by the Institutional Ethics Committee of Riga Stradiņš University (protocol code No. 22-2/264/2021).

Informed Consent Statement: Informed consent was obtained from all subjects involved in this study.

Data Availability Statement: All images utilised for model training in this study are publicly available. The complete dataset has been deposited in the Zenodo repository and can be accessed via the following DOI: https://doi.org/10.5281/zenodo.14900511. Additionally, the software developed to implement and test the proposed model is openly available on GitHub at https://github.com/edImar/MorpHista (accessed on 4 April 2025).

Acknowledgments: The authors would like to acknowledge the Riga Stradiņš University Department of Doctoral Studies for their support in acquiring the reagents and the article processing charges.

Conflicts of Interest: The authors declare no conflicts of interest.

Abbreviations

The following abbreviations are used in this manuscript:

AI	Artificial intelligence
ANO1	Anoctamin 1
ASA	American Society of Anaesthesiologists
CI	Confidence interval
DNN	Deep neural network
FFPE	Formalin-fixed and paraffin-embedded
F1	F1 Score (harmonic mean of precision and recall)
GI	Gastrointestinal
HD	Haemorrhoidal disease
HRP	Horseradish peroxidase
IHC	Immunohistochemistry
IQR	Interquartile range
LH	LigaSure haemorrhoidectomy
ML	Machine learning
mAP50	Mean average precision at 50% intersection over union (IoU)
mAP50-95	Mean average precision averaged over IoU thresholds from 50% to 95%
TMEM16A	Transmembrane protein 16A (alternative name for ANO1)
VAS	Visual Analogue Scale
WSI	Whole slide image(s)
TIFF	Tagged Image File Format

References

1. Lohsiriwat, V. Anatomy, Physiology, and Pathophysiology of Hemorrhoids. In *Hemorrhoids. Coloproctology*; Ratto, C., Parello, A., Litta, F., Eds.; Springer International Publishing: Cham, Switzerland, 2018; Volume 2, pp. 9–17, ISBN 978-3-319-53356-8.
2. Yuan, C.; Zhou, C.; Xue, R.; Jin, X.; Jin, C.; Zheng, C. Outcomes of Modified Tissue Selection Therapy Stapler in the Treatment of Prolapsing Hemorrhoids. *Front. Surg.* **2022**, *9*, 838742. [CrossRef] [PubMed]
3. Alhamdany, A.; Wahhab, R.A.S.A.; Lateef, N.F. Ligasure^{TM} Hemorrhoidectomy versus Conventional Hemorrhoidectomy: Comparison in Outcome. *Open Access Maced. J. Med. Sci.* **2022**, *10*, 68–73. [CrossRef]
4. Wei, D.; Jiang, P.; Gao, R.; Zhao, Y. Prevention and Treatment of Anastomotic Strictures After Procedure for Prolapse and Hemorrhoids. *Risk Manag. Healthc. Policy* **2023**, *16*, 1351–1357. [CrossRef] [PubMed]
5. Durgun, C.; Yiğit, E. Laser Hemorrhoidoplasty Versus Ligasure Hemorrhoidectomy: A Comparative Analysis. *Cureus* **2023**, *15*, 43119. [CrossRef] [PubMed]
6. Gardner, I. Benign Anorectal Disease: Hemorrhoids, Fissures, and Fistulas. *Ann. Gastroenterol.* **2019**, *33*, 9. [CrossRef]
7. Elnaim, A.L.K.; Musa, S.; Wong, M.P.-K.; Sagap, I. A Prospective Interventional Study on LigaSureTM Haemorrhoidectomy as a Daycare Procedure. *Malays. J. Med. Sci.* **2021**, *28*, 102–107. [CrossRef]
8. Cheng, K.-C.; Song, L.-C.; Wu, K.-L.; Chen, H.-H.; Lee, K.-C. Risk Factors of Delayed Hemorrhage after LigaSure Hemorrhoidectomy. *BMC Surg.* **2022**, *22*, 361. [CrossRef]
9. Chen, C.-W.; Lu, T.-J.; Hsiao, K.-H. Surgical Outcomes of LigaSure Hemorrhoidectomy in the Elderly Population: A Retrospective Cohort Study. *BMC Gastroenterol.* **2021**, *21*, 413. [CrossRef]
10. Bibi, S.; Saqib, K.; Irfan, I.; Tabbasam, S.; Ahmad, H. LigaSure Hemorrhoidectomy vs Milligan Morgan Hemorrhoidectomy: A Quasi-Experimental Study. *Prof. Med. J.* **2023**, *30*, 680–683. [CrossRef]
11. Jin, J.; Unasa, H.; Bahl, P.; Mauiliu-Wallis, M.; Svirskis, D.; Hill, A. Can Targeting Sphincter Spasm Reduce Post-Haemorrhoidectomy Pain? A Systematic Review and Meta-Analysis. *World J. Surg.* **2023**, *47*, 520–533. [CrossRef]
12. Robinson, A.; McIntosh, J.; Peberdy, H.; Wishart, D.; Brown, G.; Pope, H.; Kumar, S. The Effectiveness of Physiotherapy Interventions on Pain and Quality of Life in Adults with Persistent Post-Surgical Pain Compared to Usual Care: A Systematic Review. *PLoS ONE* **2019**, *14*, e0226227. [CrossRef] [PubMed]
13. Amir, A.; Nazir, A.; Umair, A.; Khan, M.A.; Maqbool, S.; Anwar, M.I.; Fazal, F. Comparison of Pedicle Coagulation Hemorrhoidectomy With LigaSure Versus Conventional Milligan Morgan Hemorrhoidectomy in Reducing Post-Operative Pain: A Randomized Controlled Trial. *Cureus* **2023**, *15*, 45015. [CrossRef] [PubMed]

14. Foong, D.; Zhou, J.; Zarrouk, A.; Ho, V.; O'Connor, M.D. Understanding the Biology of Human Interstitial Cells of Cajal in Gastrointestinal Motility. *Int. J. Mol. Sci.* **2020**, *21*, 4540. [CrossRef] [PubMed]
15. Mah, S.A.; Du, P.; Avci, R.; Vanderwinden, J.-M.; Cheng, L.K. Analysis of Regional Variations of the Interstitial Cells of Cajal in the Murine Distal Stomach Informed by Confocal Imaging and Machine Learning Methods. *Cell. Mol. Bioeng.* **2022**, *15*, 193–205. [CrossRef]
16. Mah, S.A.; Avci, R.; Cheng, L.K.; Du, P. Current Applications of Mathematical Models of the Interstitial Cells of Cajal in the Gastrointestinal Tract. *WIREs Mech. Dis.* **2021**, *13*, e1507. [CrossRef] [PubMed]
17. Lu, P.; Lifshitz, L.M.; Bellve, K.; ZhuGe, R. TMEM16A in Smooth Muscle Cells Acts as a Pacemaker Channel in the Internal Anal Sphincter. *Commun. Biol.* **2024**, *7*, 151. [CrossRef] [PubMed]
18. Le, S.C.; Yang, H. An Additional Ca^{2+} Binding Site Allosterically Controls TMEM16A Activation. *Cell Rep.* **2020**, *33*, 108570. [CrossRef] [PubMed]
19. Kather, J.N.; Pearson, A.T.; Halama, N.; Jäger, D.; Krause, J.; Loosen, S.H.; Marx, A.; Boor, P.; Tacke, F.; Neumann, U.P.; et al. Deep Learning Can Predict Microsatellite Instability Directly from Histology in Gastrointestinal Cancer. *Nat. Med.* **2019**, *25*, 1054–1056. [CrossRef]
20. L'Imperio, V.; Wulczyn, E.; Plass, M.; Müller, H.; Tamini, N.; Gianotti, L.; Zucchini, N.; Reihs, R.; Corrado, G.S.; Webster, D.R.; et al. Pathologist Validation of a Machine Learning–Derived Feature for Colon Cancer Risk Stratification. *JAMA Netw. Open* **2023**, *6*, e2254891. [CrossRef]
21. Najdawi, F.; Sucipto, K.; Mistry, P.; Hennek, S.; Jayson, C.K.B.; Lin, M.; Fahy, D.; Kinsey, S.; Wapinski, I.; Beck, A.H.; et al. Artificial Intelligence Enables Quantitative Assessment of Ulcerative Colitis Histology. *Mod. Pathol.* **2023**, *36*, 100124. [CrossRef]
22. Codipilly, D.C.; Faghani, S.; Hagan, C.; Lewis, J.; Erickson, B.J.; Iyer, P.G. The Evolving Role of Artificial Intelligence in Gastrointestinal Histopathology: An Update. *Clin. Gastroenterol. Hepatol.* **2024**, *22*, 1170–1180. [CrossRef] [PubMed]
23. Yilmaz, F.; Brickman, A.; Najdawi, F.; Yakirevich, E.; Egger, R.; Resnick, M.B. Advancing Artificial Intelligence Integration Into the Pathology Workflow: Exploring Opportunities in Gastrointestinal Tract Biopsies. *Lab. Investig.* **2024**, *104*, 102043. [CrossRef] [PubMed]
24. Jocher, G.; Qiu, J. Ultralytics YOLO11. 2024. Available online: https://docs.ultralytics.com/models/yolo11/ (accessed on 4 April 2025).
25. Sheikh, P.; Régnier, C.; Goron, F.; Salmat, G. The Prevalence, Characteristics and Treatment of Hemorrhoidal Disease: Results of an International Web-Based Survey. *J. Comp. Eff. Res.* **2020**, *9*, 1219–1232. [CrossRef] [PubMed]
26. Oakland, K.; Chadwick, G.; East, J.E.; Guy, R.; Humphries, A.; Jairath, V.; McPherson, S.; Metzner, M.; Morris, A.J.; Murphy, M.F.; et al. Diagnosis and Management of Acute Lower Gastrointestinal Bleeding: Guidelines from the British Society of Gastroenterology. *Gut* **2019**, *68*, 776–789. [CrossRef]
27. Brown, S.R. Haemorrhoids: An Update on Management. *Ther. Adv. Chronic Dis.* **2017**, *8*, 141–147. [CrossRef]
28. Kibret, A.A.; Oumer, M.; Moges, A.M. Prevalence and Associated Factors of Hemorrhoids among Adult Patients Visiting the Surgical Outpatient Department in the University of Gondar Comprehensive Specialized Hospital, Northwest Ethiopia. *PLoS ONE* **2021**, *16*, e0249736. [CrossRef]
29. Onder, T.; Altiok, M. A Retrospective Comparative Study of Hemorrhoidal Artery Ligation versus Ligasure Hemorrhoidectomy for the Third Degree Hemorrhoidal Disease. *Asian J. Surg.* **2023**, *46*, 4385–4388. [CrossRef]
30. Prokopakis, E.P.; Lachanas, V.A.; Vardouniotis, A.S.; Velegrakis, G.A. The Use of the Ligasure Vessel Sealing System in Head and Neck Surgery: A Report on Six Years of Experience and a Review of the Literature. *B-ENT* **2010**, *6*, 19–25. [PubMed]
31. McGenity, C.; Clarke, E.L.; Jennings, C.; Matthews, G.; Cartlidge, C.; Freduah-Agyemang, H.; Stocken, D.D.; Treanor, D. Artificial Intelligence in Digital Pathology: A Systematic Review and Meta-Analysis of Diagnostic Test Accuracy. *Npj Digit. Med.* **2024**, *7*, 114. [CrossRef] [PubMed]
32. Lohsiriwat, V.; Jitmungngan, R. Strategies to Reduce Post-Hemorrhoidectomy Pain: A Systematic Review. *Med. Kaunas Lith.* **2022**, *58*, 418. [CrossRef] [PubMed]
33. Huang, Y.-J.; Chen, C.-Y.; Chen, R.-J.; Kang, Y.-N.; Wei, P.-L. Topical Diltiazem Ointment in Post-Hemorrhoidectomy Pain Relief: A Meta-Analysis of Randomized Controlled Trials. *Asian J. Surg.* **2018**, *41*, 431–437. [CrossRef] [PubMed]
34. Nagaty, M. A Comparison between the Outcome of LigaSure Hemorrhoidectomy Versus Conventional Milligan Morgan's Technique. *Al-Azhar Int. Med. J.* **2022**, *3*, 52–56. [CrossRef]
35. Uzzaman, M.M.; Siddiqui, M.R.S. A Brief Literature Review on the Management of Post-Haemorrhoidectomy Pain. *Surg. Tech. Dev.* **2011**, *1*, e32. [CrossRef]
36. Emile, S.H. Evidence-Based Review of Methods Used to Reduce Pain after Excisional Hemorrhoidectomy. *J. Coloproctology* **2019**, *39*, 081–089. [CrossRef]
37. Perera, N.; Liolitsa, D.; Iype, S.; Croxford, A.; Yassin, M.; Lang, P.; Ukaegbu, O.; Van Issum, C. Phlebotonics for Haemorrhoids. *Cochrane Database Syst. Rev.* **2012**, *8*, CD004322. [CrossRef]

38. Orefice, R.; Litta, F.; Parello, A.; De Simone, V.; Campennì, P.; Marra, A.A.; Ratto, C. A Prospective Study on the Efficacy of Two Different Phlebotonic Therapies as a Bridge to Surgery in Patients with Advanced Hemorrhoidal Disease. *J. Clin. Med.* **2021**, *10*, 1549. [CrossRef]
39. Al-Sajee, D.; Huizinga, J.D. Interstitial Cells of Cajal: Pathology, Injury and Repair. *Sultan Qaboos Univ. Med. J.* **2012**, *12*, 411–421. [CrossRef]
40. Torihashi, S.; Horisawa, M.; Watanabe, Y. C-Kit Immunoreactive Interstitial Cells in the Human Gastrointestinal Tract. *J. Auton. Nerv. Syst.* **1999**, *75*, 38–50. [CrossRef]
41. Brunenieks, I.; Pekarska, K.; Kasyanov, V.; Groma, V. Biomechanical and Morphological Peculiarities of the Rectum in Patients with Obstructed Defecation Syndrome. *Rom. J. Morphol. Embryol.* **2017**, *58*, 1193–1200. [PubMed]
42. Hagger, R.; Gharaie, S.; Finlayson, C.; Kumar, D. Distribution of the Interstitial Cells of Cajal in the Human Anorectum. *J. Auton. Nerv. Syst.* **1998**, *73*, 75–79. [CrossRef] [PubMed]
43. Kaji, N.; Hori, M. Interstitial Cells of Cajal in Gastrointestinal Inflammatory Diseases. *J. Smooth Muscle Res.* **2023**, *59*, 1–13. [CrossRef] [PubMed]
44. Wu, C.-E.; Tzen, C.-Y.; Wang, S.-Y.; Yeh, C.-N. Clinical Diagnosis of Gastrointestinal Stromal Tumor (GIST): From the Molecular Genetic Point of View. *Cancers* **2019**, *11*, 679. [CrossRef] [PubMed]
45. Yin, J.; Chen, J.D.Z. Roles of Interstitial Cells of Cajal in Regulating Gastrointestinal Motility: *In Vitro versus in Vivo* Studies. *J. Cell. Mol. Med.* **2008**, *12*, 1118–1129. [CrossRef] [PubMed]
46. Chevalier, N.R.; Ammouche, Y.; Gomis, A.; Teyssaire, C.; De Santa Barbara, P.; Faure, S. Shifting into High Gear: How Interstitial Cells of Cajal Change the Motility Pattern of the Developing Intestine. *Am. J. Physiol.-Gastrointest. Liver Physiol.* **2020**, *319*, G519–G528. [CrossRef] [PubMed]
47. Hwang, S.J.; Blair, P.J.A.; Britton, F.C.; O'Driscoll, K.E.; Hennig, G.; Bayguinov, Y.R.; Rock, J.R.; Harfe, B.D.; Sanders, K.M.; Ward, S.M. Expression of Anoctamin 1/TMEM16A by Interstitial Cells of Cajal Is Fundamental for Slow Wave Activity in Gastrointestinal Muscles. *J. Physiol.* **2009**, *587*, 4887–4904. [CrossRef]
48. Lees-Green, R.; Gibbons, S.J.; Farrugia, G.; Sneyd, J.; Cheng, L.K. Computational Modeling of Anoctamin 1 Calcium-Activated Chloride Channels as Pacemaker Channels in Interstitial Cells of Cajal. *Am. J. Physiol.-Gastrointest. Liver Physiol.* **2014**, *306*, G711–G727. [CrossRef]
49. Sanders, K.M. Spontaneous Electrical Activity and Rhythmicity in Gastrointestinal Smooth Muscles. In *Smooth Muscle Spontaneous Activity*; Hashitani, H., Lang, R.J., Eds.; Advances in Experimental Medicine and Biology; Springer: Singapore, 2019; Volume 1124, pp. 3–46, ISBN 978-981-13-5894-4.
50. Forrest, A.S.; Hennig, G.W.; Jokela-Willis, S.; Park, C.D.; Sanders, K.M. Prostaglandin Regulation of Gastric Slow Waves and Peristalsis. *Am. J. Physiol.-Gastrointest. Liver Physiol.* **2009**, *296*, G1180–G1190. [CrossRef]
51. Huizinga, J.D.; Hussain, A.; Chen, J.-H. Interstitial Cells of Cajal and Human Colon Motility in Health and Disease. *Am. J. Physiol.-Gastrointest. Liver Physiol.* **2021**, *321*, G552–G575. [CrossRef]
52. Choi, E.L.; Taheri, N.; Tan, E.; Matsumoto, K.; Hayashi, Y. The Crucial Role of the Interstitial Cells of Cajal in Neurointestinal Diseases. *Biomolecules* **2023**, *13*, 1358. [CrossRef]
53. Sweet, T.; Abraham, C.M.; Rich, A. Origin and Development of Interstitial Cells of Cajal. *Int. J. Dev. Biol.* **2024**, *68*, 93–102. [CrossRef]
54. Strege, P.R.; Ou, Y.; Sha, L.; Rich, A.; Gibbons, S.J.; Szurszewski, J.H.; Sarr, M.G.; Farrugia, G. Sodium Current in Human Intestinal Interstitial Cells of Cajal. *Am. J. Physiol.-Gastrointest. Liver Physiol.* **2003**, *285*, G1111–G1121. [CrossRef] [PubMed]
55. Won, K.-J.; Sanders, K.M.; Ward, S.M. Interstitial Cells of Cajal Mediate Mechanosensitive Responses in the Stomach. *Proc. Natl. Acad. Sci. USA* **2005**, *102*, 14913–14918. [CrossRef] [PubMed]
56. Truong Thuy Nguyen, V.; Taheri, N.; Choi, E.L.; Kellogg, T.A.; Linden, D.R.; Hayashi, Y. Insulin-Like Growth Factor1 Preserves Gastric Pacemaker Cells and Motor Function in Aging via ERK1/2 Activation. *Cell. Mol. Gastroenterol. Hepatol.* **2023**, *16*, 369–383. [CrossRef] [PubMed]
57. Du, P.; Hameed, A.; Angeli, T.R.; Lahr, C.; Abell, T.L.; Cheng, L.K.; O'Grady, G. The Impact of Surgical Excisions on Human Gastric Slow Wave Conduction, Defined by High-resolution Electrical Mapping and in Silico Modeling. *Neurogastroenterol. Motil.* **2015**, *27*, 1409–1422. [CrossRef]
58. Camilleri, M.; Tack, J. Is the Quantification of Interstitial Cells of Cajal in Gastric Biopsy Samples in Patients with Gastroparesis Ready for Prime Time? *Gastroenterology* **2023**, *165*, 1–4. [CrossRef] [PubMed]
59. Patel, V.; Khan, M.N.; Shrivastava, A.; Sadiq, K.; Ali, S.A.; Moore, S.R.; Brown, D.E.; Syed, S. Artificial Intelligence Applied to Gastrointestinal Diagnostics: A Review. *J. Pediatr. Gastroenterol. Nutr.* **2020**, *70*, 4–11. [CrossRef] [PubMed]

60. Lecuelle, J.; Truntzer, C.; Basile, D.; Laghi, L.; Greco, L.; Ilie, A.; Rageot, D.; Emile, J.-F.; Bibeau, F.; Taïeb, J.; et al. Machine Learning Evaluation of Immune Infiltrate through Digital Tumour Score Allows Prediction of Survival Outcome in a Pooled Analysis of Three International Stage III Colon Cancer Cohorts. *eBioMedicine* **2024**, *105*, 105207. [CrossRef] [PubMed]
61. Zhou, J.; Hu, N.; Huang, Z.-Y.; Song, B.; Wu, C.-C.; Zeng, F.-X.; Wu, M. Application of Artificial Intelligence in Gastrointestinal Disease: A Narrative Review. *Ann. Transl. Med.* **2021**, *9*, 1188. [CrossRef]